CHEMICAL REVIEWS

Review

Cite This: *Chem. Rev.* 2019, 119, 902−956

pubs.acs.org/CR

Radioactive Main Group and Rare Earth Metals for Imaging and Therapy

Thomas I. Kostelnik* and Chris Orvig*

Medicinal Inorganic Chemistry Group, Department of Chemistry, University of British Columbia, Vancouver, British Columbia V6T 1Z1, Canada

ABSTRACT: Radiometals possess an exceptional breadth of decay properties and have been applied to medicine with great success for several decades. The majority of current clinical use involves diagnostic procedures, which use either positron-emission tomography (PET) or single-photon imaging to detect anatomic abnormalities that are difficult to visualize using conventional imaging techniques (e.g., MRI and X-ray). The potential of therapeutic radiometals has more recently been realized and relies on ionizing radiation to induce irreversible DNA damage, resulting in cell death. In both cases, radiopharmaceutical development has been largely geared toward the field of oncology; thus, selective tumor targeting is often essential for efficacious drug use. To this end, the rational design of four-component radiopharmaceuticals has become popularized. This Review introduces fundamental concepts of drug design and applications, with particular emphasis on bifunctional chelators (BFCs), which ensure secure consolidation of the radiometal and targeting vector and are integral for optimal drug performance. Also presented are detailed accounts of production, chelation chemistry, and biological use of selected main group and rare earth radiometals.

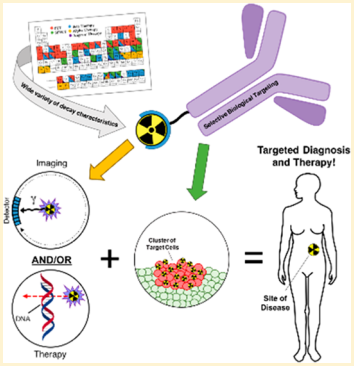

CONTENTS

Special Issue: Metals in Medicine

Received: May 8, 2018
Published: October 31, 2018

DOI: 10.1021/acs.chemrev.8b00294
Chem. Rev. 2019, 119, 902−956

1. INTRODUCTION TO RADIOPHARMACEUTICALS

Nuclear medicine is a rapidly growing, interdisciplinary field based on the use of radioactive nuclides for diagnostic and therapeutic purposes. The development of radiopharmaceuticals is a key aspect of expanding the clinical capabilities of nuclear medicine physicians and is achieved by continually improving the existing framework of current drug design. Radiopharmaceuticals are divided into two broad classes: organically derived and metal-based. These classes primarily differ in their strategy of radionuclide incorporation. Organically derived radiopharmaceuticals incorporate nonmetal radionuclides (e.g., ^{18}F, ^{11}C, ^{13}N, ^{15}O, and ^{123}I) by covalent bond formation, often replacing one hydrogen atom, whereas metal-based tracers rely on coordination chemistry. The short half-lives and limited decay characteristics of most "organic" radionuclides severely limit their applications. As seen in Figure 1, radiometals offer a broad variety of decay characteristics and, as such, will be the focus of this Review. With a complementary scope to the transition metal focus of Boros and Packard,[1] we describe the production, purification, chelation, and biological use of metal-based radiopharmaceuticals, with emphasis on main group and rare earth radiometals.

2. DESIGN OF RADIOPHARMACEUTICALS

Within the realm of metal-based radiopharmaceuticals, two prominent categories exist: metal-essential and metal-nonessential. The distinction between these classes is the role of the radiometal. In metal-essential drugs, the radiometal is fundamental for biological targeting. For example, ^{99m}Tc-sestamibi (Cardiolite) is a cardiac imaging agent composed of a ^{99m}Tc^{+} center coordinated by six methoxyisobutylisonitrile (MIBI) ligands. The arrangement of these lipophilic ligands around the metal facilitates heart uptake of ^{99m}Tc-sestamibi; however, if ^{99m}Tc^{+} was replaced by a different metal ion or was absent altogether, the resulting biodistribution would be profoundly different.[15] Although metal-essential drugs are simple to synthesize, they are challenging to derivatize. In contrast, metal-nonessential tracers are modular by design and in theory exhibit metal-independent in vivo behavior. Readers are cautioned that, in practice, metal choice can influence drug biodistribution (see sections 3.3 and 9); however, compared to metal-essential radiopharmaceuticals, this influence is relatively small. Most metal-nonessential design strategies divide the drug into four parts: radiometal, ligand/chelator, linker, and bioconjugate/targeting vector (Figure 2). In this case, the decay properties of the radiometal are the root of diagnostic/therapeutic function, while the bioconjugate ensures drug accumulation at target cells. The chelator and linker integrate the two otherwise incompatible components. This design is very popular, as it permits alteration of individual components to tune drug function, providing enormous potential for "plug-and-play" drug discovery. Unless otherwise stated, all discussed radiotracers emulate this design.

3. DECAY PROPERTIES OF RADIOMETALS IN MEDICINE

Radiometal decay properties determine radiopharmaceutical function. Diagnostic radiometals emit radiation that minimally interacts with biological tissue, allowing it to easily escape the body and reach external detectors. Therapeutic radiometals emit radiation intended to maximally interact with surrounding tissue in order to exert a toxic effect locally. These differences in radiation behavior are heavily reliant on radiometal decay characteristics. Table 1 presents decay properties, applications, and production routes of popular radiometals and may be helpful for reference in the following discussion. Figure 3 illustrates decay-specific applications.

3.1. Diagnostic Radiometals

Diagnostic radiotracers emit or indirectly produce photons, which are detected by high-density material to produce spatial representations of drug distribution in vivo. Positron-emission tomography (PET) and single-photon emission computed tomography (SPECT) are the most prevalent imaging modalities for this purpose.

PET imaging requires the use of positron (β^{+}) emitters, which are normally neutron-deficient radionuclides that balance their nuclear composition through the conversion of a proton to a neutron by β^{+} emission. When these positrons meet nearby electrons (β^{-}), a process known as "annihilation" results in the simultaneous emission of near-coincident (~180 °) γ-rays, with a characteristic energy of 511 keV. When PET scanners detect these simultaneous γ-rays, computational methods precisely calculate the radiotracer location by determining the point of annihilation.[22] The distance a β^{+} travels before annihilation is proportional to its energy; thus, emission of low-energy positrons is preferred due to their close proximity to the radiotracer at the point of annihilation.[23] By far the most commonly used PET radiotracer is the glucose analogue, [^{18}F]FDG (^{18}F-fluorodeoxyglucose), which has a natural propensity to be selectively taken up by aggressively growing tumors because of its similarity to glucose. The high radiotracer concentration in tumors and low background activity facilitate acquisition of high-resolution images.[24]

Similar to traditional two-dimensional scintigraphy, SPECT is based on the detection of γ-rays emitted from radiotracers, often as a result of electron capture (EC) or isomeric transition (IT). Unlike scintigraphy, however, SPECT renders three-dimensional images to produce more spatially oriented representations of tracer behavior. Because of its reliance on single-emission events (as opposed to simultaneous events), SPECT detectors require narrow γ-ray filtering, or "collima-

DOI: 10.1021/acs.chemrev.8b00294
Chem. Rev. 2019, 119, 902−956

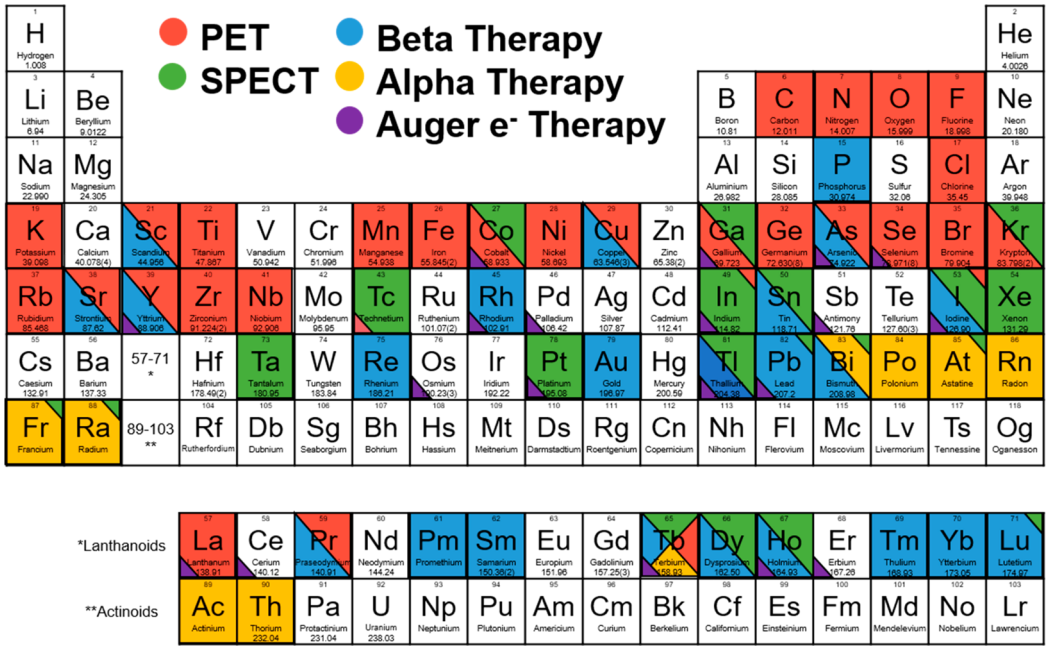

Figure 1. Color-coded periodic table with current or potential applications of each element in diagnostic and/or therapeutic radiopharmaceuticals.[2−14] Periodic table reproduced by permission of International Union of Pure and Applied Chemistry. Copyright © 2018 International Union of Pure and Applied Chemistry.

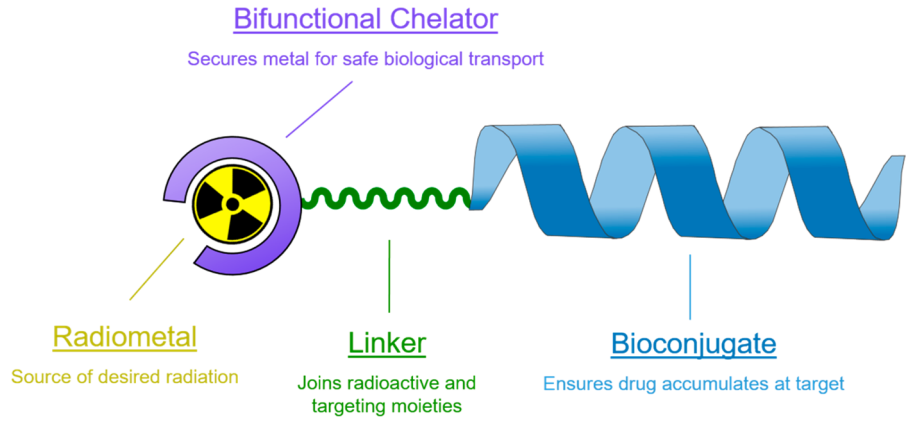

Figure 2. Standard, four-component radiopharmaceutical design.

tion", for decay localization and sharp image construction. Low-energy γ-rays (100−250 keV) are ideal for SPECT as they are more easily filtered by collimators and efficiently attenuated by SPECT detectors.[25,26] The vast majority of SPECT scans are based on ^{99m}Tc radionuclides, with one of the most frequently used radiotracers being ^{99m}Tc-sestamibi for heart perfusion imaging.[15]

Of the two techniques, PET has superior sensitivity and resolution but is far more expensive than SPECT as a result of higher instrumentation costs and lower radionuclide availability.[26−28] PET and SPECT provide high-quality morphological information but lack anatomical perspective. Accordingly, they are often combined with computed tomography (CT) to produce a more complete biological representation.[27]

3.2. Therapeutic Radiometals

Therapeutic radiometals primarily induce their cytotoxic effects through irreversible DNA damage, resulting in deletions, chromosome aberrations, and cell death.[29] DNA damage can be achieved with the emission of beta (β^-) particles, alpha (α) particles, or low-energy electrons (henceforth, Auger electrons). The ability of an emitted particle to damage DNA is heavily dependent on its linear energy transfer (LET), which is a measure of atom ionization/excitation per unit length and is commonly reported in keV/μm for biological systems. High LET is typical of highly ionizing radiation and signifies dense energy deposition. Particles with high LET deposit their energy over shorter distances than those with low LET and are more effective at causing biological and/or chemical damage.[29,30] Tissue range is dependent on both a particle's LET and kinetic energy. For example, if two particles have identical energy but different LET, the particle with higher LET will deposit its energy more rapidly, resulting in shorter tissue range. Alternatively, if two particles have identical LET but different energies, the higher-energy particle will take longer to deposit its energy, resulting in greater tissue range. Long tissue range can be useful for treatment of large tumors but is increasingly regarded as undesirable because it is directly linked to off-target toxicity.[31−33] Particle LET and tissue range vary among

DOI: 10.1021/acs.chemrev.8b00294
Chem. Rev. 2019, 119, 902−956

Table 1. Popular Subject Radiometals with Relevant Production Routes, Decay Parameters, and Applications[16−21]

radionuclide	production	half life (h)	decay mode and branching	average energy of decay particle (keV)[a]	max gamma energy (keV) (intensity %)	application
^{44}Sc	^{44}Ca(p,n)^{44}Sc	4.04	β^+ (94%)	632	1157 (100%)	PET
	^{44}Ti/^{44}Sc generator		EC (6%)			
^{47}Sc	^{47}Ti(n,p)^{47}Sc	80.4	β^- (100%)	162	159 (68%)	β^- therapy
	^{46}Ca(n,γ)^{47}Ca→^{47}Sc					SPECT
^{66}Ga	^{66}Zn(p,n)^{66}Ga	9.49	β^+ (57%)	1747	1039 (37%)	PET
			EC (43%)		2752 (23%)	
^{67}Ga	^{67}Zn(p,n)^{67}Ga	78.2	EC (100%)		93 (39%)	SPECT
			4.7 e$^-$/decay[b]	Auger: 6.3[b]	185 (21%)	
					300 (17%)	
^{68}Ga	^{68}Ge/^{68}Ga generator	1.13	β^+ (89%)	830		PET
			EC (11%)			
^{86}Y	^{86}Sr(p,n)^{86}Y	14.7	β^+ (32%)	664	777 (22%)	PET
			EC (68%)		1077 (83%)	
					1153 (31%)	
^{90}Y	^{90}Sr/^{90}Y generator	64.0	β^- (100%)	934		β^- therapy
^{110m}In	^{110}Cd(p,n)^{110m}In	1.15	β^+ (61%)	1011	658 (98%)	PET
			EC (39%)			
^{111}In	^{nat}Cd(p,xn)^{111}In	67.2	EC (100%)		245 (94%)	SPECT
			14.7 e$^-$/decay[b]	Auger: 6.8[b]	171 (91%)	
^{114m}In	^{114}Cd(p,n)^{114m}In	1188	IT (97%)		190 (16%)	Auger electron therapy
^{149}Tb	spallation of Ta-foil	4.12	α (17%)	α: 3970	165 (26%)	α therapy
	^{152}Gd(p,4n)^{149}Tb		β^+ (7%)	β^+: 728	352 (29%)	PET
	^{142}Nd(^{12}C,5n)^{149}Dy→^{149}Tb		EC (76%)		389 (18%)	
					817 (12%)	
					853 (16%)	
^{152}Tb	spallation of Ta-foil	17.5	β^+ (20%)	1142	344 (64%)	PET
	^{152}Gd(p,n)^{152}Tb		EC (80%)			
^{155}Tb	spallation of Ta-foil	128	EC (100%)		87 (32%)	SPECT
	^{155}Gd(p,n)^{155}Tb				105 (25%)	
	^{159}Tb(p,5n)^{155}Dy→^{155}Tb					
^{161}Tb	^{160}Gd(n,γ)^{161}Gd→^{161}Tb	165	β^- (100%)	β^-: 154	26 (23%)	β^- and Auger electron therapy
			12.4 e$^-$/decay[c]	Auger: 46.5[c]	49 (17%)	SPECT
					75 (10%)	
^{177}Lu	^{176}Lu(n,γ)^{177}Lu	159	β^- (100%)	134	113 (6%)	β^- therapy
	^{176}Yb(n,γ)^{177}Yb→^{177}Lu				208 (10%)	SPECT
^{212}Bi	^{228}Th/^{212}Pb/^{212}Bi generator	1.01	α (36%)	α: 6210		α and β^- therapy
			β^- (64%)	α: 8780 (daughter)		
				β^-: 771		
^{213}Bi	^{225}Ac/^{213}Bi generator	0.76	α (2%)	α: 8.35 MeV[d] (daughter)	440 (26%)	α and β^- therapy
			β^- (98%)	β^-: 435		
^{225}Ac	^{229}Th/^{225}Ac generator	238	α (100%)	α: 5.8−8.4 MeV[d] (chain average)		α therapy
	^{226}Ra(p,2n)^{225}Ac					
	^{232}Th(p,2p6n)^{225}Ac					

[a]Ref 16; weighted average of average values. [b]Refs 18 and 19. [c]Ref 20. [d]Ref 21.

therapeutic radionuclides and are heavily influenced by the decay type and energy.

β^- particles have variable energy (0.1−2.2 MeV) and relatively low LET, which typically falls in the realm of 0.2 keV/μm. Although β^- emitters are the most developed class of radiotherapeutics, it is known that their low LET results in a high decay range (0.5−10 mm; 50−1000 cell diameters) that often extends beyond the diameter of targeted tumors.[10] This can lead to the death of healthy cells ("cross-fire") and is a major deterrent of β^- therapy. Currently, low-energy β^- emitters (e.g., ^{177}Lu) are being heavily investigated due to their lower decay range relative to high-energy β^- emitters (e.g., ^{90}Y).[34] Alpha particles have high energies (5−8 MeV) and extremely high LET (~80 keV/μm), resulting in a low decay range (40−100 μm; <10 cell diameters).[10] Their highly ionizing nature and short tissue range is the cause of current enthusiastic efforts to explore targeted alpha therapy (TAT), notably with ^{225}Ac. Auger electrons are low-energy particles ejected as a result of energy released during the filling of inner electron-shell vacancies. These particles have high LET (4−26 keV/μm) and very low energy (1−10 keV), resulting in tissue range (1−20 μm) that is often less than the diameter of a single cell (~10 μm).[10] This makes cross-fire effects essentially nonexistent and presents the potential to treat single-cell

DOI: 10.1021/acs.chemrev.8b00294
Chem. Rev. 2019, 119, 902−956

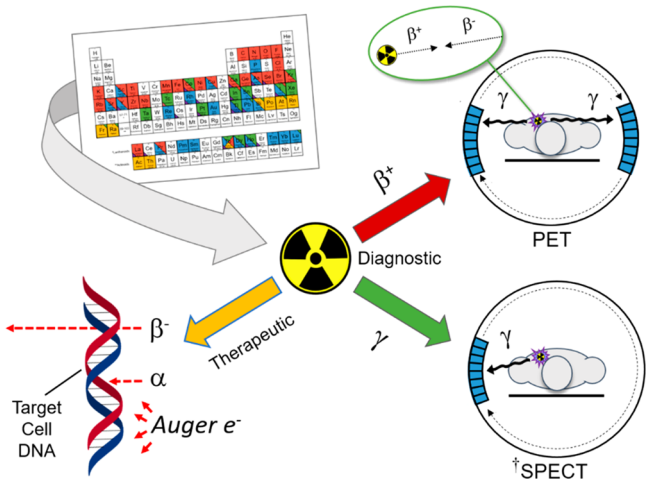

Figure 3. Radiometal decay types and their corresponding applications in nuclear medicine. †Indicates that degree of rotation, number of detectors, and orbital path may vary depending on instrument.

tumor metastasis. Auger electrons are the least explored therapeutic and are currently limited by their need for cell or nucleus internalization to exert any degree of toxic effects.[35]

3.3. Theranostics

Combined therapeutic and diagnostic ("theranostic") isotopes are an emerging concept and are desirable because of their ability to diagnose, treat, and evaluate treatment, simultaneously or following a therapeutic regimen. Some radiometals are inherently theranostic, generally by virtue of a therapeutic nuclide having an imageable γ-line (e.g., ^{47}Sc, ^{177}Lu); however, the most ideal theranostic agents are composed of chemically identical radioisotope pairs with similar half-lives and complementary emission. In this way, the diagnostic and therapeutic decay modes are optimal (i.e., high branching and appropriate energy) and the radioisotopes exhibit identical (bio)chemical behavior, notably with respect to the chelator. This ensures the therapeutic radiotracer behaves identically to the diagnostic radiotracer in vivo, which is crucial for accurate dosimetry. This is in contrast to nonchemically identical matched pairs (e.g., ^{111}In/^{90}Y), where diagnostic information is less representative of therapeutic dose distribution due to differences in radiotracer behavior.[36]

4. INTRODUCTION TO RADIONUCLIDE PRODUCTION AND PURITY

The next two sections will briefly summarize core concepts of radiometal production and purity that are relevant in later discussion. It should be noted that this description is by no means all-encompassing but rather an introduction for those interested but unfamiliar with the topic.

4.1. Production of Radionuclides

Cyclotrons and nuclear reactors are commonly used for radionuclide production. Cyclotrons use magnetic fields to accelerate charged particles (e.g., protons, deuterons, and α-particles) and produce proton-rich nuclides, which (if radioactive) typically decay by EC or β^+ emission in order to balance their unstable nuclear composition. Cyclotron-based production is contingent on the accelerated particle having sufficient energy to overcome the threshold energy of a given nuclear reaction, which is influenced by the mass difference between nuclear reactants (i.e., target nuclide, irradiating particle) and products (i.e., product nucleus, emitted particles), as well as the electrostatic repulsion between the accelerated particle and the target nuclide. These parameters are referred to as the Q value and the Coulomb barrier, respectively.[30] Biomedical cyclotrons are most common and have beam energies below 20 MeV. These small cyclotrons are typically found in hospitals or universities; thus, production routes that are compatible with low-energy cyclotrons are desirable due to their greater potential for clinical use. Intermediate- (20−35 MeV) and high-energy (>35 MeV) cyclotrons are also useful for medical radionuclide production but are far less common.[37] Reactor production is based around the spontaneous fission of fissile materials (within fuel rods) that release neutrons capable of inducing fission or neutron activation of target material. In the latter case, the resulting nuclides are neutron-rich and (if radioactive) normally decay via β^- emission. Unlike nuclide production via charged particle bombardment, no Coulomb barrier exists for neutron reactions because they are not repulsed by the positively charged nucleus or negatively charged electrons of target atoms. As such, low-energy neutrons are generally more desirable for production via neutron capture due to their greater probability of interactions with surrounding nuclei, compared to high-energy neutrons. For example, thermal neutrons have relatively low kinetic energy (E = 0.025 eV) and are commonly used to produce a variety of radionuclides. For production via fission, however, neutron energies must be on the order of MeV.[30] Cyclotrons and reactors are both vital means of radionuclide production and are often said to have complementary roles in the field of nuclear medicine due to the contrasting nature of produced radionuclides.[38] Linear accelerators (LINACS) also can be used for medical radionuclide production[39] but are far less common.

In a simplified sense, activity production is proportional to the number of target atoms, beam intensity (or flux), and formation cross section, which is a measure of likelihood that a nuclear reaction will occur.[30] For those unfamiliar, cross sections can be conceptualized through the analogy of trying to hit a target with a projectile. In the same way that a target with a large surface area will be easier to hit, so too does a large cross-section communicate a high probability that a nuclear reaction will occur. Cross sections (σ) are measured in barns (1b = 10^{-24} cm^2) and are a function of beam energy.[30,40] The relationship between cross sections and beam energy is often of great interest in order to achieve maximum production yields and radionuclidic purity. Investigations of this nature are often complicated by the coproduction of isotopic contaminants, which are especially problematic if long-lived and chemically identical (e.g., ^{177}Lu/^{177m}Lu, ^{225}Ac/^{227}Ac).[41,42] Contaminant production can be mitigated through the use of isotopically enriched target material; however, the enrichment process can be prohibitively expensive.[43] Natural targets are far less expensive but tend to yield lower radionuclidic purity and require careful optimization of irradiation parameters. The most desirable elements for target material are naturally monoisotopic (e.g., ^{45}Sc, ^{89}Y), but unfortunately few exist.

Generators are an extremely desirable means of production and rely on long-lived parent radionuclides that can be chemically separated from desired daughters. The parent radionuclides are loaded onto a resin and eluted or "milked" once they near equilibrium (transient or secular) with their daughters, ideally resulting in isolation of activity with high

DOI: 10.1021/acs.chemrev.8b00294
Chem. Rev. 2019, 119, 902−956

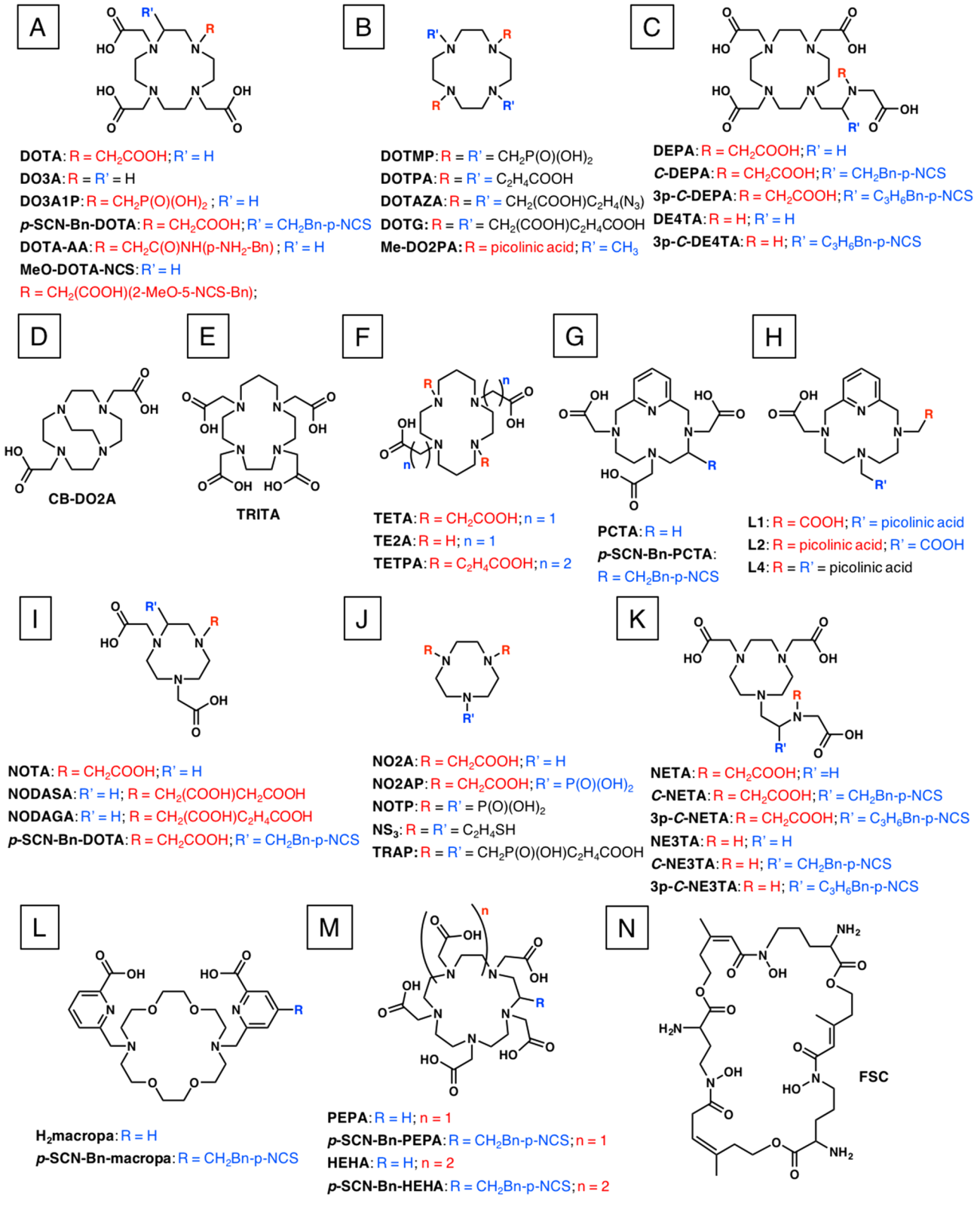

Figure 4. Selected macrocyclic chelators and their respective BFCs.

radionuclidic purity. The main benefit of generator use is cyclotron-/reactor-independent radionuclide accesses, which drastically increases radionuclide availability and makes clinical use more feasible. For other examples of developing and established generator systems not presented here, see Review by Boros and Packard.[1]

4.2. Purity of Radioactive Material

Radionuclidic purity is defined as the absence of other radionuclides and is often expressed as a percentage of desired radioactivity from total radioactivity. Not to be confused with radiochemical purity, which refers to the purity of chemical species of a given radionuclide (e.g., ^{99m}Tc-sestamibi versus

DOI: 10.1021/acs.chemrev.8b00294
Chem. Rev. 2019, 119, 902−956

$^{99m}TcO_4^-$), the term radionuclidic purity describes the purity of a given radionuclide with respect to other radionuclides (e.g., ^{72}As versus ^{73}As, ^{72}Ga, ^{71}Ge).[44] While these terms are frequently used to describe purity of radioactive species, they are limited in their ability to describe nonradioactive contaminants, notably those of the same chemical identity as the radionuclide of interest. The nonquantitative terms "no-carrier-added" (nca) and "carrier-added" (ca) are convenient in this respect, as they indicate a level of specific/molar activity (vide infra), often as a consequence of stable impurities.[44] The term ca indicates a relatively high concentration of stable nuclides of the corresponding element, while nca suggests the activity is essentially free from such contamination. The two caveats of this classification are (1) the word "essentially" is a vital component of the nca definition, as the absence of stable isotopes is both rare and challenging to prove, and (2) these classifications only consider isotopes of the element of interest; thus, contaminants of different elements may be present. Although these terms are less precise than "radionuclidic purity", they are more practical as colloquial descriptors and are commonly used to distinguish radionuclides that have been chemically separated from their target material (nca) from those that have not (ca).

The foundation of isolating nca activity is chemical distinctness of the produced radionuclide from the target material, which permits physical separation of the two components through a variety of chemical differences (e.g., solubility, resin affinity, and redox potential). For example, production of nca ^{68}Ga is possible via ^{68}Zn(p,n)^{68}Ga, resulting in a zinc target that can be chemically separated from the nano-to-picomolar concentrations of produced gallium.[45] This is in contrast to ca activity, where the sample may be elementally pure but the isotope composition is impure. This is often the case with production via neutron activation (e.g., ^{152}Sm-(n,γ)^{153}Sm) and is due to the shared chemical identity of the product and target, which results in an inextricable mixture of isotopes. Use of ca activity results in undesired nonradioactive isotopes occupying coordination sites, which is rarely permissible during subsequent use. The quantity of desirable decays per unit material is commonly described as molar activity (Bq/mol). Thus, it can be said that nca material is more desirable than ca, as it results in higher molar activity. It should be noted that specific activity (Bq/g) is also commonly used to describe activity concentration. Readers are cautioned to pay particular attention to these units, as molar activity is frequently described as specific activity in the current literature.

5. ROLE OF CHEMISTRY IN RADIOPHARMACEUTICALS

Chemistry is often referred to as the central science due to its tendency to bridge the gap between physical and life sciences. Similarly, the use of fundamental chemical concepts is vital for the consolidation of radioactive and biological components in modern radiopharmaceuticals. Covalent bond formation (e.g., [^{18}F]FDG) is one way to achieve "radiolabeling"; however, a wider variety of radionuclides are accessible through the use of radiometals and coordination chemistry. To this end, development of molecules capable of forming strong coordinative bonds with metals is imperative.

Biological and radioactive drug components are often coupled through the use of bifunctional chelators (BFCs), which serve the dual purpose of radiometal complexation and bioconjugation (section 5.3). The primary goal of radiometal complexation is the formation of robust coordination complexes to prevent the release of free metals in vivo. Stable complexes are formed through identification of compatible chelate−metal matches.[11]

5.1. Chelators for Metal Complexation

DOTA (1,4,7,10-tetraazacyclododecane-1,4,7,10-tetraacetic acid; Figure 4A) is the most frequently used chelator in nuclear medicine. While the use of DOTA is appropriate in many cases, wide and indiscriminate use has resulted in many instances of poor radiotracer performance due to nonideal chelator−metal interactions.[46−50] Lacking in these cases is consideration of fundamental metal ion characteristics (i.e., atomic number, charge, and radius), which vary from metal ion to metal ion and result in distinct preferences for geometry, coordination number, and ionic/covalent bond contribution. For optimal stability, the coordinating functional groups of the chelator should adopt the favored geometry of the metal ion while simultaneously satisfying metal coordination requirements to prevent competition from extraneous ligands, especially in biological systems (see section 5.2). Developed by Pearson in 1968,[51] hard−soft acid−base (HSAB) theory is a convenient way to discuss ionic/covalent bond character.

In the context of HSAB theory, hard metal ions have high charge density, have nonpolarizable electron shells, and tend to form predominantly ionic bonds, where electrostatic attraction is the primary driving force of bond formation (e.g., Fe^{3+}). As a rule, hard metal ions prefer hard donating groups, which possess dense anionic character (e.g., carboxylic acids). Conversely, soft metals have low charge density (e.g., Tl^+) and polarizable electron shells. They prefer more covalent bonding than do hard metal ions, which is achieved through coordination from softer, more electron-disperse donor groups (e.g., thiols). A useful metric for hard−soft character is the Drago−Wayland parameter, I_A, which conveys the electrostatic (E_A) and covalent (C_A) contributions to the formation constants of Lewis acid−base complexes (includes metal complexes) in aqueous solution ($I_A = E_A/C_A$).[52] From an energetic perspective, these differences in bonding arise due to energy differences between the highest occupied molecular orbital (HOMO) of the coordinating group and the lowest unoccupied molecular orbital (LUMO) of the metal ion. Hard metal ions generally have high-energy LUMOs that have poor orbital overlap with low-energy HOMOs of hard coordinating groups, resulting in minimal sharing of electrons and electrostatic-dominant bonding. Soft metal ions have lower-energy LUMOs that overlap with high-energy HOMOs of soft coordinating groups, resulting in significant sharing of electrons and relatively high covalent bond character.[53] Table 2 presents relevant chemical parameters of further discussed metal ions.

When coordinated to a metal ion, a chelator that satisfies the aforementioned criteria will form a highly stable, low-energy complex with a large energetic cost of dissociation. Multidentate chelators are especially effective at forming robust complexes due to "the chelate effect", which (in a simplified sense) describes the higher entropic cost of coordination from multiple, monodentate ligands relative to a single, multidentate ligand.[54,55] For this reason, high-denticity chelators are preferable. Along the same lines, preorganized binding pockets are known to have an extraordinary effect on metal complex inertness due to the lower entropic cost of complexation. This

DOI: 10.1021/acs.chemrev.8b00294
Chem. Rev. 2019, 119, 902−956

Table 2. Relevant Chemical Parameters of Discussed Metal Cations

metal ion	ionic radius[a]	hardness[b] (I_A)	pka[c]
Sc^{3+}	0.87 (CN = 8)	hard (10.49)	4.3
Ga^{3+}	0.62 (CN = 6)	hard (7.07)	2.6
Y^{3+}	1.02 (CN = 8)	hard (10.64)	7.7
In^{3+}	0.92 (CN = 8)	borderline hard (6.3)	4.0
Tb^{3+}	1.04 (CN = 8)	hard (10.07−10.30[d])	7.9
Lu^{3+}	0.98 (CN = 8)	hard (10.07)	7.6
Bi^{3+}	1.17 (CN = 8)	borderline hard (6.39)	1.1
La^{3+}	1.03 (CN = 6)	hard (10.30)	8.5
Ac^{3+}	1.12 (CN = 6)	borderline hard?	<10.4

[a]Ref 715. [b]Ref 52, p 37; ($I_a = E_A/C_A$). [c]As hydrated metal cation ($M^{3+}_{(aq)} \rightarrow MOH^{2+}_{(aq)}$). Ref 716, pp 128, 137, 319, 327, and 383. [d]Lanthanide series range.

effect is especially pronounced for macrocyclic ligands and has thus been deemed the "macrocyclic effect".[56] Two classes of chelators (macrocyclic (Figure 4) and acyclic (Figure 5)) have emerged due to the practical repercussions of this principle.

In general, macrocyclic chelators are more kinetically inert than their acyclic counterparts due to their rigid, preorganized binding sites. The disadvantage of using these scaffolds is their slow binding kinetics, which necessitate high temperatures and (long) waiting periods for optimal radiolabeling. These conditions are incompatible with heat-sensitive bioconjugates, such as antibodies, which rely on relatively weak domain interactions to maintain structural integrity.[57,58] Conversely, acyclic ligands exhibit rapid radiolabeling at ambient temperature as a result of unrestricted bond rotation in their free form. The consequence of such freedom is the high entropic cost of complexation, which results in a greater likelihood of decomplexation in vivo, compared to macrocycles.

Historically, the benefits and drawbacks of macrocyclic versus acyclic chelators were unambiguous and unavoidable; however, continued research in the field of chelator development has worked to undermine the disadvantages of each class and has proven quite successful. For example, it is well-known that DOTA suffers from sluggish labeling kinetics and requires heating up to 95 °C for radiolabeling of most metal ions. Development of pyridine-containing (PCTA, 3,6,9,15-tetraazabicyclo[9.3.1]pentadeca-1(15),11,13-triene-3,6,9-triacetic acid; Figure 4G) and iminodiacetic acid-functionalized (DEPA, 7-[2-(biscarboxymethylamino)ethyl]-4,10-biscarboxymethyl-1,4,7,10-tetraazacyclododec-1-yl-acetic acid; Figure 4C) DOTA derivatives has addressed this issue and permits more facile radiolabeling while maintaining high kinetic inertness.[59,60] Conversely, DTPA (1,1,4,7,7-diethylenetriaminepentaacetic acid; Figure 5A) complexes are known to frequently dissociate in vivo. The development of the more preorganized CHX-DTPA (cyclohexane-1,2-diamine-*N*,*N*,*N*′,*N*′-tetraacetate; Figure 5B) has alleviated this issue while maintaining rapid labeling kinetics and is now widely used with radioimmunoconjugates.[61−63] Although the choice between macrocyclic and acyclic chelators remains a matter of cost−benefit, the stereotypical shortcomings of each chelator class has been largely diminished. For lists of selected chelators, see Tables 3, 5, 7, 9, 11, 13, 15, and 17.

5.2. Evaluation of Chelators

Assessment and comparison of chelators is crucial for the continued improvement of radiotracers. As chemists, we seek to probe the thermodynamic stability, kinetic inertness, and in vivo performance of chelators to build a clear picture of how chelator−metal interactions affect biological behavior.

Evaluation of a chelator's metal affinity requires knowledge of its acid−base properties (protonation constants) and the thermodynamic stability of its metal complexes. Potentiometric, spectrophotometric, calorimetric, and NMR (nuclear magnetic resonance) titrations are commonly employed to study these parameters.[64,65] Thermodynamic stability is evaluated through the calculation of formation constants (log *K*), which are based around the complex equilibrium of metal ions, protons, and ligands (chelators), conventionally written as $pM + qH + rL \leftrightarrow M_pH_qL_r$. Metal ion affinity of different chelators is commonly compared in terms of their stability constants (log K_{MpHqLr}); however, a more useful thermodynamic parameter is the pM value (pM = −log[M]). Introduced by Raymond and co-workers,[66] pM values are linearly correlated with stability constants and express the extent to which a metal ion complex is formed in solution under physiologically relevant conditions. pM is normally reported under standard conditions ([L] = 10 μM, [M] = 1 μM, pH 7.4) and permits the most suitable comparison of the ability of different ligands with diverse basicities, protonation states, and metal complex stoichiometries to sequester specific metal ions.[67,68] High pM values are desirable, as they express low free metal concentrations at physiological pH. Although useful for comparison, thermodynamic parameters are less meaningful than kinetic studies for predicting in vivo behavior.

Kinetic inertness is normally evaluated through competition studies to determine the degree and/or rate at which extraneous factors induce complex dissociation. As discussed, metal ion complexation is dependent on proton, metal, and chelator concentrations. Competition studies aim to expose potential avenues of decomplexation by overloading a given equilibrium element and studying the repercussions from a kinetic standpoint. Subjecting metal complexes to acidic conditions (pH ≤ 2) often induces acid-catalyzed dissociation[69,70] and is a measure of how effectively protons can compete with metals for coordinating atoms. Acid dissociation studies are relatively uncommon due to their lack of direct applicability to physiological conditions. Conversely, in vitro tansmetalation studies emulate in vivo conditions relevant to dissociation and are extremely common. Incubation of radiometal complexes with a large excess of biologically relevant metal ions (e.g., Fe^{3+}, Zn^{2+}, Ca^{2+}, and Cu^{2+}) probes the likelihood of free radiometal ion release in vivo as a result of displacement by endogenous ions.[71] Incubation with serum proteins or enzymes explores the potential of radiometal transmetalation by endogenous ligands.[72] Methods to distinguish free radiometal ions from complexes are well-established and commonly involve thin-layer chromatography (TLC) or high-performance liquid chromatography (HPLC).

The most decisive evaluation of chelator utility is observation of in vivo performance with PET or SPECT. Mice are common models for this purpose, although nonhuman primates and pigs are occasionally reported.[73−75] Common signs of free metal ion release are bone,[76,77] kidney,[78] or liver[9] accumulation; however, the latter two are somewhat ambiguous as they are common sites of bioconjugate accumulation and/or excretion. Studies can also be done with nonfunctionalized, "naked" chelators; however, with no targeting moiety, most metal ion−chelate complexes are rapidly excreted due to their small/hydrophilic nature.[79−81] These studies are not particularly useful for probing long-term

DOI: 10.1021/acs.chemrev.8b00294
Chem. Rev. 2019, 119, 902−956

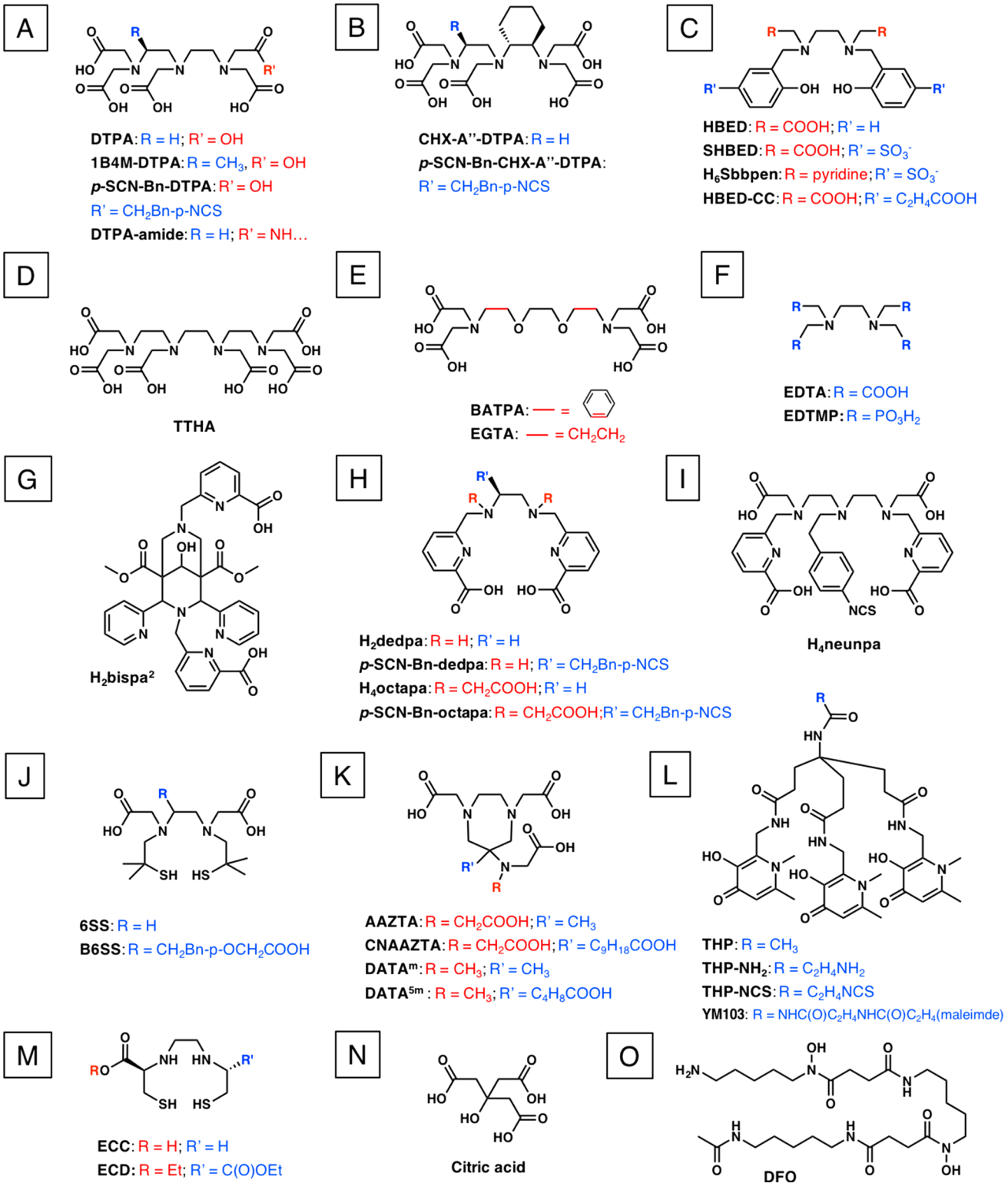

Figure 5. Selected acyclic chelators and their respective BFCs.

Table 3. Selected Sc^{3+} Chelators, Metal Complex Geometry, and Thermodynamic Parameters

metal ion	chelator	coordinating nuclei	geometry	log K_{ML}	pM	reference
Sc^{3+}	DOTA	N_4O_4	square antiprism	27.0−30.8	23.9−26.5	132−134
	NOTA	N_3O_3	distorted octahedral	16.5	19.2	92, 133
	DTPA	N_3O_5	distorted square antiprism	26.3−27.4		100, 134
	AAZTA	N_3O_4	irregular dodecahedron (1:4:3)	27.7	24.7	142

DOI: 10.1021/acs.chemrev.8b00294
Chem. Rev. 2019, 119, 902−956

decomplexation but rather are a gauge of short-term instability or the fate of a chelator if it were cleaved from its bioconjugate. Proper BFC design should, however, minimize this possibility.

5.3. Bifunctional Chelators and Linkers

Bifunctional chelators serve two purposes: (1) to secure the radiometal ion (see section 5.1) and (2) to provide a covalent link between the complex and the targeting vector. BFCs are normally adapted from nonbifunctional analogues through the addition of pendant arms bearing a functional group available for facile bioconjugate coupling. For synthetic ease, coordinating groups are sometimes replaced by coupling groups (e.g., DO3A; Figure 4A); however, this strategy can negatively impact complex stability.[82−84] The alternative is functionalization at a less critical position, such as an ethylene diamine bridge (e.g., *p*-SCN-Bn-DOTA; Figure 4A), which avoids direct interference with metal binding but is generally more synthetically challenging.

Coupling of the targeting vector to the BFC often relies on nucleophilic attack from the bioconjugate. Free amines from the N-terminus, amino acid side-chains (e.g., lysine), or linker are common for this purpose. Amine coupling to carboxylic acids is achieved through the use of coupling agents (e.g., 1-ethyl-3-[3-dimethylamoniopropyl]carbodiimide [EDC], *N,N′*-dicyclohexylurea [DCC], or hydroxybenzotriazole [HOBt]) or by first activating the electrophile (e.g., *N*-hydroxysuccinimide [NHS]).[85] A very common amine coupling strategy employs isothiocyanate groups, which are installed through the reduction and subsequent conversion (via thiophosgene) of *p*-NO_2−Bn groups.[86−88] The benefit of such an approach is facile coupling to the highly electrophilic carbon, which results in a stable thiourea linkage. The drawback of this approach is the use of highly toxic thiophosgene, as well as the tendency of the product to degrade due to the reactive isothiocyanate group. Thiol coupling via maleimide groups is possible given the presence of free cysteine residues. The use of copper-mediated "click-chemistry" and Diels−Alder coupling have also been demonstrated.[85]

Linkers are often employed to separate the chelator and the bioconjugate in order to avoid detrimental interactions (i.e., bioconjugate interference with coordination or chelate disruption of receptor targeting). Aliphatic, amino acid, or polyethylene glycol (PEG) chains are frequently used. Although often overlooked, linker properties are rather important, as the addition of side groups can be used as a powerful tool to optimize radiotracer pharmacokinetics and biodistribution.[89] A recent and notable example of this phenomenon is PSMA-617, which is discussed in many instances below.

6. TARGETING VECTORS

Bioconjugates (also known as targeting vectors) dictate the biodistribution and pharmacokinetics of the radiopharmaceutical. Accurate targeting is crucial to obtain meaningful diagnostic information and/or selectively kill diseased cells (Figure 6). Promising bioconjugates exhibit high affinity for (or are internalized by) receptors that are highly expressed on target cells but are absent or minimally expressed on healthy cells. Other desirable bioconjugate characteristics include minimal renal/hepatic accumulation, high thermal and in vivo stability, and a compatible (biological) half-life with the radiometal (physical half-life). Because of the already broad scope of this Review, categories and examples of targeting

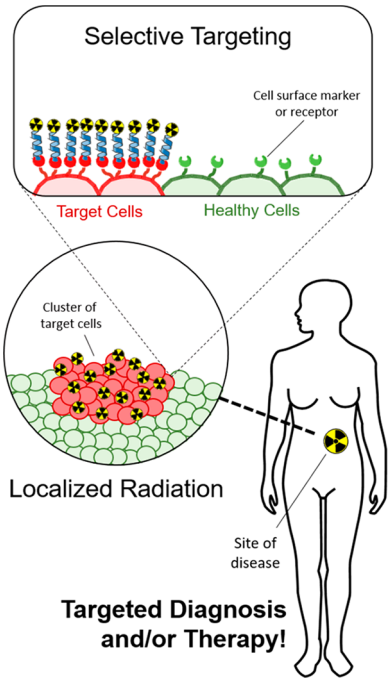

Figure 6. Simplified illustration of radiopharmaceutical targeting.

vectors will only briefly be discussed. For lists of selected radiopharmaceuticals, see Tables 4, 6, 8, 10, 12, 14, 16, and 18.

Peptides (or, more specifically, oligopeptides) are of growing interest for use in radiopharmaceuticals largely due to their size, which has ramifications on stability, biological circulation, and synthesis. As short chains (2−20 amino acids), peptides do not rely on high-level structures (i.e., secondary, tertiary, and quaternary) and exhibit considerable thermal stability. Although endogenous peptides are readily degraded by numerous biological processes in vivo, structural modifications can drastically slow degradation without altering receptor affinity, making the application of endogenous peptides to radiotracers viable.[90] In a simplified sense, biological circulation time is inversely proportional to size. Accordingly, peptides experience fast circulation and can rapidly accumulate at target receptors. Unbound peptide radiotracers quickly clear from circulation, resulting in high tumor-to-background ratios.[91−93] A caveat to this point is that excessively high rates of circulation and clearance can prevent adequate tumor accumulation. Lastly, unlike larger biomolecules (e.g., proteins and antibodies), the simple structure of peptides makes them amenable to straightforward ex vivo synthesis, which can be achieved through increasingly powerful solid-phase peptide synthesis.[94] Common peptide bioconjugates are Arg-Gly-Asp (RGD) analogues for integrin targeting; PSMA-specific peptides for prostate-specific membrane antigen (PSMA) targeting; bombesin (BBN) fragments for gastrin-releasing peptide (GRP) receptor targeting; and DOTA-conjugated octreotide analogues (i.e., DOTATATE, DOTATOC, and DOTANOC) for somatostatin (SST) receptor targeting.

Antibodies are large, Y-shaped glycoproteins central to the human immune system. The appeal of using antibodies as targeting vectors is their highly specialized targeting capabilities, which can facilitate very selective tumor localization.[95] Because of their large size, antibodies experience slow circulation, have long biological half-lives, and are suitable for use only with long-lived radiometals. While this extended

DOI: 10.1021/acs.chemrev.8b00294
Chem. Rev. 2019, 119, 902−956

period of circulation is beneficial for tumor targeting, slow clearance rates generally require long waiting periods to achieve high tumor-to-background ratios.[96] Antibodies also heavily rely on weakly bound domains to exert their biological function and as such are frequently sensitive to thermal degradation.[57,58] The use of antibody fragments is increasingly popular, as aforementioned disadvantages are alleviated while maintaining high receptor affinity and specificity.[97] Common antibody bioconjugates are Trastuzumab for human epidermal growth factor receptor 2 (HER2) targeting; J591 for PSMA targeting; HuM195 for CD33 targeting; Rituximab for CD20 targeting; and Cetuximab for epidermal growth factor receptor (EGFR) targeting.

Interlude

The remainder of this Review will summarize production, purification, chemistry, chelator development, and biological studies of selected radiometals, which are organized by their chemical identities. The discussed radiometals range from frequent clinical use (e.g., ^{68}Ga and ^{90}Y) to early-stage research (e.g., $^{149/152/155/161}$Tb) and were selected based on their current or potential clinical significance. Transition metals were intentionally omitted, as they are presented in the companion Review by Boros and Packard.[1]

7. SCANDIUM

Scandium-44 has garnered attention as a PET radionuclide due to its high β^+ branching ratio ($E\beta^+_{avg}$ = 632 keV, 94%) and long physical half-life ($t_{1/2}$ = 4.04 h).[98] The latter is advantageous for several reasons, most notably the potential to acquire images at later time points than common β^+ emitters, such as ^{18}F ($t_{1/2}$ = 1.83 h) and ^{68}Ga ($t_{1/2}$ = 1.13 h). Background signals typically decrease with time due to progressive radiotracer clearance; thus, delayed imaging with ^{44}Sc may improve tumor-to-tissue ratios and lead to higher image quality.[99] Imaging later time points also presents the opportunity to investigate pharmacokinetics of slower-circulating bioconjugates. Lastly, the extended half-life may permit cost-effective use of ^{44}Sc through centralized production and regional distribution,[100] which would not be feasible with a shorter-lived radionuclide. Scandium-44 is considered a diagnostic match for the common β^- emitters ^{90}Y and ^{177}Lu, due to the chemical similarities of rare-earth metals. More appealing, however, is the prospect of combined use with ^{47}Sc due to their shared chemical identity.

Scandium-47 ($t_{1/2}$ = 80.4 h) is a high branching, low-energy β^- emitter ($E\beta^-_{avg}$ = 162 keV, 100%) suitable for treatment of small tumors and cancer metastasis.[101] β^- emission is accompanied by coemission of low-energy γ-rays ($E\gamma$ = 159 keV; Iγ = 68%) useful for SPECT imaging.[102] Unfortunately, regular clinical use of ^{47}Sc is a distant prospect due to inconvenient production methodology. Other useful radioisotopes for scandium-based radiopharmaceuticals include the β^+ emitter ^{43}Sc ($t_{1/2}$ = 3.89 h, $E\beta^+_{avg}$ = 476 keV, 88%), which is free of high-energy gamma emission, unlike ^{44}Sc ($E\gamma$ = 1157 keV; Iγ = 100%) and ^{44m}Sc ($t_{1/2}$ = 58.6 h), due to its potential as an in vivo ^{44}Sc generator.[40,103−108]

7.1. Scandium-44 Production

The primary means of ^{44}Sc production is via ^{44}Ca(p,n)^{44}Sc, which reaches a broad cross-sectional maximum (650 mb) between 8 and 13 MeV.[40] Historically, solvent extraction[109,110] has been used to purify Sc^{3+} from Ca^{2+}; however, extraction chromatography is more robust and is now the standard. Separation is achieved through target dissolution, followed by loading of the 6 M HCl solution onto DGA (*N,N,N′,N′*-tetra-*n*-octyldiglycolamide) solid-phase resin. Washing with 6 M HCl results in retention of Sc^{3+} and elution of Ca^{2+}.[111] If significant metal impurities (e.g., Fe and Zn) are present, they may be separately eluted with 1 M HNO_3. This is crucial if enriched ^{44}Ca (<2.09% natural abundance) is to be recovered and reused.[107,111] Elution of ^{44}Sc with dilute HCl yields a high molar activity solution.[111] A similar method using UTEVA (uranium and tetravalent actinides) resin has also been demonstrated.[112] If desired, further purification may be achieved with cation-exchange chromatography, which requires NH_4OAc for elution.[113]

A promising alternative source of ^{44}Sc is the ^{44}Ti/^{44}Sc generator system. Clinical use of this system remains to be seen due to suboptimal separation of parent and daughter radionuclides, resulting in ^{44}Ti breakthrough after prolonged elution.[114−116] Furthermore, production of ^{44}Ti ($t_{1/2}$ = 60 years) is somewhat challenging and requires high-flux protons due to the long physical half-life and low ^{45}Sc(p,2n)^{44}Ti reaction cross section (40.3 mb at 24.1 MeV).[115,117]

7.2. Scandium-47 Production

Early studies investigated ^{47}Sc production by proton irradiation of ^{nat}Ti;[118,119] however, neutron irradiation is a superior strategy. Irradiation of enriched $^{47}TiO_2$ with high-energy neutrons (E_n > 1 MeV) has been shown to induce ^{47}Ti(n,p)^{47}Sc, with a theoretical yield of 2.8 TBq (75 Ci) after 3.35 days of irradiation on a 10 g target. Production of GBq quantities has been reported to date.[36,120] Use of $Li_2{}^{47}TiF_6$ as target material was shown to be beneficial, as it produced comparable yields to $^{47}TiO_2$ while requiring just minutes to dissolve in 1 M HF, as opposed to 2−4 h at 80 °C.[43] Although good radionuclidic purity (99.5%) has been reported,[36,120,121] controlling the coproduction of ^{46}Sc remains challenging and is a major drawback of this method.[101] Unsurpisingly, use of natural targets ($^{nat}TiO_2$) leads to decreased radionuclidic purity.[43,122]

Purification of Sc^{3+} from Ti^{4+} requires dissolution in concentrated H_2SO_4, followed by solvent evaporation and redissolution in water containing 0.3% H_2O_2. Cation-exchange chromatography retains Sc^{3+} while Ti^{4+} is recovered by several washes with increasingly acidic HCl (0.2−2.5 M). Scandium-47 is eluted with a mixture of 4 M HCl/0.1 M HF. Several column cycles are required to completely remove titanium.[120] Separation has also been achieved through liquid−liquid extraction, precipitation followed by anion-exchange chromatography, and silica gel chromatography.[123−125]

Scandium-47 can also be produced indirectly through a ^{47}Ca ($t_{1/2}$ = 109 h) pseudogenerator using thermal neutrons to induce ^{46}Ca(n,γ)^{47}Ca → ^{47}Sc. The apparent 10-fold increase in activity yield compared to the direct method is a result of the higher cross section (700 mb) and higher flux of thermal neutrons compared to fast neutrons.[101] The separation of ^{47}Ca from ^{47}Sc can be achieved following the same protocol as described above for ^{44}Ca(p,n)^{44}Sc. Although the indirect method requires long waiting periods and expensive ^{46}Ca target material (even relative to enriched $^{47}TiO_2$ due to <0.01% natural abundance), the superior purity and yield over direct production appears to make it a promising direction for the future of ^{47}Sc production.

LINACS have been used to produce ^{47}Sc, both directly and indirectly. Titanium-based production via ^{48}Ti(γ,p)^{47}Sc was

DOI: 10.1021/acs.chemrev.8b00294
Chem. Rev. 2019, 119, 902−956

originally proposed in 1977;[124] however, recently it was reported that beam energies above 22 MeV cause excess ^{46}Sc contamination due to the ^{48}Ti(γ,np) reaction.[126] The limited yield and stringent energy requirements make this route an unlikely candidate for future production. Calcium-based LINAC production occurs via ^{48}Ca(γ,n)^{47}Ca → ^{47}Sc; however, only preliminary studies on natural targets are available.[127]

7.3. Scandium Chemistry and Chelator Development

Scandium is found almost exclusively as a trivalent cation (Sc^{3+}) and is the smallest of the rare-earth metals, with an ionic radius of 0.75−0.87 Å (CN = 6−8). In many ways, the chemistry of Sc^{3+} is a mix of first-row transition metals and the lanthanides.[128] For example, VSEPR (valence shell electron-pair repulsion) theory groups Sc^{3+} with nearby transition metals (Fe^{3+}, Co^{3+}, and Ni^{3+}), yet the high coordination preference (CN = 6−8) and ionic bonding tendency (I_A = 10.49) of Sc^{3+} are characteristics more akin to the lanthanides. Unlike other rare-earth metals, the high acid dissociation constant of hydrated Sc^{3+} (pK_a = 4.3, $Sc^{3+}_{(aq)} \rightarrow ScOH^{2+}_{(aq)}$) results in a high propensity to hydrolyze, which begins at pH 2.5. Precipitation as $Sc(OH)_3$ occurs at neutral-to-basic pH (pH 7−11).[129]

DOTA is widely used for scandium-based radiopharmaceuticals. This compatibility may be surprising when considering the hexadentate environment of other Sc^{3+} coordination complexes (e.g., Sc[acac]$_3$) and hydrated salts (e.g., $ScCl_3$, $ScBr_3$, $Sc(ClO_4)_3$, and $Sc(NO_3)_3$).[128,130] However, like other rare-earth metals, Sc^{3+} has a high preference for hard donating groups and favors a coordination number of eight, even in its hydrated form.[52,131] In the solid-state structure of [Sc(DOTA)]$^-$, the Sc^{3+} center adopts square-antiprism geometry and is sandwiched between the N_4 (macrocycle) and O_4 (acetate) planes. Unlike many other Ln-DOTA structures, the size of Sc^{3+} does not allow a water molecule to cap the O_4 plane. The generally longer Sc−N (~2.44 Å) than Sc−O (~2.15 Å) bond distances are expected due to trivalent scandium's preference for electrostatic bonding. DOTA can near-quantitatively radiolabel $^{44/47}$Sc over 10−30 min to achieve high molar activities (Table 4); however, elevated temperatures are required. Microwave heating may be used to truncate waiting time,[132] but it is still unsuitable for heat-sensitive bioconjugates. Competition experiments with ^{44}Sc-DOTATOC demonstrate complex robustness, as complexes remained >96% intact after 24 h in the presence of competing serum proteins (calf or human serum) or metals (Fe^{3+}, Cu^{2+}, Ca^{2+}, or Cu^{2+}).[132] Moreover, the high stability (log K_{ML} = 27.0−30.8) and pM value (23.9−26.5) support DOTA use for the majority of Sc^{3+}-based radiopharmaceuticals.[133,134]

The small size of scandium has led some to study its compatibility with the smaller macrocycle NOTA (1,4,7-triazacyclononane-1,4,7-triacetic acid; Figure 4I).[92] This match is clearly unsuitable, as evidenced by low [Sc(NOTA)] stability (log K_{ML} = 16.5) and poor $^{44/47}$Sc radiolabeling capabilities.[133] During a comparison of ^{44}Sc-NODAGA- and ^{44}Sc-DOTA-conjugated peptides, authors noted that labeling 1,4,7-triazacyclononane,1-glutaric acid-4,7-acetic acid (NODAGA) conjugates with ^{44}Sc was unreliable and highly susceptible to metal impurities, overall concluding that DOTA is superior to NODAGA for ^{44}Sc radiolabeling.[92]

In terms of acyclic chelators, DTPA is a satisfactory alternative to DOTA, as suggested by the comparable stability constant (log K_{ML} = 26.3−27.4).[134] The solid-state structure of [Sc(DTPA)]$^{2-}$ reveals distorted square antiprism metal center geometry, with an N_3O_5 bonding environment and no additional coordinating water, unlike other [Ln(DTPA)]$^{2-}$ complexes.[134,135] On the basis of similar systems, it is presumed that [Sc(CHX-A″-DTPA)]$^{2-}$ is superior to [Sc(DTPA)]$^{2-}$ due to increased resistance to decomplexation.[136]

AAZTA (1,4-bis[carboxymethyl]-6-[bis{carboxymethyl}]-amino-6-methylperhydro-1,4-diazepine; Figure 5K) is most widely known for its use in MRI (magnetic resonance imaging) contrast agents with Gd^{3+}[137−141] but has also been found to form highly stable complexes with Sc^{3+} (log K_{ML} = 27.7). The preorganized cyclic backbone results in comparable inertness to DOTA, while permitting room-temperature radiolabeling due to backbone flexibility.[142] PET/MRI imaging was conducted following RGD conjugation to the bifunctional analogue, CNAAZTA (Figure 5K). The trial served as a solid proof of concept, although significant uptake of the gall bladder and intestinal tract was observed. Continued work in the realm of bioconjugation should be of interest in the future.

Other potentially useful acyclic ligands include EGTA (ethylene glycol bis[2-aminoethyl ether]-*N,N,N′,N′*-tetraacetic acid; Figure 5E) and EDTMP (ethylenediamine tetra[methylene phosphonic acid]; Figure 5F). The [^{46}Sc(EGTA)]$^-$ complex remained largely intact against competition from 0.9% NaCl or 0.1 M PBS solutions over 6 days and outperformed other common acyclic ligands such as BATPA (1,2-bis[2-aminophenoxy]ethane-*N,N,N′,N′*-tetraacetic acid; Figure 5E), TTHA (triethylenetetramine-*N,N,N′,N″,N‴,N⁗*-hexaacetic acid; Figure 5D) and HBED (*N,N′*-bis[2-hydroxybenzyl]ethylenediamine-*N,N′*-diacetic acid; Figure 5C).[143] Preliminary in vivo studies with ^{46}Sc(EDTMP)$^{5-}$ illustrate the capacity for bone targeting while mitigating intestinal/hepatic uptake typical of free Sc^{3+}.[144]

7.4. Scandium-44/47 Biological Studies

The increasing availability of ^{44}Sc and its compatibility with DOTA has led to a number of studies exploring a variety of bioconjugates including DOTATATE, DOTANOC, DOTA-Puromycin, DOTA-cRGD, DOTA-BBN[2−14]NH_2, DOTA-NAPamide DOTA-PSMA-617, and DOTA- $Z_{HER2-2891}$.[145−152] CHX-A″-DTPA has also been successfully used for radiolabeling of the monoclonal antibody (mAb), Cetuximab.[100] Most interesting are the studies that directly compare ^{44}Sc to ^{68}Ga or investigate the capability of ^{44}Sc as a diagnostic match for ^{177}Lu.

Comparison of ^{44}Sc and ^{68}Ga for imaging of animals with melanocortin-1 receptor (MC1-R) positive tumors using DOTA-NAPamide after 4 h revealed significantly higher tumor uptake of ^{44}Sc (81.7 ± 7.7%ID/g) over ^{68}Ga (17.3 ± 1.85%ID/g).[150] With DOTA-PSMA-617, ^{44}Sc and ^{68}Ga were observed to exhibit similar in vivo behavior, with ^{44}Sc-PSMA-617 displaying higher tumor-to-liver ratios at 15 min (18.8 ± 5.0 vs 6.02 ± 0.59) and 30 min (55.6 ± 7.36 vs 19.0 ± 2.3). Not only is this alone a desirable characteristic, but these values correlate more closely to ^{177}Lu-PSMA-617 than to ^{68}Ga-PSMA-617 and therefore would be more useful for pretherapeutic dosimetry.[151] The first in-human trial of ^{44}Sc-PSMA-617 was conducted by Eppard et al. on patients with metastasized castrate-resistant prostate cancer.[99] No adverse side-effects were observed and standardized uptake values (SUVs) in kidneys were significantly decreased in ^{44}Sc-PSMA-617 compared to ^{68}Ga-PSMA-11 (14.0 vs 30.5, respectively). No significant difference existed in any other SUV. Images

DOI: 10.1021/acs.chemrev.8b00294
Chem. Rev. 2019, 119, 902−956

Table 4. Selected $^{44/47}$Sc Radiopharmaceuticals with Targets and Relevant Labeling Parameters[a]

radioisotope	chelator (BFC)	standard labeling conditions	bioconjugate	target	molar/specific activity (% RCY)	reference
^{44}Sc	DOTA (DO3A)	0.25−0.5 M NH_4OAc pH 4, 95 °C, 10−30 min	BBN[2-14]NH_2	GRPR	4.8 GBq/μmol (>80)	149
			Tyr^3-octreotate (TATE)	SSTR	8 GBq/μmol (>95)	108
			PSMA-617	PSMA	6.7 ± 0.8 GBq/μmol (>98)	99
			Z-HER:2891	HER2	7.8 GBq/μmol (98 ± 2)	152
			NAP-amide	MC1-R	19 GBq/μmol (60−70)	150
	DOTA (*p*-SCN-Bn)	0.5 M NaOAc pH 4.5, 90 °C, 15 min	$c(RGD)_2$	integrin $\alpha_v\beta_3$	7.1 GBq/μmol (>90)	148
	AAZTA (CNAAZTA)	0.25 M NH_4OAc pH 4, RT, 5 min	c(RGDfK)	integrin $\alpha_v\beta_3$	0.36 GBq/μmol (99)	142
	CHX-A′′-DTPA (*p*-SCN-Bn)	0.5 M NaOAc pH 4.5, RT, 30 min	Cetuximab Fab	EGFR	63 GBq/μmol (66 ± 5)	100
^{47}Sc	DOTA (DO3A)	0.25−0.5 M NH_4OAc pH 4, 95 °C, 10−25 min	folate (cm10)	FR	13 GBq/μmol (>96)	102
			NaI^3-octreotide (NOC)	SSTR	10 GBq/μmol (96.6−99)	101

[a]GRPR (gastrin-releasing peptide receptor); SSTR (somatostatin receptor); PSMA (prostate-specific membrane antigen); HER2 (human epidermal growth factor receptor 2); MC1-R (melanocortin 1 receptor); EGFR (epidermal growth factor receptor); and FR (folate receptor).

could also be obtained at a 19 h time point! This is beneficial both for imaging purposes, due to lower background activity, and for dosimetry calculations of long-lived ^{177}Lu-PSMA-617. The authors do, however, point out that potential limitations of ^{44}Sc are the additional high-energy gammas (Eγ = 1157 keV; Iγ = 100%) and limited clinical availability.[99] The compatibility of ^{44}Sc/^{177}Lu as a theranostic pair was also suggested for DOTA-folate (Table 4).[113]

Research surrounding the therapeutic capacity of ^{47}Sc has only begun to reach animal models but is encouraging for the future of the ^{44}Sc/^{47}Sc theranostic pair. ^{47}Sc-DOTA-folate studies revealed a significant difference in relative tumor volume and survival time between treated and nontreated groups. High tumor accumulation after 4 h (17.96 ± 2.17%ID/g) and increasing tumor-to-blood ratios over the 7-day trial was noted in biodistribution data. SPECT/CT images obtained from the low-energy γ emission of ^{47}Sc illustrated high liver and kidney uptake.[102]

8. GALLIUM

Gallium-68 ($t_{1/2}$ = 1.13 h) is the leading β^+ emitting radiometal for PET imaging due to its high branching ratio ($E\beta^+_{avg}$ = 830 keV, 89%) and widespread availability. The ^{68}Ge/^{68}Ga generator obviates the need for on-site cyclotron production and makes clinical use more convenient and economic.[153] Historically, EDTA (ethylenediamine tetraacetic acid; Figure 5F) was used as a generator eluent, and the $[^{68}Ga(EDTA)]^-$ complex was directly used to monitor organ blood perfusion;[154] however, elution as $GaCl_3$ is more common in contemporary generators. The short physical half-life of ^{68}Ga makes it compatible with fast-circulating, low-molecular-weight bioconjugates, such as peptides, antibody fragments, aptamers, and oligonucleotides.[155] Gallium-68 radiotracers are at the forefront of nuclear drug development, as evidenced by the FDA (U.S. Food and Drug Administration) approval in June 2016 of ^{68}Ga-DOTATATE (NETSPOT) for imaging SST receptor-expressing neuroendocrine tumors, as well as clinical consideration of numerous other candidates (i.e., ^{68}Ga-DOTATOC, ^{68}Ga-DOTANOC, ^{68}Ga-PSMA-617, ^{68}Ga-Neo-BOMB1, and ^{68}Ga-penntixafor).[156,157]

Gallium-66 ($t_{1/2}$ = 9.49 h) is also a β^+ emitter ($E\beta^+_{avg}$ = 1747 keV, 57%) and is of interest due to its long physical half-life relative to ^{68}Ga, which is well-matched to bioconjugates with slow in vivo kinetics.[158] Recent use of ^{66}Ga appears to have been spurred by well-established Ga-based radiotracers; however, studies to date have been limited.

Gallium-67 ($t_{1/2}$ = 78.2 h) is a low-energy γ emitter (Eγ = 93, 184, and 300 keV; Iγ = 39, 21, and 17%, respectively) that decays purely by EC and is suitable for SPECT imaging. [^{67}Ga]Gallium citrate has been used for inflammation or tumor imaging due to its chemical similarity to Fe^{3+} (see section 8.4), which facilitates selective transport and accumulation. Gallium-67 lymphoma imaging has drastically decreased since the advent of [^{18}F]FDG PET/CT; however, the tracer is still commonly used in countries where no PET/CT service is available.[159] Moreover, the emission of Auger electrons has prompted some interest into ^{67}Ga therapy.[160]

8.1. Gallium-68 Production

Gallium-68 is widely available due to the ^{68}Ge/^{68}Ga generator system. Germanium-68 is cyclotron produced via ^{69}Ga(p,2n)^{68}Ge and (if necessary) can be purified from contaminants using ion-exchange, extraction, volatilization, or precipitation.[161,162] The generator consists of ^{68}Ge ($t_{1/2}$ = 270.95 days) loaded onto a resin (SnO_2, TiO_2, ZrO_2, pyrogallol formaldehyde, and nanoceria polyacrylonitrile), from which $^{68}GaCl_3$ is eluted with 0.1−1 M HCl.[162]

8.2. Gallium-67 Production

The production of ^{67}Ga is most often achieved through low-energy (20−22 MeV) proton irradiation of zinc targets via ^{67}Zn(p,n)^{67}Ga.[163−167] Other proven methods of ^{67}Ga production include ^{67}Zn(d,2n)^{67}Ga, ^{64}Zn(α,n)^{67}Ga, and ^{65}Cu(α,2n)^{67}Ga.[164,168,169] Attempts to avoid expensive enriched targets have led to the use of ^{nat}Zn or ^{nat}Ge/^{nat}Zn targets as well as heavy ion beams to induce ^{59}Co(^{11}B,3n)^{67}Ge → ^{67}Ga or ^{59}Co(^{11}C,4n)^{67}As → → ^{67}Ga and achieve indirect production.[170−173] Normally purification of Ga^{3+} from Zn^{2+} is accomplished by ion-exchange chromatography, where the target is dissolved in 10 M HCl and the solution is loaded onto a cation-exchange resin.[170,174−177] Washing with 9 M HCl removes potential contaminants (e.g., Cu^{2+} and Zn^{2+}), and elution of ^{67}Ga is achieved with 6 M HCl. For fine purification, the eluate is directly loaded onto an anion-exchange resin, which is eluted with 2 M HCl to yield nca $^{67}GaCl_3$.[177] Elution

DOI: 10.1021/acs.chemrev.8b00294
Chem. Rev. 2019, 119, 902−956

Table 5. Selected Ga^{3+} Chelators, Metal Complex Geometry, and Thermodynamic Parameters

metal ion	chelator	coordinating nuclei	geometry	log K_{ML}	pM	reference
Ga^{3+}	DOTA	N_4O_2	distorted octahedral	21.3, 25.0−26.1	15.2	190, 197, 211, 686
	PCTA	N_4O_2?	distorted octahedral[a]			83, 193, 194, 686
	NOTA	N_3O_3	distorted octahedral	29.0−31.0	26.4	197, 199, 200, 211, 687
	TRAP	N_3O_3	distorted octahedral	26.2		213−216, 688
	NOA2P	N_3O_3	distorted octahedral	34.4		211
	DTPA	N_3O_4	pentagonal-bipyramidal[b]	24.3	20.2	221, 689
	HBED	N_2O_4	distorted octahedral	38.51−39.57	30.8	223, 225, 229, 230, 232−234, 240, 244
	THP (CP256)	O_6	distorted octahedral[c]			247, 249−251,690
	H_2dedpa	N_4O_2	distorted octahedral	28.1	27.4	81, 255
	AAZTA	N_3O_3/N_2O_4	distorted octahedral[d]	21.2	22.4	260
	DATA	N_3O_3	distorted octahedral	21.5		262−265
	6SS	$N_2O_2S_2$	(distorted) octahedral[e]	41.0	31.6	221, 279

[a]On the basis of $[Ga(DOTA)]^-$. [b]On the basis of $[Fe(III)DTPA]^{2-}$. [c]On the basis of $[Ga(dpp)_3]$. [d]On the basis of $[Cu(H_2AAZTA)]$. [e]On the basis of $[(Ga)4SS(2H_2O)]^+$.

with 0.1 M citrate is also effective for fine purification, as zinc and copper are retained on the anion-exchange column, while gallium is eluted.[176,178] It has been demonstrated that, during high-current (250 μA, 23.5 MeV, 6 h) proton irradiation of ^{68}Zn, modest amounts of the PET radionuclide, ^{64}Cu, are coproduced and can be separated from ^{67}Ga and ^{68}Zn. Although fine purification would likely be necessary for further use, the dual-production proof of concept is interesting.[167] Other purification methods include liquid−liquid extraction,[174,179] precipitation,[166] complexation,[180] and thermal diffusion,[165] where the Zn target is heated to 300 °C for 2 h and the ^{67}Ga is extracted with acetic acid.

8.3. Gallium-66 Production

Many approaches to ^{67}Ga production can be applied to obtain ^{66}Ga, such as ^{66}Zn(p,n)^{66}Ga, ^{63}Cu(α,n)^{66}Ga, ^{59}Co(^{11}B,4n)^{66}Ge → ^{66}Ga, and ^{59}Co(^{12}C,5n)^{66}As → → ^{66}Ga.[172,181,182] The most common production method is proton bombardment of ^{nat}Zn or ^{66}Zn targets with a 10−15 MeV beam to induce ^{66}Zn-(p,n)^{66}Ga.[183] Purification has been achieved using liquid−liquid extraction and/or cation-exchange chromatography;[172,181,182,184−186] however, Fe^{3+} contamination is common and often overlooked.[158] Engle et al. reported the highest specific activity to date (740 GBq/μmol) by employing an ion-exchange purification method originally used for ^{67}Ga.[158,178]

8.4. Gallium Chemistry and Chelator Development

Trivalent gallium (Ga^{3+}) has an ionic radius of 0.47−0.62 Å (CN = 4−6) and is most commonly found with a coordination number of six. Neighboring the transition metals, Ga^{3+} is classified as a hard metal (I_A = 7.07) and is notorious for having analogous chemistry to the abundant endogenous ferric ion (Fe^{3+}), which is tightly regulated by the blood plasma glycoprotein, transferrin. Concern over $^{66/67/68}Ga^{3+}$ trans-chelation by transferrin (log K_{ML} = 19.75)[187] has spurred the development of extremely inert Ga^{3+} complexes capable of withstanding high concentrations of competing serum proteins. Another major challenge of Ga-based radiotracers is the propensity to form hydroxide species at low pH (pK_a = 2.6, $Ga^{3+}_{(aq)}$ → $GaOH^{2+}_{(aq)}$), often requiring radiolabeling to be done under acidic conditions or in the presence of an intermediary ligand (e.g., citrate or oxalate). Furthermore, the tendency to form $[Ga(OH)_4]^-$ at neutral pH requires high complex stability and kinetic inertness over a broad pH range. Despite these stringent requirements, several candidates have emerged and have been proven worthy for in vivo use.

DOTA has been widely used for $^{66/67/68}$Ga-based tracers despite the clear nonoptimal match. The solid-state structure of doubly deprotonated $[Ga(H_2DOTA)]^+$ reveals N_4O_2 bonding with distorted octahedral geometry.[188] The large ring size is the cause of significant distortion and hampers thermodynamic stability of the complex (log K_{ML} = 21.3−26.1). Heteroatomic and extended ring derivatives ([13]ane and [14]ane) have been studied with Ga^{3+}; however, decreased stability was observed.[189,190] Cross-bridged DOTA (CB-DO2A, 4,10-bis[carboxymethyl]-1,4,7,10-tetraazabicyclo[5.5.2]tetradecane; Figure 4D) appears to be an improvement over DOTA based on decreased Ga−N and Ga−O bond distances, as well as more ideal bond angles in the solid-state structure.[191] The pyridine-containing DOTA derivative, PCTA (Figure 4G), originally synthesized and studied with lanthanides for use as a potential MRI relaxation agent,[192] is an enormous improvement over DOTA for $^{67/68}$Ga-radiotracers, achieving quantitative radiolabeling at room temperature and maintaining good kinetic inertness during apo-transferrin challenge experiments.[193] Following encouraging stability studies,[83] in vivo experiments demonstrated good tumor accumulation and clearance from main tissues (i.e., kidney, liver, and muscle).[194] It is worth noting that, although TETA (1,4,8,11-tetraazacyclotetradecane-1,4,8,11-tetraacetic acid; Figure 4F) is extremely useful for $^{64/67}$Cu, the [14]aneN_4 macrocycle is irrelevant for $^{67/68}$Ga radiotracers (log K_{ML} = 19.7, pM = 14.1).[195−197]

NOTA (Figure 4I) is an excellent chelate match with Ga^{3+} due its appropriate ring size and coordination number, reflected in the high stability constant (log K_{ML} = 29.0−31.0) and pM value (pM = 26.4).[197] NOTA quantitatively radiolabels $^{67/68}$Ga at ambient temperature, making it clearly superior to DOTA.[198] Solid-state structures of [Ga(NOTA)] have been reported and reveal N_3O_3 coordination with slightly distorted octahedral geometry.[199,200] Bond angles deviate 5−8° from the ideal 90° octahedral geometry. On the basis of ^{71}Ga NMR spectroscopy studies, these structures are representative of solution geometry.[201] Similar solid-state geometries have been reported for bifunctional analogues NO2A and NODASA.[202,203] NODAGA achieved excellent radiolabeling yields at ambient temperature over 10 min,[198] and when targeting SST receptors, ^{67}Ga-NODAGA-TOC demonstrated superior tumor uptake and nearly double the tumor-to-blood/liver/kidney ratios compared to those of ^{111}In-DOTATOC 4 h postinjection.[204] *p*-SCN-Bn-NOTA is also commonly em-

DOI: 10.1021/acs.chemrev.8b00294
Chem. Rev. 2019, 119, 902−956

ployed as a bifunctional chelate derivative and has demonstrated superiority over DTPA and DOTA analogues during in vivo $^{67/68}$Ga use, as evidenced by lower $^{67/68}Ga^{3+}$ bone uptake.[193,205]

Phosphonate- and phosphinate-containing NOTA analogues have been increasingly reported as of late.[201,206−212] One of the most impressive analogues is [9]aneN$_3$ functionalized with three phosphinate arms extending to carboxylic acid groups for bioconjugation. The ligand, denoted TRAP (triazacyclononate phosphinic acids; Figure 4J) forms stable Ga^{3+} complexes (log K_{ML} = 26.2) and can achieve high radiochemical yields at ambient temperature with nM ligand concentrations.[213] Very high specific activity (2009 ± 61 GBq/μmol) can be achieved while maintaining good radiochemical yields. The benefit of functionalizing each ligand arm is reflected in the low IC$_{50}$ of ^{68}Ga-TRAP-(RGD)$_3$, which is 7-fold lower than that of [^{18}F]Galacto-RGD (44 vs 319 nM). Moreover, the tumor % ID/g of ^{68}Ga-TRAP-(RGD)$_3$ is nearly 4-fold greater than that of [^{18}F]Galacto-RGD with similar tumor-to-blood ratios.[214] A comparative study of fully automated ^{68}Ga labeling of TRAP-(RGD)$_3$, DOTATOC, and NODAGA-RGD demonstrated the superiority of TRAP over NOTA (NODAGA) and DOTA (DO3A), achieving specific activity 10- and 20-fold greater, respectively.[215] A 3-fold increase in tumor uptake of ^{68}Ga-TRAP-(RGD)$_3$ was also revealed in a comparison with ^{68}Ga-NODAGA-RGD and [^{18}F]Galacto-RGD; however, high adrenal uptake was also observed (27.8 ± 10%ID/g).[216] Another notable [9]aneN$_3$ analogue is NOA2P, which has a higher Ga^{3+} stability constant than even NOTA (log K_{ML} = 34.4).[211]

Many acyclic ligands have been reported to form exceptionally strong coordination complexes with Ga^{3+}. Some published works have investigated the use of DTPA with $^{67/68}$Ga;[217−220] however, the relatively low stability constant (log K_{ML} = 24.3)[221] and observed complex dissociaton[205] has largely deterred modern use, especially with the large variety of exceptional Ga^{3+} chelators currently available.

HBED (Figure 5C) is likely the most heavily investigated acyclic chelator for Ga^{3+}. Its outstanding complex stability (log K_{ML} = 38.5−39.6) is among the highest of discussed chelators. The chemical similarity between Ga^{3+} and Fe^{3+} is further emphasized here, as high $[Fe(HBED)]^-$ stability (log K_{ML} = 39.7) facilitated HBED use for iron-overload therapy.[222] Stability studies of HBED and other polycarboxyphenols demonstrate a clear preference for small, hard metal ions over softer or larger metals such as Mg^{2+}, Ca^{2+}, Mn^{2+}, Cu^{2+}, Co^{2+}, Zn^{2+}, Ni^{2+}, In^{3+}, or Gd^{3+}.[54,223−226] Modification of the phenol arms with SO_3^- groups (SHBED, *N,N′*-bis[2-hydroxy-5-sulfobenzyl]ethylenediaminediacetic acid; Figure 5C) and replacement of the COOH with pyridine arms (H_6Sbbpen, *N,N′*-bis-[2-hydroxy-5-sulfonylbenzyl]-*N,N′*-bis[2-methylpyridyl]ethylenediamine; Figure 5C) increase stability with larger ions, such as In^{3+} and Gd^{3+}.[226,227] Although the high selectivity of HBED for small, hard metals hampers its versatility, it is a major benefit for $^{67/68}$Ga-specific use.[228] HBED can quantitatively radiolabel $^{67/68}$Ga at ambient temperature with high specific activity and demonstrates high resistance to decomplexation.[229−232] Preparation at room temperature results in 50% formation of unfavored isomers, which are resolved during HPLC purification and have been studied by ^{71}Ga NMR spectroscopy.[233] At pH 4, conversion to the thermodynamic product occurs within a few hours, while at pH 7 solutions require days to overcome the kinetic barriers for stable isomer formation.[234,235] To ensure the thermodynamically favored isomer is predominant, radiolabeling is often done at elevated temperature.[235] From a physiological standpoint, the presence of multiple diastereomers can be a concern;[236] however, in the case of HBED, some evidence suggests metal-complex isomers have no effect on bioconjugate behavior.[235] The crystal structure of [Ga(HBED)H$_2$O] has recently been reported.[233] The structure features N_2O_3 ligand coordination with a coordinating water and noncoordinated, protonated phenolate group. The resulting distorted octahedral geometry is expected and resembles the solid-state structures of $[Fe(HBED)]^-$ and [Ti(HBED)].[237,238] The most common bifunctional HBED derivative is HBED-CC, which contains ethylene−carboxylic acid groups linked para to phenol hydroxyl group.[229] Functionalization of the acid groups can be achieved by protecting coordination groups using Fe^{3+}, followed by ester activation with tetrafluorophenolate (TFP) using DCC as a coupling agent. Iron(III) can then be removed by loading the complex onto a C18 cartridge and washing with 1 M HCl and water. The metal-free chelate is then eluted with a mixture of MeOH and H$_2$O.[229] Conjugation to biomolecules via amide coupling has been thoroughly investigated using this method.[229,239−242] The most investigated HBED radiotracer has been ^{68}Ga-PSMA-11 (^{68}Ga-(HBED-CC)-PSMA), which detects prostate cancer with good sensitivity and excellent specificity.[243] To date, clinical pilot studies have concluded, and several are awaiting recruitment.[244,245]

Tris(3,4-hydroxypyridinone) (THP, also known as CP256; Figure 5L) is a hexadentate ligand based on 3,4-hydroxylpyridinone coordinating groups. Like HBED, THP was originally studied for its high stability with ferric ions;[246] however, its affinity for Ga^{3+} was realized by Blower and co-workers, who pioneered work with $^{67/68}$Ga. Early studies demonstrated superior ^{68}Ga labeling of THP (pH 6.5, 5 min, RT) to DOTA (pH 4.4, 30 min, 100 °C), NOTA (pH 3.6, 10 min, RT), and HBED (pH 4.6, 10 min, RT) at each ligand's optimized radiolabeling conditions. Incubation with 130 equiv of apotransferrin led to no complex decomposition.[247] A notable experiment compared the radiochemical yield of competition experiments between DOTA, NOTA, NOTP (1,4,7-triazacyclononane-1,4,7-tri[methylene phosphonic acid]; Figure 4J), TRAP, HBED, and THP. Every paired combination of the six chelators (500 μM each) was tested at pH 3.5 and 6.5, at both 25 and 90 °C. In every ambient competition experiment, THP achieved upward of 95% radiochemical yield, with the exception of NOTP, where 92% and 94% labeling were observed at pH 3.5 and 6.5, respectively. High-temperature experiments had slightly lower labeling for THP but still demonstrated THP as the superior Ga^{3+} sequestering agent.[233] Bioconjugation of the bifunctional derivative (YM103; Figure 5L) has been demonstrated via thiol−maleimide coupling[247,248] and SCN−amide coupling.[249,250] A ^{68}Ga radiolabeling kit has been developed to simplify use of THP analogues, where 5 mL of eluent from a ^{68}Ge/^{68}Ga generator (0.1 M HCl, 600−660 MBq) is added to a lyophilized solid containing sodium bicarbonate (44 mg), sodium phosphate (17.5 mg), and THP-vector (4 μg, 26 nmol for THP-PSMA) to yield a solution with pH 6−7. After 5 min, radiochemical purity by iTLC is >95% with specific activity up to 22 MBq/nmol.[251] THP has been coupled and studied in vivo with a PSMA-targeting peptide,[251] Tyr^3-octreotate,[250] and RGD.[249,252] In general, images show no signs of instability; however, high liver and kidney uptake are common. This may

DOI: 10.1021/acs.chemrev.8b00294
Chem. Rev. 2019, 119, 902−956

Table 6. Selected $^{66/68}$Ga Radiopharmaceuticals with Targets and Relevant Labeling Parameters[a]

radioisotope	chelator (BFC)	standard labeling conditions	bioconjugate	target	molar/specific activity (% RCY)	reference
^{66}Ga	NOTA (*p*-SCN-Bn)	0.25 M NH_4OAc pH 7.2, 37 °C, 30 min	TRC-105	CD105	>74−222 GBq/μmol (>80)	691
	DFO	TRIS-buffered saline pH 7.4, 50 °C, 15 min	folate	FR		692
^{68}Ga	DOTA (DO3A)	0.1 M OAc pH 5.5, 100 °C, 10 min	Tyr^3-octreotate (TATE)	SSTR	185−260 GBq/7−45 mg (64)	693
	HBED (HBED-CC)	NaOAc, pH 4.5, 85 °C, 3 min	PSMA-11	PSMA	70 ± 20 GBq/μmol (86.5 ± 4.1)	244
	PCTA (*p*-SCN-Bn)	10 mM NaOAc pH 4.5, 30 min, RT	c(RGDyK)	integrin $\alpha_v\beta_3$	55 GBq/μmol (96.2 ± 0.5)	194
	THP (SCN)	0.6 M NH_4OAc, pH 6.5, RT, 2−5 min	c(RGDfK)	integrin $\alpha_v\beta_3$	60−80 GBq/μmol (>95)	250
	H_2dedpa (*p*-SCN-Bn)	10 mM NaOAc pH 4.5, RT, 10 min	c(RGDyK)	integrin $\alpha_v\beta_3$	34 GBq/μmol (97)	255
	TRAP	HEPES buffer pH 2, 95 °C, 5 min	$(RGD)_3$	integrin $\alpha_v\beta_3$	2009 ± 61 GBq/μmol (90.0 ± 2.7)	215

[a]FR (folate receptor); SSTR (somatostatin receptor); and PSMA (prostate-specific membrane antigen).

be a result of relatively high chelator lipophilicity, which is reflected in the partition coefficient.[250] The formation of colloids due to free $^{68}Ga^{3+}$ may also be problematic but could be avoided through postlabeling purification.[250,253] Interested readers are directed to a more in-depth review on hydroxypyridinone chelators by Cusnir et al.[254]

H_2dedpa (1,2-[{6-(carboxylato-)pyridin-2-yl}methylamino]-ethane; Figure 5H) is a picolinic acid-based scaffold that has shown promise for $^{67/68}$Ga imaging. The solid-state structure of $[Ga(dedpa)]^+$ reveals distorted octahedral geometry. The $[Ga(dedpa)]^+$ stability (log K_{ML} = 28.1) is greater than that of DOTA (log K_{ML} = 21.3−26.1) and comparable to that of NOTA (log K_{ML} = 29.0−31.0). Quantitative radiolabeling at low ligand concentrations and high kinetic inertness during apo-transferrin challenge experiments has been reported.[81] ^{68}Ga-dedpa-RGD demonstrates good tumor uptake with significant clearance from the liver, kidney, and muscles in RAG2M mice bearing U87MG human glioblastoma xenografts.[255] Several other derivatives have been made to alter kinetic inertness[256] and heart uptake,[257] as well as hypoxia[258] and bone-targeting capabilities.[259]

AAZTA (Figure 5K) forms reasonably stable Ga^{3+} complexes (log K_{ML} = 21.2) and has been modestly applied to gallium-based radiotracers.[260] Despite encouraging radiolabeling results, concerns over multiple isomers (N_3O_3/N_2O_4) resulted in favored use of hexadentate DATA (6-amino-1,4-diazepine triacetic acid; Figure 5K) analogues, which coordinate with distorted octahedral geometry.[261,262] Comparative radiolabeling of the family of DATA chelators identified DATA^m (Figure 5K) as the most promising candidate, although all derivatives performed well during DTPA, serum stability, and metal (Ca^{2+}, Cu^{2+}, and Fe^{3+}) competition experiments.[263] The bifunctional analogue (DATA^{5m}; Figure 5K) demonstrates similar radiolabeling to DATA^m following octreotide conjugation.[264] Kit-based formulations are currently under investigation for use in vivo.[263,264] Recent potentiometric data suggests fair stability (log K_{ML} = 21.5) and predominantly hydrolyzed speciation at physiological pH.[265]

Several other chelators have been studied with Ga^{3+} that will only briefly be mentioned here. The common reagent used for iron-overload therapy, deferoxamine (DFO; Figure 5O), was studied with Ga^{3+} due to its known chemical similarity with Fe^{3+}. Nonfunctionalized DFO−metal complexes are known to be excreted rapidly in the urine[266,267] but can facilitate tumor uptake when bifunctionalized at the N-terminus, as demonstrated in studies with lectins,[217] MoAb OST7,[268] octreotide,[269] and folate.[270,271] Knowledge that Ga^{3+}-siderophores mimic Fe^{3+}-siderophores and are taken up by some fungi[272,273] has spurred interest in using DFO analogues as bacterial imaging agents.[274] The cyclic siderophore analogue, fusarinine (FSC; Figure 5N), has demonstrated high radiochemical yields and kinetic inertness with ^{68}Ga, as well as good tumor uptake when conjugated to RGD.[272,275,276] Despite its hard Lewis acid properties, several sulfur-based ligands have been studied with $^{67/68}$Ga, including [9]aneN_3 analogues and a tetracoordinate NS_3 ligand.[277−279] The acyclic SNNS motif was thoroughly explored with variable acetate arms and carbon-bridge derivatization.[280−283] Ultimately, it was determined that the six-coordinate ligand, 6SS (*N,N′*-bis[2,2-dimethyl-2-mercaptoethyl]ethylenediamine-*N,N′*-diacetic acid; Figure 5J), was the most optimal structure, boasting a log K_{ML} of 41.0.[221] Despite a bifunctional derivative (B6SS, Figure 5J), to the best of our knowledge no bioconjugated analogue has been published.[279] More recently, thiol-containing ligands, ECC (ethylenecysteamine cysteine; Figure 5M) and ECD (ethyl cysteinate dimer; Figure 5M), which are popular with ^{99m}Tc tracers, were shown to be useful for ^{68}Ga-based renal and cerebral blood flow imaging, respectively.[284,285] A number of polyaminopolyphenol Schiff base complexes have demonstrated the ability to form stable complexes with Ga^{3+} and radiolabeled $^{67/68}$Ga for use in myocardial imaging,[286,287] P-glycoprotein mediated transport imaging,[288] and most recently as metalloprobes for rat cardiomyoblasts and human breast carcinoma cells.[289]

8.5. Gallium-68 Biological Studies

For brevity, this section will focus solely on clinically considered ^{68}Ga tracers. SST receptor targeting has been a major focus area due to high expression rates on neuroendocrine tumors (~80%), which are challenging to visualize using conventional anatomic imaging.[157,290] The June 2016 FDA approval of ^{68}Ga-DOTATATE (NETSPOT) is the most significant development in recent years. Clinical trials revealed superiority of ^{68}Ga-DOTATATE to ^{111}In-pentetreotide in imaging neuroendocrine tumors, and since then, high degrees of clinical implementation have been reported.[157,291] ^{68}Ga-DOTATOC and ^{68}Ga-DOTANOC have also been well-

DOI: 10.1021/acs.chemrev.8b00294
Chem. Rev. 2019, 119, 902−956

studied and are considered suitable for clinical application.[292−296]

PSMA is another highly attractive target for nuclear probes due to its high expression and poor differentiation in metastatic and hormone-refractory carcinoma.[297] In many respects, ^{68}Ga-PSMA is superior to ^{18}F/^{11}C-choline for PET/CT and has been recommended for preferred use during primary and secondary staging of castration-resistant prostate cancer.[298] ^{68}Ga-PSMA-11 (^{68}Ga-HBED-CC-PSMA) is among the most successful PSMA imaging tracers and interestingly has exhibited superior tumor accumulation (3.5−7.7%ID/g) than its DOTA counterpart (1−3%ID/g) in animal models as a consequence of hydrophobic chelator interactions.[299] Clinical studies have demonstrated high contrast in tumor metastasis and excellent detection rates at low PSA levels.[300] Structural modification of PSMA-11 to permit radiolabeling of other radiometals (e.g., ^{177}Lu and ^{225}Ac) led to the development of ^{68}Ga-PSMA-617 (^{68}Ga-DOTA-PSMA), which has a higher membrane antigen affinity and is now also of interest in clinical trials.[243] Other noteworthy tracers are ^{68}Ga-Neo-BOMB1,[301,302] ^{68}Ga-pentixafor,[303] and ^{68}Ga-OPS202 (^{68}Ga-NODAGA JR-11) (Table 6).[304]

9. YTTRIUM

Yttrium-90 ($t_{1/2}$ = 64.0 h) is a well-established, pure β^- emitting radionuclide with high-energy emission ($E\beta^-_{avg}$ = 934 keV, 100%) and relatively long soft-tissue range (11 mm).[305,306] The multiday half-life of ^{90}Y makes it most suitable for use with antibodies, although studies with peptides and other small bioconjugates are not uncommon.[220,307,308] Zevalin (^{90}Y-tiuxetan-ibritumomab) was approved for radio-immunotherapy of non-Hodgkin lymphomas by the FDA in 2002. Yttrium-90-bearing microspheres (SIR-spheres, TheraSphere) are also FDA approved, but for brachytherapy of hepatocellular carcinoma.[309]

The pure β^- emission is one of the major benefits of ^{90}Y therapy; however, dose calculations are challenging due to the lack of γ-emission. High uncertainties are typically associated with organ-specific dosimetry of ^{90}Y due to a reliance on bremsstrahlung radiation. In the 1990s, ^{111}In was commonly used as a diagnostic pair with ^{90}Y to better quantify radiation dose;[310,311] however, opinions regarding this matched pair have since shifted, as the use of ^{111}In with ^{90}Y-labeled mAb has been abandoned and was recently described as "at best... hazardous" due to the striking dissimilarities in In^{3+}/Y^{3+} biochemistry.[36,312] Although many radionuclides[313] have been considered as diagnostic matches for ^{90}Y, use of ^{86}Y is an especially attractive option due to the identical chemical behavior, which would mitigate concern over nonrepresentative image information.

Yttrium-86 ($t_{1/2}$ = 14.7 h) is a β^+ emitter whose use with ^{90}Y constitutes one of the earliest examples of a chemically identical theranostic pair. Despite low branching (32%), the broad range of positron energies, and a high level of prompt gamma coincidences that negatively impact image quality,[13,314] the benefits of the chemically identical diagnostic match have resulted in considerable attention. The availability of ^{86}Y is, however, low, and thus research has focused on production and purification of the β^+ emitter for eventual clinical use.[312]

9.1. Yttrium-90 Production

Production of ^{90}Y is well-developed, with interest dating back >50 years.[315,316] Despite the proven clinical applicability of ^{90}Y, widespread use has yet to be realized due to insufficient radionuclide availability, stemming from the lack of commercially viable generator systems.[317]

Direct ^{90}Y production has been demonstrated by ^{89}Y-(n,γ)^{90}Y; however, this method results in low specific activity as a consequences of low reaction cross section (1 mb) and a chemically identical target.[318] Specific activity can be improved using a high-flux neutron source;[319] however, it is generally accepted that the inherent inability to separate $^{89/90}$Y precludes in vivo use. Reactor production via ^{90}Zr(n,p)^{90}Y has also been explored, but target cost and the need for fast neutrons has stifled progress of this method.[318]

The most important ^{90}Y source is ^{90}Sr, which is the fission decay product of ^{235}U and is present at concentrations of up to 74−740 GBq/L in high-level liquid waste.[161] The long half-life of ^{90}Sr ($t_{1/2}$ = 28.8 years) makes it an excellent candidate for a ^{90}Y generator system and is the motivation behind the continued pursuit of large quantities of ^{90}Sr.[320−325] Isolation of ^{90}Sr from high-level liquid waste can be achieved by precipitation, solvent extraction, ion-exchange, or extraction chromatography, normally requiring at least two purification steps for adequate purity. The isotopic dilution of strontium limits the specific activity of the isolated ^{90}Sr to 1.1−1.9 TBq/g.[161]

9.2. Yttrium-86 Production

Many cyclotron-based routes to ^{86}Y production have been demonstrated, including ^{86}Sr(p,n)^{86}Y, ^{88}Sr(p,3n)^{86}Y, ^{90}Zr-(p,2p3n)^{86}Y, ^{nat}Rb(^{3}He,xn)^{86}Y, and, most recently, indirectly via ^{89}Y(p,4n)^{86}Zr → ^{86}Y.[326−329] Currently the most practical production route is ^{86}Sr(p,n)^{86}Y, as low-energy protons (7−14 MeV) can be used to achieve good yields. The drawback of this strategy is the need for enriched ^{86}Sr to minimize the coproduction of radioisotopic impurities ($^{87/88}$Y), which necessitates diligent recycling of the target material.[330] Strontium salts, such as $^{86}SrCO_3$ or $^{86}SrCl_2$, are generally employed as targets, although liquid targets have also been reported.[331] Following irradiation, Sr^{2+}/Y^{3+} separation can be achieved via precipitation, ion-exchange chromatography, liquid−liquid extraction, or solid-phase extraction chromatography.[332−335] One of the most effective separation strategies is through coprecipitation of ^{86}Y with $La(OH)_3$ using NH_4OH, followed by cation-exchange chromatography.[327] This method has been shown to yield 3.5 GBq of activity with an extremely low concentration of metal contaminants.[336] Two-step electrolytic separation also proved to be quite effective in purifying clinical-scale activity.[337−339] The method works by first dissolving the $SrCO_3$ target in 2.8 M HNO_3 and electroplating ^{86}Y onto a cathode with 2000 mA of current for 40 min. The electrodes are then placed into a second HNO_3 solution (3.5 mM), and the electrode currents are arranged to reinduce electrolysis onto a separate Pt wire electrode, at 400 mA for 15 min. The deposited activity is finally dissolved in 0.05 M HCl in the barrel of a syringe to yield high-purity ^{86}Y, suitable for radiolabeling.[339]

9.3. Yttrium Chemistry and Chelator Development

Yttrium is predominantly found as a trivalent cation (Y^{3+}) and, like scandium, is considered a rare-earth element despite its typical positioning among the transition metals. Unlike Sc^{3+}, however, Y^{3+} chemistry closely resembles that of the lanthanides, reflected in its comparable ionic radius (0.9−1.08 Å, CN = 6−9) and preferred coordination number of 8 or 9. Despite hard Lewis acid behavior (I_A = 10.64), the relatively

DOI: 10.1021/acs.chemrev.8b00294
Chem. Rev. 2019, 119, 902−956

Table 7. Selected Y^{3+} Chelators, Metal Complex Geometry, and Thermodynamic Parameters

metal ion	chelator	coordinating nuclei	geometry	log K_{ML}	pM	reference
Y^{3+}	DOTA	N_4O_4	square antiprism	24.3−24.9	19.3−19.8	340, 362, 694−697
	DTPA	N_3O_5	monocapped square antiprism	21.9−22.5	17.6−18.3	343, 362, 687, 694, 696, 698, 699
	CHX-A-DTPA	N_3O_5	monocapped square antiprism[a]	24.7	19.0	63, 136, 219, 341, 347,377
	PCTA	N_4O_3	square antiprism[b]	20.3	17.0	83, 348, 349
	L2	N_5O_3	tricapped trigonal prism	22.4	20.3	349, 351
	L4	N_6O_3	tricapped trigonal prism[a]	23.1	21.5	351
	NETA	N_4O_4	capped trigonal prism?			352−356
	DE4TA	N_5O_4	square antiprism?			354
	H_4octapa	N_4O_4	square antiprism	18.3	18.1	362, 363

[a]On the basis of $[Y(DTPA)]^{2-}$. [b]On the basis of [Y(PCTMB)].

diffuse charge distribution of Y^{3+} precludes hydrolysis at low pH (pK_a = 7.7, $Y^{3+}_{(aq)} \rightarrow YOH^{2+}_{(aq)}$).[52]

The majority of $^{86/90}Y$ tracers employ either DOTA (Figure 4A) or CHX-A″-DTPA (Figure 5B) for chelation. As would be expected with a midsized trivalent rare-earth metal, DOTA and CHX-A″-DTPA form highly stable Y^{3+}complexes (log K_{ML} = 24.3−24.9 and 24.7, respectively), quantitatively radiolabel $^{86/90}Y$ at low concentrations, and exhibit excellent kinetic inertness against serum protein and endogenous metal competition.[63,340,341] Solid-state structures of $[Y(DOTA)]^-$ and $[Y(DTPA\text{-}BA_2)(CH_3OH)]$, a diamide DTPA analogue, confirm similar Y^{3+} geometry (square antiprism) and coordinating bond lengths ($Y-O_{avg} \approx 2.3$ Å, $Y-N_{avg} \approx 2.6$ Å) for each complex.[342,343] A detailed report of ^{90}Y-labeled compounds[344] underscores the preferred use of DOTA but also reveals moderate use of CHX-A″-DTPA. Although DTPA itself can effectively radiolabel $^{86/90}Y$, the rigid backbone of CHX-A″-DTPA is beneficial for minimizing metal release, as evidenced by studies with long-lived ^{88}Y ($t_{1/2}$ = 107 days).[219,345] Interestingly, the stereochemistry of CHX-DTPA was shown to be of major importance, with markedly higher stability observed with CHX-A″-DTPA, compared to CHX-B″-DTPA, during serum challenge experiments over 17 days.[346] This translated into 2-fold higher bone uptake in animals administered ^{88}Y-CHX-B″-DTPA versus ^{88}Y-CHX-A″-DTPA, 4 days postinjection.[347] Particularly noteworthy is a comparative study of *p*-SCN-Bn-DOTA, *p*-SCN-Bn-DTPA, *p*-SCN-Bn-CHX-A″-DTPA, *p*-SCN-Bn-NOTA, and *p*-SCN-Bn-PCTA that suggests CHX-A″-DTPA is most suitable for $^{86/90}Y$ radiopharmaceuticals, based on serum stability and metal competition experiments (Fe^{3+}, Cu^{2+}, Zn^{2+}, and Ca^{2+}).[341] Alternative chelator development for $^{86/90}Y$ has been dominated by four main ligand classes: PCTA and derivatives, NETA, DEPA, and H_4octapa.

In 2006, Tircso et al. began thoroughly investigating the stability and kinetics of LnPCTA (Figure 4G) complex formation to address the slow kinetics of DOTA labeling.[59] The solid-state structure of [Y(PCTMB)], a phosphinate-substituted PCTA derivative, suggests square antiprismatic geometry about the metal center.[348] Although less thermodynamically stable (log K_{ML} = 20.3), PCTA lanthanide complex-formation kinetics are 10 times faster than DOTA and adequately slow acid-catalyzed dissociation.[83] The *p*-NO_2-Bn-PCTA analogue only exhibits a modest decrease in Y^{3+} complex stability.[83] To the best of our knowledge, no $^{86/90}Y$-PCTA animal studies have been conducted.

Monopicolinic acid PCTA derivatives have been described, with one derivative (L2; Figure 4H) demonstrating improved Y^{3+} stability (log K_{ML} = 22.4) over PCTA and a superior pM value (20.3) versus Y^{3+}-DOTA.[349] Interestingly, the tricapped trigonal prismatic geometry reveals the importance of the capping groups, as the weaker of the two Y^{3+} complexes (L1; Figure 4H) is capped by a carboxylic acid group, whereas the more robust complex (L2) is water-capped. It is suggested by the authors that protonation of the capped carboxylic acid leads to decomplexation via proton transfer to a coordinated amine, resulting in the rapid proton-assisted dissociation rate of L1 ($t_{1/2}$ = 27 min) but not L2 ($t_{1/2}$ = 357 min).[349] The proposed "capping bond effect" builds upon water exchange-rate studies with Gd^{3+} for use as MRI contrast agents[350] and may influence the rational design of highly inert complexes for nuclear medicine. Dipicolinic acid PCTA derivatives have very recently been reported, with one derivative (L4; Figure 4H) exhibiting a 1000-fold increase in acid-dissociation half-life compared to PCTA and a 300-fold increase compared to L2, in 1 M HCl. Although a small drawback was the need for elevated temperatures for optimized radiolabeling, stability studies with human serum and EDTA (0.1 M) showed excellent ^{90}Y retention over 72 h.[351]

NETA ([2-{4,7-biscarboxymethyl(1,4,7)triazacyclonona-1-yl-ethyl}carbonylmethylamino]acetic acid; Figure 4K) is a NOTA derivative and, like PCTA, was designed to maintain the high stability constants of macrocycles, while achieving rapid radiolabeling at low temperature. The octadentate chelator is essentially identical to NOTA, with the exception of one iminodiacetic acid-functionalized nitrogen, linked via ethylene bridge. Early studies demonstrated excellent ^{88}Y-NETA inertness against serum challenge over 14 days and rapid in vivo clearance after 24 h. Iminodiacetic acid linkage via propylene bridge was also synthesized; however, a higher degree of decomplexation during in vitro and in vivo studies was observed.[352] Follow-up studies have reported improved syntheses via aziridinium intermediates to produce bifunctional derivatives that maintain impressive radiolabeling and inertness with ^{90}Y when conjugated to c(RGDyK) or trastuzumab.[353−357] A lower denticity analogue, 3p-*C*-NE3TA (Figure 4K), has also been synthesized but demonstrates inferior radiolabeling capabilities and serum stability than the original octadentate chelate.[354] A similar DOTA derivative, DEPA (Figure 4C), and bifunctional analogues were synthesized, and although initial studies suggested an unideal match with Y^{3+}, the lower denticity analogue, 3p-*C*-DE4TA (Figure 4C), shows improved ^{90}Y radiolabeling and performance against serum protein competition.[354,358] In vivo experiments with both chelators are focused mainly on ^{177}Lu and will be discussed in section 12.2.[354−356]

H_4octapa (*N*,*N*′-bis[6-carboxy-2-pyridylmethyl]-ethylenediamine-*N*,*N*′-diacetic acid; Figure 5H) is an octa-

DOI: 10.1021/acs.chemrev.8b00294
Chem. Rev. 2019, 119, 902−956

Table 8. Selected $^{86/90}$Y Radiopharmaceuticals with Targets and Relevant Labeling Parameters[a]

radioisotope	chelator (BFC)	standard labeling conditions	bioconjugate	target	molar/specific activity (% RCY)	reference
^{86}Y	DOTA (DO3A)	0.15 M NH_4OAc pH 4.5, 100 °C, 15 min	Phe^1-Tyr^3-octreotide (TOC)	SSTR	28 GBq/μmol (>98.5)	372, 374
	DOTA (*p*-SCN-Bn)	0.2 M NH_4OAc pH 5.5−6, 95 °C, 20 min	PSMA peptide "6"	PSMA	>83.9 GBq/μmol (90−95)	376
	CHX-A″-DTPA (*p*-SCN-Bn)	0.1 M NH_4OAc pH 5−6, RT, 30−60 min	Antimindin/RG-1	Mindin/RG-1	29.6−39.6 MBq/mg (82−96)	378
			Panitumomab	HER1	2 GBq/mg (60−75)	379, 380
^{90}Y	DOTA (DO3A)	0.4 M NH_4OAc pH 5, 90 °C, 25 min	Phe^1-Tyr^3-octreotide (TOC)	SSTR	50 GBq/μmol (>98)	700
			Tyr^3-octreotate (TATE)	SSTR	74.7 GBq/μmol	370
	DOTA (*p*-SCN-Bn)	0.25 M NH_4OAc pH 5.4, RT, 10 min	hLL2	CD22	78.1 MBq/mg (78)	61
	1B4M-DTPA (*p*-SCN-Bn)	50 mM NaOAc RT, 5 min	Ibritumomab	CD20	740 MBq/mg (>96)	701
	CHX-A″DTPA (*p*-SCN-Bn)	0.4 M NaOAc pH 5.5, RT, 30 min	hu3S193	EGFR	85.1 MBq/mg	702
	NETA (3p-C)	0.25 M NH_4OAc pH 5.5, RT, 5 min	Trastuzumab	HER2	(99.6 ± 0.2)	355
	H_4octapa (*p*-SCN-Bn)	0.2 M NH_4OAc pH 5.5, 37 °C, 15−60 min	Trastuzumab	HER2	66.6 MBq/mg (99)	363

[a]SSTR (somatostatin receptor); PSMA (prostate-specific membrane antigen); HER1 (human epidermal growth factor receptor 1); EGFR (epidermal growth factor receptor); and HER2 (human epidermal growth factor receptor 2).

dentate analogue of H_2dedpa (section 8.4) based around a picolinic acid scaffold. Originally studied with ^{111}In,[359] H_4octapa was also determined to form highly stable lanthanide[360,361] and Y^{3+} complexes (log K_{ML} = 18.3).[362] Bifunctional *p*-SCN-Bn-octapa was synthesized and, following bioconjugation to trastuzumab, demonstrated high radiochemical yields (>95%) over 15 min at ambient temperature. Furthermore, following 96 h serum stability experiments, octapa-trastuzumab retained more ^{90}Y than CHX-A″-DTPA-trastuzumab (94.8 ± 0.6% vs 87.1 ± 0.9%).[363] Comparative in vivo studies in mice bearing HER2-expressing SKOV3 tumors revealed an identical therapeutic effect of both tracers.[363]

9.4. Yttrium-90/86 Biological Studies

Because of the low availability of ^{86}Y, the majority of yttrium-based radiopharmaceuticals are ^{90}Y therapeutics. The biological half-life of antibody bioconjugates is compatible with the physical half-life of ^{90}Y and has led to extensive investigation of ^{90}Y radioimmunotherapy. The most popular compound is FDA-approved Zevalin (^{90}Y-tiuxetan-ibritumomab) for treatment of non-Hodgkin's lymphoma.[364] After first-line therapy, treatment with Zevalin improves survival rates for patients in remission, as demonstrated over a 7-year period.[365] Although some clinicians are still hesitant to prescribe Zevalin, it is predicted that its use will become more prominent in coming years.[366] Another promising candidate for therapy is ^{90}Y-DOTA-clivatuzumab tetraxetan for treatment of advanced pancreatic ductal carcinoma. Fractioned dosing with simultaneous low-dose gemcitabine has demonstrated increased patient survival rates during phase Ib trials.[367] Use as a third-line treatment has been proposed, pending results from phase III trials.[368]

Peptide receptor radionuclide therapy (PRRT) has also been an active area of ^{90}Y research;[344] however, in recent years ^{177}Lu has replaced ^{90}Y as the preferred β^- emitter for PRRT, notably with modified SST receptor-targeting analogues. This switch is due to the decreased β^- range of ^{177}Lu (2 mm vs 11 mm), which reduces cross-fire effects and has allowed clinicians a means for addressing the relatively high rate of myelosuppression and renal failure when using ^{90}Y. The use of combination therapy with ^{90}Y-DOTATOC/^{177}Lu-DOTATOC and ^{90}Y-DOTATATE/^{177}Lu-DOTATATE has been proven to be beneficial over ^{90}Y-DOTATOC[369] and ^{90}Y-DOTATATE,[370] respectively; however, a direct comparison of combination therapy with standalone ^{177}Lu analogues has yet to be conducted despite being more pertinent.

Another clinically relevant application of ^{90}Y are glass microspheres, which contain ^{90}Y-embedded glass and are typically administered via hepatic arterial blood flow. Microsphere diameter (20−60 μm) and increased arterial blood flow ensures preferential tumor uptake and retention, facilitating β^- mediated tumor destruction. FDA-approved microspheres are under trade names Therasphere and SIR-Spheres.[371]

The utility of ^{86}Y is best encapsulated in a 2004 comparative study in which ^{86}Y-DOTATOC was compared to ^{111}In-pentetreotide for pretreatment dosimetry of ^{90}Y-DOTATOC. When compared to ^{86}Y-DOTATOC, doses calculated from ^{111}In-pentetreotide were underestimated for liver and overestimated for kidney and spleen.[372] Other notable studies with ^{86}Y have been conducted with ^{86}Y-DOTATOC,[372−375] ^{86}Y-DOTA-PSMA,[376] ^{86}Y-CHX-A″-DTPA-bevacizumab,[377] ^{86}Y-CHX-A″-DTPA-antimindin/RG-1,[378] ^{86}Y-CHX-A″-DTPA-cetuximab,[63,379] and ^{86}Y-CHX-A″-DTPA-panitumomab (Table 8)[379,380]

10. INDIUM

Indium-111 ($t_{1/2}$ = 67.2 h) is a common and widely used SPECT radionuclide and decays by EC (100%), releasing two low-energy gammas (Eγ = 171 and 245 keV; Iγ = 91 and 94%, respectively) in the process. Indium-111 is clinically approved for use in numerous drugs including Octreoscan (^{111}In-pentetreotide), Prostascint (^{111}In-capromab), CEA-Scan (^{111}In-arcitumonab), MPI indium DTPA In111 (^{111}In-DTPA), and indium In111 oxyquinoline (^{111}In-oxyquinoline) and is most commonly used for imaging of SST receptor-expressing neuroendocrine tumors and prostate cancer.[381] Indium-111 also emits Auger electrons and has been considered for therapy.[382] Other relevant indium radioisotopes include the β^+ emitter ^{110m}In ($t_{1/2}$ = 1.15 h) and the Auger electron emitter ^{114m}In ($t_{1/2}$ = 1188 h).

DOI: 10.1021/acs.chemrev.8b00294
Chem. Rev. 2019, 119, 902−956

Table 9. Selected In^{3+} Chelators, Metal Complex Geometry, and Thermodynamic Parameters

metal ion	chelator	coordinating nuclei	geometry	log K_{ML}	pM	reference
In^{3+}	DOTA	N_4O_4	square antiprism[a]	23.9	18.8	190, 435, 703
	DTPA	N_3O_5	square antiprism	29.0−29.5	24.4−25.7	421, 422, 703−705
	CHX-A″-DTPA	N_3O_5	square antiprism[b]			381
	H_4octapa	N_4O_4	square antiprism	26.8	26.5	359
	H_4neunpa	N_4O_4	square antiprism?	28.2	23.6	86
	H_2bispa[2]	N_6O_2	square antiprism	24.4	25.0	72

[a]On the basis of $[In(DOTAZA)]^-$. [b]On the basis of $[In(DTPA)]^-$.

10.1. Indium-111 Production

The production of ^{111}In is well-established and can be achieved directly via $^{nat}Cd(d,xn)$, $^{nat}Cd(p,xn)$, $^{nat}Cd(\alpha,x)$, $^{nat}Ag(\alpha,xn)$, $^{nat}Ag(^7Li,x)$, or $^{nat}Ag(^{11}B,x)$ or indirectly by $^{nat}Rh(^{12}C, x)^{111}Sb \rightarrow {}^{111}Sn \rightarrow {}^{111}In$, $^{nat}Sn(n,x)^{111}Sn \rightarrow {}^{111}In$, or $^{nat}Sn(p,x)^{111}Sn \rightarrow {}^{111}In$.[383−398] The most common production methods are proton or deuteron bombardment of natural or enriched cadmium targets or α bombardment of silver targets. These methods are popular because they can achieve high yields of nca ^{111}In while avoiding or minimizing the production of the long-lived contaminant ^{114m}In ($t_{1/2}$ = 1188 h). Proton irradiation of natural cadmium is the dominant means of commercial ^{111}In production.[179] Interestingly, cross section data on $^{nat}Cd(p,xn)$ reveal two maxima, likely corresponding to $^{111}Cd(p,n)$, $^{112}Cd(p,2n)$, and $^{113}Cd(p,3n)$ at 24 MeV (~325 mb) and $^{114}Cd(p,4n)$ at 40 MeV (~257 mb).[394] Separation of ^{111}In from Cd targets is most commonly achieved using ion-exchange chromatography, liquid−liquid extraction, solvent extraction, or precipitation, where In^{3+} is coprecipitated with $Fe(OH)_3$ in the presence of NH_4OH. Following dissolution of the precipitate in 8 M HCl, Fe^{3+} is extracted with isopropyl ether.[383] Separation of ^{111}In from Ag targets is commonly achieved by ion-exchange chromatography. For example, successful separation has been reported with anion-exchange chromatography using 4 M KCN to retain anionic $^{111}In(KCN)_x$, which is subsequently eluted with 1 M HCl.[399] Cation-exchange chromatography has also been demonstrated for fine purification, where column loading of target material in 9 M HBr results in ^{111}In retention, followed by elution with concentrated HCl.[385,400] Liquid−liquid extraction is also a common Ag/In separation method.[384,391,397] Interested readers are directed to the recent in-depth review by Lahiri et al.[400]

10.2. Indium-110m Production

Production of the β^+ emitter ^{110m}In ($t_{1/2}$ = 1.15 h, β^+ = 61.25%) has been investigated due to the ease with which established ^{111}In SPECT tracers can be converted to PET tracers. The most promising methods for direct production of ^{110m}In include $^{110}Cd(p,n)$, $^{107}Ag(\alpha,n)$, and $^{109}Ag(^3He,2n)$; however, coproduction of ^{110g}In ($t_{1/2}$ = 4.9 h) tends to dilute isotopic purity and remains problematic.[401] For example, following yield-optimizing calculations, Kakavand et al. irradiated ^{nat}Cd with 15 MeV protons (100 μA, 1 h) and produced 44.3 ± 8.8 GBq/C (gigabecquerel per Coulomb) with 1.25 ± 0.25 GBq/C ^{110g}In impurity.[402,403] Indirect production using ^{110}Sn ($t_{1/2}$ = 4.11 h, EC 100%) as a parent radionuclide can yield ^{110g}In-free ^{110m}In following electron capture and is achieved via $^{113}In(p,4n)$, $^{113}In(d,5n)$, $^{110}Cd(^3He,3n)$, $^{108}Cd(\alpha,2n)$, or $^{110}Cd(\alpha,4n)$.[401,404−406] To make future use viable, production of $^{111/113}In$ must be mitigated through the use of enriched targets and beam energy optimization.[406] A clinical proof-of-concept study with ^{110m}In-DTPA-D-Phe[1]-octreotide was conducted in 2002 to demonstrate the superiority of ^{110m}In PET compared to ^{111}In SPECT. Indeed, improved phantom and metastatic carcinoma image quality was observed.[407]

10.3. Indium-114m Production

The Auger electron emitter ^{114m}In ($t_{1/2}$ = 1188 h) has been studied due to its applicability as a therapeutic match pair with ^{111}In tracers. The radionuclide also emits 190 keV photons, suitable for γ-detection. The daughter radioisotope, ^{114g}In ($t_{1/2}$ = 72 s), is a high-energy β^- emitter (β^-_{avg} = 779 keV, 99.5%) and contributes to the desired therapeutic effect. Indium-114m production is primarily achieved through proton or deuteron irradiation of cadmium targets, via $^{114}Cd(p,n)^{114m}In$, $^{114}Cd(d,2n)^{114m}In$, and $^{116}Cd(p,3n)^{114m}In$.[179] Production was achieved by Tolmachev et al. by irradiating enriched ^{114}Cd plates with 6.5−12.6 MeV protons. Separation was demonstrated by thermal diffusion (306 °C, 2 h, etched 0.05 M HCl), followed by cation-exchange chromatography to yield 60% of the produced activity. Radiolabeling of DTPA-D-Phe[1]-octreotide to achieve high specific activity confirmed the quality of the nca ^{114m}In method. In vivo behavior was analogous to that of ^{111}In-DTPA-D-Phe[1]-octreotide.[408] The use of ^{nat}Cd targets has been investigated, but coproduction of $^{111,113m}In$ is unavoidable and yields are drastically decreased.[408,409] Neutron irradiation of enriched ^{113}In has also been reported.[410] In lieu of a detailed summary below, here we simply report that ^{114m}In is capable of damaging cell DNA and the β^- particle decay appears suitable for treatment of large tumors (>1 cm^3).[411,412] Indium-114m has undergone preclinical studies for palliative treatment of advanced lymphoid malignancy and for targeting of HER2-expressing malignant tumors, as well as clinical studies to treat lymphoid cell malignancy.[410,413−415]

10.4. Indium Chemistry and Chelator Development

Indium is found almost exclusively as a trivalent cation (In^{3+}), has an ionic radius of 0.62−0.92 Å (CN = 4−8), and requires a coordination number of eight to become coordinatively saturated. Although considered a borderline-hard metal, among the metal ions currently discussed, In^{3+} is relatively soft (I_A = 6.3). Indium(III) is a versatile metal that can form stable complexes with soft donating groups, such as thiols,[279,280,416,417] as well as hard donating groups, such as phenolates.[224,418−420] Although not as convenient as in the case of the lanthanides, the pK_a of aquated In^{3+} (pK_a = 4.0, $In^{3+}_{(aq)} \rightarrow InOH^{2+}_{(aq)}$) is generally nonproblematic for radiolabeling.

Because of its propensity for a range of chelators and coordinating groups, the majority of ^{111}In-tracers utilize the most readily available chelators, namely, CHX-A″-DTPA (Figure 5B) and DOTA (Figure 4A). $[In(DTPA)]^{2-}$ and $[In(CHX\text{-}A''\text{-}DTPA)]^{2-}$ are highly stable and have been used extensively for peptide- and antibody-based imaging, notably in

DOI: 10.1021/acs.chemrev.8b00294
Chem. Rev. 2019, 119, 902−956

Table 10. Selected ^{111}In Radiopharmaceuticals with Targets and Relevant Labeling Parameters[a]

radionuclide	chelator (BFC)	standard labeling conditions	bioconjugate	target	molar/specific activity (% RCY)	reference
^{111}In	DOTA (DO3A)	0.4 M NH_4OAc pH 5−7, 65−90 °C, 30−40 min	BBN(7-14)NH_2	GRPR	<1722 GBq/μmol (35−89)	427
			BASS	SSTR	12 GBq/μmol (>95)	446
	DTPA (DTPA-amide)	0.1−0.2 M NaOAc pH 5.5, 25−40 °C, 10−40 min	Phe^1-octreotide	SSTR	17−25 GBq/mg (>95)	706
	CHX-A″-DTPA (*p*-NH_2-Bn)		(Arg^{11})CCMSH	MC1-R	4.44 MBq/mg	220
	H_4octapa	0.2 M NH_4OAc pH 5.5, RT, 15 min	Trastuzumab	HER2	148 MBq/mg (94)	87
	H_4neunpa	0.15 M NH_4OAc pH 6, RT, 15−30 min	Trastuzumab	HER2	1036 MBq/mg (92.6)	86

[a]GRPR (gastrin-releasing peptide receptor); SSTR (somatostatin receptor); MC1-R (melanocortin 1 receptor); and HER2 (human epidermal growth factor receptor 2).

a number of clinically approved drugs including Octreoscan (In-pentreotide), Prostascint (In-capromab), CEA-Scan (In-arcitumomab), and In-DTPA.[381] The crystal structure of $[In(DTPA)]^{2-}$ reveals an eight-coordinate metal center, with N_3O_5 bonding and square antiprismatic geometry. Bond lengths are quite uniform, with the exception of one carboxylic oxygen stemming from a terminal backbone nitrogen, which is 0.1 Å longer than other In−O bonds.[421] The uniformity of the structure and the coordinatively saturated metal center likely contribute to high complex stability (log K_{ML} = 29.5).[422] A number of studies have investigated derivatives with alternative functional groups to increase stability[224,423] and bifunctional strategies,[424,425] but the current gold standard is *p*-SCN-Bn-(CHX-A″-DTPA).

Indium-111 radiotracers are a prime example of indiscriminate use of DOTA. Despite the need for elevated radiolabeling temperatures and lower log K_{ML} and pM values than DTPA, DOTA continues to be applied to ^{111}In radiopharmaceuticals.[340,426−432] Although no $[In(DOTA)]^-$ crystal structure has been reported, based on a number of closely related DOTA analogues (In[DO3A], In[DOTA-AA], and In-$[DOTAZA]^-$), the In^{3+} center likely adopts square antiprismatic geometry.[433−435] Compared to other macrocyclic ligands, the size of In^{3+} is best suited to DOTA, which was found to form slightly more stable complexes (log K_{ML} = 23.9) than extended cyclen analogues [13]aneN_4 (TRITA; 1,4,7,10-tetraazacyclotridecane-*N*,*N*′,*N*″*N*‴-tetraacetic acid; Figure 4E) and [14]aneN_4 (TETA; Figure 4F) (log K_{ML} = 23.00 and 21.89, respectively).[190] Smaller macrocycles have also been studied with In^{3+}; however, the low coordination number and nonideal ring size, revealed through crystal structures,[436,437] should deter future use of small macrocycles with $^{111}In^{3+}$.

The authors' research group has developed a number of ligands that form robust In^{3+} complexes. Building on an established H_2dedpa (Figure 5H) scaffold (see section 8.4), functionalization with acetate arms led to the creation of H_4octapa (Figure 5H), which can quantitatively radiolabel ^{111}In in 10 min at room temperature. $[In(octapa)]^-$ exhibits impressive complex stability at physiological pH, with higher pM values than both DTPA and DOTA.[359] Following trastuzumab bioconjugation via isothiocyanate coupling, imaging studies with ^{111}In and ^{177}Lu revealed higher tumor uptake and tumor-to-tissue ratios than DOTA-trastuzumab.[87] Several reports have since been published exploring the capabilities of this versatile ligand family by altering coordination number,[86,423] functional groups,[438] and backbone composition.[256,439]

10.5. Indium-111 Biological Studies

Thanks to its commercial availability, straightforward coordination chemistry, and compatibility with SPECT imaging, ^{111}In is commonly used to study in vivo behavior or new biological vectors, all of which will not be covered in this Review. The most recent developments in the areas of GRP receptor, SST receptor, integrin, and HER2 targeting will be discussed.

Indium-111 has been extensively used in BBN imaging studies, notably where the pharmacokinetics of BBN were improved by altering linker properties.[426,427,440] Evidence suggest that intravenous injection of BBN agonists may be biologically hazardous;[430] BBN antagonists are now under investigation for radiotracer development. A notable example is ^{111}In-DOTA-PEG$_4$-AR, which produced high-quality SPECT images with good tumor-to-tissue ratios observed after 24 h. Also promising is the use of NODAGA-PEG$_4$-AR and TE2A-PEG$_4$-AR with ^{68}Ga and ^{64}Cu, respectively.[441]

Integrin-targeting studies are increasingly utilizing ^{68}Ga or ^{64}Cu; however, Briat et al. recently used ^{111}In-RAFT-RGD and ^{111}In-DOTA-A700 to study renal uptake.[432] Co-administration with gelofusine was found to decrease renal uptake upward of 50%, greatly alleviating kidney dose. Another study used ^{111}In-DTPA-A20FMDV2 for diagnosis of idiopathic pulmonary fibrosis and revealed encouraging preclinical results, as high lung uptake was observed.[442]

Somatostatin receptor-targeting scintigraphy has been clinically practiced for over 20 years with Octreoscan (^{111}In-pentetreotide and ^{111}In-DTPA-D-Phe^1-octreotide); however, the development of ^{99m}Tc- and ^{68}Ga-tracers has significantly reduced the appeal of ^{111}In imaging.[443] Studies comparing ^{68}Ga-DOTATATE and ^{68}Ga-DOTATOC to ^{111}In-octreotide adamantly declare superiority of ^{68}Ga based on cost, radiation exposure, image quality, and acquisition speed.[444,445] Copper-64-DOTATATE was also shown to be superior to ^{111}In-octreotide. Despite these results, ^{111}In is still used clinically and for research purposes. For example, SST receptor targeting has recently changed focus from SST agonists to antagonist. Indium-111-DOTA-BASS (^{111}In-DO3A-pNO_2-Phe-c(DCys-Tyr-D-Trp-Lys-Thr-Cys)D-Tyr-NH_2) is the first clinical SST antagonist applied as a tracer. Higher tumor uptake and improved visualization of metastatic neuroendocrine tumors compared to ^{111}In-pentetreotide were reported.[446]

Because of slow antibody clearance and consequently low tumor-to-blood and tumor-to-tissue ratios, HER2 targeting has focused on the use of antibody fragments to increase clearance while maintaining specificity. The most recent reports of ^{111}In HER2 targeting include ^{111}In-PEP09239,[447] ^{111}In-ABY-002,[447,448] ^{111}In-trastuzumab,[449] and ^{111}In-ABY-025.[450] In general, high tumor uptake is observed, but the trade-off

DOI: 10.1021/acs.chemrev.8b00294
Chem. Rev. 2019, 119, 902−956

between specificity and body clearance is still a challenge. The use of the first synthetic affibody, ^{111}In-ABY-002, is especially noteworthy.[448]

11. TERBIUM

Terbium radioisotopes are of interest due to the existence of four clinically relevant radioisotopes with applications across each major modality of nuclear medicine (i.e., PET, SPECT, β^- therapy, α therapy, and Auger electron therapy). For this reason, terbium has been deemed the "Swiss knife of nuclear medicine".[451]

With respect to therapeutic radionuclides, ^{149}Tb ($t_{1/2}$ = 4.12 h) is a low-branching, low-energy α emitter (Eα = 3970 keV, 17%) with short soft-tissue range of 28 μm.[21] Terbium-149 is the only radiolanthanide with a suitable physical half-life for α therapy and is most compatible with fast-circulating bioconjugates, such as peptides. Terbium-149 also emits β^+ suitable for PET imaging (Eβ^+_{avg} = 728 keV, 7%), which may allow approximate dose quantification during therapy. Terbium-161 ($t_{1/2}$ = 165 h) is a high-branching, low-energy β^- emitter (Eβ^-_{avg} = 154 keV, 100%) that coemits therapeutic Auger electrons, which account for up to 71% of the radionuclide's biological dose.[452] Terbium-161 also emits γ-rays (Eγ = 26, 49, and 75 keV; Iγ = 23, 17, and 10%, respectively) suitable for SPECT imaging. In terms of diagnostic radionuclides, ^{152}Tb ($t_{1/2}$ = 17.5 h) is a low-branching β^+ emitter (Eβ^+_{avg} = 1142 keV, 20%) suitable for PET imaging and ^{155}Tb ($t_{1/2}$ = 128 h) is a low-energy γ emitter (Eγ = 87 and 105; Iγ = 32 and 25%, respectively) for SPECT imaging. The advantages of terbium radioisotopes are the versatility with which they can be applied; however, availability is still a major issue that has limited use.

11.1. Terbium-149/152/155 Production via Spallation

Production of ^{149}Tb, ^{152}Tb, and ^{155}Tb are most common via proton-induced spallation of tantalum targets, which has been demonstrated using the ISOLDE (Isotope Mass Separator Online Facility) facility at CERN (European Organization for Nuclear Research). After collision of 1.4 GeV protons, the spallation products are ionized, separated by mass-to-charge ratio, and implanted into a Zn-coated Au target.[3,453] Purification of Tb from the target material, decay products, and isobaric monoxide contaminants is achieved with cation-exchange chromatography, where the resin is loaded with 0.1 M HCl target solution and eluted with α-hydroxyisobutyric acid (α-HIBA) at pH 4.75.[3,453−456] Use of molten KNO_3 on aluminum as an implantation target has also been described and permits purification with high radiochemical yield (>90%) in just 1 h.[457] It has been speculated that, for clinical applicability, electromagnetic separation may be the only means of producing sufficient quantities of high-purity $^{149/152/155}$Tb. A dedicated compact facility may be a potential direction for the future.[458]

11.2. Alternative Terbium-149 Production

Beyond spallation, ^{149}Tb ($t_{1/2}$ = 4.12 h) can be produced by light particle (p, $^{3/4}$He) irradiation of ^{152}Gd targets. The advantage of the ^{152}Gd(p,4n)^{149}Tb approach is the high cross section (248 mb) at medium-high proton energy (41 MeV), which is bested only by ^{152}Gd(α,7n)^{149}Tb; however, the need for a high-energy (>100 MeV) α-beam makes broad use of the latter impractical.[457,458] The disadvantage of the (p,4n) reaction is the chemical similarity of Gd and Tb, which makes separation under a short time frame challenging.[457] The cost of enriched ^{152}Gd targets is also unappealing and has resulted in the investigation of ^{nat}Eu targets. With the use of a ^{3}He beam, the natural isotope composition of europium (47.81% ^{151}Eu, 52.19% ^{153}Eu) lends itself nicely to ^{151}Eu(^{3}He,5n)^{149}Tb and ^{153}Eu(^{3}He, 7n)^{149}Tb at medium-high beam energies (30−70 MeV). This method can efficiently produce ^{149}Tb, along with ^{152}Tb and ^{155}Tb, which could potentially be useful as match pairs for ^{149}Tb therapy.[459,460]

A variety of heavy ion beams ($^{10/11}$B, ^{12}C, $^{14/15}$N, $^{16/18}$O, and ^{19}F) can also be used to directly produce ^{149}Tb, typically via irradiation of early lanthanide targets. Unfortunately, coproduction of ^{149m}Tb is common and rather detrimental, as it hinders ^{149g}Tb production and has an extremely low probability of decaying to ^{149g}Tb.[461,462] The most promising method of ^{149}Tb production is an indirect route, which follows ^{nat}Nd(^{12}C, xn)^{149}Dy ($t_{1/2}$ = 4.23 min, EC 56%) → ^{149}Tb and is favored over direct methods due to the large cross section.[463] Production of 2.6 MBq was demonstrated with 1.25 h of irradiation (108 MeV, 1uA) followed by 20 min of wait time.[463,464] Cation-exchange chromatography was used to separate the ^{149}Tb from the Nd_2O_3 target and coproduced radiolanthanides. Following target dissolution in 2 M HCl, the solution was loaded onto the resin, washed with NH_4Cl (0.1−1.2 M), and eluted with α-HIBA (0.2−0.4 M). Terbium-149 is separated from other rare-earth elements during this process by altering the eluent concentration. Given these results, it was proposed that under optimized conditions (97% ^{142}Nd, 50−100 uA, 8−10 h) a dedicated cyclotron would permit routine clinical use of ^{149}Tb by continuous batch production of 10−20 GBq.[457]

11.3. Alternative Terbium-152/155 Production

Alternate routes to $^{152/155}$Tb production have also been studied as a means of avoiding cumbersome ISOLDE separation. The PET radionuclide, ^{152}Tb, can be produced by ^{139}La(^{16}O,3n), ^{143,144}Nd(^{12}C, xn)^{152}Dy → ^{152}Tb, ^{152}Gd(p,n), and ^{155}Gd(p,4n).[455,458,465,466] Production of the SPECT radionuclide, ^{155}Tb, using gadolinium targets is of interest due to the relatively high natural isotope composition of ^{155}Gd (14.8%). Deuteron-induced reactions have proved to be nonideal, as both ^{155}Gd(d,2n)^{155}Tb and ^{155}Gd(d,n)^{156}Tb occur at similar beam energies and produce radioisotopes with similar half-lives. Nca ^{155}Tb is therefore unachievable using this production strategy.[467] ^{155}Gd(p,n)^{155}Tb appears to be a promising approach, provided a highly enriched (∼100%) target is used.[466] In terms of indirect methods, the ^{156}Dy(γ,n)^{155}Dy → ^{155}Tb photonuclear reaction was realized in 1981; however, despite excellent radionuclide purity, low production quantities hampered clinical applicability.[458] Despite the need for high-energy protons, the indirect ^{159}Tb(p,5n)^{155}Dy → ^{155}Tb route appears to be the most favorable nca approach.[468]

11.4. Terbium-161 Production

Of the discussed terbium radioisotopes, ^{161}Tb is the only one with large-scale production capabilities. Terbium-161 is not produced by proton-induced spallation of tantalum and is generally obtained indirectly via ^{160}Gd(n,γ)^{161}Gd → ^{161}Tb.[469] The use of enriched ^{160}Gd is key for this process, because the thermal neutron cross section of ^{157}Gd (15.68%) is massive (254 000 b) and will produce a significant amount of stable ^{158}Gd, the natural abundance of which is already high (24.87%). The natural and beam-produced ^{158}Gd then form stable terbium via ^{158}Gd(n,γ)^{159}Gd → ^{159}Tb, resulting in

DOI: 10.1021/acs.chemrev.8b00294
Chem. Rev. 2019, 119, 902−956

Table 11. Selected Tb^{3+} Chelators, Metal Complex Geometry, and Thermodynamic Parameters

metal ion	chelator	coordinating nuclei	geometry	log K_{ML}	pM	reference
Tb^{3+}	DOTA	N_4O_4	monocapped square antiprism[a]	23.6−27.0		490−492, 496, 707−709
	DTPA	N_3O_5	monocapped square antiprism[b]	22.8		495, 699, 710

[a]On the basis of $[Tb(DO3AP)]^-$. [b]On the basis of $[Gd(DTPA)]^{2-}$.

isotopic dilution of ^{161}Tb and low molar activity.[319] Similar to $^{149/152/155}Tb$ purification following proton-induced spallation, ^{161}Tb is purified from the Gd target using cation-exchange chromatography. A Ln resin based on di(2-ethylhexyl)-orthophosphoric acid (HDEHP) has also shown excellent separation of ^{161}Tb from Gd.[470]

11.5. Terbium Chemistry and Chelator Development

Terbium is most commonly found as a trivalent cation (Tb^{3+}), has an ionic radius of 0.92−1.10 Å (CN = 6−9), and favors a coordination number of 8 or 9.[471] As with Y^{3+}, this diffuse charge distribution makes hydroxide formation (pK_a = 7.9, $Tb^{3+}_{(aq)} \rightarrow TbOH^{2+}_{(aq)}$) nonproblematic. Characteristic of lanthanides, Tb^{3+} exhibits a preference for oxygen-based bonding, dominated by electrostatic interactions (I_A = 10.07−10.30). Interestingly, Bünzli reported that, as of 2014, 75% of all structurally characterized lanthanide complexes had at least one Ln−O bond and 40% had exclusively Ln−O bonds.[472] Terbium is best known for its luminescent properties, which have led to its application in biomedical probes and supramolecular luminescent sensors.[473,474] Tuning of these radiative properties has been investigated with a variety of chelators,[475−479] including DOTA[480−486] and DTPA (Table 11).[484,485,487−489]

Terbium-based radiotracers almost exclusively use DOTA (Figure 4A) for chelation. No solid-state structure of $[Tb(DOTA)]^-$ has been reported; however, the bonding environment is presumed to be monocapped twisted square antiprism based on crystallographic data for $[Tb(DO3AP)(H_2O)]^-$ and $[Tb(DOTG)(H_2O)]^-$. Typical bond distances reveal closer proximity of Tb^{3+} to the oxygen plane ($Tb-O_{avg} \approx 0.8$ Å, $Tb-N_{avg} \approx 1.6$ Å).[490−492] DOTA forms robust complexes with Tb^{3+} (log K_{ML} = 23.6−27.0) and can achieve quantitative radiolabeling at low concentrations, but does require elevated temperatures.[20,93,453,454,493,494]

Of the few studies that use alternative chelators, CHX-A″-DTPA (Figure 5B) is most favored and is typically employed as a result of heat-sensitive targeting vectors.[495] DTPA (Figure 5A) stability among the lanthanides peaks between Tb^{3+} and Ho^{3+} (log K_{ML} = 22.8),[495,496] making CHX-A″-DTPA use appealing, given the rapid radiolabeling capabilities at ambient temperatures.[75] New ligand development or existing ligand application for terbium-based radiopharmaceuticals should be of interest in the future, especially considering the chemical similarity of Tb^{3+} to Lu^{3+}.

11.6. Terbium-149/152/155/161 Biological Studies

The therapeutic potential of ^{149}Tb has yet to be realized in humans but has proven to be encouraging in animal models. Treatment with ^{149}Tb-CHX-A″-DTPA-rituximab 2 days post-injection of Daudi cells (human lymphoma model) led to 89% of mice having no pathological changes after 120 days. This is quite impressive compared to the control group, which all died within 40 days. Bone, spleen, and liver accumulation were problematic, as 28.4 ± 4% of long-lived daughter radionuclide activity (^{145}Sm, ^{149}Eu) remained in the body; however, it was suggested that post-tracer administration of EDTA or DTPA may remedy this accumulation.[497] Animal studies with ^{149}Tb-DOTA-folate have demonstrated a dose-dependent relationship, with both tumor growth and survival time.[453] Most recently, ^{149}Tb-DOTANOC has demonstrated the ability to accumulate in AR42J xenografts and was imaged using PET/CT.[93] Comparison of ^{149}Tb- and ^{213}Bi-labeled antibodies (d9 mAb) revealed that ^{149}Tb treatment led to a lower degree of cell killing due to low α-branching (17%).[75] This conclusion may serve as a drawback; however, if highly specific targeting is achieved, an advantage could be realized through decreased cross-fire effects. This is especially true when considering the off-target dose received from short-lived ^{213}Bi (see section 13) due to slow circulation of antibodies. The longer physical half-life of ^{149}Tb is more congruent with antibody circulation and may be more suitable for radioimmunotherapy despite lower cell-killing capabilities.[75]

Terbium-161 β^- therapy has received attention due to significant coemission of conversion and Auger electrons. Monte Carlo (CELLDOSE) calculations estimate that, for small metastases, 71% of the ^{161}Tb dose comes from conversion electron (CE) or Auger electrons. As tumor size decreases, the effectiveness of ^{161}Tb over ^{47}Sc and ^{67}Cu increases due to higher effectiveness of low-range radiation.[452] Similar advantages were noted in a comparison of ^{161}Tb with ^{90}Y, ^{177}Lu, and ^{111}In.[498] In vitro experiments on radiolabeled DOTA-folate (cm09) exhibited superior IC_{50} for ^{161}Tb versus ^{177}Lu in KB and IGROV-1 cell lines, requiring 4.5- and 1.7-fold less activity to exert the same therapeutic effect, respectively. Comparable SPECT images were obtained during in vivo experiments for both radiotracers, but ^{161}Tb-DOTA-folate reduced tumor growth more efficiently than ^{177}Lu-DOTA-folate.[494] Terbium-161 is also less toxic to kidneys than ^{177}Lu due to the large dose contribution from CE and Auger electrons. Through a comparison of equal activity administration, it was shown that, despite the higher renal dose, ^{161}Tb (3.0 Gy/MBq) therapy displayed comparable renal toxicity to ^{177}Lu (2.3 Gy/MBq) therapy, suggesting the emission of low-energy electrons led to no adverse side-effects.[20]

In a preclinical study of ^{152}Tb-DOTANOC, spallation of Ta-targets at ISOLDE/CERN produced 600 MBq of ^{152}Tb after purification. Quantitative radiolabeling with DOTANOC was confirmed by HPLC, and animal studies showed good tumor uptake in AR42J tumor-bearing mice.[93] Not only did this study produce record amounts of purified ^{152}Tb and demonstrate efficacious use, it seems to have spurred the first in-human trial, where PET/CT images of ^{152}Tb-DOTATOC showed clear tumor uptake in small tumor metastases, especially 24 h postinjection.[493] Although high background signals were observed as a result of low positron branching ratio (20.3%), the prospect of identifying a (nearly) identical theranostic pair with $^{149}Tb/^{161}Tb/^{177}Lu$ capable of long-time-point imaging makes the use of ^{152}Tb for PET attractive.

The utility of the four combined radioisotopes was demonstrated in a study that conducted ^{149}Tb and ^{161}Tb therapy and imaged tumors using ^{152}Tb for PET/CT and

DOI: 10.1021/acs.chemrev.8b00294
Chem. Rev. 2019, 119, 902−956

Table 12. Selected $^{149/152/155/161}$Tb Radiopharmaceuticals with Targets and Relevant Labeling Parameters[a]

radioisotope	chelator (BFC)	standard labeling conditions	bioconjugate	target	molar/specific activity (% RCY)	reference
^{149}Tb	DOTA (DO3A)	0.15 M α-HIBA pH 5, 95 °C, 15 min	folate (cm09)	FR	0.48 GBq/μmol (>96)	3
	CHX-A′′-DTPA (*p*-SCN-Bn)	3 M NH_3OAc pH 5.5, RT, 10 min	Rituximab	CD20	1.11 GBq/mg (99)	497
^{152}Tb	DOTA (DO3A)	0.15 M α-HIBA pH 4.75, 95 °C, 15 min	folate (cm09)	FR	1.33 GBq/μmol (>96)	3
			NaI^3-octreotide (NOC)	SSTR	10 GBq/μmol	93
		0.4 M NaOAc pH 4.6, 95 °C, 40 min	Phe^1-Tyr^3-octreotide (TOC)	SSTR	10 GBq/μmol	493
^{155}Tb	DOTA (DO3A)	0.15 M α-HIBA pH 4.75, 95 °C, 15 min	folate (cm09)	FR	0.64 GBq/μmol (>96)	3
^{161}Tb	DOTA (DO3A)	0.5 M NaOAc pH 5, 95 °C, 15 min	folate (cm09)	FR	6−27 GBq/μmol (>98)	3

[a]FR (folate receptor) and SSTR (somatostatin receptor).

Table 13. Selected Lu^{3+} Chelators, Metal Complex Geometry, and Thermodynamic Parameters

metal ion	chelator	coordinating nuclei	geometry	log K_{ML}	pM	reference
Lu^{3+}	DOTA	N_4O_4	square antiprism	21.6−29.2	17.1	87, 518, 521, 707, 711
	DTPA	N_3O_5	tricapped trigonal prism[a]	22.4−22.6	19.1	521, 699, 703, 712
	NETA	N_4O_4	tricapped trigonal prism?			355, 356
	DE4TA	N_4O_5/N_5O_4?	square antiprism?			354
	PCTA	N_4O_3	square antiprism?			79, 524
	H_4octapa	N_4O_4	square antiprism	20.1−20.5	19.8	87, 361, 439

[a]On the basis of $[Yb(DTPA)]^{2-}$.

^{155}Tb for SPECT/CT. Although no meaningful comparison of effectiveness of ^{149}Tb/^{161}Tb could be made due to low sample size, both groups showed decreased tumor growth and significantly increased survival time compared to untreated control groups. Phantom studies of ^{152}Tb were not ideal; however, the 24 h PET/CT time point of ^{152}Tb revealed good tumor uptake.[3] Overall the benefits of $^{149/152/155/161}$Tb-based theranostics are exciting; unfortunately, concerns over production yields, costs, and the need for highly sophisticated facilities at present has led to uncertainty regarding potential clinical use.[7]

12. LUTETIUM

Lutetium-177 ($t_{1/2}$ = 159 h) decays purely via β^- emission, releasing low-energy electrons ($E\beta^-_{avg}$ = 134 keV, 100%) and coemitting low-energy gammas (Eγ = 113 and 208 keV; Iγ = 6 and 10%, respectively) that are useful for SPECT imaging and dose determination.[79] The physical half-life of ^{177}Lu makes it compatible with both short- and long-circulating bioconjugates and allows off-site production centers to distribute activity to clinics over a long range.[319] Lutetium-177 is generally seen as superior to ^{90}Y (see section 9) due to the lower β^- energy, which results in shorter tissue range and decreased cross-fire to healthy cells. This results in lower toxicity and improved patient tolerance during clinical treatment.[499−501] Very recently, the first ^{177}Lu-based drug, Lutathera (^{177}Lu-DOTATATE), received FDA approval for treatment of somatostatin receptor-positive gastroenteropancreatic neuroendocrine tumors.[502] Given the success of ^{177}Lu therapeutics and the adequate commercial availability, signs point to continued clinical trials and approval of ^{177}Lu-based therapeutics in the years to come.

12.1. Lutetium-177 Production

Reactor production of ^{177}Lu is accomplished by both direct and indirect methods. Direct reactor production is the most inexpensive, high-yielding, and common route of generating ^{177}Lu.[503] Irradiation of enriched $^{176}Lu_2O_3$ follows ^{176}Lu-(n,γ)^{177}Lu, which has a thermal neutron capture cross section of ∼2020 b and resonance integral of ∼1087 b.[16,41,504] A drawback of this method is the production of ca activity, which generally results in specific activity of 0.74−1.1 TBq/mg—only a quarter of the theoretical 4.07 TBq/mg. Specific activity levels of 2.59 TBq/mg at high thermal neutron flux (2 × 1015 n/cm^2 s) have been reported.[505] Coproduction of the long-lived radioisotope ^{177m}Lu ($t_{1/2}$ = 160.5 days) is another drawback; however, by using medium-flux reactors, the impurity can be kept to <0.02%.[506] Conveniently, no postirradiation processing is necessary due to the elementally pure target. The high yield of direct reactor production has made it the most commercially viable means of ^{177}Lu production.

The reactor-based indirect strategy involves irradiation of Yb_2O_3 targets to induce ^{176}Yb(n,γ)^{177}Yb → ^{177}Lu. The main advantages of this method are the low levels of ^{177m}Lu produced and the high specific activity. Although challenging, many have demonstrated separation to yield nca ^{177}Lu.[507−514] For example, small-scale reversed-phase ion pair chromatography has led to ^{177}Lu with high radionuclidic purity and an 84% yield. The dissolved Yb_2O_3 target (5 mg) was loaded onto a reverse-phase column and ^{177}Lu eluted with 0.25 M α-HIBA/0.1 M octanesulfonate.[510] Liquid−liquid extraction has also proved useful for Yb/Lu separation, with 1 M HCl and 1% HDEHP (di[2-ethylhexyl]orthophosphoric acid) in cyclohexane preferentially extracting Lu into the organic phase.[507] The most developed separation strategy is a three-step extraction chromatography method, where each separation stage (front-end, primary, and secondary) involves multicolumn use. This purification method is favored because of its effective separation factor (10^6) and activity with high radionuclidic purity, which is eluted in a form amenable to standard radiolabeling conditions. The excellent separation is also useful for recycling of ^{176}Yb. The process has achieved a 73% yield from a 300 mg target within 4 h.[509] The main

DOI: 10.1021/acs.chemrev.8b00294
Chem. Rev. 2019, 119, 902−956

disadvantage of the indirect method is the relatively low cross section (2.85 b) combined with a need for enriched ^{176}Yb. This high cost and relatively low-yielding process makes production expensive. Some commercial sources are available for studies requiring nca ^{177}Lu.

Cyclotron production of ^{177}Lu has also been demonstrated, but use of these routes is quite limited. The typical (p,n) approach is impossible for ^{177}Lu production because ^{177}Yb is a short-lived radioactive nuclide. Production via ^{nat}Yb(d,n), ^{nat}Hf(p,2pxn), and ^{181}Ta(p,3p2n) has been explored, but the coproduction of various Yb and Lu radioisotopes necessitates the use of enriched targets, which are too expensive to justify their use for such low-yielding reactions.[515,516] Indirect production via ^{176}Yb(d,p)^{177}Yb → ^{177}Lu has also been explored.[517] Even though production of undesired radioisotopes can be avoided below a deuteron beam energy of 11 MeV and high specific activity is achievable, the low cross section for this reaction makes it inferior to reactor-based production methods.

12.2. Lutetium Chemistry and Chelator Development

Lutetium is most commonly found as a trivalent cation (Lu^{3+}) and is the smallest of the lanthanide series with an ionic radius of 0.86−1.03 (CN = 6−9). Lutetium(III) prefers a coordination number between 8 and 9, with a slight preference for 8, as is common with the late lanthanides.[471] As mentioned, the ionic bonding preference of Lu^{3+} (I_A = 10.07) is typical of the lanthanides, which prefer oxygen-donating groups due to their ionic-donating compatibility. As with Y^{3+} and Tb^{3+}, the high pK_a (7.6, $Lu^{3+}_{(aq)}$ → $LuOH^{2+}_{(aq)}$) of aquated Lu^{3+} makes metal hydrolysis nonproblematic during radiolabeling.

The most commonly used chelators for ^{177}Lu radiotracers are DOTA (Figure 4A) and DTPA (Figure 5A) analogues. The molecular structure of $[Lu(DOTA)(H_2O)]^-$ demonstrates water-capped square antiprismatic geometry.[518] As with other rare-earth metals, the high stability and inertness of $[Lu(DOTA)]^-$ (log K_{ML} = 21.6−29.2) has led to frequent use. Lutetium-177 has a physical half-life that is well-suited to the biological half-life of most antibodies; therefore, the slow labeling kinetics of DOTA, which necessitate heating, are not ideal for many ^{177}Lu applications. When appropriate, however, the preference for DOTA is supported not only by thermodynamics but also by high kinetic inertness against serum proteins.[519,520] This degree of long-term stability is especially crucial due to the long half-life of ^{177}Lu, which would lead to prolonged and elevated dose if released in vivo.

In cases where heat-sensitive bioconjugates are employed, DTPA analogues can be used to rapidly radiolabel at room temperature. The structure of $[Lu(DTPA)]^{2-}$ is unknown; however, based on the $[Yb(DTPA)]^{2-}$ solid-state structure, tricapped trigonal prismoidal metal center geometry with N_3O and O_4 planes is assumed. Compared to DOTA, $[Lu(DTPA)]^{2-}$ complexes exhibit decreased thermodynamic stability (log K_{ML} = 22.4−22.6) and kinetic inertness (serum stability and acid dissociation);[519−521] however, radiolabeling ^{177}Lu in the presence of Ca^{2+}, Zn^{2+}, and Fe^{2+} revealed superior selectivity of DTPA over DOTA.[521] Other studies have also confirmed that metal competition from Zn^{2+}, Cu^{2+}, Co^{2+}, Pb^{2+}, and Ni^{2+} can obstruct DOTA labeling of ^{177}Lu, highlighting the promiscuous chelation of DOTA.[522] CHX-A″-DTPA is preferred for ^{177}Lu labeling over less-rigid DTPA analogues due to its superior kinetic inertness, which is reflected during in vitro challenge studies and in vivo experiments.[520]

Other studies have used less conventional ligands for ^{177}Lu with variable success. Pandey et al. compared *p*-SCN-Bn-NOTA with *p*-SCN-Bn-CHX-A″-DTPA and unsurprisingly found the latter better resisted decomplexation, likely due to the inadequate coordination number and small ring size of NOTA.[523] As discussed with ^{90}Y, NETA (Figure 4K) and DE4TA (Figure 4C) have also shown promise for use with ^{177}Lu. NETA and the RGD-bioconjugated analogue, 3p-C-NETA-c(RGDyK), were found to quantitatively radiolabel ^{177}Lu at ambient temperature within 1 min and showed minimal signs of decomplexation during in vitro and in vivo studies.[356] Follow-up experiments compared 3p-*C*-NETA-trastuzumab and 3p-*C*-DEPA-trastuzumab with DOTA-p-SCN-Bn-trastuzumab and DTPA-p-SCN-Bn-trastuzumab. 3p-*C*-NETA-trastuzumab and DTPA-p-SCN-Bn-trastuzumab were radiolabeled >99% within 1 min, while 3p-*C*-DEPA-trastuzumab required 30 min and DOTA-p-SCN-Bn-trastuzumab required 60 min to reach maximum labeling (97.9% and 97.8%, respectively). In vivo studies with ^{177}Lu-3p-*C*-NETA-trastuzumab showed excellent tumor uptake (10.10 ± 0.45% ID/g) and good clearance from blood, liver, and kidneys with no sign of bone accumulation after 120 h.[355] Ten-coordinate 3p-*C*-DEPA is an nonideal match for ^{177}Lu; however, the nine-coordinate analogue, 3p-*C*-DE4TA, shows improved in vitro stability with ^{177}Lu and good in vivo clearance of the naked BFC after 24 h.[354] No experiments with targeting vectors have been published to date.

PCTA (Figure 4G) has recently been considered for use with ^{177}Lu. Labeling, stability, and biodistribution of naked *p*-SCN-Bn-PCTA is comparable to those of *p*-SCN-Bn-DOTA. It was also demonstrated that in vitro cell binding of cetuximab and panitumumab was not affected by use of PCTA versus DOTA.[524] Despite good in vivo clearance of ^{177}Lu-(*p*-SCN-Bn-PCTA) after 24 h, no bioconjugated analogue has been reported.[79]

As with ^{90}Y and ^{111}In, H_4octapa (Figure 5H) has been found to form highly stable Lu^{3+} complexes (log K_{ML} = 20.1−20.5), notably at physiological pH (pM = 19.8). Near-quantitative radiolabeling at low ligand concentrations of ^{177}Lu can be achieved at ambient temperature in 15 min. Low decomplexation rates during in vitro competition studies with serum proteins are also impressive. A comparison between ^{177}Lu-octapa-trastuzumab and ^{177}Lu-DOTA-trastuzumab revealed significantly higher tumor uptake of the former after 24 h, leading to speculation that some degree of antibody damage incurred during DOTA radiolabeling. Decreased kidney and slightly increased bone uptake were also observed for ^{177}Lu-octapa-trastuzumab.[87]

12.3. Lutetium-177 Biological Studies

Research surrounding the use of ^{177}Lu-DOTATATE has been an intense area of research in recent years[525−534] and has led to FDA approval for treatment of inoperable, progressive SST receptor-positive midgut carcinoid tumors, sold under the trade name Lutathera.[502] During a randomized phase III trial that took place over >3 years with 229 patients, the estimated rate of progression-free survival was 65.2% for the treatment group and 10.8% for the control group, after 20 months.[532] A related therapeutic, ^{177}Lu-DOTATOC, recently underwent phase II clinical trials for treatment of gastroenteropancreatic neuroendocrine tumors and is currently recruiting for phase III.[245,535] Treatment of prostate cancer with ^{177}Lu-PSMA-I&T and ^{177}Lu-PSMA-617 is another highly active area of research,

DOI: 10.1021/acs.chemrev.8b00294
Chem. Rev. 2019, 119, 902−956

Table 14. Selected ^{177}Lu Radiopharmaceuticals with Targets and Relevant Labeling Parameters[a]

radionuclide	chelator (BFC)	standard labeling conditions	bioconjugate	target	molar/specific activity (% RCY)	reference
^{177}Lu	DOTA (DO3A)	0.5 M NaAscorbate pH 4.5, 80−95 °C, 30 min	Tyr^3-octreotate (TATE)	SSTR	19.5 GBq/mg (>98)	501
			PSMA-617	PSMA	89.7 ± 13.6 GBq/mg (>95)	537
		0.3 M NH_4OAc pH 7, 37 °C, 20 min	J591	PSMA	185−481 MBq/mg (78 ± 8)	550
	NETA (3p-C)	0.25 M NH_4OAc pH 5.5, RT, 15 min	Trastuzumab	HER2	23.7 GBq/μmol (92)	355
	H_4octapa (p-SCN-Bn)	0.2 M NH_4OAc pH 5.5, RT, 15 min	Trastuzumab	HER2	130 MBq/mg (95)	87

[a]SSTR (somatostatin receptor); PSMA (prostate-specific membrane antigen); and HER2 (human epidermal growth factor receptor 2).

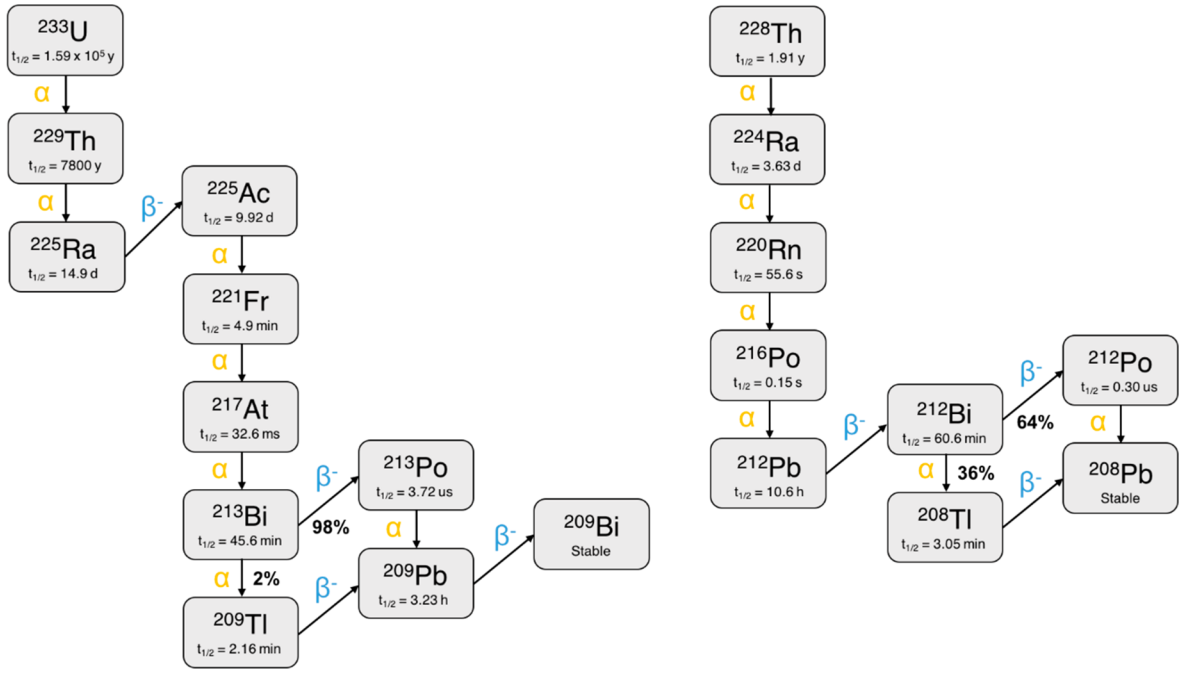

Figure 7. ^{233}U and ^{228}Th decay chains.

with the latter currently awaiting phase II trials.[536−544] Several reviews have discussed these therapeutics in detail.[545−548] Other noteworthy compounds coming down the proverbial pipeline are ^{177}Lu-J591 for radioimmunotherapy of prostate cancer[549−553] and the SST antagonist ^{177}Lu-OPS201.[73,554,555]

Very recently, click-mediated pretargeted radioimmunotherapy of colorectal carcinoma has been demonstrated with huA33-TCO and ^{177}Lu-DOTA-PEG$_7$-Tz. This approach combines the favorable pharmacokinetics of small molecules with the specificity and affinity of antibodies. Monoclonal antibody pretargeting is performed 24 h prior to injection of the radioactive component, which then selectively undergoes a Diels−Alder reaction with the *trans*-cyclooctene-functionalized antibody to achieve highly selective accumulation while retaining rapid background clearance. This appears to be an extremely promising therapeutic strategy, as treatment led to a 100% survival rate over 70 days, while no mice from the control group survived past 47 days.[556] Future work should be of great interest.

13. BISMUTH

There are two therapeutic radioisotopes of bismuth that have been studied for TAT. Bismuth-212 ($t_{1/2}$ = 1.01 h) is part of the natural thorium (^{232}Th) decay chain and is the direct daughter radionuclide of ^{212}Pb. Although ^{212}Pb has been thoroughly investigated as an in vivo generator for ^{212}Bi, it will not be further discussed.[557] Bismuth-212 decays to stable ^{208}Pb by two independent pathways; the major route involves emission of high-energy β^- (Eβ^- = 771 keV, 64%) to ^{212}Po ($t_{1/2}$ = 0.3 μs), followed by α decay (Eα = 8780 keV, 100%). The minor route involves α emission (Eα_{avg} = 6210 keV, 36%) to ^{208}Tl ($t_{1/2}$ = 3.05 m), followed by high-energy β^- particle decay (Eβ^-_{avg} = 560 keV, 100%). Low-energy gammas emitted from the intermediate daughter ^{208}Tl are useful for scintigraphy; unfortunately, a high-energy, high-intensity gamma (Eγ = 2614 keV; Iγ = 99%) is also emitted and places high shielding requirements on nuclear medicine staff. This is seen as a major drawback to clinical applicability of ^{212}Bi.[319]

Bismuth-213 ($t_{1/2}$ = 0.76 h) is a daughter radionuclide of ^{225}Ac (see section 14) and decays to stable ^{209}Bi primarily through medium-energy β^- emission (Eβ^-_{avg} = 435 keV, 98%) to ^{213}Po ($t_{1/2}$ = 4.2 μs), followed by α emission (Eα = 8350 keV, 100%) to ^{209}Pb. A minor route (2%) to ^{209}Pb occurs by α decay (Eα = 5848 keV, 2%) to ^{209}Tl, followed by β^- particle decay. Lead-209 ($t_{1/2}$ = 3.23 h) emits a medium-energy β^- (Eβ^-_{avg} = 198 keV, 100%) to yield ^{209}Bi. Due to the nonstagnant nature of radiopharmaceuticals in vivo and the relatively long physical half-life of ^{209}Pb, this β^- has a lower probability of reaching target cells and exerting a therapeutic effect. Bismuth-213 also emits a medium-energy γ-ray (Eγ =

DOI: 10.1021/acs.chemrev.8b00294
Chem. Rev. 2019, 119, 902−956

Table 15. Selected Bi^{3+} Chelators, Metal Complex Geometry, and Thermodynamic Parameters

metal ion	chelator	coordinating nuclei	geometry	log K_{ML}	pM	reference
Bi^{3+}	DOTA	N_4O_4	square antiprism	30.3	27.0	84, 587
	Me-DO2PA	N_6O_2	square antiprism	34.2	28.6	587, 591
	DTPA	N_3O_5	square antiprism	33.9−35.2		592, 597
	CHX-DTPA	N_3O_5	square antiprism	34.9−35.6		592, 597
	NETA	N_4O_4	square antiprism?			358, 598−601
	DEPA	N_4O_5/N_5O_4?	distorted dodecahedron?			60, 358, 598, 602
	H_4neunpa	N_5O_4	distorted dodecahedron?	28.8	27	86

440 keV; Iγ = 26.5%), which can be used for imaging.[319] It should be noted that ^{205}Bi ($t_{1/2}$ = 15.3 days), ^{206}Bi ($t_{1/2}$ = 6.2 days), and ^{207}Bi ($t_{1/2}$ = 31.6 years) are sometimes used as long-lived surrogates for $^{212/213}$Bi.

The short half-lives of both radioisotopes make them most suitable for bioconjugates with fast in vivo kinetics; however, simultaneous interest in $^{212/213}$Bi and radioimmunotherapy appears to have influenced substantial investigation in radiolabeling of slower-circulating antibodies.[49,62,558−573] The therapeutic effects of $^{212/213}$Bi come from a combination of α and β^- particle decay, which is beneficial for treatment of large tumors but can lead to cross-fire effects for smaller tumors or metastasis. Despite the therapeutic potential of $^{212/213}$Bi, radioisotope cost and availability have hampered drug development.[319,574]

13.1. Bismuth-212/213 Production

Bismuth-212 ($t_{1/2}$ = 60.6 min) and ^{213}Bi ($t_{1/2}$ = 45.6 min) are both short-lived radioisotopes that heavily rely on generators for production. Briefly, ^{212}Bi can be obtained from ^{224}Ra ($t_{1/2}$ = 3.6 days), a daughter radionuclide of the ^{228}Th ($t_{1/2}$ = 1.9 years) decay chain.[575] The ^{224}Ra is separated from ^{228}Th by dissolving the thorium in 8 M HNO_3 and running the solution through an anion-exchange resin, which retains anionic thorium(IV) nitrate while eluting $^{224}Ra^{2+}$ and accompanying daughter nuclides. As seen in Figure 7, the first α-decay of ^{224}Ra is followed by two additional α-particles from ^{220}Rn ($t_{1/2}$ = 55.6 s) and ^{216}Po ($t_{1/2}$ = 0.15 s) to produce ^{212}Pb ($t_{1/2}$ = 10.6 h), which undergoes β^-decay to ^{212}Bi. The ^{212}Bi generator is prepared by loading the ^{224}Ra onto a cation-exchange resin and ^{212}Bi eluted using 0.5−2 M HCl or HI. Elution of ^{212}Pb can be minimized by using lower acid concentration; however, both radionuclides are often eluted and labeled in transient equilibrium.[576−578] Interestingly, ^{212}Bi can also be obtained by isolating gaseous or aqueous ^{220}Rn; however, these methods have not been further explored due to limited ^{228}Th availability.[579−582] As discussed, the ^{212}Bi daughter, ^{208}Tl, emits high-energy, high-intensity gammas and places high shielding requirements on nuclear medicine staff. This is seen as a major drawback to clinical applicability of ^{212}Bi, and for this reason, ^{213}Bi is the preferred bismuth radioisotope and will be the focus of further discussion.

Bismuth-213 ($t_{1/2}$ = 45.6 m) can be obtained from ^{225}Ac ($t_{1/2}$ = 10.0 days), which is part of the ^{229}Th ($t_{1/2}$ = 7340 years) decay chain (see section 14). The ^{213}Bi generator is produced by batch-loading ^{225}Ac onto a cation-exchange resin and eluting ^{213}Bi with a 0.1 M NaI/0.1 M HCl solution. Elution of ^{213}Bi comes in the form of $[BiI_5]^{2-}$, which is not strongly retained on the cation-exchange resin and allows separation not only from ^{225}Ac but from ^{221}Fr as well. Interestingly, batch-loading the resin (which leads to more uniform distribution of ^{225}Ac throughout the resin) is essential, as top-loading results in severe resin radiolysis and limits the long-term viability of the generator system.[62] Although ^{225}Ac breakthrough remains somewhat problematic, it can be minimized by prewashing the resin with dilute HCl and employing a postcolumn guard resin. Another issue is the presence of the ^{213}Bi daughter radionuclide, ^{209}Pb ($t_{1/2}$ = 3.25 h), which is a result of β^- particle decay to ^{213}Po ($t_{1/2}$ = 4.2 μs, 98%), followed by α-decay. Although not ideal, removal of ^{209}Pb postradiolabeling appears to be an adequate strategy.[583] Despite the therapeutic potential of ^{213}Bi, the cost of the ^{225}Ac/^{213}Bi generator is considered its main drawback and has largely hindered development.[319,574]

13.2. Bismuth Chemistry and Chelator Development

Bismuth is most commonly found as a trivalent cation (Bi^{3+}) due to the inert pair effect. Several pentavalent bismuth (Bi^{5+}) species are known oxidizing agents and will oxidize water to revert to their preferred trivalent species.[584,585] The ionic radius of Bi^{3+} is 0.96−1.17 Å (CN = 5−8), and although some low-coordinate Bi^{3+} complexes have been reported, the most stable species are typically octadentate. Like In^{3+}, Bi^{3+} exhibits borderline-hard bonding preferences due to a relatively high covalent bonding contribution. The first pK_a of aquated Bi^{3+} is extremely low (pK_a = 1.1, $Bi^{3+} \rightarrow BiOH^{2+}_{(aq)}$) and results in metal ion hydrolysis beginning at pH 0.[586] Weakly coordinating buffers, such as citrate or acetate, are used to prevent hydrolysis at typical labeling pH (3−5).[587]

Chelator development for $^{213}Bi^{3+}$ radiopharmaceuticals has seen sustained interest over the years, likely due to the adequate, but nonideal performance of DOTA (Figure 4A) and DTPA (Figure 5A). Crystallographic data of [Bi(DOTA)]$^-$ reveals that the Bi^{3+} center adopts square antiprism geometry. Interestingly, Bi^{3+} is more deeply embedded in the macrocycle than smaller metals, such as Lu^{3+}, due to the soft Lewis acid character of Bi^{3+}, which prefers coordination by nitrogen. Conversely, Lu^{3+} prefers acetate arm coordination, causing Lu^{3+} to lie further outside the ring despite its smaller size.[84] The ability of DOTA to stably complex Bi^{3+} (log K_{ML} = 30.3) and adequately resist decomplexation in vivo has been demonstrated and has even been shown to assist in superior treatment of critically located gliomas or prostate cancer than β^- emitters (i.e., ^{90}Y and ^{177}Lu).[588,589] Rather than signify [^{213}Bi(DOTA)]$^-$ as an ideal chelator−radiometal pair, these outcomes are a consequence of the short radionuclide half-life, which only requires a few hours of stable coordination to exert a therapeutic effect. In vivo studies with a longer-lived bismuth radioisotope, ^{206}Bi ($t_{1/2}$ = 6.42 days), reveal a substantial degree of ^{206}Bi kidney accumulation (12.08%ID/g) after just 4 h.[46] Similar biodistribution occurs when the [15]aneN$_5$ macrocycle, PEPA (1,4,7,10,13-pentaazocyclopentadecane pentaacetic acid; Figure 4M), is labeled with ^{206}Bi and studied in vivo, indicating an equally (if not more) labile metal−ligand match.[590] Recently, DOTA derivatives bearing pyridine arms have shown very selective ^{207}Bi radiolabeling.[71] Another

DOI: 10.1021/acs.chemrev.8b00294
Chem. Rev. 2019, 119, 902−956

interesting derivative is Me-DO2PA (Figure 4B), which is a [12]aneN$_4$ backbone bearing two picolinic acid arms and two methyl-capped amines. Increased Bi^{3+} complex stability over DOTA was reported.[587,591] Although DOTA analogues are passable as $^{212/213}$Bi chelators, several superior options are available.

DTPA analogues have seen considerable use as Bi^{3+} chelators. The solid-state structure of $[Bi(CHX\text{-}DTPA)]^-$ reveals square antiprism geometry about the Bi^{3+} center, with evidence supporting the presence of a lone pair due to dodecahedron-like distortion. The closely matched Bi−O (2.4−2.5 Å) and Bi−N bond lengths (2.5−2.6 Å) are a result of softer bonding preferences of Bi^{3+} versus harder metals (e.g., Sc^{3+}, Y^{3+}, and Lu^{3+}). The lack of H_2O coordination despite the large size of Bi^{3+} is either a result of a coordinatively saturated metal center or the more preorganized binding site with less potential for hydrate species to form.[592] The high stability of $[Bi(DTPA)]^{2-}$ (log K_{ML} = 33.9−35.2) is misleading, as early work revealed inadequate kinetic inertness for $^{212/213}$Bi-based pharmaceuticals, resulting in kidney accumulation during in vivo studies. A slight improvement in performance is noted with $[^{212/213}Bi(1B4M\text{-}DTPA)]^{2-}$, but kidney uptake remains problematic.[46,593−595] Contemporary ^{213}Bi TAT studies almost exclusively use CHX-A″-DTPA[596,597] over DTPA due to its equivalent stability (log K_{ML} = 34.9−35.6) and greatly enhanced inertness when complexing trivalent bismuth.[49,62,558−568,571,573] Comparison of renal uptake of B72.3-mAb radiolabeled with ^{206}Bi using DTPA, 1B4M-DTPA, and CHX-A-DTPA as chelators shows a clear effect of backbone rigidity on ^{206}Bi release. After 6 h, kidney uptake for DTPA groups was 27.2%ID/g, for 1B4M was 13.2%ID/g, and for CHX-A-DTPA was 7.8%ID/g.[595] Moderate kidney uptake suggests that CHX-A″-DTPA is not an ideal match with Bi^{3+}, but its widespread availability and adequate performance during in vivo studies appear to have popularized its use for $^{212/213}$Bi therapeutics.

NETA (Figure 4K) derivatives radiolabel $^{205/206}$Bi at low metal-to-ligand concentrations and demonstrate less degradation than that of CHX-A″-DTPA during in vitro challenge experiments.[598−600] Interestingly, biodistribution studies of naked $[^{205/206}Bi(C\text{-}NETA)]^-$ in nontumor-bearing mice resulted in high kidney accumulation (24.63 ± 2.79%ID/g) after 1 h, whereas the biodistribution of the seven-coordinate derivative $[^{205/206}Bi(C\text{-}NE3TA)]$ led to significantly less accumulation (4.69 ± 0.55%ID/g) despite a presumably noncoordinatively saturated Bi^{3+} metal center.[600] The continued use of NETA (as opposed to NE3TA) with an extended linker between the coordinating functional groups and pendant isothiocyanate group (*p*-SCN-Bn) in the following experiments suggests the observed instability was related to coupling group interference. 3p-*C*-NETA-trastuzumab demonstrated superior $^{205/206}$Bi labeling to DOTA-trastuzumab, and in vivo studies on mice bearing subcutaneous tumors (LS-174T) demonstrated impressive tumor uptake without elevating kidney accumulation over 24 h.[601]

DEPA (Figure 4C) has also been studied with $^{205/206}$Bi to reveal equally encouraging results.[60,358] After $^{205/206}$Bi radiolabeling of *C*-DEPA-trastuzumab, complexes remained 100% intact after serum stability studies over 72 h, whereas 23% of $^{205/206}$Bi-DTPA-trastuzumab complexes degraded.[60] The extended linker derivative, $^{205/206}$Bi 3p-*C*-DEPA-trastuzumab, showed good tumor uptake in tumor-bearing (LS-174T) mice.[602] As noted by Price and Orvig,[11] a comparison of NETA versus DEPA for Bi-based radiopharmaceuticals would be useful to determine the "gold standard" of bismuth chelators.

One final notable chelator for Bi^{3+} is the inherently bifunctional picolinic acid-based scaffold, H_4neunpa (Figure 5I). Although stability with Bi^{3+} (log K_{ML} = 28.8) is lower than that of DOTA and DTPA, the pM value is the same as DOTA (pM = 27), providing auspicious evidence for in vivo use.[86] To date, no radiolabeling studies have been reported.

13.3. Bismuth-213 Biological Studies

Bismuth-213 will be the focus of this section due to its prevalence in recent literature over ^{212}Bi. The most influential tracers for ^{213}Bi TAT have involved radiolabeling anti-CD33 agents, specifically the mAb HuM195 (Lintuzumab), for treatment of advanced myeloid leukemia. Clinical preparation of ^{213}Bi-CHX-A″-DTPA-HuM195 was first demonstrated in 1999 and was followed by pharmacokinetic and dosimetric studies that utilized the γ-emission of ^{213}Bi (440 keV, I = 26%).[566,603] Compared to β^- emitting radionuclides, ^{213}Bi therapy resulted in a 1000-fold increase in the target-to-whole-body dose ratio due to increased target (bone marrow, liver, and spleen) dose and lower whole-body dose. In an effort to fully treat myeloid leukemia (requires 99.9% diseased cell death), cytarabine therapy was followed with ^{213}Bi-CHX-A″-DTPA-HuM195 therapy. Despite reductions in circulating blasts (14/15, 93%) and bone marrow blasts (14/18, 78%), no patients achieved complete remission.[567] A more intensive trial used a nonremittive dose of cytarabine and found some patients (2/21) receiving a dose of 37 MBq/kg achieved complete remission.[568] The most recent studies point toward use of ^{225}Ac (see section 14) over ^{213}Bi due to its more manageable half-life and ability to emit four α particles.[569,570] Other promising mAb uses for ^{213}Bi have also been demonstrated with J591[571,572] and bevacizumab[49] for prostate cancer, anti-EGFR-mAb[558,559] for bladder carcinoma, anti-CD38-mAb[560] and anti-CD138[561] for multiple myeloma, d9-mAb[562] for diffuse-type gastric cancer, anti-CD45-mAb[563] for leukemia, and bevacizumab[564,604] for colorectal cancer. Use with the monovalent antibody fragment (Fab′), CO17-1A for treatment of colon cancer is also notable.[32]

In terms of peptide bioconjugates, preclinical studies with ^{213}Bi-DOTATOC on SST receptor-expressing pancreatic tumors demonstrated effectiveness in controlling growth of small tumors and displayed a dose-dependent response in large tumors over >20 days.[605] In vitro studies evidenced the superiority of ^{213}Bi-DOTATOC over ^{177}Lu-DOTATOC by demonstrating decreased target cell survival rate of the former with identical doses.[606] Interestingly, a study exploring the use of contrast-enhanced ultrasound in humans noted treatment with ^{177}Lu/^{90}Y-DOTATOC led to a decrease in tumor vascularity and diameter, while ^{213}Bi-DOTATOC therapy led to decreased tumor vascularity with little change in tumor diameter after several months. This suggests that, prior to tumor shrinkage, α-therapy first induces changes in tumor microcirculation.[607] A retrospective study of patients treated with ^{213}Bi-DOTATOC as a result of ineffective β^- therapy (i.e., ^{90}Y and ^{177}Lu) demonstrated enduring responses between 6 and 34 months (median = 21 months), with seven (87.5%) patients declared progression-free survival and one (12.5%) having a complete response. Long-term renal toxicity following ^{213}Bi treatment was expected due to considerable kidney dose during prior β therapy; however, no patients display kidney

DOI: 10.1021/acs.chemrev.8b00294
Chem. Rev. 2019, 119, 902−956

Table 16. Selected ^{213}Bi Radiopharmaceuticals with Targets and Relevant Labeling Parameters[a]

radionuclide	chelator (BFC)	standard labeling conditions	bioconjugate	target	molar/specific activity (% RCY)	reference
^{213}Bi	CHX-A′′-DTPA (*p*-SCN-Bn)	0.2 M NH_4OAc pH 4−4.5, RT, 10 min	Lintuzumab (HuM195)	CD33	329−766 MBq/mg (81 ± 9)	603
		0.4 M NH_4OAc pH 5.3, RT, 7 min	anti-EGFR mAb	EGFR	0.35−1.4 GBq/mg (95−97)	558
	DOTA (DO3A)	0.15 M TRIS buffer pH 8.5−8.7, 95 °C, 5 min	Tyr^3-octreotate (TATE)	SSTR	6.7−13.3 GBq/μmol (>99)	609, 610
			PESIN	GRPR	83.6 GBq/μmol (97.8 ± 2.4)	589

[a]EGFR (epidermal growth factor receptor); SSTR (somatostatin receptor); and GRPR (gastrin-releasing peptide receptor).

failure 2 years post-treatment. Low acute hematological toxicity was reported.[608]

Animal studies with ^{213}Bi-DOTATATE have been detailed by Chan et al., who noted >10% ID/g tumor uptake after 10 min.[609−611] When L-lysine (35 mg) was preinjected prior to ^{213}Bi-DOTATATE administration, renal clearance was improved and led to decreased kidney dose (0.56 Gy/MBq vs 1.1 Gy/MBq). This benefit led to higher survival rates over 90 days for high-dose (>28 MBq; 0% vs >70%) and medium-dose (>20 MBq; 60% vs 100%) groups.[609] A separate study investigated the influence of tumor size on ^{213}Bi-DOTATATE treatment efficacy and found smaller tumors generally received higher doses compared to large tumors (both for H69 and CA20948 cell lines). Slowing tumor growth was, however, more effective for larger tumors. In all cases, treated groups lived substantially longer than control groups.[610]

Bismuth-213-PSMA-617 has shown great promise in treating metastatic castration-resistant prostate cancer, as summarized in the brief report of the first in-human treatment.[612] The patient received two cycles with a total dose of 592 MBq and after 11 months showed no sign of cancerous regions by ^{68}Ga-PSMA-617 PET/CT. Another study used fluorescent biomarkers to quantify ^{213}Bi-induced double-strand breaks during therapy. In vitro studies revealed double-strand breaks in 20.91 ± 1.23% of cells from LNCaP xenografts after 1 h, compared to <1% in the control group. Indications of double-strand breaks decreased to 2.51 ± 0.21% after 24 h.[29] Dosimetry calculations and experiments report the maximum single dose of ^{213}Bi should be 2 GBq per cycle with a maximum dose for cumulative treatment of 3.6 GBq, to limit dose to kidneys, salivary glands, and red marrow. The authors also emphasize the superiority of ^{225}Ac over ^{213}Bi based on therapeutic index.[613]

Other noteworthy ^{213}Bi peptide bioconjugates include DOTA-PESIN, substance P, PAI2, F3, and IMP288. DOTA-PESIN (DO3A-PEG_4-BBN[7-14]) is an 8-amino acid bombesin derivative with a high affinity for all three human BBN receptors (i.e., NMB-R, GRPR, and BBN receptor subtype 3).[614] A study comparing ^{213}Bi-DOTA-PESIN with ^{177}Lu-DOTA-PESIN demonstrated superior tumor-growth control and survival rates for the α-treated group.[589] When labeled with ^{213}Bi, substance P has demonstrated improved median survival time for treatment of malignant primary brain tumors (Glioblastoma multiforme, GBM), compared to conventional treatment (25.2 vs 14.6 months).[615] Plasminogen activator inhibitor type 2 (PAI2) has been heavily investigated and shown promise with ^{213}Bi for treatment of breast, prostate, pancreatic, and ovarian cancer.[616−620] The most recent ^{213}Bi-PAI2 study was dosimetry based with aspirations of phase I clinical trials;[621] however, over the past decade no such studies have been published. Pretargeted TF2/IMP288 therapy for treatment of carinoembryonic antigen (CEA)-expressing tumors and vascular tumor homing peptide, F3, have also been studied with ^{213}Bi.[565,622]

14. ACTINIUM

Actinium-225 ($t_{1/2}$ = 240 h) is an α emitter believed by many to be among the most promising therapeutic radionuclides. This belief is centered around the potent cell-killing capability of the ^{225}Ac decay chain, which releases four α particles during its decay to stable ^{209}Bi (Figure 7). The initial α decay (Eα = 5790 keV) is followed shortly by two subsequent α emissions (Eα = 6300 and 7070 keV) due to the short physical half-lives of intermediate daughter radionuclides ^{221}Fr ($t_{1/2}$ = 4.9 m) and ^{217}At ($t_{1/2}$ = 32 ms), which produces ^{213}Bi ($t_{1/2}$ = 0.76 h). Bismuth-213 itself is a therapeutic radionuclide (see section 13), leading many to describe ^{225}Ac as an in vivo ^{213}Bi generator. This description undermines the importance of the first three decays, which result in a 1 000−10 000-fold toxicity increase.[623] The high LET of the four α decays (80, 75, 64, and 61 keV/μm) limits the soft-tissue range to a maximum of 85 μm.[319] Francium-221 and bismuth-213 release low-/medium-energy gammas (^{221}Fr Eγ = 218 keV, Iγ = 11%; ^{213}Bi Eγ = 440 keV, Iγ = 26) suitable for SPECT.[624] The long physical half-life of ^{225}Ac makes it suitable for slow-circulating bioconjugates; however, many promising examples with fast-circulating peptides have been reported.[613,625−628] There is currently clinical interest in several actinium-based therapeutics, including ^{225}Ac-J591, ^{225}Ac-PSMA-617, and ^{225}Ac-HuM195.[245] The major issues with current ^{225}Ac use are the challenges associated with retaining intact complexation of ^{225}Ac and chemically dissimilar daughter radionuclides, as well as a lack of availability, resulting in high activity cost ($1200/mCi).[629]

14.1. Actinium-225 Production

The primary global source of clinical-grade ^{225}Ac is the ^{233}U ($t_{1/2}$ = 1.59 × 10^5 years) decay chain, which produces ^{229}Th ($t_{1/2}$ = 7340 years) as a long-lived parent (Figure 7). In an effort to manufacture nuclear weapons in the 1960s, kilogram quantities of ^{233}U were produced via neutron irradiation of natural thorium to induce ^{232}Th(n,γ)^{233}Th → → ^{233}U.[630] Chemical separation of ^{229}Th from the ^{233}U stockpile has allowed assembly of three main ^{229}Th/^{225}Ac generators, which are located at Oak Ridge National Lab, U.S.A. (5.55 GBq ^{229}Th and 22.2 GBq/y ^{225}Ac), Institute of Physics and Power Engineering, Russia (5.55 GBq ^{229}Th and 26.2 GBq/y ^{225}Ac), and the Institute for Transuranium Elements, Germany (1.7 GBq ^{229}Th and 13 GBq/y ^{225}Ac), totaling 63 GBq of ^{225}Ac per year.[631] The separation of ^{229}Th from daughter radionuclides is

DOI: 10.1021/acs.chemrev.8b00294
Chem. Rev. 2019, 119, 902−956

Table 17. Selected Ac^{3+} Chelators; La^{3+} Complex Geometry and Thermodynamic Parameters Are Reported in Lieu of a "Cold" Ac^{3+} Analogue

metal ion	chelator	coordinating nuclei	geometry	log K_{ML}	pM	reference
La^{3+} (Ac^{3+})	DOTA	N_4O_4	square antiprism	20.7−22.9		707, 713
	DTPA	N_3O_5	monocapped square antiprism	19.5		361, 699, 714
	H_2macropa	N_4O_6	irregular tridecahedron (4:6:1)	15.0		664, 665
	HEHA	N_6O_6	distorted hexagonal antiprism?	19.1		699
	PEPA	N_5O_5	distorted pentagonal antiprism?	13.6		699
	H_2bispa^2	N_6O_2	square antiprism?	11.4	12.0	72

well-established with anion-exchange chromatography in 8 M HNO_3, due to the formation and retention of anionic thorium(IV) nitrate[576] and elution of ^{225}Ac and ^{225}Ra.[632,633] Establishment of the nonproliferation policy has rendered the current quantity of ^{229}Th finite, and it is now widely accepted that the global demand for ^{225}Ac will quickly outgrow current supply.[634−636] Accordingly, research into the use of ^{232}Th and ^{226}Ra targets for ^{225}Ac production has become an active area of research.

Radium-226 ($t_{1/2}$ = 1600 years) targets are attractive for ^{225}Ac production due the relatively high reaction cross sections; however, a disadvantage is the radioactive nature of ^{226}Ra, which necessitates extra precautions during target preparation and postirradiation recovery.[319,637] The most promising ^{226}Ra-based method is direct production via ^{226}Ra-(p,2n)^{225}Ac, which has a maximum cross section (710 mb) at 16.8 MeV beam energy.[637] Following irradiation of $RaCl_2$ (30 mg), the target is dissolved in 0.01 M HCl and loaded onto a Ln-spec column. The column is washed with 0.1 M HCl to elute ^{226}Ra, Pb, and Po impurities, and ^{225}Ac is then eluted and washed through a Sr-spec column with 2 M HCl. This purification strategy has been used to isolate clinical-grade ^{225}Ac, with comparable purity to that of a ^{229}Th/^{225}Ac generator system. After 45.3 h of irradiation (15.9 MeV, 50 uA), 485 MBq of ^{225}Ac was obtained with negligible ^{226}Ac and ^{224}Ac contamination.[637]

Several other routes to ^{225}Ac production using ^{226}Ra targets have been reported. An indirect method via ^{226}Ra(3n, 2β^-)^{229}Th → ^{225}Ac has been demonstrated; however, this strategy produces nearly 10^4 times more ^{228}Th due to its shorter half-life ($t_{1/2}$ = 1.91 years) and need for only two neutrons, rendering this method unfeasible.[638,639] The use of photonuclear reactions to induce ^{226}Ra(γ,n)^{225}Ra → ^{225}Ac has also been considered due to the possibility of using larger targets than cyclotrons, presenting the opportunity to produce more overall activity despite lower efficiency.[640] This method was also found to be impractical due to limitations with current LINAC facilities, which provide inadequate current, pulse length, and frequency.[640,641] The use of high-energy neutrons is now under investigation to induce ^{226}Ra(n, 2n)^{225}Ra → ^{225}Ac. Theoretical calculations supporting the production of practical amounts of activity have been reported.[642]

Proton irradiation of natural thorium (^{232}Th) is another potential avenue for the future of ^{225}Ac production. Building on early reports,[643−646] Zhuikov et al. demonstrated a method capable of producing GBq amounts of ^{225}Ac using high-energy protons (90, 110, and 135 MeV). The dominant production reactions include ^{232}Th(p,p7n)^{225}Th → ^{225}Ac and ^{232}Th-(p,2p6n)^{225}Ac, with the latter contributing 45.8% and 86.5% of produced ^{225}Ac at 90 and 135 MeV proton energy, respectively.[647] Follow-up cross section studies in the energy range of 21−141 MeV revealed more clearly the need for proton energies of >100 MeV to reach cumulative reaction cross sections above 10 mb and produce useful amounts of ^{225}Ac while minimizing relative production of the long-lived contaminant ^{227}Ac ($t_{1/2}$ = 27.8 years).[42] Cross sections for production of other impurities (e.g., ^{139,141,143,144}Ce, ^{140}La, ^{140}Ba, ^{99} Mo, and ^{226}Ac) have also been reported.[636,648,649] Production rates were calculated and experimentally validated using an 800 MeV proton beam at Los Alamos National Laboratory, and it was estimated that 747 GBq of ^{225}Ac could be produced at a rate of 3.5 MBq/uAh over 10 days of irradiation. If successful, one irradiation of this scale would yield 20 times the activity of current annual worldwide production.[650] Similar reports for potential use of a 78−200 MeV beams are also available.[636,648]

Purification from ^{232}Th has been demonstrated with a combination of liquid−liquid extraction and solid-phase extraction chromatography;[647] however, recent reports almost exclusively rely on ion-exchange and/or solid-phase extraction chromatography. For example, as reported by Weidner et al., following target dissolution, the solution matrix is adjusted to 8 M HNO_3 to retain anionic thorium(IV) nitrate upon loading of an anion-exchange resin, while Ac^{3+} and Ra^{2+} have minimal retention and are quickly eluted. Thorium is stripped using dilute HNO_3. This method may be repeated several times, as large amounts of ^{232}Th may saturate the resin and lead to ^{232}Th breakthrough. Separation of ^{225}Ac from ^{225}Ra is then achieved with cation-exchange chromatography, which is loaded in 0.1 M HNO_3, ^{225}Ra eluted with 1.2 M HNO_3, and finally ^{225}Ac eluted with 8 M HNO_3.[650] Recently, there have been a number of studies attempting to develop simple and robust purification systems for ^{225}Ac, many of which employ either UTEVA or DGA, among other resins.[651−655]

14.2. Actinium Chemistry and Chelator Development

Actinium is only chemically stable in the trivalent oxidation state (Ac^{3+}) and, with the largest ionic radii among the *f*-block, is the most basic trivalent ion known.[656] X-ray absorption fine structure (XAFS) spectroscopy studies have recently revealed that aqueous Ac^{3+} is surrounded by 10.9 ± 0.5 inner-sphere water molecules, while DFT (density functional theory) predicts a nonacoordinated hydrate species, $[Ac(H_2O)_9]^{3+}$. The authors noted that higher lanthanide and actinide hydration values are typically calculated by XAFS than what are observed in solid-state structures.[657] Actinium does not easily hydrolyze, with evidence supporting only 74% $[Ac(OH)]^{2+}$ and 26% $[Ac(OH)_2]^{+}$ speciation at pH 8.[656] Chelation chemistry has been a major challenge of ^{225}Ac drug development. Not only is the chemical behavior of actinium still a point of contention (including placement on the periodic table[658]), but the absence of a nonradioactive or "cold" actinium isotope makes even rudimentary experiments to identify promising chelator candidates time-consuming and

DOI: 10.1021/acs.chemrev.8b00294
Chem. Rev. 2019, 119, 902−956

logistically challenging. Because of its chemical similarities and behavior during complexation, La^{3+} is often used as a chemical surrogate for Ac^{3+}. Chelator development is further complicated when considering the ^{225}Ac decay chain, which produces six chemically different daughter radionuclides, with variable coordination number and electronic donor preferences. The most elusive daughter radionuclides are ^{221}Fr ($t_{1/2}$ = 4.8 min) and ^{217}At ($t_{1/2}$ = 32.2 ms), as both species are very chemically different than $^{225}Ac^{3+}$ and are therefore unlikely to remain stable in the coordination environment designed for the trivalent actinide. Moreover, some are skeptical that the "recoil energy" released during ^{225}Ac α-decay (100 keV, or 2 keV if considering mass of total complex) is too great to be overcome by coordinative bonds (≈eV).[659]

Actinium chelator development has been primarily focused on macrocycles due to their enhanced kinetic inertness over acyclic ligands, which is a crucial parameter when considering the lengthy half-life of ^{225}Ac ($t_{1/2}$ = 240 h). Through a comparison of common ligands (DTPA, TETA, DOTA, DOTPA TETPA, and DOTMP) and bifunctional analogues (MeO−DOTA-NCS and *p*-SCN-Bn-DOTA), it was determined that DOTA is the only candidate that can achieve quantitative ^{225}Ac radiolabeling. All other tested chelates had essentially no labeling, with the exception of DOTMP (78% radiolabeling). Serum stability testing revealed >75% intact complexes of ^{225}Ac-DOTA over 50 days, while ^{225}Ac-DOTMP rapidly dissociates over a few days.[660] Use of CHX-DTPA with ^{225}Ac is also clearly unsuitable, as a 100% mortality rate of mice 8 days postinjection (185 kBq) was demonstrated.[661] Antibody radiolabeling (HuM195 and Ritiuximab) using *p*-SCN-Bn-DOTA compared to DO3A revealed superior radiochemical yield and higher obtainable specific activity (129 GBq/g vs 27.4 GBq/g) with eight-coordinate *p*-SCN-Bn-DOTA over seven-coordinate DO3A. This result underscores the need for high-coordinate chelates for ^{225}Ac radiopharmaceuticals.[662] Moreover, the lack of time-dependent liver accumulation of the ^{225}Ac-DOTA-NCS-HuM195 complex suggests good in vivo stability.

The large radius and high coordination number of Ac^{3+} has led some to apply larger macrocycles such as PEPA and HEHA (1,4,7,10,13,16-hexaazocyclooctadecane hexaacetic acid; Figure 4M) to ^{225}Ac-based tracers. Although early studies with nonfunctionalized HEHA boasted "exceptional stability in vivo" and rapid clearance, follow-up studies with HEHA-Bn-p-NCS-(BL-3) demonstrated high rates of decomplexation (69% intact over 5 h).[661,663] PEPA is even less suitable for ^{225}Ac than HEHA.[661] Most recently, a promising new 18-membered macrocycle has been applied to ^{225}Ac by Thiele et al.[664] First synthesized by Roca-Sabio et al.,[665] H_2macropa (*N*,*N*′-bis[(6-carboxy-2-pyridil)methyl]-4,13-diaza-18-crown-6; Figure 4L) quantitatively radiolabels ^{225}Ac within 5 min at room temperature (1:1800 M/L ratio) and is stable over 7 days against La^{3+} or human serum competition.[664] The PSMA/albumin dual-targeting bioconjugate, H_2macropa-Bn-p-NCS-RPS-070, was synthesized and exhibited similar labeling capabilities to the nonfunctionalized analogue.[664] During animal studies (LNCaP xenografts) ^{225}Ac-macropa-NCS-RPS-070 displayed essentially no tissue or organ uptake besides that of the kidney and tumor; after 96 h kidney activity is mostly excreted, while a significant amount of activity remains in the tumor.[664]

Although most common acyclic ligands (i.e., EDTA, DTPA, and CHX-DTPA) have demonstrated instability with ^{225}Ac complexation,[661] a bispidine analogue functionalized with picolinic acid (H_2bispa^2, 6,6′-[{9-hydroxy-1,5-bis(methoxycarbonyl)-2,4-di(pyridin-2-yl)-3,7-diazabicyclo[3.3.1]nonane-3,7-diyl}bis(methylene)]dipicolinic acid; Figure 5G) has demonstrated excellent radiolabeling capabilities. Interestingly, the [In(bispa^2)]$^+$ complex exhibited higher thermodynamic stability than did either [Lu(bispa^2)]$^+$ or [La(bispa^2)]$^+$ by over 12 orders of magnitude. Although this may be explained by a better fit of In^{3+} into the bispidine pocket than larger La^{3+} or smaller Lu^{3+}, this trend would seem contrary to stability testing with ^{225}Ac, which is larger than La^{3+}, yet exhibited excellent stability against serum protein competition experiments.[72] Bioconjugated analogues have yet to be reported.

As a response to concerns over daughter nuclei and recoil energy of ^{225}Ac alpha decay, several alternatives to BFC for radionuclide delivery have been reported. Although this topic is beyond the scope of this Review, interested readers are directed to the following articles regarding nanoparticles, polymer vesicles, and liposomes: refs 666−671.

14.3. Actinium-225 Biological Studies

Despite intense interest and proven superiority of ^{225}Ac over other therapeutic radionuclides (i.e., ^{90}Y, ^{177}Lu, and ^{213}Bi),[625,672] low availability and high associated cost have limited studies exploring preclinical or clinical use of ^{225}Ac. Initial studies focused primarily on monoclonal antibody labeling, likely due to the compatible physical/biological half-lives, as well as the established interest in ^{213}Bi-mAb therapy.

Toxicity was extremely problematic during early ^{225}Ac preclinical studies with HEHA-mAb-201b and HEHA-CC49/ΔHu-CH$_2$CC49.[659,673] Although treatment resulted in decreased tumor mass, slow release of daughter radionuclides led to unacceptable rates of renal toxicity. This issue has since been diminished, but not completely eliminated, through use of DOTA. For example, nonequilibrium ^{213}Bi dose following ^{225}Ac-DOTA-Lintuzumab administration still accounts for 60% (0.46 ± 0.11 Gy/kBq) of the total kidney dose (0.77 ± 0.21 Gy/kBq).[674] In this study, the authors stressed the need for methods to reduce renal accumulation of daughter radionuclides, such as the use of coadministered metal chelates or diuretics.[674−676] Vector internalization has also been suggested as a way to overcome challenges of daughter radionuclide distribution.[677,678]

DOTA-Trastuzumab (anti-HER2/*neu*) and DOTA-HuM195 (anti-CD33) have been the subjects of many ^{225}Ac biological studies. Thermal sensitivity of the antibodies requires two-step labeling procedures, where *p*-SCN-Bn-DOTA is radiolabeled with ^{225}Ac, purified via cation-exchange resin (C18 Sephadex), and subsequently bioconjugated by adding the complex to an antibody solution. Although this method results in low radiochemical yield and specific activity (1/1000 antibodies labeled), it has been sufficient to draw clinically relevant conclusions, such as the benefit of fractioned therapy.[677] Preclinical studies with ^{225}Ac-HuM195 to treat human prostate cancer xenografts have revealed improved survival over control groups, as well as tumor regression and prolonged survival without toxicity in a substantial fraction of animals.[679] Dosimetry of ^{225}Ac-DOTA-HuM195 in nonhuman primates for treatment of acute myeloid leukemia was determined by monitoring hemoglobin levels after escalating doses. Although the study was imperfect due to a difference in tracer biological half-life between nonhuman primates and

DOI: 10.1021/acs.chemrev.8b00294
Chem. Rev. 2019, 119, 902−956

Table 18. Selected ^{225}Ac Radiopharmaceuticals with Targets and Relevant Labeling Parameters[a]

radionuclide	chelator (BFC)	standard labeling conditions	bioconjugate	target	molar/specific activity (% RCY)	reference
^{225}Ac	HEHA (*p*-SCN-Bn)	NaOAc, pH 5, RT, 10 min	Hu-ΔCH$_2$CC49	LS174T tumors	18.5 MBq/mg	673
	DOTA (*p*-SCN-Bn)	2 M TMAA buffer pH 5.5, 56 °C, 42 min	Lintuzumab (HuM195)	CD33	2.59−4.07 MBq/mg (93 ± 8)	660, 676
		0.5 M NaOAc pH 5, 70 °C, 60 min	Phe^1-Tyr^3-octreotide (TOC)	SSTR	40−120 MBq/mg	625
		0.1 M Tris buffer pH 9, 95 °C, 5 min	PSMA-617	PSMA	0.17 ± 0.05 GBq/μmol	628

[a]SSTR (somatostatin receptor) and PSMA (prostate-specific membrane antigen).

humans, a suggested dose level of 28 kBq/kg was reported.[680] Phase I clinical trials for treatment of advanced acute myeloid lymphoma showed antileukemic activity across all dose levels (37−148 kBq/kg). Moreover, 67% (10/15) of patients receiving ≥37 kBq/kg exhibited a decrease in bone marrow blasts at 4 weeks, with upward of 50% decrease noted in more than half of the evaluable patients.[623,681] Additional clinical trials for ^{225}Ac-DOTA-HuM195 are currently awaiting patient recruitment. Treatment of neuroblastomas with ^{225}Ac-DOTA-3F8 was also encouraging and demonstrated a 2-fold survival increase (16−34 days) in a nude rat xenograft model of meningeal carcinomatosis.[682] Radioimmunoconjugates ^{225}Ac-B4 and ^{225}Ac-J591 have also shown promising therapeutic potential, with the latter being of particular clinical interest.[679,683,684]

Despite seemingly incompatible physical and biological half-lives, ^{225}Ac has been applied to PRRT. The less thermally sensitive bioconjugates provide the benefit of one-step labeling and therefore higher specific activity, relative to two-step labeling procedures used for antibody bioconjugates. A comparative study of ^{177}Lu- and ^{225}Ac-DOTATOC over 4 days revealed significant accumulation of both tracers in neuroendocrine xenograft tumors, with improved efficacy of ^{225}Ac-DOTATOC over ^{177}Lu-DOTATOC.[625] Another study examined ^{225}Ac-DOTA-c(RGDyK) distribution and, by using Cerenkov luminescence imaging, was able to visualize and quantify the difference in tracer accumulation between blocked (excess c(RGDyK)) and nonblocked animal populations. Although kidney uptake remained problematic, tumor uptake and retention was good, and the proof-of-concept imaging was an interesting alternative to using a diagnostic pair (^{68}Ga/^{111}In).[626]

Most notably, ^{225}Ac-PSMA-617 has exhibited astounding antitumor activity and may have a large clinical impact in coming years. In a short communication, Kratochwil et al. reported two patients whose prostate-specific antigen (PSA) decreased to below measurable levels following ^{225}Ac-PSMA-617 treatment. One patient's treatment was in 3 cycles of 9−10 MBq (100kBq/kg) at bimonthly intervals, and after 2 months, PSMA-positive lesions could no longer be visualized by ^{68}Ga-PSMA-617 PET/CT and the PSA level dropped from 3000 to 0.26 ng/mL.[628] In the full study, not all subjects responded as dramatically, but results remain encouraging as decreased PSA response was observed in 75% of patients, with a dose of ≥100 kBq/kg required for a response. The authors concluded that 100 kBq/kg is a reasonable clinical dose to elicit a therapeutic response while minimizing xerostomia (dry mouth).[627] In the most recent retrospective analysis of data, authors report that, in patients surviving >8 weeks, 87% (33/38) demonstrated PSA decline, with a decrease of ≥50% in 63% (24/38) of patients.[685]

15. CONCLUSIONS

The use of controlled internal radiation is remarkably effective at selectively diagnosing and treating cancer, as well as other complex diseases. Radiopharmaceutical development has vastly expanded the breadth and efficacy of modern drugs, which are increasingly attractive compared to traditional chemotherapeutics, whose use is comparatively crude and has scantily developed in the last 20 years. Advances in the fields of radionuclide production/purification, BFC development, and bioconjugate discovery have collectively contributed to the success of contemporary four-component radiopharmaceuticals. Indeed, the future of nuclear medicine and radiopharmaceuticals appears bright!

AUTHOR INFORMATION

Corresponding Authors

*E-mail: tkostelnik@chem.ubc.ca.
*E-mail: orvig@chem.ubc.ca.

ORCID

Chris Orvig: 0000-0002-2830-5493

Notes

The authors declare no competing financial interest.

Biographies

Thomas Kostelnik received his undergraduate education at Mount Allison University in Sackville, New Brunswick, Canada, where he completed his honours B.Sc. (2015) in chemistry under Dr. Stephen Westcott. Thomas is an NSERC scholar at University of British Columbia and has been working with Prof. Chris Orvig since 2015. His research is partially conducted at TRIUMF, Canada's national particle accelerator centre, and is focused on radiochemistry and chelator development for exotic, medically relevant radiometals.

Chris Orvig completed his honours B.Sc. in chemistry at McGill University in Montreal, Quebec, Canada. He earned his doctorate as an NSERC of Canada scholar at MIT with Alan Davison, FRS, and completed postdoctoral fellowships with Kenneth N. Raymond at the University of California, Berkeley, and the late Colin J. L. Lock at McMaster University. In 1984, he joined the University of British Columbia, and is now a Professor of Chemistry and Pharmaceutical Sciences and a Fellow of the Royal Society of Canada.

ACKNOWLEDGMENTS

We gratefully acknowledge the Natural Sciences and Engineering Research Council (NSERC) of Canada for CGSM/CGSD fellowships (T.I.K.) and many years of Discovery Grant support (C.O.), as well as the University of British Columbia for a 4YF fellowship (T.I.K.). We also thank the IsoSiM NSERC CREATE program at TRIUMF and the Canadian Institutes of Health Research (CIHR) for their generous

DOI: 10.1021/acs.chemrev.8b00294
Chem. Rev. 2019, 119, 902−956

support, as well as Dr. Maria de Guadalupe (Lupe) Jaraquemada-Peláez and Mr. Luke Wharton for stimulating discussion and thoughtful editing. C.O. dedicates this article to the memory of his dear friend Paul O'Brien, CBE, FRS, FREng.

ABBREVIATIONS[717]

α=alpha; representative of helium nucleus
α-HIBA=alpha-hydroxyisobutyric acid
β^+=positron; representative of an antielectron
β^-=beta; representative of an electron
γ=gamma
σ=cross section
6SS=*N,N′*-bis(2,2-dimethyl-2-mercaptoethyl)-ethylenediamine-*N,N′*-diacetic acid
[9]aneN$_3$=triazacyclononane
AAZTA=1,4-bis(carboxymethyl)-6-(bis[carboxymethyl])-amino-6-methylperhydro-1,4-diazepine
B=barn, 1 b = 10^{-24} cm^2
BATPA=1,2-bis(2-aminophenoxy)ethane-*N,N,N′,N′*-tetra-acetic acid
BBN=bombesin
BFC=bifunctional chelator
Bq=becquerel, SI unit of radioactivity (s^{-1})
Bq/C=becquerel per Coulomb
Bq/g=becquerel per gram
Bq/mol=becquerel per mole
ca=carrier-added
c(RGDfK)=cyclic Arg-Gly-Asp-D-Phe-Lys
c(RGDyK)=cyclic Arg-Gly-Asp-D-Tyr-Lys
C_A=covalent contribution to hardness parameter (I_A)
CB-DO2A=4,10-bis(carboxymethyl)-1,4,7,10-tetraazabicyclo[5.5.2]tetradecane
CE=conversion electron
CEA=carcinoembryonic antigen
CERN=European Organization for Nuclear Research
CHX-DTPA=cyclohexane-1,2-diamine-*N,N,N′,N′*-tetraacetate
CT=computed tomography
DATA=6-amino-1,4-diazepine triacetic acid
DCC=*N,N′*-dicyclohexylcarbodiimide
DEPA=7-[2-(bis-carboxymethylamino)-ethyl]-4,10-biscarboxymethyl-1,4,7,10-tetraazacyclododec-1-yl-acetic acid
DFO=deferoxamine
DFT=density functional theory
DGA=*N,N,N′,N′*-tetra-*n*-octyldiglycolamide
DOTA=1,4,7,10-tetraazacyclododecane-1,4,7,10-tetraacetic acid
DTPA=1,1,4,7,7-diethylenetriaminepentaacetic acid
E_A=electrostatic contribution to hardness parameter (I_A)
EC=electron capture
ECC=ethylenecysteamine cysteine
ECD=ethyl cysteinate dimer
EDC=1-ethyl-3-(3-(dimethylamino)propyl)carbodiimide
EDTA=ethylenediaminetetraacetic acid
EDTMP=ethylenediamine tetra(methylene phosphonic acid)
EGFR=epidermal growth factor receptor
EGTA=ethylene glycol bis(2-aminoethyl ether)-*N,N,N′,N′*-tetraacetic acid
eV=electronvolt
Fab=antibody fragment or antigen-binding fragment
FDA=U.S. Food and Drug Administration
[^{18}F]FDG=^{18}F-fluorodeoxyglucose
FR=folate receptor
FSC=fusarinine
GBM=glioblastoma multiforme
GBq/C=gigabecquerel per Coulomb
GI=gastrointestinal
GRP=gastrin-releasing peptide
GRPR=gastrin-releasing peptide receptor
Gy=gray, SI unit of absorbed dose, m^2/s^2
H$_2$bispa^2=6,6′-[{9-hydroxy-1,5-bis(methoxycarbonyl)-2,4-di(pyridin-2-yl)-3,7-diazabicyclo[3.3.1]nonane-3,7-diyl}bis-(methylene)]dipicolinic acid
H$_2$dedpa=1,2-[{6-(carboxylato)pyridin-2-yl}methylamino]-ethane
H$_2$macropa=*N,N′*-bis[(6-carboxy-2-pyridil)methyl]-4,13-diaza-18-crown-6
H$_4$octapa=*N,N′*-bis(6-carboxy-2-pyridylmethyl)-ethylenediamine-*N,N′*-diacetic acid
H$_6$Sbbpen=*N,N′*-bis(2-hydroxy-5-sulfonylbenzyl)-*N,N′*-bis-(2-methylpyridyl)ethylenediamine
HBED=*N,N′*-bis(2-hydroxybenzyl)ethylenediamine-*N,N′*-diacetic acid
HDEHP=di(2-ethylhexyl)orthophosphoric acid
HEHA=1,4,7,10,13,16-hexaazocyclooctadecane hexaacetic acid
HEPES=4-(2-hydroxyethyl)-1-piperazineethanesulfonic acid
HER2=human epidermal growth factor 2
HOBt=hydroxybenzotriazole
HPLC=high-performance liquid chromatography
HSAB theory=hard−soft acid−base theory
I_A=hardness parameter, $I_A = E_A/C_A$
ID/g=injected dose per gram of tissue
ISOLDE=Isotope Mass Separator Online Facility
IT=isomeric transition
LET=linear energy transfer
LINAC=linear accelerator
log *K*=formation constant
mAb=monoclonal antibody
mb=millibarn
MC1-R=melanocortin-1 receptor
MIBI=methoxyisobutylisonitrile
MRI=magnetic resonance imaging
nca=no-carrier-added
NETA=[2-{4,7-biscarboxymethyl(1,4,7)triazacyclonona-1-yl-ethyl}carbonylmethylamino]acetic acid
NHS=*N*-hydroxysuccinimide
NMR=nuclear magnetic resonance
NOC=NaI^3-octreotide
NODAGA=1,4,7-triazacyclononane,1-glutaric acid-4,7-acetic acid
NOTA=1,4,7-triazacyclononane-1,4,7-triacetic acid
NOTP=1,4,7-triazacyclononane-1,4,7-tri(methylene phosphonic acid)
PAI2=plasminogen activator inhibitor type 2
PBS=phosphate-buffered saline
PCTA=3,6,9,15-tetraazabicyclo[9.3.1]pentadeca-1-(15),11,13-triene-3,6,9-triacetic acid
PEG=polyethylene glycol
PEPA=1,4,7,10,13-pentaazocyclopentadecane pentaacetic acid
PESIN=DO3A-PEG$_4$-BBN[7-14]
PET=positron-emission tomography
PRRT=peptide receptor radionuclide therapy

DOI: 10.1021/acs.chemrev.8b00294
Chem. Rev. 2019, 119, 902−956

PSA=prostate-specific antigen
PSMA=prostate-specific membrane antigen
RAFT=regioselectively addressable functionalized template
RGD=arginylglycylaspartic acid, Arg-Gly-Asp
SHBED=*N,N′*-bis(2-hydroxy-5-sulfobenzyl)-ethylenediaminediacetic acid
SPECT=single-photon emission computed tomography
SST=somatostatin
SSTR=somatostatin receptor
SUV=standard uptake value
TAT=targeted alpha therapy
TATE=Tyr^3-octreotate
TETA=1,4,8,11-tetraazacyclotetradecane-1,4,8,11-tetraacetic acid
TFP=tetrafluorophenolate
THP=Tris(3,4-hydroxypyridinone)
TLC=thin-layer chromatography
TOC=Phe^1-Tyr^3-octreotide
TRAP=triazacyclononate phosphinic acids
TRITA=1,4,7,10-tetraazacyclotridecane-*N,N′,N″N‴*-tetracetic acid
TTHA=triethylenetetramine-*N,N,N′,N″,N‴,N⁗*-hexaacetic acid
UTEVA=uranium and tetravalent actinides
VSPER=valence shell electron pair repulsion
XAFS=X-ray absorption fine structure

REFERENCES

(1) Boros, E.; Packard, A. B. Radioactive Transition Metals for Imaging and Therapy. *Chem. Rev.* **2018**, *118*, DOI: 10.1021/acs.chemrev.8b00281.
(2) Qaim, S. M. Nuclear Data for Production and Medical Application of Radionuclides: Present Status and Future Needs. *Nucl. Med. Biol.* **2017**, *44*, 31−49.
(3) Müller, C.; Zhernosekov, K.; Köster, U.; Johnston, K.; Dorrer, H.; Hohn, A.; Van der Walt, N. T.; Türler, A.; Schibli, R. A Unique Matched Quadruplet of Terbium Radioisotopes for PET and SPECT and for α- and β-Radionuclide Therapy: An in Vivo Proof-of-Concept Study with a New Receptor-Targeted Folate Derivative. *J. Nucl. Med.* **2012**, *53*, 1951−1959.
(4) Amoroso, A. J.; Fallis, I. A.; Pope, S. J. A. Chelating Agents for Radiolanthanides: Applications to Imaging and Therapy. *Coord. Chem. Rev.* **2017**, *340*, 198−219.
(5) Mulford, D. A.; Scheinberg, D. A.; Jurcic, J. G. The Promise of Targeted α-Particle Therapy. *J. Nucl. Med.* **2005**, *46*, 199S−204S.
(6) Cutler, C. S.; Hennkens, H. M.; Sisay, N.; Huclier-Markai, S.; Jurisson, S. S. Radiometals for Combined Imaging and Therapy. *Chem. Rev.* **2013**, *113*, 858−883.
(7) Aluicio-Sarduy, E.; Ellison, P. A.; Barnhart, T. E.; Cai, W.; Nickles, R. J.; Engle, J. W. PET Radiometals for Antibody Labeling. *J. Labelled Compd. Radiopharm.* **2018**, *61*, 636−651.
(8) McDevitt, M. R.; Sgouros, G.; Sofou, S. Targeted and Nontargeted α-Particle Therapies. *Annu. Rev. Biomed. Eng.* **2018**, *20*, 73−93.
(9) Valdovinos, H. F. Production, Labeling and in Vivo Studies with the Theranostic Positron-Emitting Radiometals ^{44}Sc, $^{55/58m/58g}$Co, $^{61/64}$Cu, ^{86}Y and ^{69}Ge. Ph.D. Thesis, University of Wisconsin—Madison, 2017.
(10) Ramogida, C. F.; Orvig, C. Tumour Targeting with Radiometals for Diagnosis and Therapy. *Chem. Commun.* **2013**, *49*, 4720−4739.
(11) Price, E. W.; Orvig, C. Matching Chelators to Radiometals for Radiopharmaceuticals. *Chem. Soc. Rev.* **2014**, *43*, 260−290.
(12) Blower, P. J. A. Nuclear Chocolate Box: The Periodic Table of Nuclear Medicine. *Dalton Trans* **2015**, *44*, 4819−4844.
(13) Braad, P. E. N.; Hansen, S. B.; Thisgaard, H.; Høilund-Carlsen, P. F. PET Imaging with the Non-Pure Positron Emitters: ^{55}Co, ^{86}Y and ^{124}I. *Phys. Med. Biol.* **2015**, *60*, 3479−3497.
(14) Bernhardt, P.; Forssell-Aronsson, E.; Jacobsson, L.; Skarnemark, G. Low-Energy Electron Emitters for Targeted Radiotherapy of Small Tumours. *Acta Oncol.* **2001**, *40*, 602−608.
(15) Boros, E.; Marquez, B. V.; Ikotun, O. F.; Lapi, S. E.; Ferreira, C. L. Coordination Chemistry and Ligand Design in the Development of Metal Based Radiopharmaceuticals. In *Ligand Design in Medicinal Inorganic Chemistry*; Storr, T., Ed.; John Wiley & Sons: Chichester, U.K., 2014; pp 47−79.
(16) Livechart, Table of Nuclides, Nuclear Structure and Decay Data; https://www-nds.iaea.org/relnsd/vcharthtml/VChartHTML.html (accessed Apr 1, 2018).
(17) Chu, S. Y. F.; Ekstrom, L. P.; Firestone, R. B. WWW table of radioactive isotopes, database version 2/28/1999; http://nucleardata.nuclear.lu.se/toi/ (accessed Apr 1, 2018).
(18) O'Donoghue, J. A.; Wheldon, T. E. Targeted Radiotherapy Using Auger Electron Emitters. *Phys. Med. Biol.* **1996**, *41*, 1973−1992.
(19) Howell, R. W. Radiation Spectra for Auger-Electron Emitting Radionuclides: Report No. 2 of AAPM Nuclear Medicine Task Group No. 6. *Med. Phys.* **1992**, *19*, 1371−1383.
(20) Haller, S.; Pellegrini, G.; Vermeulen, C.; Van der Meulen, N. P.; Köster, U.; Bernhardt, P.; Schibli, R.; Müller, C. Contribution of Auger/Conversion Electrons to Renal Side Effects after Radionuclide Therapy: Preclinical Comparison of ^{161}Tb-Folate and ^{177}Lu-Folate. *EJNMMI Res.* **2016**, *6*, 13.
(21) Seidl, C. Radioimmunotherapy with α-Particle-Emitting Radionuclides. *Immunotherapy* **2014**, *6*, 431−458.
(22) Orsini, F.; Lorenzoni, A.; Puta, E.; Mariani, G. Positron-Emitting Radiopharmaceuticals for Diagnostic Applications. In *Nuclear Oncology*; Springer: Cham, 2017; pp 85−98.
(23) Cherry, S. R.; Dahlbom, M. PET: Physics, Instrumentation, and Scanners. In *PET*; Phelps, M. E., Ed.; Springer: New York, 2004.
(24) Alauddin, M. M. Positron Emission Tomography (PET) Imaging with ^{18}F-Based Radiotracers. *Am. J. Nucl. Med. Mol. Imaging* **2012**, *2*, 55−76.
(25) Sorenson, J. A.; Phelps, M. E. The Anger Camera: Performance Characteristics. In *Physics in Nuclear Medicine*; Grune & Stratton: Orlando, 1987; pp 331−345.
(26) Rahmim, A.; Zaidi, H. PET versus SPECT: Strengths, Limitations and Challenges. *Nucl. Med. Commun.* **2008**, *29*, 193−207.
(27) Van der Wall, E. E. Cost Analysis Favours SPECT over PET and CTA for Evaluation of Coronary Artery Disease: The SPARC Study. *Neth. Hear. J.* **2014**, *22*, 257−258.
(28) Fornell, D. SPECT Scanner vs. PET, Which is Best? https://www.dicardiology.com/article/spect-scanner-vs-pet-which-best (accessed Apr 1, 2018).
(29) Nonnekens, J.; Chatalic, K. L.; Molkenboer-Kuenen, J. D.; Beerens, C. E.; Bruchertseifer, F.; Morgenstern, A.; Veldhoven-Zweistra, J.; Schottelius, M.; Wester, H.-J.; van Gent, D. C.; et al. ^{213}Bi-Labeled Prostate-Specific Membrane Antigen-Targeting Agents Induce DNA Double-Strand Breaks in Prostate Cancer Xenografts. *Cancer Biother.Radiopharm.* **2017**, *32*, 67−73.
(30) Saha, G. B. *Fundamentals of Nuclear Pharmacy*; Springer-Verlag: New York, 2018.
(31) Kassis, A. I. Therapeutic Radionuclides: Biophysical and Radiobiologic Principles. *Semin. Nucl. Med.* **2008**, *38*, 358−366.
(32) Behr, T. M.; Béhé, M.; Stabin, M. G.; Wehrmann, E.; Apostolidis, C.; Molinet, R.; Strutz, F.; Fayyazi, A.; Wieland, E.; Gratz, S.; et al. High-Linear Energy Transfer (LET) α versus Low-LET ß Emitters in Radioimmunotherapy of Solid Tumors: Therapeutic Efficacy and Dose-Limiting Toxicity of ^{213}Bi- versus ^{90}Y-Labeled CO17−1A Fab' Fragments in a Human Colonic Cancer Model. *Cancer Res.* **1999**, *59*, 2635−2643.
(33) Zalutsky, M. R.; Pozzi, O. R. Radioimmunotherapy with α-Particle Emitting Radionuclides. *Q. J. Nucl. Med. Mol. Imaging* **2004**, *48*, 289−296.

DOI: 10.1021/acs.chemrev.8b00294
Chem. Rev. 2019, 119, 902−956

(34) Romer, A.; Seiler, D.; Marincek, N.; Brunner, P.; Koller, M. T.; Ng, Q. K. T.; Maecke, H. R.; Müller-Brand, J.; Rochlitz, C.; Briel, M.; et al. Somatostatin-Based Radiopeptide Therapy with [^{177}Lu-DOTA]-TOC versus [^{90}Y-DOTA]-TOC in Neuroendocrine Tumours. *Eur. J. Nucl. Med. Mol. Imaging* **2014**, *41*, 214−222.
(35) Kassis, A. I. Therapeutic Ratios or Targeted Radionuclides. In *Targeted Radionuclide Therapy*; Lippincott Williams & Wilkins: 2012; pp 249−257.
(36) Srivastava, S. C. Paving the Way to Personalized Medicine: Production of Some Promising Theragnostic Radionuclides at Brookhaven National Laboratory. *Semin. Nucl. Med.* **2012**, *42*, 151−163.
(37) Synowiecki, M. A.; Perk, L. R.; Nijsen, J. F. W. Production of Novel Diagnostic Radionuclides in Small Medical Cyclotrons. *EJNMMI Radiopharm. Chem.* **2018**, *3*, 3.
(38) Qaim, S. M. The Present and Future of Medical Radionuclide Production. *Radiochim. Acta* **2012**, *100*, 635−651.
(39) Starovoitova, V. N.; Tchelidze, L.; Wells, D. P. Production of Medical Radioisotopes with Linear Accelerators. *Appl. Radiat. Isot.* **2014**, *85*, 39−44.
(40) Carzaniga, T. S.; Auger, M.; Braccini, S.; Bunka, M.; Ereditato, A.; Nesteruk, K. P.; Scampoli, P.; Türler, A.; Van der Meulen, N. Measurement of ^{43}Sc and ^{44}Sc Production Cross-Section with an 18 MeV Medical PET Cyclotron. *Appl. Radiat. Isot.* **2017**, *129*, 96−102.
(41) Banerjee, S.; Pillai, M. R. A.; Knapp, F. F. Lutetium-177 Therapeutic Radiopharmaceuticals: Linking Chemistry, Radiochemistry, and Practical Applications. *Chem. Rev.* **2015**, *115*, 2934−2974.
(42) Ermolaev, S. V.; Zhuikov, B. L.; Kokhanyuk, V. M.; Matushko, V. L.; Kalmykov, S. N.; Aliev, R. A.; Tananaev, I. G.; Myasoedov, B. F. Production of Actinium, Thorium and Radium Isotopes from Natural Thorium Irradiated with Protons up to 141 MeV. *Radiochim. Acta* **2012**, *100*, 223−229.
(43) Bartoś, B.; Majkowska, A.; Krajewski, S.; Bilewicz, A. New Separation Method of No-Carrier-Added ^{47}Sc from Titanium Targets. *Radiochim. Acta* **2012**, *100*, 457−461.
(44) Coenen, H. H.; Gee, A. D.; Adam, M.; Antoni, G.; Cutler, C. S.; Fujibayashi, Y.; Jeong, J. M.; Mach, R. H.; Mindt, T. L.; Pike, V. W.; et al. Consensus Nomenclature Rules for Radiopharmaceutical Chemistry — Setting the Record Straight. *Nucl. Med. Biol.* **2017**, *55*, v−xi.
(45) Pandey, M. K.; Byrne, J. F.; Jiang, H.; Packard, A. B.; DeGrado, T. R. Cyclotron Production of ^{68}Ga via the ^{68}Zn(p, n)^{68}Ga Reaction in Aqueous Solution. *Am. J. Nucl. Med. Mol. Imaging* **2014**, *4*, 303−310.
(46) Gansow, O. A. Newer Approaches to the Radiolabeling of Monoclonal Antibodies by Use of Metal Chelates. *Nucl. Med. Biol.* **1991**, *18*, 369−381.
(47) Ruble, G.; Wu, C.; Squire, R. A.; Gansow, O. A.; Strand, M. The Use of ^{212}Pb-Labeled Monoclonal Antibody in the Treatment of Murine Erythroleukemia. *Int. J. Radiat. Oncol., Biol., Phys.* **1996**, *34*, 609−616.
(48) Horak, E.; Hartmann, F.; Garmestani, K.; Wu, C.; Brechbiel, M.; Gansow, O. A.; Landolfi, N. F.; Waldmann, T. A. Radioimmunotherapy Targeting of HER2/Neu Oncoprotein on Ovarian Tumor Using Lead-212-DOTA-AE1. *J. Nucl. Med.* **1997**, *38*, 1944−1950.
(49) Rizvi, S. N. F.; Visser, O. J.; Vosjan, M. J. W. D.; van Lingen, A.; Hoekstra, O. S.; Zijlstra, J. M.; Huijgens, P. C.; van Dongen, G. A. M. S.; Lubberink, M. Biodistribution, Radiation Dosimetry and Scouting of ^{90}Y-Ibritumomab Tiuxetan Therapy in Patients with Relapsed B-Cell Non-Hodgkin's Lymphoma Using ^{89}Zr-Ibritumomab Tiuxetan and PET. *Eur. J. Nucl. Med. Mol. Imaging* **2012**, *39*, 512−520.
(50) Rolleman, E. J.; Krenning, E. P.; Bernard, B. F.; de Visser, M.; Bijster, M.; Visser, T. J.; Vermeij, M.; Lindemans, J.; de Jong, M. Long-Term Toxicity of [^{177}Lu-DOTA^{0},Tyr^{3}]Octreotate in Rats. *Eur. J. Nucl. Med. Mol. Imaging* **2007**, *34*, 219−227.
(51) Pearson, R. G. Hard and Soft Acids and Bases, HSAB, Part I: Fundamental Principles. *J. Chem. Educ.* **1968**, *45*, 581−587.
(52) Martell, A. E.; Hancock, R. D. *Metal Complexes in Aqueous Solutions*; Plenum Press: New York, 1996.
(53) Pearson, R. G. Hard and Soft Acids and Bases, HSAB, Part II: Underlying Theories. *J. Chem. Educ.* **1968**, *45*, 643−648.
(54) Eplattenier, F. L.; Murase, I.; Martell, A. E. New Multidentate Ligands. VI. Chelating Tendencies of N,N'-Di(2-Hydroxybenzyl)-Ethylenediamine-N,N'-Diacetic Acid. *J. Am. Chem. Soc.* **1967**, *89*, 837−843.
(55) Frausto da Silva, J. J. R. The Chelate Effect Redefined. *J. Chem. Educ.* **1983**, *60*, 390−392.
(56) Hancock, R. D. Chelate Ring Size and Metal Ion Selection. The Basis of Selectivity for Metal Ions in Open-Chain Ligands and Macrocycles. *J. Chem. Educ.* **1992**, *69*, 615−621.
(57) Ionescu, R. M.; Vlasak, J.; Price, C.; Kirchmeier, M. Contribution of Variable Domains to the Stability of Humanized IgG1Monoclonal Antibodies. *J. Pharm. Sci.* **2008**, *97*, 1414−1426.
(58) Vermeer, A. W. P.; Norde, W. The Thermal Stability of Immunoglobulin: Unfolding and Aggregation of a Multi-Domain Protein. *Biophys. J.* **2000**, *78*, 394−404.
(59) Tircsó, G.; Kovács, Z.; Sherry, A. D. Equilibrium and Formation/Dissociation Kinetics of Some Ln^{III}PCTA Complexes. *Inorg. Chem.* **2006**, *45*, 9269−9280.
(60) Dadwal, M.; Kang, C. S.; Song, H. A.; Sun, X.; Dai, A.; Baidoo, K. E.; Brechbiel, M. W.; Chong, H. S. Synthesis and Evaluation of a Bifunctional Chelate for Development of Bi(III)-Labeled Radioimmunoconjugates. *Bioorg. Med. Chem. Lett.* **2011**, *21*, 7513−7515.
(61) Griffiths, G. L.; Govindan, S. V.; Sharkey, R. M.; Fisher, D. R.; Goldenberg, D. M. ^{90}Y-DOTA-HLL2: An Agent for Radioimmunotherapy of Non-Hodgkin's Lymphoma. *J. Nucl. Med.* **2003**, *44*, 77−84.
(62) McDevitt, M. R.; Finn, R. D.; Sgouros, G.; Ma, D.; Scheinberg, D. A. An ^{225}Ac/^{213}Bi Generator System for Therapeutic Clinical Applications: Construction and Operation. *Appl. Radiat. Isot.* **1999**, *50*, 895−904.
(63) Nayak, T. K.; Regino, C. A. S.; Wong, K. J.; Milenic, D. E.; Garmestani, K.; Baidoo, K. E.; Szajek, L. P.; Brechbiel, M. W. PET Imaging of HER1-Expressing Xenografts in Mice with ^{86}Y-CHX-A″-DTPA-Cetuximab. *Eur. J. Nucl. Med. Mol. Imaging* **2010**, *37*, 1368−1376.
(64) Liu, B.; Dong, L.; Yu, Q.; Li, X.; Wu, F.; Tan, Z.; Luo, S. Thermodynamic Study on the Protonation Reactions of Glyphosate in Aqueous Solution: Potentiometry, Calorimetry and NMR Spectroscopy. *J. Phys. Chem. B* **2016**, *120*, 2132−2137.
(65) Vaiana, L.; Esteban-Gómez, D.; Mato-Iglesias, M.; Platas-Iglesias, C.; de Blas, A.; Rodríguez-Blas, T. Anion Coordination Effect on the Nuclearity of CoII, NiII, CuII, and ZnII Complexes with a Benzimidazole Pendant-Armed Crown. *Eur. J. Inorg. Chem.* **2009**, *2009*, 400−411.
(66) Harris, W. R.; Carrano, C. J.; Raymond, K. N. Spectrophotometric Determination of the Proton-Dependent Stability Constant of Ferric Enterobactin. *J. Am. Chem. Soc.* **1979**, *101*, 2213−2214.
(67) Liu, Z. D.; Khodr, H. H.; Liu, D. Y.; Lu, S. L.; Hider, R. C. Synthesis, Physicochemical Characterization, and Biological Evaluation of 2-(1′-Hydroxyalkyl)-3-Hydroxypyridin-4-Ones: Novel Iron Chelators with Enhanced pFe^{3+} Values. *J. Med. Chem.* **1999**, *42*, 4814−4823.
(68) Aaseth, J.; Criponi, G.; Andersen, O. Chelating Agents as Therapeutic Compounds—Basic Principles. In *Chelation Therapy in the Treatment of Metal Intoxication*; Academic Press: Boston, 2016.
(69) Wedeking, P.; Kumar, K.; Tweedle, M. F. Dissociation of Gadolinium Chelates in Mice: Relationship to Chemical Characteristics. *Magn. Reson. Imaging* **1992**, *10*, 641−648.
(70) Graham, P.; Weatherburn, D. Dissociation Kinetics of Metal Complexes in Acid. Copper Complexes of Triazamacrocycles. *Aust. J. Chem.* **1981**, *34*, 291−300.
(71) Wilson, J. J.; Ferrier, M.; Radchenko, V.; Maassen, J. R.; Engle, J. W.; Batista, E. R.; Martin, R. L.; Nortier, F. M.; Fassbender, M. E.; John, K. D.; et al. Evaluation of Nitrogen-Rich Macrocyclic Ligands for the Chelation of Therapeutic Bismuth Radioisotopes. *Nucl. Med. Biol.* **2015**, *42*, 428−438.

DOI: 10.1021/acs.chemrev.8b00294
Chem. Rev. 2019, 119, 902−956

(72) Comba, P.; Jermilova, U.; Orvig, C.; Patrick, B. O.; Ramogida, C. F.; Rück, K.; Schneider, C.; Starke, M. Octadentate Picolinic Acid-Based Bispidine Ligand for Radiometal Ions. *Chem. - Eur. J.* **2017**, *23*, 15945−15956.
(73) Beykan, S.; Dam, J. S.; Eberlein, U.; Kaufmann, J.; Kjærgaard, B.; Jødal, L.; Bouterfa, H.; Bejot, R.; Lassmann, M.; Jensen, S. B. ^{177}Lu-OPS201 Targeting Somatostatin Receptors: In Vivo Biodistribution and Dosimetry in a Pig Model. *EJNMMI Res.* **2016**, *6*, 50.
(74) Kasten, B. B.; Azure, M. T.; Schoeb, T. R.; Fisher, D. R.; Zinn, K. R. Imaging, Biodistribution, and Toxicology Evaluation of ^{212}Pb-TCMC-Trastuzumab in Nonhuman Primates. *Nucl. Med. Biol.* **2016**, *43*, 391−396.
(75) Miederer, M.; Seidl, C.; Beyer, G.-J.; Charlton, D. E.; Vranjes-Duric, S.; Comor, J. J.; Huber, R.; Nikula, T.; Apostolidis, C.; Schuhmacher, C.; et al. Comparison of the Radiotoxicity of Two Alpha-Particle-Emitting Immunoconjugates, Terbium-149 and Bismuth-213, Directed against a Tumor-Specific, Exon 9 Deleted (D9) E-Cadherin Adhesion Protein. *Radiat. Res.* **2003**, *159*, 612−620.
(76) Sephton, R. G.; Hodgson, G. S.; De Abrew, S.; Harris, A. W. Ga-67 and Fe-59 Distributions in Mice. *J. Nucl. Med.* **1978**, *19*, 930−935.
(77) Abou, D. S.; Ku, T.; Smith-Jones, P. M. In Vivo Biodistribution and Accumulation of ^{89}Zr in Mice. *Nucl. Med. Biol.* **2011**, *38*, 675−681.
(78) Nikula, T. K.; McDevitt, M. R.; Finn, R. D.; Wu, C.; Kozak, R. W.; Garmestani, K.; Brechbiel, M. W.; Curcio, M. J.; Pippin, C. G.; Tiffany-Jones, L.; et al. Alpha-Emitting Bismuth Cyclohexylbenzyl DTPA Constructs of Recombinant Humanized Anti-CD33 Antibodies: Pharmacokinetics, Bioactivity, Toxicity and Chemistry. *J. Nucl. Med.* **1999**, *40*, 166−176.
(79) Pandey, U.; Gamre, N.; Kumar, Y.; Shetty, P.; Sarma, H. D.; Dash, A. A Systematic Evaluation of the Potential of PCTA-NCS Ligand as a Bifunctional Chelating Agent for Design of ^{177}Lu Radiopharmaceuticals. *J. Radioanal. Nucl. Chem.* **2016**, *307*, 187−194.
(80) Lee, S.; Hong, Y.; Kim, H.; Choi, S. Synthesis and Application of a Novel Cysteine-Based DTPA-NCS for Targeted Radioimmunotherapy. *Nucl. Med. Biol.* **2013**, *40*, 424−429.
(81) Boros, E.; Ferreira, C. L.; Cawthray, J. F.; Price, E. W.; Patrick, B. O.; Wester, D. W.; Adam, M. J.; Orvig, C. Acyclic Chelate with Ideal Properties for ^{68}Ga PET Imaging Agent Elaboration. *J. Am. Chem. Soc.* **2010**, *132*, 15726−15733.
(82) Kumar, K.; Tweedle, M. F. Macrocyclic Polyaminocarboxylate Complexes of Lanthanides as Magnetic Resonance Imaging Contrast Agents. *Pure Appl. Chem.* **1993**, *65*, 515−520.
(83) Tircsó, G.; Benyó, E. T.; Suh, E. H.; Jurek, P.; Kiefer, G. E.; Sherry, A. D.; Kovács, Z. (S)-5-(p-Nitrobenzyl)-PCTA, a Promising Bifunctional Ligand with Advantageous Metal Ion Complexation Kinetics. *Bioconjugate Chem.* **2009**, *20*, 565−575.
(84) Csajbók, É.; Baranyai, Z.; Bányai, I.; Brücher, E.; Király, R.; Müller-Fahrnow, A.; Platzek, J.; Radüchel, B.; Schäfer, M. Equilibrium, ^{1}H and ^{13}C NMR Spectroscopy, and X-Ray Diffraction Studies on the Complexes Bi(DOTA)$^{-}$ and Bi(DO3A-Bu). *Inorg. Chem.* **2003**, *42*, 2342−2349.
(85) Lattuada, L.; Barge, A.; Cravotto, G.; Giovenzana, G. B.; Tei, L. The Synthesis and Application of Polyamino Polycarboxylic Bifunctional Chelating Agents. *Chem. Soc. Rev.* **2011**, *40*, 3019−3049.
(86) Spreckelmeyer, S.; Ramogida, C. F.; Rousseau, J.; Arane, K.; Bratanovic, I.; Colpo, N.; Jermilova, U.; Dias, G. M.; Dude, I.; Jaraquemada-Peláez, M. de G.; et al. p-NO_2−Bn−H_4neunpa and H_4neunpa−Trastuzumab: Bifunctional Chelator for Radiometalpharmaceuticals and ^{111}In Immuno-Single Photon Emission Computed Tomography Imaging. *Bioconjugate Chem.* **2017**, *28*, 2145−2159.
(87) Price, E. W.; Zeglis, B. M.; Cawthray, J. F.; Ramogida, C. F.; Ramos, N.; Lewis, J. S.; Adam, M. J.; Orvig, C. H4Octapa-Trastuzumab: Versatile Acyclic Chelate System for ^{111}In and ^{177}Lu Imaging and Therapy. *J. Am. Chem. Soc.* **2013**, *135*, 12707−12721.
(88) Brechbiel, M. W.; Gansow, O. A. Backbone-Substituted DTPA Ligands for ^{90}Y Radioimmunotherapy. *Bioconjugate Chem.* **1991**, *2*, 187−194.
(89) Liu, S.; Edwards, D. S. Bifunctional Chelators for Therapeutic Lanthanide Radiopharmaceuticals. *Bioconjugate Chem.* **2001**, *12*, 7−34.
(90) Ruzza, P.; Calderan, A. Radiolabeled Peptide-Receptor Ligands in Tumor Imaging. *Expert Opin. Med. Diagn.* **2011**, *5*, 411−424.
(91) Benešová, M.; Bauder-Wüst, U.; Schäfer, M.; Klika, K. D.; Mier, W.; Haberkorn, U.; Kopka, K.; Eder, M. Linker Modification Strategies To Control the Prostate-Specific Membrane Antigen (PSMA)-Targeting and Pharmacokinetic Properties of DOTA-Conjugated PSMA Inhibitors. *J. Med. Chem.* **2016**, *59*, 1761−1775.
(92) Domnanich, K. A.; Müller, C.; Farkas, R.; Schmid, R. M.; Ponsard, B.; Schibli, R.; Türler, A.; Van der Meulen, N. P. ^{44}Sc for Labeling of DOTA- and NODAGA-Functionalized Peptides: Preclinical in Vitro and in Vivo Investigations. *EJNMMI Radiopharm. Chem.* **2017**, *1*, 8.
(93) Müller, C.; Vermeulen, C.; Johnston, K.; Köster, U.; Schmid, R.; Türler, A.; Van der Meulen, N. P. Preclinical in Vivo Application of ^{152}Tb-DOTANOC: A Radiolanthanide for PET Imaging. *EJNMMI Res.* **2016**, *6*, 35.
(94) Mijalis, A. J.; Thomas, D. A.; Simon, M. D.; Adamo, A.; Beaumont, R.; Jensen, K. F.; Pentelute, B. L. A Fully Automated Flow-Based Approach for Accelerated Peptide Synthesis. *Nat. Chem. Biol.* **2017**, *13*, 464−466.
(95) Chari, R. V. J. Targeted Cancer Therapy: Conferring Specificity to Cytotoxic Drugs. *Acc. Chem. Res.* **2008**, *41*, 98−107.
(96) Boswell, C. A.; Brechbiel, M. W. Development of Radioimmunotherapeutic and Diagnostic Antibodies: An Inside-Out View. *Nucl. Med. Biol.* **2007**, *34*, 757−778.
(97) Holliger, P.; Hudson, P. J. Engineered Antibody Fragments and the Rise of Single Domains. *Nat. Biotechnol.* **2005**, *23*, 1126−1136.
(98) García-Toraño, E.; Peyrés, V.; Roteta, M.; Sánchez-Cabezudo, A. I.; Romero, E.; Martínez Ortega, A. Standardisation and Precise Determination of the Half-Life of ^{44}Sc. *Appl. Radiat. Isot.* **2016**, *109*, 314−318.
(99) Eppard, E.; de la Fuente, A.; Benešová, M.; Khawar, A.; Bundschuh, R. A.; Gärtner, F. C.; Kreppel, B.; Kopka, K.; Essler, M.; Rösch, F. Clinical Translation and First In-Human Use of [^{44}Sc]Sc-PSMA-617 for PET Imaging of Metastasized Castrate-Resistant Prostate Cancer. *Theranostics* **2017**, *7*, 4359−4369.
(100) Chakravarty, R.; Goel, S.; Valdovinos, H. F.; Hernandez, R.; Hong, H.; Nickles, R. J.; Cai, W. Matching the Decay Half-Life with the Biological Half-Life: ImmunoPET Imaging with ^{44}Sc-Labeled Cetuximab Fab Fragment. *Bioconjugate Chem.* **2014**, *25*, 2197−2204.
(101) Domnanich, K. A.; Müller, C.; Benešová, M.; Dressler, R.; Haller, S.; Köster, U.; Ponsard, B.; Schibli, R.; Türler, A.; Van der Meulen, N. P. ^{47}Sc as Useful Bβ− Emitter for the Radiotheragnostic Paradigm: A Comparative Study of Feasible Production Routes. *EJNMMI Radiopharm. Chem.* **2017**, *2*, 5.
(102) Muller, C.; Bunka, M.; Haller, S.; Koster, U.; Groehn, V.; Bernhardt, P.; Van der Meulen, N.; Turler, A.; Schibli, R. Promising Prospects for ^{44}Sc-/^{47}Sc-Based Theragnostics: Application of ^{47}Sc for Radionuclide Tumor Therapy in Mice. *J. Nucl. Med.* **2014**, *55*, 1658−1664.
(103) Domnanich, K. A.; Eichler, R.; Müller, C.; Jordi, S.; Yakusheva, V.; Braccini, S.; Behe, M.; Schibli, R.; Türler, A.; Van der Meulen, N. P. Production and Separation of ^{43}Sc for Radiopharmaceutical Purposes. *EJNMMI Radiopharm. Chem.* **2017**, *2*, 14.
(104) Szkliniarz, K.; Jastrzębski, J.; Bilewicz, A.; Chajduk, E.; Choiński, J.; Jakubowski, A.; Janiszewska, Ł.; Leszczuk, E.; Łyczko, M.; Sitarz, M.; et al. Medical Radioisotopes Produced Using the Alpha Particle Beam from the Warsaw Heavy Ion Cyclotron. *Acta Phys. Pol., A* **2015**, *127*, 1471−1474.
(105) Walczak, R.; Krajewski, S.; Szkliniarz, K.; Sitarz, M.; Abbas, K.; Choiński, J.; Jakubowski, A.; Jastrzębski, J.; Majkowska, A.; Simonelli, F.; et al. Cyclotron Production of ^{43}Sc for PET Imaging. *EJNMMI Phys.* **2015**, *2*, 33.
(106) Szkliniarz, K.; Sitarz, M.; Walczak, R.; Jastrzębski, J.; Bilewicz, A.; Choiński, J.; Jakubowski, A.; Majkowska, A.; Stolarz, A.; Trzcińska,

DOI: 10.1021/acs.chemrev.8b00294
Chem. Rev. 2019, 119, 902−956

A.; et al. Production of Medical Sc Radioisotopes with an Alpha Particle Beam. *Appl. Radiat. Isot.* **2016**, *118*, 182−189.
(107) Alliot, C.; Kerdjoudj, R.; Michel, N.; Haddad, F.; Huclier-Markai, S. Cyclotron Production of High Purity ^{44m,44}Sc with Deuterons from $^{44}CaCO_3$ Targets. *Nucl. Med. Biol.* **2015**, *42*, 524−529.
(108) Huclier-Markai, S.; Kerdjoudj, R.; Alliot, C.; Bonraisin, A. C.; Michel, N.; Haddad, F.; Barbet, J. Optimization of Reaction Conditions for the Radiolabeling of DOTA and DOTA-Peptide with $^{44m/44}$Sc and Experimental Evidence of the Feasibility of an in Vivo PET Generator. *Nucl. Med. Biol.* **2014**, *41*, e36−e43.
(109) Zhang, P.; You, S.; Zhang, L.; Feng, S.; Hou, S. A Solvent Extraction Process for the Preparation of Ultrahigh Purity Scandium Oxide. *Hydrometallurgy* **1997**, *47*, 47−56.
(110) Radhakrishnan, K. P.; Owens, T. C. Separation of Scandium and Calcium by Liquid-Liquid Extraction Using Tributyl Phosphate as Solvent. *J. Chem. Eng. Data* **1972**, *17*, 478−482.
(111) Hoehr, C.; Oehlke, E.; Benard, F.; Lee, C. J.; Hou, X.; Badesso, B.; Ferguson, S.; Miao, Q.; Yang, H.; Buckley, K.; et al. ^{44g}Sc Production Using a Water Target on a 13 MeV Cyclotron. *Nucl. Med. Biol.* **2014**, *41*, 401−406.
(112) Valdovinos, H. F.; Hernandez, R.; Barnhart, T. E.; Graves, S.; Cai, W.; Nickles, R. J. Separation of Cyclotron-Produced ^{44}Sc from a Natural Calcium Target Using a Dipentyl Pentylphosphonate Functionalized Extraction Resin. *Appl. Radiat. Isot.* **2015**, *95*, 23−29.
(113) Muller, C.; Bunka, M.; Reber, J.; Fischer, C.; Zhernosekov, K.; Turler, A.; Schibli, R. Promises of Cyclotron-Produced ^{44}Sc as a Diagnostic Match for Trivalent ß$^-$-Emitters: In Vitro and In Vivo Study of a ^{44}Sc-DOTA-Folate Conjugate. *J. Nucl. Med.* **2013**, *54*, 2168−2174.
(114) Pruszyński, M.; Loktionova, N. S.; Filosofov, D. V.; Rösch, F. Post-Elution Processing of ^{44}Ti/^{44}Sc Generator-Derived ^{44}Sc for Clinical Application. *Appl. Radiat. Isot.* **2010**, *68*, 1636−1641.
(115) Filosofov, D. V.; Loktionova, N. S.; Rösch, F. A ^{44}Ti/^{44}Sc Radionuclide Generator for Potential Application of ^{44}Sc-Based PET-Radiopharmaceuticals. *Radiochim. Acta* **2010**, *98*, 149−156.
(116) Radchenko, V.; Engle, J. W.; Medvedev, D. G.; Maassen, J. M.; Naranjo, C. M.; Unc, G. A.; Meyer, C. A. L.; Mastren, T.; Brugh, M.; Mausner, L.; et al. Proton-Induced Production and Radiochemical Isolation of ^{44}Ti from Scandium Metal Targets for ^{44}Ti/^{44}Sc Generator Development. *Nucl. Med. Biol.* **2017**, *50*, 25−32.
(117) Daraban, L.; Adam Rebeles, R.; Hermanne, A.; Tarkanyi, F.; Takacs, S. Study of the Excitation Functions for ^{43}K, ^{43,44,44m}Sc and ^{44}Ti by Proton Irradiation on ^{45}Sc up to 37MeV. *Nucl. Instrum. Methods Phys. Res., Sect. B* **2009**, *267*, 755−759.
(118) Kopecky, P.; Szelecsényi, F.; Molnár, T.; Mikecz, P.; Tárkányi, F. Excitation Functions of (p,xn) Reactions on ^{Nat}Ti: Monitoring of Bombarding Proton Beams. *Appl. Radiat. Isot.* **1993**, *44*, 687−692.
(119) Mausner, L. F.; Kolsky, K. L.; Mease, R. C.; Chinol, M.; Meinken, G. E.; Straub, R. F.; Srivastava, S. C.; Pietrelli, L.; Steplewski, Z. Production and Evaluation of Sc-47 for Radioimmunotherapy. *J. Labelled Compd. Radiopharm.* **1993**, *32*, 388−390.
(120) Kolsky, K. L.; Joshi, V.; Mausner, L. F.; Srivastava, S. C. Radiochemical Purification of No-Carrier-Added Scandium-47 for Radioimmunotherapy. *Appl. Radiat. Isot.* **1998**, *49*, 1541−1549.
(121) Mausner, L. F.; Kolsky, K. L.; Joshi, V.; Srivastava, S. C. Radionuclide Development at BNL for Nuclear Medicine Therapy. *Appl. Radiat. Isot.* **1998**, *49*, 285−294.
(122) Deilami-nezhad, L.; Moghaddam-Banaem, L.; Sadeghi, M.; Asgari, M. Production and Purification of Scandium-47: A Potential Radioisotope for Cancer Theranostics. *Appl. Radiat. Isot.* **2016**, *118*, 124−130.
(123) Lahiri, S.; Banerjee, S.; Das, N. R. LLX Separation of Carrier-Free ^{47}Sc, ^{48}V and ^{48,49,51}Cr Produced in α-Particle Activated Titanium with HDEHP. *Appl. Radiat. Isot.* **1996**, *47*, 1−6.
(124) Yagi, M.; Kondo, K. Preparation of Carrier-Free ^{47}Sc by the ^{48}Ti (γ, p) Reaction. *Int. J. Appl. Radiat. Isot.* **1977**, *28*, 463−468.
(125) Bokhari, T. H.; Mushtaq, A.; Khan, I. U. Separation of No-Carrier-Added Radioactive Scandium from Neutron Irradiated Titanium. *J. Radioanal. Nucl. Chem.* **2010**, *283*, 389−393.
(126) Mamtimin, M.; Harmon, F.; Starovoitova, V. N. Sc-47 Production from Titanium Targets Using Electron Linacs. *Appl. Radiat. Isot.* **2015**, *102*, 1−4.
(127) Rane, S.; Harris, J. T.; Starovoitova, V. N. ^{47}Ca Production for ^{47}Ca/^{47}Sc Generator System Using Electron Linacs. *Appl. Radiat. Isot.* **2015**, *97*, 188−192.
(128) Horovitz, C. T. *Biochemistry of Scandium and Yttrium, Part 1: Physical and Chemical Fundamentals*; Springer: Boston, 1999.
(129) Melson, G. A. Chemical Properties. In *Scandium: Its Occurrence, Chemistry, Physics, Metallurgy, Biology, and Technology*; Horvitz, C. T., Ed.; Academic: London, 1975; pp 111−138.
(130) Anderson, T. J.; Neuman, M. A.; Melson, G. A. Coordination Chemistry of Scandium. V. Crystal and Molecular Structure of Tris (Acetylacetonato)Scandium(III). *Inorg. Chem.* **1973**, *12*, 927−930.
(131) Migliorati, V.; D'Angelo, P. Unraveling the Sc^{3+} Hydration Geometry: The Strange Case of the Far-Coordinated Water Molecule. *Inorg. Chem.* **2016**, *55*, 6703−6711.
(132) Pruszyński, M.; Majkowska-Pilip, A.; Loktionova, N. S.; Eppard, E.; Roesch, F. Radiolabeling of DOTATOC with the Long-Lived Positron Emitter ^{44}Sc. *Appl. Radiat. Isot.* **2012**, *70*, 974−979.
(133) Majkowska-Pilip, A.; Bilewicz, A. Macrocyclic Complexes of Scandium Radionuclides as Precursors for Diagnostic and Therapeutic Radiopharmaceuticals. *J. Inorg. Biochem.* **2011**, *105*, 313−320.
(134) Pniok, M.; Kubíček, V.; Havlíčková, J.; Kotek, J.; Sabatie-Gogová, A.; Plutnar, J.; Huclier-Markai, S.; Hermann, P. Thermodynamic and Kinetic Study of Scandium(III) Complexes of DTPA and DOTA: A Step Toward Scandium Radiopharmaceuticals. *Chem. - Eur. J.* **2014**, *20*, 7944−7955.
(135) Hermann, P.; Kotek, J.; Kubíček, V.; Lukeš, I. Gadolinium-(III) Complexes as MRI Contrast Agents: Ligand Design and Properties of the Complexes. *Dalton Trans* **2008**, *23*, 3027−3047.
(136) McMurry, T. J.; Pippin, C. G.; Wu, C.; Deal, K. A.; Brechbiel, M. W.; Mirzadeh, S.; Gansow, O. A. Physical Parameters and Biological Stability of Yttrium(III) Diethylenetriaminepentaacetic Acid Derivative Conjugates. *J. Med. Chem.* **1998**, *41*, 3546−3549.
(137) Aime, S.; Calabi, L.; Cavallotti, C.; Gianolio, E.; Giovenzana, G. B.; Losi, P.; Maiocchi, A.; Palmisano, G.; Sisti, M. [Gd-AAZTA]$^-$: A New Structural Entry for an Improved Generation of MRI Contrast Agents. *Inorg. Chem.* **2004**, *43*, 7588−7590.
(138) Gianolio, E.; Giovenzana, G. B.; Ciampa, A.; Lanzardo, S.; Imperio, D.; Aime, S. A Novel Method of Cellular Labeling: Anchoring MR-Imaging Reporter Particles on the Outer Cell Surface. *ChemMedChem* **2008**, *3*, 60−62.
(139) Gugliotta, G.; Botta, M.; Giovenzana, G. B.; Tei, L. Fast and Easy Access to Efficient Bifunctional Chelators for MRI Applications. *Bioorg. Med. Chem. Lett.* **2009**, *19*, 3442−3444.
(140) Baranyai, Z.; Uggeri, F.; Giovenzana, G. B.; Bényei, A.; Brücher, E.; Aime, S. Equilibrium and Kinetic Properties of the Lanthanoids(III) and Various Divalent Metal Complexes of the Heptadentate Ligand AAZTA. *Chem. - Eur. J.* **2009**, *15*, 1696−1705.
(141) Briley-Saebo, K. C.; Geninatti-Crich, S.; Cormode, D. P.; Barazza, A.; Mulder, W. J. M.; Chen, W.; Giovenzana, G. B.; Fisher, E. A.; Aime, S.; Fayad, Z. A. High-Relaxivity Gadolinium-Modified High-Density Lipoproteins as Magnetic Resonance Imaging Contrast Agents. *J. Phys. Chem. B* **2009**, *113*, 6283−6289.
(142) Nagy, G.; Szikra, D.; Trencsényi, G.; Fekete, A.; Garai, I.; Giani, A. M.; Negri, R.; Masciocchi, N.; Maiocchi, A.; Uggeri, F.; et al. AAZTA: An Ideal Chelating Agent for the Development of ^{44}Sc PET Imaging Agents. *Angew. Chem., Int. Ed.* **2017**, *56*, 2118−2122.
(143) Połosak, M.; Piotrowska, A.; Krajewski, S.; Bilewicz, A. Stability of ^{47}Sc-Complexes with Acyclic Polyamino-Polycarboxylate Ligands. *J. Radioanal. Nucl. Chem.* **2013**, *295*, 1867−1872.
(144) Deilami-nezhad, L.; Moghaddam-Banaem, L.; Sadeghi, M. Development of Bone Seeker Radiopharmaceuticals by Scandium-47 and Estimation of Human Absorbed Dose. *Appl. Radiat. Isot.* **2017**, *129*, 108−116.

DOI: 10.1021/acs.chemrev.8b00294
Chem. Rev. 2019, 119, 902−956

(145) Koumarianou, E.; Pawlak, D.; Korsak, A.; Mikolajczak, R. Comparison of Receptor Affinity of ^{Nat}Sc-DOTA-TATE versus ^{Nat}Ga-DOTA-TATE. *Nucl. Med. Rev.* **2011**, *14*, 85−89.
(146) Van der Meulen, N. P.; Bunka, M.; Domnanich, K. A.; Müller, C.; Haller, S.; Vermeulen, C.; Türler, A.; Schibli, R. Cyclotron Production of ^{44}Sc: From Bench to Bedside. *Nucl. Med. Biol.* **2015**, *42*, 745−751.
(147) Eigner, S.; Vera, D. R. B.; Fellner, M.; Loktionova, N. S.; Piel, M.; Lebeda, O.; Rösch, F.; Roß, T. L.; Henke, K. E. Imaging of Protein Synthesis: In Vitro and In Vivo Evaluation of ^{44}Sc-DOTA-Puromycin. *Mol. Imaging Biol.* **2013**, *15*, 79−86.
(148) Hernandez, R.; Valdovinos, H. F.; Yang, Y.; Chakravarty, R.; Hong, H.; Barnhart, T. E.; Cai, W. ^{44}Sc: An Attractive Isotope for Peptide-Based PET Imaging. *Mol. Pharmaceutics* **2014**, *11*, 2954−2961.
(149) Koumarianou, E.; Loktionova, N. S.; Fellner, M.; Roesch, F.; Thews, O.; Pawlak, D.; Archimandritis, S. C.; Mikolajczak, R. ^{44}Sc-DOTA-BN[2−14]NH_2 in Comparison to ^{68}Ga-DOTA-BN[2−14]NH_2 in Pre-Clinical Investigation. Is ^{44}Sc a Potential Radionuclide for PET? *Appl. Radiat. Isot.* **2012**, *70*, 2669−2676.
(150) Nagy, G.; Dénes, N.; Kis, A.; Szabó, J. P.; Berényi, E.; Garai, I.; Bai, P.; Hajdu, I.; Szikra, D.; Trencsényi, G. Preclinical Evaluation of Melanocortin-1 Receptor (MC1-R) Specific ^{68}Ga- and ^{44}Sc-Labeled DOTA-NAPamide in Melanoma Imaging. *Eur. J. Pharm. Sci.* **2017**, *106*, 336−344.
(151) Umbricht, C. A.; Benešová, M.; Schmid, R. M.; Türler, A.; Schibli, R.; van der Meulen, N. P.; Müller, C. ^{44}Sc-PSMA-617 for Radiotheragnostics in Tandem with ^{177}Lu-PSMA-617—Preclinical Investigations in Comparison with ^{68}Ga-PSMA-11 and ^{68}Ga-PSMA-617. *EJNMMI Res.* **2017**, *7*, 9.
(152) Honarvar, H.; Müller, C.; Cohrs, S.; Haller, S.; Westerlund, K.; Karlström, A. E.; Van der Meulen, N. P.; Schibli, R.; Tolmachev, V. Evaluation of the First ^{44}Sc-Labeled Affibody Molecule for Imaging of HER2-Expressing Tumors. *Nucl. Med. Biol.* **2017**, *45*, 15−21.
(153) Velikyan, I. Prospective of ^{68}Ga-Radiopharmaceutical Development. *Theranostics* **2014**, *4*, 47−80.
(154) Spang, P.; Herrmann, C.; Roesch, F. Bifunctional Gallium-68 Chelators: Past, Present, and Future. *Semin. Nucl. Med.* **2016**, *46*, 373−394.
(155) Fani, M.; André, J. P.; Maecke, H. R. ^{68}Ga-PET: A Powerful Generator-Based Alternative to Cyclotron-Based PET Radiopharmaceuticals. *Contrast Media Mol. Imaging* **2008**, *3*, 53−63.
(156) Jadvar, H.; Chen, X.; Cai, W.; Mahmood, U. Radiotheranostics in Cancer Diagnosis and Management. *Radiology* **2018**, *286*, 388−400.
(157) NETSPOT (kit for the preparation of gallium Ga 68 dotatate injection); https://www.accessdata.fda.gov/drugsatfda_docs/nda/2016/208547Orig1s000TOC.cfm (accessed Apr 1, 2018).
(158) Engle, J. W.; Lopez-Rodriguez, V.; Gaspar-Carcamo, R. E.; Valdovinos, H. F.; Valle-Gonzalez, M.; Trejo-Ballado, F.; Severin, G. W.; Barnhart, T. E.; Nickles, R. J.; Avila-Rodriguez, M. A. Very High Specific Activity $^{66/68}$Ga from Zinc Targets for PET. *Appl. Radiat. Isot.* **2012**, *70*, 1792−1796.
(159) Al-Suqri, B.; Al-Bulushi, N. Gallium-67 Scintigraphy in the Era of Positron Emission Tomography and Computed Tomography: Tertiary Centre Experience. *Sultan Qaboos Univ. Med. J.* **2015**, *15*, e338−343.
(160) bin Othman, M. F.; Mitry, N. R.; Lewington, V. J.; Blower, P. J.; Terry, S. Y. A. Re-Assessing Gallium-67 as a Therapeutic Radionuclide. *Nucl. Med. Biol.* **2017**, *46*, 12−18.
(161) *Production of Long Lived Parent Radionuclides for Generators: ^{68}Ge, ^{82}Sr, ^{90}Sr and ^{188}W*; An International Atomic Energy Agency Publication: Vienna, 2010.
(162) Velikyan, I. ^{68}Ga-Based Radiopharmaceuticals: Production and Application Relationship. *Molecules* **2015**, *20*, 12913−12943.
(163) Little, F. E.; Lagunas-Solar, M. C. Cyclotron Production of ^{67}Ga. Cross Sections and Thick-Target Yields for the ^{67}Zn(p, n) and ^{68}Zn(p, 2n) Reactions. *Int. J. Appl. Radiat. Isot.* **1983**, *34*, 631−637.
(164) Nagame, Y.; Unno, M.; Nakahara, H.; Murakami, Y. Production of ^{67}Ga by Alpha Bombardment of Natural Zinc. *Int. J. Appl. Radiat. Isot.* **1978**, *29*, 615−619.
(165) Andrade Martins, P. de; Osso, J. A. Thermal Diffusion of ^{67}Ga from Irradiated Zn Targets. *Appl. Radiat. Isot.* **2013**, *82*, 279−282.
(166) Sadeghi, M.; Mokhtari, L. Rapid Separation of ^{67,68}Ga from ^{68}Zn Target Using Precipitation Technique. *J. Radioanal. Nucl. Chem.* **2010**, *284*, 471−473.
(167) Al.Rayyes, A. H.; Ailouti, Y. Routine Simultaneous Production of No-Carrier-Added High Purity ^{64}Cu and ^{67}Ga. *Nukleonika* **2011**, *56*, 259−262.
(168) Gul, K. Calculations for the Excitation Functions of 3−26 MeV Proton Reactions on ^{66}Zn, ^{67}Zn and ^{68}Zn. *Appl. Radiat. Isot.* **2001**, *54*, 311−318.
(169) Steyn, J.; Meyer, B. R. Producion of ^{67}Ga by Deuteron Bombardment of Natural Zinc. *Int. J. Appl. Radiat. Isot.* **1973**, *24*, 369−372.
(170) Van der Meulen, N. P.; Van der Walt, T. N. The Separation of Fe from Ga to Produce Ultrapure ^{67}Ga. *Z. Naturforsch., B: J. Chem. Sci.* **2007**, *62*, 483−486.
(171) Naidoo, C.; Van der Walt, T. N. Cyclotron Production of ^{67}Ga(III) with a Tandem ^{Nat}Ge−^{Nat}Zn Target. *Appl. Radiat. Isot.* **2001**, *54*, 915−919.
(172) Nayak, D.; Lahiri, S. Alternative Methods for the Production of Carrier-Free ^{66,67}Ga. *Appl. Radiat. Isot.* **2001**, *54*, 189−193.
(173) Nayak, D.; Banerjee, A.; Lahiri, S. Separation of No-Carrier-Added ^{66,67}Ga Produced in Heavy Ion-Induced Cobalt Target Using Alginate Biopolymers. *Appl. Radiat. Isot.* **2007**, *65*, 891−896.
(174) Aardaneh, K.; Shirazi, B. Radiochemical Separation of ^{67}Ga from Zn and Cu Using the Adsorbent Resin Amberlite XAD-7. *J. Radioanal. Nucl. Chem.* **2005**, *265*, 47−51.
(175) Massaoud, A.; Hanafi, H.; Siyam, T.; Saleh, Z.; Ali, F. Separation of Ga(III) from Cu(II), Ni(II) and Zn(II) in Aqueous Solution Using Synthetic Polymeric Resins. *Cent. Eur. J. Chem.* **2008**, *6*, 39−45.
(176) Hassan, K. F. Rapid Separation of Radiogallium from Zn and Cu Targets Using Anion Exchange Technique. *J. Radioanal. Nucl. Chem.* **2011**, *289*, 801−804.
(177) Azadeh, P.; Yousef, F.; Reza, J. A.; Abbas, A.; Shahzad, F.; Mohsen, K. D.; Ali, R.; Ali, K. Radiosynthesis and Quality Control of [^{67}Ga]-3,4-Dimethoxylated Porphyrin Complex as a Possible Imaging Agent. *Iran J. Pharm. Res.* **2013**, *12*, 735−744.
(178) El-Azony, K. M.; Ferieg, K.; Saleh, Z. A. Direct Separation of ^{67}Ga Citrate from Zinc and Copper Target Materials by Anion Exchange. *Appl. Radiat. Isot.* **2003**, *59*, 329−331.
(179) Cyclotron Produced Radionuclides. *Physical Characteristics and Production Methods*; An International Atomic Energy Agency Publication: Vienna, 2009.
(180) Dumortier, R.; Weber, M. E.; Vera, J. H. Removal and Recovery of Gallium from Aqueous Solutions by Complexation with Sodium Di-(n-Octyl) Phosphinate. *Hydrometallurgy* **2005**, *76*, 207−215.
(181) Zweit, J.; Sharma, H.; Downey, S. Production of Gallium-66, a Short-Lived, Positron Emitting Radionuclide. *Int. J. Rad. Appl. Instrum. A* **1987**, *38*, 499−501.
(182) Lewis, M. R.; Reichert, D. E.; Laforest, R.; Margenau, W. H.; Shefer, R. E.; Klinkowstein, R. E.; Hughey, B. J.; Welch, M. J. Production and Purification of Gallium-66 for Preparation of Tumor-Targeting Radiopharmaceuticals. *Nucl. Med. Biol.* **2002**, *29*, 701−706.
(183) Szelecsényi, F.; Boothe, T. E.; Tavano, E.; Plitnikas, M. E.; Tárkányi, F. Compilation of Cross Sections/Thick Target Yields for ^{66}Ga, ^{67}Ga and ^{68}Ga Production Using Zn Targets up to 30 MeV Proton Energy. *Appl. Radiat. Isot.* **1994**, *45*, 473−500.
(184) Jalilian, A. R.; Rowshanfarzad, P.; Sabet, M.; Novinrooz, A.; Raisali, G. Preparation of [^{66}Ga]Bleomycin Complex as a Possible PET Radiopharmaceutical. *J. Radioanal. Nucl. Chem.* **2005**, *264*, 617−621.
(185) Hong, H.; Zhang, Y.; Engle, J. W.; Nayak, T. R.; Theuer, C. P.; Nickles, R. J.; Barnhart, T. E.; Cai, W. In Vivo Targeting and Positron

DOI: 10.1021/acs.chemrev.8b00294
Chem. Rev. 2019, 119, 902−956

Emission Tomography Imaging of Tumor Vasculature with ^{66}Ga-Labeled Nano-Graphene. *Biomaterials* **2012**, *33*, 4147−4156.
(186) Pourjavadi, A.; Akhlaghi, M.; Jalilian, A. R. Preparation and Evaluation of a [^{66}Ga]Gallium Chitosan Complex in Fibrosarcoma Bearing Animal Models. *Nukleonika* **2011**, *56*, 35−40.
(187) Harris, W. R.; Chen, Y.; Wein, K. Equilibrium Constants for the Binding of Indium(III) to Human Serum Transferrin. *Inorg. Chem.* **1994**, *33*, 4991−4998.
(188) Kubícek, V.; Havlícková, J.; Kotek, J.; Tircsó, G.; Hermann, P.; Tóth, E.; Lukes, I. Gallium(III) Complexes of DOTA and DOTA-Monoamide: Kinetic and Thermodynamic Studies. *Inorg. Chem.* **2010**, *49*, 10960−10969.
(189) Knetsch, P. A.; Petrik, M.; Rangger, C.; Seidel, G.; Pietzsch, H.-J.; Virgolini, I.; Decristoforo, C.; Haubner, R. [^{68}Ga]NS_3-RGD and [^{68}Ga]Oxo-DO3A-RGD for Imaging $\alpha_v\beta_3$ Integrin Expression: Synthesis, Evaluation, and Comparison. *Nucl. Med. Biol.* **2013**, *40*, 65−72.
(190) Clarke, E. T.; Martell, A. E. Stabilities of Trivalent Metal Ion Complexes of the Tetraacetate Derivatives of 12-, 13- and 14-Membered Tetraazamacrocycles. *Inorg. Chim. Acta* **1991**, *190*, 37−46.
(191) Niu, W.; Wong, E. H.; Weisman, G. R.; Peng, Y.; Anderson, C. J.; Zakharov, L. N.; Golen, J. A.; Rheingold, A. L. Structural and Dynamic Studies of Zinc, Gallium, and Cadmium Complexes of a Dicarboxylate Pendant-Armed Cross-Bridged Cyclen. *Eur. J. Inorg. Chem.* **2004**, *2004*, 3310−3315.
(192) Aime, S.; Botta, M.; Geninatti Crich, S.; Giovenzana, G. B.; Jommi, G.; Pagliarin, R.; Sisti, M. Synthesis and NMR Studies of Three Pyridine-Containing Triaza Macrocyclic Triacetate Ligands and Their Complexes with Lanthanide Ions. *Inorg. Chem.* **1997**, *36*, 2992−3000.
(193) Ferreira, C. L.; Lamsa, E.; Woods, M.; Duan, Y.; Fernando, P.; Bensimon, C.; Kordos, M.; Guenther, K.; Jurek, P.; Kiefer, G. E. Evaluation of Bifunctional Chelates for the Development of Gallium-Based Radiopharmaceuticals. *Bioconjugate Chem.* **2010**, *21*, 531−536.
(194) Ferreira, C. L.; Yapp, D. T. T.; Mandel, D.; Gill, R. K.; Boros, E.; Wong, M. Q.; Jurek, P.; Kiefer, G. E. ^{68}Ga Small Peptide Imaging: Comparison of NOTA and PCTA. *Bioconjugate Chem.* **2012**, *23*, 2239−2246.
(195) Anderson, C. J.; Dehdashti, F.; Cutler, P. D.; Schwarz, S. W.; Laforest, R.; Bass, L. A.; Lewis, J. S.; McCarthy, D. W. ^{64}Cu-TETA-Octreotide as a PET Imaging Agent for Patients with Neuroendocrine Tumors. *J. Nucl. Med.* **2001**, *42*, 213−221.
(196) Lewis, J. S.; Lewis, M. R.; Cutler, P. D.; Srinivasan, A.; Schmidt, M. A.; Schwarz, S. W.; Morris, M. M.; Miller, J. P.; Anderson, C. J. Radiotherapy and Dosimetry of ^{64}Cu-TETA-Tyr^3-Octreotate in a Somatostatin Receptor-Positive, Tumor-Bearing Rat Model. *Clin. Cancer Res.* **1999**, *5*, 3608−3616.
(197) Martell, A. E.; Motekaitis, R. J.; Clarke, E. T.; Delgado, R.; Sun, Y.; Ma, R. Stability Constants of Metal Complexes of Macrocyclic Ligands with Pendant Donor Groups. *Supramol. Chem.* **1996**, *6*, 353−363.
(198) Velikyan, I.; Maecke, H.; Langstrom, B. Convenient Preparation of ^{68}Ga-Based PET-Radiopharmaceuticals at Room Temperature. *Bioconjugate Chem.* **2008**, *19*, 569−573.
(199) Jyo, A.; Kohno, T.; Terazono, Y.; Kawano, S. Crystal Structure of Gallium(III) Complex of 1,4,7-Triazacyclonane-N,N′,N″-Triacetate. *Anal. Sci.* **1990**, *6*, 323−324.
(200) Craig, A. S.; Parker, D.; Adams, H.; Bailey, N. A. Stability, ^{71}Ga NMR, and Crystal Structure of a Neutral Gallium(III) Complex of 1,4,7-Triazacyclononanetriacetate: A Potential Radiopharmaceutical? *J. Chem. Soc., Chem. Commun.* **1989**, *23*, 1793−1794.
(201) Prata, M. I. M.; Santos, A. C.; Geraldes, C. F. G. C.; de Lima, J. J. P. Structural and in Vivo Studies of Metal Chelates of Ga(III) Relevant to Biomedical Imaging. *J. Inorg. Biochem.* **2000**, *79*, 359−363.
(202) Shetty, D.; Choi, S. Y.; Jeong, J. M.; Hoigebazar, L.; Lee, Y. S.; Lee, D. S.; Chung, J. K.; Lee, M. C.; Chung, Y. K. Formation and Characterization of Gallium(III) Complexes with Monoamide Derivatives of 1,4,7-Triazacyclononane-1,4,7-Triacetic Acid: A Study of the Dependency of Structure on Reaction PH. *Eur. J. Inorg. Chem.* **2010**, *2010*, 5432−5438.
(203) André, J. P.; Maecke, H. R.; André, J. P.; Zehnder, M.; Macko, L.; Akyel, K. G. 1,4,7-Triazacyclononane-1-Succinic Acid-4,7-Diacetic Acid (NODASA): A New Bifunctional Chelator for Radio Gallium-Labelling of Biomolecules. *Chem. Commun.* **1998**, *12*, 1301−1302.
(204) Eisenwiener, K.-P.; Prata, M. I. M.; Buschmann, I.; Zhang, H.-W.; Santos, A. C.; Wenger, S.; Reubi, J. C.; Mäcke, H. R. NODAGATOC, a New Chelator-Coupled Somatostatin Analogue Labeled with [$^{67/68}$Ga] and [^{111}In] for SPECT, PET, and Targeted Therapeutic Applications of Somatostatin Receptor (Hsst2) Expressing Tumors. *Bioconjugate Chem.* **2002**, *13*, 530−541.
(205) Lee, J.; Garmestani, K.; Wu, C.; Brechbiel, M. W.; Chang, H. K.; Choi, C. W.; Gansow, O. A.; Carrasquillo, J. A.; Paik, C. H. In Vitro and in Vivo Evaluation of Structure-Stability Relationship of ^{111}In- and ^{67}Ga-Labeled Antibody via 1B4M or C-NOTA Chelates. *Nucl. Med. Biol.* **1997**, *24*, 225−230.
(206) Šimeček, J.; Notni, J.; Kapp, T. G.; Kessler, H.; Wester, H.-J. Benefits of NOPO As Chelator in Gallium-68 Peptides, Exemplified by Preclinical Characterization of ^{68}Ga-NOPO−c(RGDfK). *Mol. Pharmaceutics* **2014**, *11*, 1687−1695.
(207) Šimeček, J.; Zemek, O.; Hermann, P.; Notni, J.; Wester, H.-J. Tailored Gallium(III) Chelator NOPO: Synthesis, Characterization, Bioconjugation, and Application in Preclinical Ga-68-PET Imaging. *Mol. Pharmaceutics* **2014**, *11*, 3893−3903.
(208) Fellner, M.; Riss, P.; Loktionova, N. S.; Zhernosekov, K. P.; Thews, O.; Geraldes, C. F. G. C.; Kovacs, Z.; Lukes, I.; Rösch, F. Comparison of Different Phosphorus-Containing Ligands Complexing ^{68}Ga for PET-Imaging of Bone Metabolism. *Radiochim. Acta* **2011**, *99*, 43−51.
(209) Poty, S.; Désogère, P.; Šimeček, J.; Bernhard, C.; Goncalves, V.; Goze, C.; Boschetti, F.; Notni, J.; Wester, H. J.; Denat, F. MA-NOTMP: A Triazacyclononane Trimethylphosphinate Based Bifunctional Chelator for Gallium Radiolabelling of Biomolecules. *ChemMedChem* **2015**, *10*, 1475−1479.
(210) Máté, G.; Šimeček, J.; Pniok, M.; Kertész, I.; Notni, J.; Wester, H.-J.; Galuska, L.; Hermann, P. The Influence of the Combination of Carboxylate and Phosphinate Pendant Arms in 1,4,7-Triazacyclononane-Based Chelators on Their ^{68}Ga Labelling Properties. *Molecules* **2015**, *20*, 13112−13126.
(211) Prata, M. I. M.; André, J. P.; Kovács, Z.; Takács, A. I.; Tircsó, G.; Tóth, I.; Geraldes, C. F. G. C. Gallium(III) Chelates of Mixed Phosphonate-Carboxylate Triazamacrocyclic Ligands Relevant to Nuclear Medicine: Structural, Stability and in Vivo Studies. *J. Inorg. Biochem.* **2017**, *177*, 8−16.
(212) Ferreira, M. F.; Pereira, G.; André, J. P.; Prata, M. I. M.; Ferreira, P. M. T.; Martins, J. A.; Geraldes, C. F. G. C. Ga[NO2A-N-(α-Amino)Propionate] Chelates: Synthesis and Evaluation as Potential Tracers for ^{68}Ga PET. *Dalton Trans* **2014**, *43*, 8037−8047.
(213) Notni, J.; Hermann, P.; Havlíčková, J.; Kotek, J.; Kubíček, V.; Plutnar, J.; Loktionova, N.; Riss, P. J.; Rösch, F.; Lukeš, I. A Triazacyclononane-Based Bifunctional Phosphinate Ligand for the Preparation of Multimeric ^{68}Ga Tracers for Positron Emission Tomography. *Chem. - Eur. J.* **2010**, *16*, 7174−7185.
(214) Notni, J.; Šimeček, J.; Hermann, P.; Wester, H. J. TRAP, a Powerful and Versatile Framework for Gallium-68 Radiopharmaceuticals. *Chem. - Eur. J.* **2011**, *17*, 14718−14722.
(215) Notni, J.; Pohle, K.; Wester, H.-J. Comparative Gallium-68 Labeling of TRAP-, NOTA-, and DOTA-Peptides: Practical Consequences for the Future of Gallium-68-PET. *EJNMMI Res.* **2012**, *2*, 28.
(216) Notni, J.; Pohle, K.; Wester, H. J. Be Spoilt for Choice with Radiolabelled RGD Peptides: Preclinical Evaluation of ^{68}Ga-TRAP-$(RGD)_3$. *Nucl. Med. Biol.* **2013**, *40*, 33−41.
(217) Kojima, S.; Jay, M. Comparisons of Labeling Efficiency, Biological Activity and Biodistribution among ^{125}I-, ^{67}Ga-DTPA-and ^{67}Ga-DFO-Lectins. *Eur. J. Nucl. Med.* **1987**, *13*, 366−370.
(218) Koop, B.; Reske, S. N.; Neumaier, B. Labelling of a Monoclonal Antibody with ^{68}Ga Using Three DTPA-Based Bifunc-

DOI: 10.1021/acs.chemrev.8b00294
Chem. Rev. 2019, 119, 902−956

tional Ligands and Their in Vitro Evaluation for Application in Radioimmunotherapy. *Radiochim. Acta* **2007**, *95*, 39−42.
(219) Camera, L.; Kinuya, S.; Garmestani, K.; Wu, C.; Brechbiel, M. W.; Pai, L. H.; McMurry, T. J.; Gansow, O. A.; Pastan, I.; Paik, C. H.; et al. Evaluation of the Serum Stability and in Vivo Biodistribution of CHX-DTPA and Other Ligands for Yttrium Labeling of Monoclonal Antibodies. *J. Nucl. Med.* **1994**, *35*, 882−889.
(220) Wei, L.; Zhang, X.; Gallazzi, F.; Miao, Y.; Jin, X.; Brechbiel, M. W.; Xu, H.; Clifford, T.; Welch, M. J.; Lewis, J. S.; et al. Melanoma Imaging Using ^{111}In-, ^{86}Y- and ^{68}Ga-Labeled CHX-A″-Re(Arg^{11})-CCMSH. *Nucl. Med. Biol.* **2009**, *36*, 345−354.
(221) Sun, Y.; Anderson, C. J.; Pajeau, T. S.; Reichert, D. E.; Hancock, R. D.; Motekaitis, R. J.; Martell, A. E.; Welch, M. J. Indium(III) and Gallium(III) Complexes of Bis(Aminoethanethiol) Ligands with Different Denticities: Stabilities, Molecular Modeling, and in Vivo Behavior. *J. Med. Chem.* **1996**, *39*, 458−470.
(222) Bergeron, R. J.; Wiegand, J.; Brittenham, G. M. HBED: The Continuing Development of a Potential Alternative to Deferoxamine for Iron-Chelating Therapy. *Blood* **1999**, *93*, 370−375.
(223) Ma, R.; Motekaitis, R. J.; Martell, A. E. Stability of Metal Ion Complexes of N,N′-Bis(2-Hydroxybenzyl)Ethylenediamine-N,N′-Diacetic Acid. *Inorg. Chim. Acta* **1994**, *224*, 151−155.
(224) Ma, R.; Murase, I.; Martell, A. E. Synthesis and Characterization of Metal Complexes with N,N″-Bis(2-Hydroxybenzyl)-Diethylenetriamine-N, N′,N″-Triacetic Acid and the Stabilities of Its Complexes with Divalent and Trivalent Metal Ions. *Inorg. Chim. Acta* **1994**, *223*, 109−119.
(225) Taliaferro, C. H.; Martell, A. New Multidentate Ligands. XXIV. Disodium-N,N′-Bis(2-Hydroxy-5-Sulfobenzyl)-Ethylenediaminediacetic Acid, a New Chelating Ligand for Trivalent Metal Ions. *Inorg. Chim. Acta* **1984**, *85*, 9−15.
(226) Wong, E.; Caravan, P.; Liu, S.; Rettig, S. J.; Orvig, C. Selectivity of Potentially Hexadentate Amine Phenols for Ga^{3+} and In^{3+} in Aqueous Solution. *Inorg. Chem.* **1996**, *35*, 715−724.
(227) Motekaitis, R. J.; Sun, Y.; Martell, A. E. N,N′-Bispyridoxylethylenediamine-N,N′-Diacetic Acid (PLED) and N,N′-Bis(2-Hydroxy-5-Sulfobenzylethylenediamine-N,N′-Diacetic Acid (SHBED). *Inorg. Chim. Acta* **1989**, *159*, 29−39.
(228) Weineisen, M.; Simecek, J.; Schottelius, M.; Schwaiger, M.; Wester, H. J. Synthesis and Preclinical Evaluation of DOTAGA-Conjugated PSMA Ligands for Functional Imaging and Endoradiotherapy of Prostate Cancer. *EJNMMI Res.* **2014**, *4*, 63.
(229) Eder, M.; Wängler, B.; Knackmuss, S.; LeGall, F.; Little, M.; Haberkorn, U.; Mier, W.; Eisenhut, M. Tetrafluorophenolate of HBED-CC: A Versatile Conjugation Agent for ^{68}Ga-Labeled Small Recombinant Antibodies. *Eur. J. Nucl. Med. Mol. Imaging* **2008**, *35*, 1878−1886.
(230) Eder, M.; Krivoshein, A. V.; Backer, M.; Backer, J. M.; Haberkorn, U.; Eisenhut, M. ScVEGF-PEG-HBED-CC and ScVEGF-PEG-NOTA Conjugates: Comparison of Easy-to-Label Recombinant Proteins for [^{68}Ga]PET Imaging of VEGF Receptors in Angiogenic Vasculature. *Nucl. Med. Biol.* **2010**, *37*, 405−412.
(231) Eder, M.; Knackmuss, S.; Le Gall, F.; Reusch, U.; Rybin, V.; Little, M.; Haberkorn, U.; Mier, W.; Eisenhut, M. ^{68}Ga-Labelled Recombinant Antibody Variants for Immuno-PET Imaging of Solid Tumours. *Eur. J. Nucl. Med. Mol. Imaging* **2010**, *37*, 1397−1407.
(232) Schuhmacher, J.; Klivényi, G.; Matys, R.; Stadler, M.; Regiert, T.; Hauser, H.; Doll, J.; Maier-Borst, W.; Zöller, M. Multistep Tumor Targeting in Nude Mice Using Bispecific Antibodies and a Gallium Chelate Suitable for Immunoscintigraphy with Positron Emission Tomography. *Cancer Res.* **1995**, *55*, 115−123.
(233) Tsionou, M. I.; Knapp, C. E.; Foley, C. A.; Munteanu, C. R.; Cakebread, A.; Imberti, C.; Eykyn, T. R.; Young, J. D.; Paterson, B. M.; Blower, P. J.; et al. Comparison of Macrocyclic and Acyclic Chelators for Gallium-68 Radiolabelling. *RSC Adv.* **2017**, *7*, 49586−49599.
(234) Schuhmacher, J.; Klivényi, G.; Hull, W. E.; Matys, R.; Hauser, H.; Kalthoff, H.; Schmiegel, W. H.; Maier-Borst, W.; Matzku, S. A Bifunctional HBED-Derivative for Labeling of Antibodies with ^{67}Ga, ^{111}In and ^{59}Fe. Comparative Biodistribution with ^{111}In-DTPA and ^{131}I-Labeled Antibodies in Mice Bearing Antibody Internalizing And Non-internalizing Tumors. *Nucl. Med. Biol.* **1992**, *19*, 809−824.
(235) Eder, M.; Neels, O.; Müller, M.; Bauder-Wüst, U.; Remde, Y.; Schäfer, M.; Hennrich, U.; Eisenhut, M.; Afshar-Oromieh, A.; Haberkorn, U.; et al. Novel Preclinical and Radiopharmaceutical Aspects of [^{68}Ga]Ga-PSMA-HBED-CC: A New PET Tracer for Imaging of Prostate Cancer. *Pharmaceuticals* **2014**, *7*, 779−796.
(236) Smith, S. W. Chiral Toxicology: It's the Same Thing···Only Different. *Toxicol. Sci.* **2009**, *110*, 4−30.
(237) Ma, M. T.; Blower, P. J. Chelators for Diagnostic Molecular Imaging with Radioisotopes of Copper, Gallium and Zirconium. In *Metal Chelation in Medicine*; Crichton, R., Ward, R. J., Hider, R. J., Eds.; The Royal Society of Chemistry: Cambridge, 2017; pp 260−312.
(238) Larsen, S. K.; Jenkins, B. G.; Memon, N. G.; Lauffer, R. B. Structure-Affinity Relationships in the Binding of Unsubstituted Iron Phenolate Complexes to Human Serum Albumin. Molecular Structure of Iron(III) N, N'-Bis(2-Hydroxybenzyl)Ethylenediamine-N,N'-Diacetate. *Inorg. Chem.* **1990**, *29*, 1147−1152.
(239) Schäfer, M.; Bauder-Wüst, U.; Leotta, K.; Zoller, F.; Mier, W.; Haberkorn, U.; Eisenhut, M.; Eder, M. A Dimerized Urea-Based Inhibitor of the Prostate-Specific Membrane Antigen for ^{68}Ga-PET Imaging of Prostate Cancer. *EJNMMI Res.* **2012**, *2*, 23.
(240) Eder, M.; Schäfer, M.; Bauder-Wüst, U.; Haberkorn, U.; Eisenhut, M.; Kopka, K. Preclinical Evaluation of a Bispecific Low-Molecular Heterodimer Targeting Both PSMA and GRPR for Improved PET Imaging and Therapy of Prostate Cancer. *Prostate* **2014**, *74*, 659−668.
(241) Eder, M.; Lohr, T.; Bauder-Wust, U.; Reber, M.; Mier, W.; Schafer, M.; Haberkorn, U.; Eisenhut, M. Pharmacokinetic Properties of Peptidic Radiopharmaceuticals: Reduced Uptake of $(EH)_3$-Conjugates in Important Organs. *J. Nucl. Med.* **2013**, *54*, 1327−1330.
(242) Baranski, A.-C.; Schäfer, M.; Bauder-Wüst, U.; Wacker, A.; Schmidt, J.; Liolios, C.; Mier, W.; Haberkorn, U.; Eisenhut, M.; Kopka, K.; et al. Improving the Imaging Contrast of ^{68}Ga-PSMA-11 by Targeted Linker Design: Charged Spacer Moieties Enhance the Pharmacokinetic Properties. *Bioconjugate Chem.* **2017**, *28*, 2485−2492.
(243) Afshar-Oromieh, A.; Hetzheim, H.; Kratochwil, C.; Benesova, M.; Eder, M.; Neels, O. C.; Eisenhut, M.; Kubler, W.; Holland-Letz, T.; Giesel, F. L.; et al. The Theranostic PSMA Ligand PSMA-617 in the Diagnosis of Prostate Cancer by PET/CT: Biodistribution in Humans, Radiation Dosimetry, and First Evaluation of Tumor Lesions. *J. Nucl. Med.* **2015**, *56*, 1697−1705.
(244) Minamimoto, R.; Hancock, S.; Schneider, B.; Chin, F. T.; Jamali, M.; Loening, A.; Vasanawala, S.; Gambhir, S. S.; Iagaru, A. Pilot Comparison of ^{68}Ga-RM2 PET and ^{68}Ga-PSMA-11 PET in Patients with Biochemically Recurrent Prostate Cancer. *J. Nucl. Med.* **2016**, *57*, 557−562.
(245) NIH U.S. National Library of Medicine. www.ClinicalTrials.gov (accessed Apr 1, 2018).
(246) Zhou, T.; Neubert, H.; Liu, D. Y.; Liu, Z. D.; Ma, Y. M.; Kong, X. Le; Luo, W.; Mark, S.; Hider, R. C. Iron Binding Dendrimers: A Novel Approach for the Treatment of Haemochromatosis. *J. Med. Chem.* **2006**, *49*, 4171−4182.
(247) Berry, D. J.; Ma, Y.; Ballinger, J. R.; Tavaré, R.; Koers, A.; Sunassee, K.; Zhou, T.; Nawaz, S.; Mullen, G. E. D.; Hider, R. C.; et al. Efficient Bifunctional Gallium-68 Chelators for Positron Emission Tomography: Tris(Hydroxypyridinone) Ligands. *Chem. Commun.* **2011**, *47*, 7068−7070.
(248) Ma, M. T.; Meszaros, L. K.; Paterson, B. M.; Berry, D. J.; Cooper, M. S.; Ma, Y.; Hider, R. C.; Blower, P. J. Tripodal Tris(Hydroxypyridinone) Ligands for Immunoconjugate PET Imaging with $^{89}Zr^{4+}$: Comparison with Desferrioxamine-B. *Dalton Trans* **2015**, *44*, 4884−4900.
(249) Ma, M. T.; Cullinane, C.; Imberti, C.; Baguña Torres, J.; Terry, S. Y. A.; Roselt, P.; Hicks, R. J.; Blower, P. J. New Tris(Hydroxypyridinone) Bifunctional Chelators Containing Isothio-

DOI: 10.1021/acs.chemrev.8b00294
Chem. Rev. 2019, 119, 902−956

cyanate Groups Provide a Versatile Platform for Rapid One-Step Labeling and PET Imaging with $^{68}Ga^{3+}$. *Bioconjugate Chem.* **2016**, *27*, 309−318.
(250) Ma, M. T.; Cullinane, C.; Waldeck, K.; Roselt, P.; Hicks, R. J.; Blower, P. J. Rapid Kit-Based ^{68}Ga-Labelling and PET Imaging with THP-Tyr^3-Octreotate: A Preliminary Comparison with DOTA-Tyr^3-Octreotate. *EJNMMI Res.* **2015**, *5*, 52.
(251) Young, J. D.; Abbate, V.; Imberti, C.; Meszaros, L. K.; Ma, M. T.; Terry, S. Y. A.; Hider, R. C.; Mullen, G. E.; Blower, P. J. ^{68}Ga-THP-PSMA: A PET Imaging Agent for Prostate Cancer Offering Rapid, Room-Temperature, 1-Step Kit-Based Radiolabeling. *J. Nucl. Med.* **2017**, *58*, 1270−1277.
(252) Imberti, C.; Terry, S. Y. A.; Cullinane, C.; Clarke, F.; Cornish, G. H.; Ramakrishnan, N. K.; Roselt, P.; Cope, A. P.; Hicks, R. J.; Blower, P. J.; et al. Enhancing PET Signal at Target Tissue in Vivo: Dendritic and Multimeric Tris(Hydroxypyridinone) Conjugates for Molecular Imaging of $\alpha_v\beta_3$ Integrin Expression with Gallium-68. *Bioconjugate Chem.* **2017**, *28*, 481−495.
(253) Brom, M.; Franssen, G. M.; Joosten, L.; Gotthardt, M.; Boerman, O. C. The Effect of Purification of Ga-68-Labeled Exendin on in Vivo Distribution. *EJNMMI Res.* **2016**, *6*, 65.
(254) Cusnir, R.; Imberti, C.; Hider, R.; Blower, P.; Ma, M. Hydroxypyridinone Chelators: From Iron Scavenging to Radiopharmaceuticals for PET Imaging with Gallium-68. *Int. J. Mol. Sci.* **2017**, *18*, 116.
(255) Boros, E.; Ferreira, C. L.; Yapp, D. T. T.; Gill, R. K.; Price, E. W.; Adam, M. J.; Orvig, C. RGD Conjugates of the H_2dedpa Scaffold: Synthesis, Labeling and Imaging with ^{68}Ga. *Nucl. Med. Biol.* **2012**, *39*, 785−794.
(256) Ramogida, C. F.; Cawthray, J. F.; Boros, E.; Ferreira, C. L.; Patrick, B. O.; Adam, M. J.; Orvig, C. H_2CHXdedpa and H_4CHXoctapa—Chiral Acyclic Chelating Ligands for ^{67,68}Ga and ^{111}In Radiopharmaceuticals. *Inorg. Chem.* **2015**, *54*, 2017−2031.
(257) Boros, E.; Ferreira, C. L.; Patrick, B. O.; Adam, M. J.; Orvig, C. New Ga Derivatives of the H_2dedpa Scaffold with Improved Clearance and Persistent Heart Uptake. *Nucl. Med. Biol.* **2011**, *38*, 1165−1174.
(258) Ramogida, C. F.; Pan, J.; Ferreira, C. L.; Patrick, B. O.; Rebullar, K.; Yapp, D. T. T.; Lin, K. S.; Adam, M. J.; Orvig, C. Nitroimidazole-Containing H_2Dedpa and H_2CHXdedpa Derivatives as Potential PET Imaging Agents of Hypoxia with ^{68}Ga. *Inorg. Chem.* **2015**, *54*, 4953−4965.
(259) Weekes, D. M.; Ramogida, C. F.; Jaraquemada-Peláez, M. D. G.; Patrick, B. O.; Apte, C.; Kostelnik, T. I.; Cawthray, J. F.; Murphy, L.; Orvig, C. Dipicolinate Complexes of Gallium(III) and Lanthanum(III). *Inorg. Chem.* **2016**, *55*, 12544−12558.
(260) Baranyai, Z.; Uggeri, F.; Maiocchi, A.; Giovenzana, G. B.; Cavallotti, C.; Takács, A.; Tóth, I.; Bányai, I.; Bényei, A.; Brucher, E.; et al. Equilibrium, Kinetic and Structural Studies of AAZTA Complexes with Ga^{3+}, In^{3+} and Cu^{2+}. *Eur. J. Inorg. Chem.* **2013**, *2013*, 147−162.
(261) Waldron, B. P. *Synthesis and Evaluation of New Ligands for Gallium Radiolabelling*; Ph.D Thesis, Durham University, 2013.
(262) Parker, D.; Waldron, B. P.; Yufit, D. S. Crystallographic and Solution NMR Structural Analyses of Four Hexacoordinated Gallium(III) Complexes Based on Ligands Derived from 6-Amino-Perhydro-1,4-Diazepine. *Dalton Trans* **2013**, *42*, 8001−8008.
(263) Seemann, J.; Waldron, B. P.; Roesch, F.; Parker, D. Approaching 'Kit-Type' Labelling with ^{68}Ga: The DATA Chelators. *ChemMedChem* **2015**, *10*, 1019−1026.
(264) Seemann, J.; Waldron, B.; Parker, D.; Roesch, F. DATATOC: A Novel Conjugate for Kit-Type ^{68}Ga Labelling of TOC at Ambient Temperature. *EJNMMI Radiopharm. Chem.* **2017**, *1*, 1−12.
(265) Farkas, E.; Nagel, J.; Waldron, B. P.; Parker, D.; Tóth, I.; Brücher, E.; Rösch, F.; Baranyai, Z. Equilibrium, Kinetic and Structural Properties of Gallium(III) and Some Divalent Metal Complexes Formed with the New DATA^m and DATA^{5m} Ligands. *Chem. - Eur. J.* **2017**, *23*, 10358−10371.
(266) Herscheid, J. D. M.; Hoekstra, A.; Vos, C. M. N-Succinyldesferrioxamine B: A Potential Radiopharmaceutical for Assessing Renal Function. *Eur. J. Nucl. Med.* **1984**, *9*, 508−510.
(267) Herscheid, J. D.; Knops, G. H.; Hoekstra, M. The Biodistribution of ^{67}Ga-Labelled N-Hydroxyamino Acid Derivatives in Tumour-Bearing Rats. *Nucl. Med. Commun.* **1986**, *7*, 53−57.
(268) Koizumi, M.; Endo, K.; Kunimatsu, M.; Sakahara, H.; Nakashima, T.; Kawamura, Y.; Watanabe, Y.; Saga, T.; Konishi, J.; Yamamuro, T.; et al. ^{67}Ga-Labeled Antibodies for Immunoscintigraphy and Evaluation of Tumor Targeting of Drug-Antibody Conjugates in Mice. *Cancer Res.* **1988**, *48*, 1189−1194.
(269) Smith-Jones, P. M.; Stolz, B.; Bruns, C.; Albert, R.; Reist, H. W.; Fridrich, R.; Mäcke, H. R. Gallium-67/Gallium-68-[DFO]-Octreotide- a Potential Radiopharmaceutical for PET Imaging of Somatostatin Receptor-Positive Tumors: Synthesis and Radiolabeling in Vitro and Preliminary in Vivo Studies. *J. Nucl. Med.* **1994**, *35*, 317−325.
(270) Mathias, C. J.; Wang, S.; Lee, R. J.; Waters, D. J.; Low, P. S.; Green, M. A. Tumor-Selective Radiopharmaceutical Targeting via Receptor-Mediated Endocytosis of Gallium-67-Deferoxamine-Folate. *J. Nucl. Med.* **1996**, *37*, 1003−1008.
(271) Wang, S.; Lee, R. J.; Mathias, C. J.; Green, M. A.; Low, P. S. Synthesis, Purification, and Tumor Cell Uptake of ^{67}Ga-Deferoxamine−Folate, a Potential Radiopharmaceutical for Tumor Imaging. *Bioconjugate Chem.* **1996**, *7*, 56−62.
(272) Zhai, C.; Summer, D.; Rangger, C.; Haas, H.; Haubner, R.; Decristoforo, C. Fusarinine C, a Novel Siderophore-Based Bifunctional Chelator for Radiolabeling with Gallium-68. *J. Labelled Compd. Radiopharm.* **2015**, *58*, 209−214.
(273) Emery, T.; Hoffer, P. B. Siderophore-Mediated Mechanism of Gallium Uptake Demonstrated in the Microorganism Ustilago Sphaerogena. *J. Nucl. Med.* **1980**, *21*, 935−939.
(274) Ioppolo, J. A.; Caldwell, D.; Beiraghi, O.; Llano, L.; Blacker, M.; Valliant, J. F.; Berti, P. J. ^{67}Ga-Labeled Deferoxamine Derivatives for Imaging Bacterial Infection: Preparation and Screening of Functionalized Siderophore Complexes. *Nucl. Med. Biol.* **2017**, *52*, 32−41.
(275) Knetsch, P. A.; Zhai, C.; Rangger, C.; Blatzer, M.; Haas, H.; Kaeopookum, P.; Haubner, R.; Decristoforo, C. [^{68}Ga]FSC-$(RGD)_3$ a Trimeric RGD Peptide for Imaging $\alpha_v\beta_3$ Integrin Expression Based on a Novel Siderophore Derived Chelating Scaffold—synthesis and Evaluation. *Nucl. Med. Biol.* **2015**, *42*, 115−122.
(276) Zhai, C.; Franssen, G. M.; Petrik, M.; Laverman, P.; Summer, D.; Rangger, C.; Haubner, R.; Haas, H.; Decristoforo, C. Comparison of Ga-68-Labeled Fusarinine C-Based Multivalent RGD Conjugates and [^{68}Ga]NODAGA-RGD—In Vivo Imaging Studies in Human Xenograft Tumors. *Mol. Imaging Biol.* **2016**, *18*, 758−767.
(277) Motekaitis, R. J.; Martell, A. E.; Koch, S. A.; Hwang, J.; Quarless, D. A.; Welch, M. J. The Gallium(III) and Indium(III) Complexes of Tris(2-Mercaptobenzyl)Amine and Tris(2-Hydroxybenzyl)Amine. *Inorg. Chem.* **1998**, *37*, 5902−5911.
(278) Notni, J.; Pohle, K.; Peters, J. A.; Görls, H.; Platas-Iglesias, C. Structural Study of Ga(III), In(III), and Fe(III) Complexes of Triaza-Macrocycle Based Ligands with N_3S_3 Donor Set. *Inorg. Chem.* **2009**, *48*, 3257−3267.
(279) Sun, Y.; Martell, A. E.; Motekaitis, R. J.; Welch, M. J. Synthesis and Stabilities of the Ga(III) and In(III) Chelates of a New Diaminodithiol Bifunctional Ligand. *Tetrahedron* **1998**, *54*, 4203−4210.
(280) Li, Y.; Martell, A. E.; Hancock, R. D.; Reibenspies, J. H.; Anderson, C. J.; Welch, M. J. N. N'-Ethylenedi-L-Cysteine (EC) and Its Metal Complexes: Synthesis, Characterization, Crystal Structures, and Equilibrium Constants. *Inorg. Chem.* **1996**, *35*, 404−414.
(281) Anderson, C. J.; John, C. S.; Li, Y. J.; Hancock, R. D.; McCarthy, T. J.; Martell, A. E.; Welch, M. J. N,N′-Ethylene-Di-L-Cysteine (EC) Complexes of Ga(III) and In(III): Molecular Modeling, Thermodynamic Stability and in Vivo Studies. *Nucl. Med. Biol.* **1995**, *22*, 165−173.

DOI: 10.1021/acs.chemrev.8b00294
Chem. Rev. 2019, 119, 902−956

(282) Zheng, Y. Y.; Saluja, S.; Yap, G. P. A.; Blumenstein, M.; Rheingold, A. L.; Francesconi, L. C. Gallium and Indium Complexes of Bis(Amino Thiol) (N_2S_2) Ligands. *Inorg. Chem.* **1996**, *35*, 6656−6666.
(283) Francesconi, L. C.; Liu, B.; Billings, J. J.; Carroll, P. J.; Graczyk, G.; Kung, H. F. Synthesis, Characterization and Solid State Structure of a Neutral Gallium(III) Amino Thiolate Complex: A Potential Radiopharmaceutical for PET Imaging. *J. Chem. Soc., Chem. Commun.* **1991**, *2*, 94−95.
(284) Mirzaei, A.; Jalilian, A. R.; Aghanejad, A.; Mazidi, M.; Yousefnia, H.; Shabani, G.; Ardaneh, K.; Geramifar, P.; Beiki, D. Preparation and Evaluation of ^{68}Ga-ECC as a PET Renal Imaging Agent. *Nucl. Med. Mol. Imaging* **2015**, *49*, 208−216.
(285) Mirzaei, A.; Jalilian, A. R.; Shabani, G.; Fakhari, A.; Akhlaghi, M.; Beiki, D. Development of ^{68}Ga Ethyl Cysteinate Dimer for PET Studies. *J. Radioanal. Nucl. Chem.* **2016**, *307*, 725−732.
(286) Tsang, B. W.; Mathias, C. J.; Fanwick, P. E.; Green, M. A. Structure-Distribution Relationships for Metal-Labeled Myocardial Imaging Agents: Comparison of a Series of Cationic Gallium(III) Complexes with Hexadentate Bis(Salicylaldimine) Ligands. *J. Med. Chem.* **1994**, *37*, 4400−4406.
(287) Hsiao, Y. M.; Mathias, C. J.; Wey, S.-P.; Fanwick, P. E.; Green, M. A. Synthesis and Biodistribution of Lipophilic and Monocationic Gallium Radiopharmaceuticals Derived from N,N′-Bis(3-Aminopropyl)-N,N′-Dimethylethylenediamine: Potential Agents for PET Myocardial Imaging with ^{68}Ga. *Nucl. Med. Biol.* **2009**, *36*, 39−45.
(288) Sharma, V.; Beatty, A.; Wey, S.-P.; Dahlheimer, J.; Pica, C.; Crankshaw, C.; Bass, L.; Green, M.; Welch, M.; Piwnica-Worms, D. Novel Gallium(III) Complexes Transported by MDR1 P-Glycoprotein: Potential PET Imaging Agents for Probing P-Glycoprotein-Mediated Transport Activity in Vivo. *Chem. Biol.* **2000**, *7*, 335−343.
(289) Sivapackiam, J.; Harpstrite, S. E.; Rath, N. P.; Sharma, V. ^{67}Ga-Metalloprobes: Monitoring the Impact of Geometrical Isomers on Accumulation Profiles in Rat Cardiomyoblasts and Human Breast Carcinoma Cells. *MedChemComm* **2017**, *8*, 158−161.
(290) Panagiotidis, E.; Alshammari, A.; Michopoulou, S.; Skoura, E.; Naik, K.; Maragkoudakis, E.; Mohmaduvesh, M.; Al-Harbi, M.; Belda, M.; Caplin, M. E.; et al. Comparison of the Impact of ^{68}Ga-DOTATATE and ^{18}F-FDG PET/CT on Clinical Management in Patients with Neuroendocrine Tumors. *J. Nucl. Med.* **2017**, *58*, 91−96.
(291) Calais, J.; Fendler, W.; Eiber, M.; Wolin, E.; Slavik, R.; Barrio, M.; Gupta, P.; Quon, A.; Schiepers, C.; Auerbach, M.; et al. High Degree of Implementation of Intended Management Changes after ^{68}Ga-DOTATATE PET/CT Imaging in Patients with Neuroendocrine Tumors. *J. Nucl. Med.* **2017**, *58*, 172.
(292) Zolghadri, S.; Naderi, M.; Yousefnia, H.; Alirezapour, B.; Beiki, D. Evaluation of the Possible Utilization of ^{68}Ga-DOTATOC in Diagnosis of Adenocarcinoma Breast Cancer. *Asia Ocean. J. Nucl. Med. Biol.* **2018**, *6*, 41−49.
(293) Graham, M. M.; Gu, X.; Ginader, T.; Breheny, P.; Sunderland, J. J. ^{68}Ga-DOTATOC Imaging of Neuroendocrine Tumors: A Systematic Review and Metaanalysis. *J. Nucl. Med.* **2017**, *58*, 1452−1458.
(294) Velikyan, I.; Sundin, A.; Sorensen, J.; Lubberink, M.; Sandstrom, M.; Garske-Roman, U.; Lundqvist, H.; Granberg, D.; Eriksson, B. Quantitative and Qualitative Intrapatient Comparison of ^{68}Ga-DOTATOC and ^{68}Ga-DOTATATE: Net Uptake Rate for Accurate Quantification. *J. Nucl. Med.* **2014**, *55*, 204−210.
(295) Ambrosini, V.; Campana, D.; Bodei, L.; Nanni, C.; Castellucci, P.; Allegri, V.; Montini, G. C.; Tomassetti, P.; Paganelli, G.; Fanti, S. ^{68}Ga-DOTANOC PET/CT Clinical Impact in Patients with Neuroendocrine Tumors. *J. Nucl. Med.* **2010**, *51*, 669−673.
(296) Campana, D.; Ambrosini, V.; Pezzilli, R.; Fanti, S.; Labate, A. M. M.; Santini, D.; Ceccarelli, C.; Nori, F.; Franchi, R.; Corinaldesi, R.; et al. Standardized Uptake Values of ^{68}Ga-DOTANOC PET: A Promising Prognostic Tool in Neuroendocrine Tumors. *J. Nucl. Med.* **2010**, *51*, 353−359.
(297) Benesova, M.; Schafer, M.; Bauder-Wust, U.; Afshar-Oromieh, A.; Kratochwil, C.; Mier, W.; Haberkorn, U.; Kopka, K.; Eder, M. Preclinical Evaluation of a Tailor-Made DOTA-Conjugated PSMA Inhibitor with Optimized Linker Moiety for Imaging and Endoradiotherapy of Prostate Cancer. *J. Nucl. Med.* **2015**, *56*, 914−920.
(298) Virgolini, I.; Decristoforo, C.; Haug, A.; Fanti, S.; Uprimny, C. Current Status of Theranostics in Prostate Cancer. *Eur. J. Nucl. Med. Mol. Imaging* **2018**, *45*, 471−495.
(299) Eder, M.; Schäfer, M.; Bauder-Wüst, U.; Hull, W.-E.; Wängler, C.; Mier, W.; Haberkorn, U.; Eisenhut, M. ^{68}Ga-Complex Lipophilicity and the Targeting Property of a Urea-Based PSMA Inhibitor for PET Imaging. *Bioconjugate Chem.* **2012**, *23*, 688−697.
(300) Afshar-Oromieh, A.; Malcher, A.; Eder, M.; Eisenhut, M.; Linhart, H. G.; Hadaschik, B. A.; Holland-Letz, T.; Giesel, F. L.; Kratochwil, C.; Haufe, S.; et al. PET Imaging with a [^{68}Ga]Gallium-Labelled PSMA Ligand for the Diagnosis of Prostate Cancer: Biodistribution in Humans and First Evaluation of Tumour Lesions. *Eur. J. Nucl. Med. Mol. Imaging* **2013**, *40*, 486−495.
(301) Dalm, S. U.; Bakker, I. L.; de Blois, E.; Doeswijk, G. N.; Konijnenberg, M. W.; Orlandi, F.; Barbato, D.; Tedesco, M.; Maina, T.; Nock, B. A.; et al. ^{68}Ga/^{177}Lu-NeoBOMB1, a Novel Radiolabeled GRPR Antagonist for Theranostic Use in Oncology. *J. Nucl. Med.* **2017**, *58*, 293−299.
(302) Nock, B. A.; Kaloudi, A.; Lymperis, E.; Giarika, A.; Kulkarni, H. R.; Klette, I.; Singh, A.; Krenning, E. P.; de Jong, M.; Maina, T.; et al. Theranostic Perspectives in Prostate Cancer with the Gastrin-Releasing Peptide Receptor Antagonist NeoBOMB1: Preclinical and First Clinical Results. *J. Nucl. Med.* **2017**, *58*, 75−80.
(303) Herrmann, K.; Lapa, C.; Wester, H.-J.; Schottelius, M.; Schiepers, C.; Eberlein, U.; Bluemel, C.; Keller, U.; Knop, S.; Kropf, S.; et al. Biodistribution and Radiation Dosimetry for the Chemokine Receptor CXCR4-Targeting Probe ^{68}Ga-Pentixafor. *J. Nucl. Med.* **2015**, *56*, 410−416.
(304) Nicolas, G. P.; Schreiter, N.; Kaul, F.; Uiters, J.; Bouterfa, H.; Kaufmann, J.; Erlanger, T. E.; Cathomas, R.; Christ, E.; Fani, M.; et al. Comparison of ^{68}Ga-OPS202 (^{68}Ga-NODAGA-JR11) and ^{68}Ga-DOTATOC (^{68}Ga-Edotreotide) PET/CT in Patients with Gastroenteropancreatic Neuroendocrine Tumors: Evaluation of Sensitivity in a Prospective Phase II Imaging. *J. Nucl. Med.* **2018**, *59*, 915−921.
(305) Jødal, L. Beta Emitters and Radiation Protection. *Acta Oncol.* **2009**, *48*, 308−313.
(306) Kong, G.; Callahan, J.; Hofman, M. S.; Pattison, D. A.; Akhurst, T.; Michael, M.; Eu, P.; Hicks, R. J. High Clinical and Morphologic Response Using ^{90}Y-DOTA-Octreotate Sequenced with ^{177}Lu-DOTA-Octreotate Induction Peptide Receptor Chemoradionuclide Therapy (PRCRT) for Bulky Neuroendocrine Tumours. *Eur. J. Nucl. Med. Mol. Imaging* **2017**, *44*, 476−489.
(307) McQuade, P.; Miao, Y.; Yoo, J.; Quinn, T. P.; Welch, M. J.; Lewis, J. S. Imaging of Melanoma Using ^{64}Cu− and ^{86}Y−DOTA−ReCCMSH(Arg^{11}), a Cyclized Peptide Analogue of α-MSH. *J. Med. Chem.* **2005**, *48*, 2985−2992.
(308) Biddlecombe, G. B.; Rogers, B. E.; de Visser, M.; Parry, J. J.; de Jong, M.; Erion, J. L.; Lewis, J. S. Molecular Imaging of Gastrin-Releasing Peptide Receptor-Positive Tumors in Mice Using ^{64}Cu- and ^{86}Y-DOTA−(Pro^1 Tyr^4)-Bombesin(1−14). *Bioconjugate Chem.* **2007**, *18*, 724−730.
(309) Westcott, M. A.; Coldwell, D. M.; Liu, D. M.; Zikria, J. F. The Development, Commercialization, and Clinical Context of Yttrium-90 Radiolabeled Resin and Glass Microspheres. *Adv. Radiat. Oncol.* **2016**, *1*, 351−364.
(310) Carrasquillo, J. A.; White, J. D.; Paik, C. H.; Raubitschek, A.; Le, N.; Rotman, M.; Brechbiel, M. W.; Gansow, O. A.; Top, L. E.; Perentesis, P.; et al. Similarities and Differences in ^{111}In- and ^{90}Y-Labeled 1B4M-DTPA AntiTac Monoclonal Antibody Distribution. *J. Nucl. Med.* **1999**, *40*, 268−276.
(311) Liu, C.; Liu, G.; Liu, N.; Zhang, Y.; He, J.; Rusckowski, M.; Hnatowich, D. J. Radiolabeling Morpholinos with ^{90}Y, ^{111}In, ^{188}Re and ^{99m}Tc. *Nucl. Med. Biol.* **2003**, *30*, 207−214.

DOI: 10.1021/acs.chemrev.8b00294
Chem. Rev. 2019, 119, 902−956

(312) Rösch, F.; Herzog, H.; Qaim, S. The Beginning and Development of the Theranostic Approach in Nuclear Medicine, as Exemplified by the Radionuclide Pair ^{86}Y and ^{90}Y. *Pharmaceuticals* **2017**, *10*, 56.
(313) Mausner, L. F.; Srivastava, S. C. Selection of Radionuclides for Radioimmunotherapy. *Med. Phys.* **1993**, *20*, 503−509.
(314) Conti, M.; Eriksson, L. Physics of Pure and Non-Pure Positron Emitters for PET: A Review and a Discussion. *EJNMMI Phys.* **2016**, *3*, 8.
(315) Rane, A. T.; Bhatki, K. S. Rapid Radiochemical Separations of Strontium-90-Yttrium-90 and Calcium-45-Scandium-46 on a Cation Exchange Resin. *Anal. Chem.* **1966**, *38*, 1598−1601.
(316) Suzuki, Y. Preparation of Carrier-Free Y^{90} from Sr^{90} with Ion Exchange. *Int. J. Appl. Radiat. Isot.* **1964**, *15*, 599−602.
(317) Chakravarty, R.; Dash, A. Availability of Yttrium-90 from Strontium-90: A Nuclear Medicine Perspective. *Cancer Biother.Radiopharm.* **2012**, *27*, 621−641.
(318) Abbasi, I. A.; Zaidi, J. H.; Arif, M.; Waheed, S.; Subhani, M. S. Measurement of Fission Neutron Spectrum Averaged Cross Sections of Threshold Reactions on Zirconium: Production Possibility of No-Carrier-Added ^{90}Y in a Nuclear Reaction. *Radiochim. Acta* **2006**, *94*, 381−384.
(319) Knapp, F. F.; Dash, A. *Radiopharmaceuticals for Therapy*; Springer: India, 2016.
(320) Chinol, M.; Hnatowich, D. J. Generator-Produced Yttrium-90 for Radioimmunotherapy. *J. Nucl. Med.* **1987**, *28*, 1465−1470.
(321) Lee, T. W.; Ting, G. Study on the Separation of Carrier-Free Yttrium-90 from Strontium-90. *Isotopenpraxis* **1991**, *27*, 269−273.
(322) Malja, S.; Schomacker, K.; Malja, E. Preparation of ^{90}Y by the ^{90}Sr-^{90}Y Generator for Medical Purpose. *J. Radioanal. Nucl. Chem.* **2000**, *245*, 403−406.
(323) Venkatesh, M.; Pandey, A. K.; Dhami, P. S.; Kannan, R.; Achuthan, P. V.; Chitnis, R. R.; Gopalakrishnan, V.; Banerjee, S.; Samuel, G.; Pillai, M. R. A.; et al. Complexation Studies with ^{90}Y from a Novel ^{90}Sr-^{90}Y Generator. *Radiochim. Acta* **2001**, *89*, 413−417.
(324) Chakravarty, R.; Pandey, U.; Manolkar, R. B.; Dash, A.; Venkatesh, M.; Pillai, M. R. A. Development of an Electrochemical ^{90}Sr-^{90}Y Generator for Separation of ^{90}Y for Targeted Therapy. *Nucl. Med. Biol.* **2008**, *35*, 245−253.
(325) Petrović, D. Z.; Trtić-Petrović, T. M.; Vladisavljević, G. T.; Stoiljković, M. M.; Slavković-Beškoski, L. J.; Kumrić, K. R. Novel ^{90}Sr−^{90}Y Generator System Based on a Pertraction through Supported Liquid Membrane in Hollow Fiber Contactor. *Chem. Eng. Res. Des.* **2015**, *97*, 57−67.
(326) Rösch, F.; Qaim, S. M.; Stöcklin, G. Nuclear Data Relevant to the Production of the Positron Emitting Radioisotope ^{86}Y via the ^{86}Sr(p, n)- and ^{Nat}Rb(^{3}He, xn)-Processes. *Radiochim. Acta* **1993**, *61*, 1−8.
(327) Rösch, F.; Qaim, S. M.; Stöcklin, G. Production of the Positron Emitting Radioisotope ^{86}Y for Nuclear Medical Application. *Appl. Radiat. Isot.* **1993**, *44*, 677−681.
(328) Zaneb, H.; Hussain, M.; Amjed, N.; Qaim, S. M. Nuclear Model Analysis of Excitation Functions of Proton Induced Reactions on ^{86}Sr, ^{88}Sr and ^{Nat}Zr: Evaluation of Production Routes of ^{86}Y. *Appl. Radiat. Isot.* **2015**, *104*, 232−241.
(329) Baimukhanova, A.; Radchenko, V.; Kozempel, J.; Marinova, A.; Brown, V.; Karandashev, V.; Karaivanov, D.; Schaffer, P.; Filosofov, D. Utilization of (p,4n) Reaction for ^{86}Zr Production with Medium Energy Protons and Development of a ^{86}Zr → ^{86}Y Radionuclide Generator. *J. Radioanal. Nucl. Chem.* **2018**, *316*, 191−199.
(330) Sadeghi, M.; Aboudzadeh, M.; Zali, A.; Zeinali, B. ^{86}Y Production via ^{86}Sr(p, n) for PET Imaging at a Cyclotron. *Appl. Radiat. Isot.* **2009**, *67*, 1392−1396.
(331) Oehlke, E.; Hoehr, C.; Hou, X.; Hanemaayer, V.; Zeisler, S.; Adam, M. J.; Ruth, T. J.; Celler, A.; Buckley, K.; Benard, F.; et al. Production of Y-86 and Other Radiometals for Research Purposes Using a Solution Target System. *Nucl. Med. Biol.* **2015**, *42*, 842−849.
(332) Avila-Rodriguez, M. A.; Nye, J. A.; Nickles, R. J. Production and Separation of Non-Carrier-Added ^{86}Y from Enriched ^{86}Sr Targets. *Appl. Radiat. Isot.* **2008**, *66*, 9−13.
(333) Kandil, S. A.; Scholten, B.; Hassan, K. F.; Hanafi, H. A.; Qaim, S. M. A Comparative Study on the Separation of Radioyttrium from Sr- and Rb-Targets via Ion-Exchange and Solvent Extraction Techniques, with Special Reference to the Production of No-Carrier-Added ^{86}Y, ^{87}Y and ^{88}Y Using a Cyclotron. *J. Radioanal. Nucl. Chem.* **2009**, *279*, 823−832.
(334) Medvedev, D. G.; Mausner, L. F.; Srivastava, S. C. Irradiation of Strontium Chloride Targets at Proton Energies above 35 MeV to Produce PET Radioisotope Y-86. *Radiochim. Acta* **2011**, *99*, 755−761.
(335) Garmestani, K.; Milenic, D. E.; Plascjak, P. S.; Brechbiel, M. W. A New and Convenient Method for Purification of ^{86}Y Using a Sr(II) Selective Resin and Comparison of Biodistribution of ^{86}Y and ^{111}In Labeled Herceptin™. *Nucl. Med. Biol.* **2002**, *29*, 599−606.
(336) Kettern, K.; Linse, K. H.; Spellerberg, S.; Coenen, H. H.; Qaim, S. M. Radiochemical Studies Relevant to the Production of ^{86}Y and ^{88}Y at a Small-Sized Cyclotron. *Radiochim. Acta* **2002**, *90*, 845−849.
(337) Reischl, G.; Rösch, F.; Machulla, H.-J. Electrochemical Separation and Purification of Yttrium-86. *Radiochim. Acta* **2002**, *90*, 225−228.
(338) Yoo, J.; Tang, L.; Perkins, T. A.; Rowland, D. J.; Laforest, R.; Lewis, J. S.; Welch, M. J. Preparation of High Specific Activity ^{86}Y Using a Small Biomedical Cyclotron. *Nucl. Med. Biol.* **2005**, *32*, 891−897.
(339) Lukić, D.; Tamburella, C.; Buchegger, F.; Beyer, G.-J.; Čomor, J. J.; Seimbille, Y. High Efficiency Production and Purification of ^{86}Y Based on Electrochemical Separation. *Appl. Radiat. Isot.* **2009**, *67*, 523−529.
(340) Breeman, W. A. P.; Jong, M.; Visser, T. J.; Erion, J. L.; Krenning, E. P. Optimising Conditions for Radiolabelling of DOTA-Peptides with ^{90}Y, ^{111}In and ^{177}Lu at High Specific Activities. *Eur. J. Nucl. Med. Mol. Imaging* **2003**, *30*, 917−920.
(341) Chakravarty, R.; Chakraborty, S.; Dash, A. A Systematic Comparative Evaluation of ^{90}Y-Labeled Bifunctional Chelators for Their Use in Targeted Therapy. *J. Labelled Compd. Radiopharm.* **2014**, *57*, 65−74.
(342) Parker, D.; Pulukkody, K.; Smith, F. C.; Batsanov, A.; Howard, J. A. K. Structures of the Yttrium Complexes of 1,4,7,10-Tetraazacyclododecane-N,N′,N″,N‴-Tetraacetic Acid (H_4Dota) and N,N″-Bis(Benzylcarbamoylmethyl)Diethylenetriamine-N,N′,N″-Triacetic Acid and the Solution Structure of a Zirconium Complex of H_4. *J. Chem. Soc., Dalton Trans.* **1994**, 689−693.
(343) Hsieh, W.-Y.; Liu, S. Synthesis, Characterization, and Structures of Indium In(DTPA-BA_2) and Yttrium Y(DTPA-BA_2)-(CH_3OH) Complexes (BA = Benzylamine): Models for ^{111}In- and ^{90}Y-Labeled DTPA-Biomolecule Conjugates. *Inorg. Chem.* **2004**, *43*, 6006−6014.
(344) Bokhari, T. H.; Butt, M. B.; Hina, S.; Iqbal, M.; Daud, M.; Imran, M. A Review on ^{90}Y-Labeled Compounds and Biomolecules. *J. Radioanal. Nucl. Chem.* **2017**, *314*, 1487−1496.
(345) Nayak, T. K.; Brechbiel, M. W. ^{86}Y Based PET Radiopharmaceuticals: Radiochemistry and Biological Applications. *Med. Chem.* **2011**, *7*, 380−388.
(346) Wu, C.; Kobayashi, H.; Sun, B.; Yoo, T. M.; Paik, C. H.; Gansow, O. A.; Carrasquillo, J. A.; Pastan, I.; Brechbiel, M. W. Stereochemical Influence on the Stability of Radio-Metal Complexes in Vivo. Synthesis and Evaluation of the Four Stereoisomers of 2-(p-Nitrobenzyl)-Trans-CyDTPA. *Bioorg. Med. Chem.* **1997**, *5*, 1925−1934.
(347) Kobayashi, H.; Wu, C.; Yoo, T. M.; Sun, B. F.; Drumm, D.; Pastan, I.; Paik, C. H.; Gansow, O. A.; Carrasquillo, J. A.; Brechbiel, M. W. Evaluation of the in Vivo Biodistribution of Yttrium-Labeled Isomers of CHX-DTPA-Conjugated Monoclonal Antibodies. *J. Nucl. Med.* **1998**, *39*, 829−836.
(348) Le Fur, M.; Beyler, M.; Lepareur, N.; Fougère, O.; Platas-Iglesias, C.; Rousseaux, O.; Tripier, R. Pyclen Tri-n-Butylphosphonate

DOI: 10.1021/acs.chemrev.8b00294
Chem. Rev. 2019, 119, 902−956

Ester as Potential Chelator for Targeted Radiotherapy: From Yttrium(III) Complexation to ^{90}Y Radiolabeling. *Inorg. Chem.* **2016**, *55*, 8003−8012.
(349) Le Fur, M.; Beyler, M.; Molnár, E.; Fougère, O.; Esteban-Gómez, D.; Tircsó, G.; Platas-Iglesias, C.; Lepareur, N.; Rousseaux, O.; Tripier, R. The Role of the Capping Bond Effect on Pyclen $^{Nat}Y^{3+}/^{90}Y^{3+}$ Chelates: Full Control of the Regiospecific N-Functionalization Makes the Difference. *Chem. Commun.* **2017**, *53*, 9534−9537.
(350) Rodríguez-Rodríguez, A.; Regueiro-Figueroa, M.; Esteban-Gómez, D.; Rodríguez-Blas, T.; Patinec, V.; Tripier, R.; Tircsó, G.; Carniato, F.; Botta, M.; Platas-Iglesias, C. Definition of the Labile Capping Bond Effect in Lanthanide Complexes. *Chem. - Eur. J.* **2017**, *23*, 1110−1117.
(351) Le Fur, M.; Beyler, M.; Molnár, E.; Fougère, O.; Esteban-Gómez, D.; Tircsó, G.; Platas-Iglesias, C.; Lepareur, N.; Rousseaux, O.; Tripier, R. Stable and Inert Yttrium(III) Complexes with Pyclen-Based Ligands Bearing Pendant Picolinate Arms: Toward New Pharmaceuticals for β-Radiotherapy. *Inorg. Chem.* **2018**, *57*, 2051−2063.
(352) Chong, H. S.; Garmestani, K.; Ma, D.; Milenic, D. E.; Overstreet, T.; Brechbiel, M. W. Synthesis and Biological Evaluation of Novel Macrocyclic Ligands with Pendent Donor Groups as Potential Yttrium Chelators for Radioimmunotherapy with Improved Complex Formation Kinetics. *J. Med. Chem.* **2002**, *45*, 3458−3464.
(353) Chong, H. S.; Ma, X.; Le, T.; Kwamena, B.; Milenic, D. E.; Brady, E. D.; Song, H. a.; Brechbiel, M. W. Rational Design and Generation of a Bimodal Bifunctional Ligand for Antibody-Targeted Radiation Cancer Therapy. *J. Med. Chem.* **2008**, *51*, 118−125.
(354) Chong, H. S.; Sun, X.; Chen, Y.; Sin, I.; Kang, C. S.; Lewis, M. R.; Liu, D.; Ruthengael, V. C.; Zhong, Y.; Wu, N.; et al. Synthesis and Comparative Biological Evaluation of Bifunctional Ligands for Radiotherapy Applications of ^{90}Y and ^{177}Lu. *Bioorg. Med. Chem.* **2015**, *23*, 1169−1178.
(355) Kang, C. S.; Sun, X.; Jia, F.; Song, H. A.; Chen, Y.; Lewis, M.; Chong, H. S. Synthesis and Preclinical Evaluation of Bifunctional Ligands for Improved Chelation Chemistry of ^{90}Y and ^{177}Lu for Targeted Radioimmunotherapy. *Bioconjugate Chem.* **2012**, *23*, 1775−1782.
(356) Kang, C. S.; Chen, Y.; Lee, H.; Liu, D.; Sun, X.; Kweon, J.; Lewis, M. R.; Chong, H. S. Synthesis and Evaluation of a New Bifunctional NETA Chelate for Molecular Targeted Radiotherapy Using ^{90}Y or ^{177}Lu. *Nucl. Med. Biol.* **2015**, *42*, 242−249.
(357) Chong, H. S.; Song, H. A.; Kang, C. S.; Le, T.; Sun, X.; Dadwal, M.; Lee, H.; Lan, X.; Chen, Y.; Dai, A. A Highly Effective Bifunctional Ligand for Radioimmunotherapy Applications. *Chem. Commun.* **2011**, *47*, 5584−5586.
(358) Chong, H. S.; Lim, S.; Baidoo, K. E.; Milenic, D. E.; Ma, X.; Jia, F.; Song, H. A.; Brechbiel, M. W.; Lewis, M. R. Synthesis and Biological Evaluation of a Novel Decadentate Ligand DEPA. *Bioorg. Med. Chem. Lett.* **2008**, *18*, 5792−5795.
(359) Price, E. W.; Cawthray, J. F.; Bailey, G. A.; Ferreira, C. L.; Boros, E.; Adam, M. J.; Orvig, C. H_4Octapa: An Acyclic Chelator for ^{111}In Radiopharmaceuticals. *J. Am. Chem. Soc.* **2012**, *134*, 8670−8683.
(360) Jaraquemada-Peláez, M. de G.; Wang, X.; Clough, T. J.; Cao, Y.; Choudhary, N.; Emler, K.; Patrick, B. O.; Orvig, C. H_4Octapa: Synthesis, Solution Equilibria and Complexes with Useful Radiopharmaceutical Metal Ions. *Dalton Trans* **2017**, *46*, 14647−14658.
(361) Kálmán, F. K.; Végh, A.; Regueiro-Figueroa, M.; Tóth, É.; Platas-Iglesias, C.; Tircsó, G. H_4Octapa: Highly Stable Complexation of Lanthanide(III) Ions and Copper(II). *Inorg. Chem.* **2015**, *54*, 2345−2356.
(362) Price, E. W.; Cawthray, J. F.; Adam, M. J.; Orvig, C. Modular Syntheses of H_4Octapa and H_2Dedpa, and Yttrium Coordination Chemistry Relevant to ^{86}Y/^{90}Y Radiopharmaceuticals. *Dalton Trans* **2014**, *43*, 7176−7190.
(363) Price, E. W.; Edwards, K. J.; Carnazza, K. E.; Carlin, S. D.; Zeglis, B. M.; Adam, M. J.; Orvig, C.; Lewis, J. S. A Comparative Evaluation of the Chelators H_4Octapa and CHX-A″-DTPA with the Therapeutic Radiometal ^{90}Y. *Nucl. Med. Biol.* **2016**, *43*, 566−576.
(364) Goldsmith, S. J. Radioimmunotherapy of Lymphoma. In *Nuclear Medicine Therapy*; Springer: New York, 2013; pp 3−25.
(365) Morschhauser, F.; Radford, J.; Van Hoof, A.; Botto, B.; Rohatiner, A. Z. S.; Salles, G.; Soubeyran, P.; Tilly, H.; Bischof-Delaloye, A.; van Putten, W. L. J.; et al. ^{90}Yttrium-Ibritumomab Tiuxetan Consolidation of First Remission in Advanced-Stage Follicular Non-Hodgkin Lymphoma: Updated Results After a Median Follow-Up of 7.3 Years From the International, Randomized, Phase III First-Line Indolent Trial. *J. Clin. Oncol.* **2013**, *31*, 1977−1983.
(366) Rizzieri, D. Zevalin® (Ibritumomab Tiuxetan): After More than a Decade of Treatment Experience, What Have We Learned? *Crit. Rev. Oncol. Hematol.* **2016**, *105*, 5−17.
(367) Ocean, A. J.; Pennington, K. L.; Guarino, M. J.; Sheikh, A.; Bekaii-Saab, T.; Serafini, A. N.; Lee, D.; Sung, M. W.; Gulec, S. A.; Goldsmith, S. J.; et al. Fractionated Radioimmunotherapy with ^{90}Y-Clivatuzumab Tetraxetan and Low-Dose Gemcitabine Is Active in Advanced Pancreatic Cancer. *Cancer* **2012**, *118*, 5497−5506.
(368) Picozzi, V. J.; Ramanathan, R. K.; Lowery, M. A.; Ocean, A. J.; Mitchel, E. P.; O'Neil, B. H.; Guarino, M. J.; Conkling, P. R.; Cohen, S. J.; Bahary, N.; et al. ^{90}Y-Clivatuzumab Tetraxetan With or Without Low-Dose Gemcitabine: A Phase Ib Study in Patients with Metastatic Pancreatic Cancer after Two or More Prior Therapies. *Eur. J. Cancer* **2015**, *51*, 1857−1864.
(369) Villard, L.; Romer, A.; Marincek, N.; Brunner, P.; Koller, M. T.; Schindler, C.; Ng, Q. K. T.; Mäcke, H. R.; Müller-Brand, J.; Rochlitz, C.; et al. Cohort Study of Somatostatin-Based Radiopeptide Therapy With [^{90}Y-DOTA]-TOC Versus [^{90}Y-DOTA]-TOC Plus [^{177}Lu-DOTA]-TOC in Neuroendocrine Cancers. *J. Clin. Oncol.* **2012**, *30*, 1100−1106.
(370) Kunikowska, J.; Królicki, L.; Hubalewska-Dydejczyk, A.; Mikołajczak, R.; Sowa-Staszczak, A.; Pawlak, D. Clinical Results of Radionuclide Therapy of Neuroendocrine Tumours with ^{90}Y-DOTATATE and Tandem ^{90}Y/^{177}Lu-DOTATATE: Which Is a Better Therapy Option? *Eur. J. Nucl. Med. Mol. Imaging* **2011**, *38*, 1788−1797.
(371) Lee, E. W.; Alanis, L.; Cho, S.-K.; Saab, S. Yttrium-90 Selective Internal Radiation Therapy with Glass Microspheres for Hepatocellular Carcinoma: Current and Updated Literature Review. *Korean J. Radiol.* **2016**, *17*, 472−488.
(372) Helisch, A.; Förster, G. J.; Reber, H.; Buchholz, H.-G.; Arnold, R.; Göke, B.; Weber, M. M.; Wiedenmann, B.; Pauwels, S.; Haus, U.; et al. Pre-Therapeutic Dosimetry and Biodistribution of ^{86}Y-DOTA-Phe1-Tyr3-Octreotide versus ^{111}In-Pentetreotide in Patients with Advanced Neuroendocrine Tumours. *Eur. J. Nucl. Med. Mol. Imaging* **2004**, *31*, 1386−1392.
(373) Förster, G. J.; Engelbach, M.; Brockmann, J.; Reber, H.; Buchholz, H.-G.; Mäcke, H. R.; Rösch, F.; Herzog, H.; Bartenstein, P. Preliminary Data on Biodistribution and Dosimetry for Therapy Planning of Somatostatin Receptor Positive Tumours: Comparison of ^{86}Y-DOTATOC and ^{111}In-DTPA-octreotide. *Eur. J. Nucl. Med. Mol. Imaging* **2001**, *28*, 1743−1750.
(374) Rösch, F.; Herzog, H.; Stolz, B.; Brockmann, J.; Köhle, M.; Mühlensiepen, H.; Marbach, P.; Müller-Gärtner, H.-W. Uptake Kinetics of the Somatostatin Receptor Ligand [^{86}Y]DOTA-DPhe^1-Tyr^3-Octreotide ([^{86}Y]SMT487) Using Positron Emission Tomography in Non-Human Primates and Calculation of Radiation Doses of the ^{90}Y-Labelled Analogue. *Eur. J. Nucl. Med. Mol. Imaging* **1999**, *26*, 358−366.
(375) Walrand, S.; Barone, R.; Pauwels, S.; Jamar, F. Experimental Facts Supporting a Red Marrow Uptake Due to Radiometal Transchelation in ^{90}Y-DOTATOC Therapy and Relationship to the Decrease of Platelet Counts. *Eur. J. Nucl. Med. Mol. Imaging* **2011**, *38*, 1270−1280.
(376) Banerjee, S. R.; Foss, C. A.; Pullambhatla, M.; Wang, Y.; Srinivasan, S.; Hobbs, R. F.; Baidoo, K. E.; Brechbiel, M. W.; Nimmagadda, S.; Mease, R. C.; et al. Preclinical Evaluation of ^{86}Y-

DOI: 10.1021/acs.chemrev.8b00294
Chem. Rev. 2019, 119, 902−956

Labeled Inhibitors of Prostate-Specific Membrane Antigen for Dosimetry Estimates. *J. Nucl. Med.* **2015**, *56*, 628−634.
(377) Nayak, T. K.; Garmestani, K.; Baidoo, K. E.; Milenic, D. E.; Brechbiel, M. W. PET Imaging of Tumor Angiogenesis in Mice with VEGF-A-Targeted ^{86}Y-CHX-A″-DTPA-Bevacizumab. *Int. J. Cancer* **2011**, *128*, 920−926.
(378) Schneider, D. W.; Heitner, T.; Alicke, B.; Light, D. R.; McLean, K.; Satozawa, N.; Parry, G.; Yoo, J.; Lewis, J. S.; Parry, R. In Vivo Biodistribution, PET Imaging, and Tumor Accumulation of ^{86}Y- and ^{111}In-Antimindin/RG-1, Engineered Antibody Fragments in LNCaP Tumor-Bearing Nude Mice. *J. Nucl. Med.* **2009**, *50*, 435−443.
(379) Nayak, T. K.; Garmestani, K.; Milenic, D. E.; Baidoo, K. E.; Brechbiel, M. W. HER1-Targeted ^{86}Y-Panitumumab Possesses Superior Targeting Characteristics than ^{86}Y-Cetuximab for PET Imaging of Human Malignant Mesothelioma Tumors Xenografts. *PLoS One* **2011**, *6*, e18198.
(380) Nayak, T. K.; Garmestani, K.; Baidoo, K. E.; Milenic, D. E.; Brechbiel, M. W. Preparation, Biological Evaluation, and Pharmacokinetics of the Human Anti-HER1Monoclonal Antibody Panitumumab Labeled with ^{86}Y for Quantitative PET of Carcinoma. *J. Nucl. Med.* **2010**, *51*, 942−950.
(381) Opacic, T.; Paefgen, V.; Lammers, T.; Kiessling, F. Status and Trends in the Development of Clinical Diagnostic Agents. *Wiley Interdiscip. Rev. Nanomed. Nanobiotech.* **2017**, *9*, e1441.
(382) Kersemans, V.; Cornelissen, B.; Minden, M. D.; Brandwein, J.; Reilly, R. M. Drug-Resistant AML Cells and Primary AML Specimens Are Killed by ^{111}In-Anti-CD33 Monoclonal Antibodies Modified with Nuclear Localizing Peptide Sequences. *J. Nucl. Med.* **2008**, *49*, 1546−1554.
(383) Gruverman, I. J.; Kruger, P. Cyclotron-Produced Carrier-Free Radioisotopes: Thick Target Yield Data and Carrier-Free Separation Procedures. *Int. J. Appl. Radiat. Isot.* **1959**, *5*, 21−31.
(384) Wood, R. A.; Wakakuwa, S. T.; Macdonald, N. S. The Carrier-Free Isolation of Indium from Silver and Cadmium by Liquid-Liquid Extraction. *J. Inorg. Nucl. Chem.* **1972**, *34*, 3517−3522.
(385) Das, M. K.; Chattopadhayay, S.; Sarkar, B. R.; Ramamoorthy, N. A Cation Exchange Method for Separation of ^{111}In from Inactive Silver, Copper, Traces of Iron and Radioactive Gallium and Zinc Isotopes. *Appl. Radiat. Isot.* **1997**, *48*, 11−14.
(386) Nayak, D.; Lahiri, S.; Ramaswami, A. Alternative Production and Separation Method of ^{111}In by Heavy Ion Activation of Silver. *Indian J. Chem.* **2002**, *41A*, 2300−2302.
(387) Mukhopadhyay, B.; Lahiri, S.; Mukhopadhyay, K.; Ramaswami, A. Separation of Carrier-Free ^{111}In, ^{116,117}Te and ^{116,116m,117}Sb from a ^{11}B-Induced Silver Target. *J. Radioanal. Nucl. Chem.* **2003**, *256*, 307−310.
(388) Thakare, S. V.; Nair, A. G. C.; Chakrabarty, S.; Tomar, B. S. Separation of Carrier-Free ^{111}In Formed in the ^{12}C+Rh Reaction. *J. Radioanal. Nucl. Chem.* **1999**, *242*, 537−539.
(389) Beták, E.; Mikołajczak, R.; Staniszewska, J.; Mikołajewski, S.; Rurarz, E. Activation Cross Sections for Reactions Induced by 14 MeV Neutrons on Natural Tin and Enriched ^{112}Sn Targets with Reference to ^{111}In Production via Radioisotope Generator ^{112}Sn(n, 2n)^{111}Sn → ^{111}In. *Radiochim. Acta* **2005**, *93*, 311−326.
(390) Hermanne, A.; Tárkányi, F.; Ditrói, F.; Takács, S.; Adam Rebeles, R.; Uddin, M. S.; Hagiwara, M.; Baba, M.; Shubin, Y.; Kovalev, S. F. Experimental Study of the Excitation Functions of Proton Induced Reactions on ^{Nat}Sn up to 65MeV. *Nucl. Instrum. Methods Phys. Res., Sect. B* **2006**, *247*, 180−191.
(391) Levin, V. I.; Kozlova, M. D.; Malinin, A. B.; Sevastianova, A. S.; Potapova, Z. M. The Production of Carrier-Free Indium-111. *Int. J. Appl. Radiat. Isot.* **1974**, *25*, 286−288.
(392) Brown, L. C.; Beets, A. L. Cyclotron Production of Carrier-Free Indium-111. *Int. J. Appl. Radiat. Isot.* **1972**, *23*, 57−58.
(393) Dahl, J. R.; Tilbury, R. S. The Use of a Compact, Multi-Particle Cyclotron for the Production of ^{52}Fe, ^{67}Ga, ^{111}In and ^{123}I for Medical Purposes. *Int. J. Appl. Radiat. Isot.* **1972**, *23*, 431−437.
(394) Khandaker, M. U.; Kim, K.; Lee, M. W.; Kim, K. S.; Kim, G. N.; Cho, Y. S.; Lee, Y. O. Production Cross-Sections for the Residual Radionuclides from the ^{Nat}Cd(p, x) Nuclear Processes. *Nucl. Instrum. Methods Phys. Res., Sect. B* **2008**, *266*, 4877−4887.
(395) Hermanne, A.; Daraban, L.; Adam Rebeles, R.; Ignatyuk, A.; Tarkanyi, F.; Takacs, S. Alpha Induced Reactions on ^{Nat}Cd up to 38.5MeV: Experimental and Theoretical Studies of the Excitation Functions. *Nucl. Instrum. Methods Phys. Res., Sect. B* **2010**, *268*, 1376−1391.
(396) Khandaker, M. U.; Kim, K.; Lee, M.; Kim, G. Investigation of Activation Cross-Sections of Alpha-Induced Nuclear Reactions on Natural Cadmium. *Nucl. Instrum. Methods Phys. Res., Sect. B* **2014**, *333*, 80−91.
(397) MacDonald, N. S.; Neely, H. H.; Wood, R. A.; Takahashi, J. M.; Wakakuwa, S. I.; Birdsall, R. L. Methods for Compact Cyclotron Production of Indium-111 for Medical Use. *Int. J. Appl. Radiat. Isot.* **1975**, *26*, 631−633.
(398) Filossofov, D. V.; Lebedev, N. A.; Novgorodov, A. F.; Bontchev, G. D.; Starodub, G. Y. Production, Concentration and Deep Purification of ^{111}In Radiochemicals. *Appl. Radiat. Isot.* **2001**, *55*, 293−295.
(399) de Pasquali, G.; von Goeler, E.; Peacock, R. N. Separation of Carrier-Free Indium-111 from Silver by Ion Exchange. *J. Inorg. Nucl. Chem.* **1959**, *11*, 257.
(400) Lahiri, S.; Maiti, M.; Ghosh, K. Production and Separation of ^{111}In: An Important Radionuclide in Life Sciences: A Mini Review. *J. Radioanal. Nucl. Chem.* **2013**, *297*, 309−318.
(401) Büyükuslu, H.; Kaplan, A.; Yildirim, G.; Aydin, A.; Tel, E.; Bölükdemir, M. H. Production Cross Sections of Medical ^{110,111}In in Radionuclides. *Kerntechnik* **2010**, *75*, 103−108.
(402) Kakavand, T.; Mirzaii, M.; Eslami, M.; Karimi, A. Nuclear Model Calculation and Targetry Recipe for Production of ^{110m}In. *Appl. Radiat. Isot.* **2015**, *104*, 60−66.
(403) Kakavand, T.; Mirzaii, M.; Eslami, M.; Karimi, A. Experimental and Monte Carlo Study on Production of ^{110m}In via ^{Nat}Cd(p,xn) Reaction. *J. Radioanal. Nucl. Chem.* **2015**, *306*, 423−427.
(404) Lundqvist, H.; Scott-Robson, S.; Einarsson, L.; Malmborg, P. ^{110}Sn/^{110}In—A New Generator System for Positron Emission Tomography. *Appl. Radiat. Isot.* **1991**, *42*, 447−450.
(405) Rösch, F.; Qaim, S. M.; Novgorodov, A. F.; Tsai, Y.-M. Production of Positron-Emitting ^{110m}In via the ^{110}Cd-(^{3}He,3n)^{110}Sn→^{110m}In Process. *Appl. Radiat. Isot.* **1997**, *48*, 19−26.
(406) Tárkányi, F.; Takács, S.; Ditrói, F.; Hermanne, A.; Baba, M.; Mohsena, B. M. A.; Ignatyuk, A. V. New Cross Section Data and Review of Production Routes of Medically Used ^{110m}In. *Nucl. Instrum. Methods Phys. Res., Sect. B* **2015**, *351*, 6−15.
(407) Lubberink, M.; Tolmachev, V.; Widström, C.; Bruskin, A.; Lundqvist, H.; Westlin, J.-E. ^{110m}In-DTPA-D-Phe^{1}-Octreotide for Imaging of Neuroendocrine Tumors with PET. *J. Nucl. Med.* **2002**, *43*, 1391−1397.
(408) Tolmachev, V.; Bernhardt, P.; Forssell-Aronsson, E.; Lundqvist, H. ^{114m}In, a Candidate for Radionuclide Therapy: Low-Energy Cyclotron Production and Labeling of DTPA-D-Phe^{1}-Octreotide. *Nucl. Med. Biol.* **2000**, *27*, 183−188.
(409) Ghosh, K.; Maiti, M.; Lahiri, S. Separation of No-Carrier-Added ^{113,117m}Sn and ^{113m,114m}In from Alpha Particle Irradiated Natural Cadmium Target. *J. Radioanal. Nucl. Chem.* **2013**, *295*, 865−870.
(410) Cowan, R. A.; Murby, B.; Gunton, D.; Owens, S. E.; Hoyes, K. P.; Sharma, H. L.; Smith, A.-M.; Chang, J.; Van Kessel, B.; Nuttall, P. M.; et al. Autologous Lymphocytes as Vectors to Target Therapeutic Radiation, Using Indium-114m, in Patients with Lymphoid Cell Malignancy. *Br. J. Haematol.* **2002**, *119*, 459−466.
(411) Kairemo, K. J. A.; Ramsay, H. A.; Tagesson, M.; Jekunen, A. P.; Paavonen, T. K.; Jaaskela-Saari, H. A.; Liewendahl, K.; Ljunggren, K.; Savolainen, S.; Strand, S.-E. Indium-111 Bleomycin Complex for Radiochemotherapy of Head and Neck Cancer - Dosimetric and Biokinetic Aspects. *Eur. J. Nucl. Med.* **1996**, *23*, 631−638.
(412) Zweit, J. Radionuclides and Carrier Molecules for Therapy. *Phys. Med. Biol.* **1996**, *41*, 1905−1914.

DOI: 10.1021/acs.chemrev.8b00294
Chem. Rev. 2019, 119, 902−956

(413) Jackson, H.; Jackson, N. C. Spleen-Targeted $^{114}In^{m}$ via Normal and Heat-Damaged Red Cells in the Mouse: Isotope Distribution and Bone Marrow Damage. *Nucl. Med. Commun.* **2000**, *21*, 839−843.
(414) Orlova, A.; Rosik, D.; Sandström, M.; Lundqvist, H.; Einarsson, L.; Tolmachev, V. Evaluation of [$^{111/114m}$In]CHX-A″-DTPA-$Z_{HER2:342}$, an Affibody Ligand Coniugate for Targeting of HER2-Expressing Malignant Tumors. *Q. J. Nucl. Med. Mol. Imaging* **2007**, *51*, 314−323.
(415) Tolmachev, V.; Wållberg, H.; Andersson, K.; Wennborg, A.; Lundqvist, H.; Orlova, A. The Influence of Bz-DOTA and CHX-A″-DTPA on the Biodistribution of ABD-Fused Anti-HER2 Affibody Molecules: Implications for ^{114m}In-Mediated Targeting Therapy. *Eur. J. Nucl. Med. Mol. Imaging* **2009**, *36*, 1460−1468.
(416) Briand, G. G.; Cooper, B. F. T.; MacDonald, D. B. S.; Martin, C. D.; Schatte, G. Preferred Bonding Motif for Indium Aminoethanethiolate Complexes: Structural Characterization of $(Me_2NCH_2CH_2S)_2InX/SR$(X = Cl, I; R = 4-MeC_6H_4,4-$MeOC_6H_4$). *Inorg. Chem.* **2006**, *45*, 8423−8429.
(417) Sullivan, M. T.; Senaratne, N. K.; Eichhorn, D. M. Synthesis and X-Ray Crystallographic Characterization of [In(Tsalen)(OAc)]-(Tsalen = N,N′-Ethylenebis(Thiosalicylideneimine)). *Polyhedron* **2016**, *114*, 152−155.
(418) Hunt, F. C. Potential Radiopharmaceuticals for the Diagnosis of Biliary Atresia and Neonatal Hepatitis: EHPG and HBED Chelates of ^{67}Ga and ^{111}In. *Nucl. Med. Biol.* **1988**, *15*, 659−664.
(419) Caravan, P.; Orvig, C. Tripodal Aminophenolate Ligand Complexes of Aluminum(III), Gallium(III), and Indium(III) in Water. *Inorg. Chem.* **1997**, *36*, 236−248.
(420) Green, M. A.; Welch, M. J.; Mathias, C. J.; Taylor, P.; Martell, A. E. Evaluation of PLED as a Chelating Ligand in the Preparation of Gallium and Indium Radiopharmaceuticals. *Int. J. Nucl. Med. Biol.* **1985**, *12*, 381−386.
(421) Maecke, H. R.; Riesen, A.; Ritter, W. The Molecular Structure of Indium-DTPA. *J. Nucl. Med.* **1989**, *30*, 1235−1239.
(422) Delgado, R.; do Carmo Figueira, M.; Quintino, S. Redox Method for the Determination of Stability Constants of Some Trivalent Metal Complexes. *Talanta* **1997**, *45*, 451−462.
(423) Price, E. W.; Ferreira, C. L.; Adam, M. J.; Orvig, C. High-Denticity Ligands Based on Picolinic Acid for ^{111}In Radiochemistry. *Can. J. Chem.* **2014**, *92*, 695−705.
(424) Safavy, A.; Smith, D. C.; Bazooband, A.; Buchsbaum, D. J. De Novo Synthesis of a New Diethylenetriaminepentaacetic Acid (DTPA) Bifunctional Chelating Agent. *Bioconjugate Chem.* **2002**, *13*, 317−326.
(425) Roselli, M.; Schlom, J.; Gansow, O. A.; Brechbiel, M. W.; Mirzadeh, S.; Pippin, C. G.; Milenic, D. E.; Colcher, D. Comparative Biodistribution Studies of DTPA-Derivative Bifunctional Chelates for Radiometal Labeled Monoclonal Antibodies. *Nucl. Med. Biol.* **1991**, *18*, 389−394.
(426) Hoffman, T. J.; Gali, H.; Smith, C. J.; Sieckman, G. L.; Hayes, D. L.; Owen, N. K.; Volkert, W. A. Novel Series of ^{111}In-Labeled Bombesin Analogs as Potential Radiopharmaceuticals for Specific Targeting of Gastrin-Releasing Peptide Receptors Expressed on Human Prostate Cancer Cells. *J. Nucl. Med.* **2003**, *44*, 823−831.
(427) Garrison, J. C.; Rold, T. L.; Sieckman, G. L.; Naz, F.; Sublett, S. V.; Figueroa, S. D.; Volkert, W. a.; Hoffman, T. J. Evaluation of the Pharmacokinetic Effects of Various Linking Group Using the ^{111}In-DOTA- X-BBN(7−14)NH_2 Structural Paradigm in a Prostate Cancer Model. *Bioconjugate Chem.* **2008**, *19*, 1803−1812.
(428) Kolenc-Peitl, P.; Mansi, R.; Tamma, M.; Gmeiner-Stopar, T.; Sollner-Dolenc, M.; Waser, B.; Baum, R. P.; Reubi, J. C.; Maecke, H. R. Highly Improved Metabolic Stability and Pharmacokinetics of Indium-111-DOTA-Gastrin Conjugates for Targeting of the Gastrin Receptor. *J. Med. Chem.* **2011**, *54*, 2602−2609.
(429) Mansi, R.; Wang, X.; Forrer, F.; Waser, B.; Cescato, R.; Graham, K.; Borkowski, S.; Reubi, J. C.; Maecke, H. R. Development of a Potent DOTA-Conjugated Bombesin Antagonist for Targeting GRPr-Positive Tumours. *Eur. J. Nucl. Med. Mol. Imaging* **2011**, *38*, 97−107.
(430) Marsouvanidis, P. J.; Nock, B. A.; Hajjaj, B.; Fehrentz, J.-A.; Brunel, L.; M'Kadmi, C.; Van der Graaf, L.; Krenning, E. P.; Maina, T.; Martinez, J.; et al. Gastrin Releasing Peptide Receptor-Directed Radioligands Based on a Bombesin Antagonist: Synthesis, ^{111}In-Labeling, and Preclinical Profile. *J. Med. Chem.* **2013**, *56*, 2374−2384.
(431) Zhou, Z.; Wagh, N. K.; Ogbomo, S. M.; Shi, W.; Jia, Y.; Brusnahan, S. K.; Garrison, J. C. Synthesis and In Vitro and In Vivo Evaluation of Hypoxia-Enhanced ^{111}In-Bombesin Conjugates for Prostate Cancer Imaging. *J. Nucl. Med.* **2013**, *54*, 1605−1612.
(432) Briat, A.; Wenk, C. H. F.; Ahmadi, M.; Claron, M.; Boturyn, D.; Josserand, V.; Dumy, P.; Fagret, D.; Coll, J. L.; Ghezzi, C.; et al. Reduction of Renal Uptake of ^{111}In-DOTA-Labeled and A700-Labeled RAFT-RGD during Integrin $\alpha_v\beta_3$ Targeting Using Single Photon Emission Computed Tomography and Optical Imaging. *Cancer Sci.* **2012**, *103*, 1105−1110.
(433) Yang, C.-T.; Li, Y.; Liu, S. Synthesis and Structural Characterization of Complexes of a DO3A-Conjugated Triphenylphosphonium Cation with Diagnostically Important Metal Ions. *Inorg. Chem.* **2007**, *46*, 8988−8997.
(434) Liu, S.; He, Z.; Hsieh, W. Y.; Fanwick, P. E. Synthesis, Characterization, and X-Ray Crystal Structure of In(DOTA-AA) (AA = p-Aminoanilide): A Model for ^{111}In-Labeled DOTA-Biomolecule Conjugates. *Inorg. Chem.* **2003**, *42*, 8831−8837.
(435) Kriemen, E.; Holzapfel, M.; Ruf, E.; Rehbein, J.; Maison, W. Synthesis and Structural Analysis of 1,4,7,10-Tetraazacyclododecane-1,4,7,10-tetraazidoethylacetic Acid (DOTAZA) Complexes. *Eur. J. Inorg. Chem.* **2015**, *2015*, 5368−5378.
(436) Matthews, R. C.; Parker, D.; Ferguson, G.; Kaitner, B.; Harrison, A.; Royle, L. Synthesis and Structure of Stable Indium and Gallium Complexes of (R)-1,4,7-Tris(2′-Methylcarboxymethyl)-Triazacyclononane. *Polyhedron* **1991**, *10*, 1951−1953.
(437) Craig, A. S.; Helps, I. M.; Parker, D.; Adams, H.; Bailey, N. A.; Williams, M. G.; Smith, J. M. A.; Ferguson, G. Crystal and Molecular Structure of a Seven-Coordinate Chloroindium(III) Complex of 1,4,7-Triazacyclononanetriacetic Acid. *Polyhedron* **1989**, *8*, 2481−2484.
(438) Price, E. W.; Zeglis, B. M.; Lewis, J. S.; Adam, M. J.; Orvig, C. H_6Phospa-Trastuzumab: Bifunctional Methylenephosphonate-Based Chelator with ^{89}Zr, ^{111}In and ^{177}Lu. *Dalton Trans* **2014**, *43*, 119−131.
(439) Price, E. W.; Zeglis, B. M.; Cawthray, J. F.; Lewis, J. S.; Adam, M. J.; Orvig, C. What a Difference a Carbon Makes: H_4octapa vs H_4C3octapa, Ligands for In-111 and Lu-177 Radiochemistry. *Inorg. Chem.* **2014**, *53*, 10412−10431.
(440) Breeman, W. A. P.; De Jong, M.; Bernard, B. F.; Kwekkeboom, D. J.; Srinivasan, A.; Van der Pluijm, M. E.; Hofland, L. J.; Visser, T. J.; Krenning, E. P. Pre-Clinical Evaluation of [^{111}In-DTPA-Pro^1, Tyr^4]Bombesin, a New Radioligand for Bombesin-Receptor Scintigraphy. *Int. J. Cancer* **1999**, *83*, 657−663.
(441) Abiraj, K.; Mansi, R.; Tamma, M.-L.; Fani, M.; Forrer, F.; Nicolas, G.; Cescato, R.; Reubi, J. C.; Maecke, H. R. Bombesin Antagonist-Based Radioligands for Translational Nuclear Imaging of Gastrin-Releasing Peptide Receptor-Positive Tumors. *J. Nucl. Med.* **2011**, *52*, 1970−1978.
(442) John, A. E.; Luckett, J. C.; Tatler, A. L.; Awais, R. O.; Desai, A.; Habgood, A.; Ludbrook, S.; Blanchard, A. D.; Perkins, A. C.; Jenkins, R. G.; et al. Preclinical SPECT/CT Imaging of $\alpha_v\beta_6$ Integrins for Molecular Stratification of Idiopathic Pulmonary Fibrosis. *J. Nucl. Med.* **2013**, *54*, 2146−2152.
(443) Mikołajczak, R.; Maecke, H. R. Radiopharmaceuticals for Somatostatin Receptor Imaging. *Nucl. Med. Rev.* **2016**, *19*, 126−132.
(444) Hofman, M. S.; Kong, G.; Neels, O. C.; Eu, P.; Hong, E.; Hicks, R. J. High Management Impact of Ga-68 DOTATATE (GaTate) PET/CT for Imaging Neuroendocrine and Other Somatostatin Expressing Tumours. *J. Med. Imaging Radiat. Oncol.* **2012**, *56*, 40−47.
(445) Schreiter, N. F.; Brenner, W.; Nogami, M.; Buchert, R.; Huppertz, A.; Pape, U. F.; Prasad, V.; Hamm, B.; Maurer, M. H. Cost Comparison of ^{111}In-DTPA-Octreotide Scintigraphy and ^{68}Ga-

DOI: 10.1021/acs.chemrev.8b00294
Chem. Rev. 2019, 119, 902−956

DOTATOC PET/CT for Staging Enteropancreatic Neuroendocrine Tumours. *Eur. J. Nucl. Med. Mol. Imaging* **2012**, *39*, 72−82.
(446) Wild, D.; Fani, M.; Behe, M.; Brink, I.; Rivier, J. E. F.; Reubi, J. C.; Maecke, H. R.; Weber, W. A. First Clinical Evidence That Imaging with Somatostatin Receptor Antagonists Is Feasible. *J. Nucl. Med.* **2011**, *52*, 1412−1417.
(447) Rosik, D.; Orlova, A.; Malmberg, J.; Altai, M.; Varasteh, Z.; Sandström, M.; Karlström, A. E.; Tolmachev, V. Direct Comparison of ^{111}In-Labelled Two-Helix and Three-Helix Affibody Molecules for in Vivo Molecular Imaging. *Eur. J. Nucl. Med. Mol. Imaging* **2012**, *39*, 693−702.
(448) Baum, R. P.; Prasad, V.; Muller, D.; Schuchardt, C.; Orlova, A.; Wennborg, A.; Tolmachev, V.; Feldwisch, J. Molecular Imaging of HER2-Expressing Malignant Tumors in Breast Cancer Patients Using Synthetic ^{111}In- or ^{68}Ga-Labeled Affibody Molecules. *J. Nucl. Med.* **2010**, *51*, 892−897.
(449) Gaykema, S. B. M.; de Jong, J. R.; Perik, P. J.; Brouwers, A. H.; Schröder, C. P.; Munnink, T. H. O.; Bongaerts, A. H. H.; de Vries, E. G. E.; Hooge, M. N. L. ^{111}In-Trastuzumab Scintigraphy in HER2-Positive Metastatic Breast Cancer Patients Remains Feasible during Trastuzumab Treatment. *Mol. Imaging* **2014**, *13*, 7290.2014.00011.
(450) Sorensen, J.; Sandberg, D.; Sandstrom, M.; Wennborg, A.; Feldwisch, J.; Tolmachev, V.; Astrom, G.; Lubberink, M.; Garske-Roman, U.; Carlsson, J.; et al. First-in-Human Molecular Imaging of HER2 Expression in Breast Cancer Metastases Using the ^{111}In-ABY-025 Affibody Molecule. *J. Nucl. Med.* **2014**, *55*, 730−735.
(451) Terbium: a new "Swiss Army knife" for Nuclear Medicine; http://www.drugdiscoverytoday.com/view/30142/terbium-a-new-swiss-army-knife-for-nuclear-medicine/ (accessed Apr 1, 2018).
(452) Champion, C.; Quinto, M. A.; Morgat, C.; Zanotti-Fregonara, P.; Hindié, E. Comparison between Three Promising SS-Emitting Radionuclides, ^{67}Cu, ^{47}Sc and ^{161}Tb, with Emphasis on Doses Delivered to Minimal Residual Disease. *Theranostics* **2016**, *6*, 1611−1618.
(453) Müller, C.; Reber, J.; Haller, S.; Dorrer, H.; Köster, U.; Johnston, K.; Zhernosekov, K.; Türler, A.; Schibli, R. Folate Receptor Targeted Alpha-Therapy Using Terbium-149. *Pharmaceuticals* **2014**, *7*, 353−365.
(454) Müller, C.; Fischer, E.; Behe, M.; Köster, U.; Dorrer, H.; Reber, J.; Haller, S.; Cohrs, S.; Blanc, A.; Grünberg, J.; et al. Future Prospects for SPECT Imaging Using the Radiolanthanide Terbium-155 — Production and Preclinical Evaluation in Tumor-Bearing Mice. *Nucl. Med. Biol.* **2014**, *41*, e58−e65.
(455) Allen, B. J.; Goozee, G.; Sarkar, S.; Beyer, G.; Morel, C.; Byrne, A. P. Production of Terbium-152 by Heavy Ion Reactions and Proton Induced Spallation. *Appl. Radiat. Isot.* **2001**, *54*, 53−58.
(456) Köster, U. ISOLDE Target and Ion Source Chemistry. *Radiochim. Acta* **2001**, *89*, 749−756.
(457) Beyer, G. J.; Čomor, J. J.; Daković, M.; Soloviev, D.; Tamburella, C.; Hagebø, E.; Allan, B.; Dmitriev, S. N.; Zaitseva, N. G.; et al. Production Routes of the Alpha Emitting ^{149}Tb for Medical Application. *Radiochim. Acta* **2002**, *90*, 247−252.
(458) Steyn, G. F.; Vermeulen, C.; Szelecsényi, F.; Kovács, Z.; Hohn, A.; van der Meulen, N. P.; Schibli, R.; Van der Walt, T. N. Cross Sections of Proton-Induced Reactions on ^{152}Gd, ^{155}Gd and ^{159}Tb with Emphasis on the Production of Selected Tb Radionuclides. *Nucl. Instrum. Methods Phys. Res., Sect. B* **2014**, *319*, 128−140.
(459) Zagryadskii, V. A.; Latushkin, S. T.; Malamut, T. Y.; Novikov, V. I.; Ogloblin, A. A.; Unezhev, V. N.; Chuvilin, D. Y. Measurement of Terbium Isotopes Yield in Irradiation of ^{151}Eu Targets by ^{3}He Nuclei. *At. Energy* **2017**, *123*, 55−58.
(460) Ogloblin, A. A.; Unezhev, V. N.; Zagryadskiy, V. A.; Ryazanov, A. I.; Novikov, V. I.; Latushkin, S. T.; Malamut, T. Y. Application of Cyclotrons in Beam Technologies. *Phys. At. Nucl.* **2017**, *80*, 968−975.
(461) Simonoff, G. N.; Alexander, J. M. Angular-Momentum Effects on Neutron Emission by Dy and Tb Compound Nuclei. *Phys. Rev.* **1964**, *133*, B104−B113.
(462) Maiti, M. New Measurement of Cross Sections of Evaporation Residues from the ^{Nat}Pr + ^{12}C Reaction: A Comparative Study on the Production of ^{149}Tb. *Phys. Rev. C: Nucl. Phys.* **2011**, *84*, 044615.
(463) Zaitseva, N. G.; Dmitriev, S. N.; Maslov, O. D.; Molokanova, L. G.; Starodub, G. Y.; Shishkin, S. V.; Shishkina, T. V.; Beyer, G. J. Terbium-149 for Nuclear Medicine. The Production of ^{149}Tb via Heavy Ions Induced Nuclear Reactions. *Czech. J. Phys.* **2003**, *53*, A455−A458.
(464) Dmitriev, S. N.; Beyer, G. J.; Zaitseva, N. G.; Maslov, O. D.; Molokanova, L. G.; Starodub, G. Y.; Shishkin, S. V.; Shishkina, T. V. Lanthanides in Nuclear Medicine: Preparation of ^{149}Tb by Irradiation with Heavy Ions. *Radiochemistry* **2002**, *44*, 171−173.
(465) Nayak, D.; Lahiri, S.; Ramaswami, A.; Manohar, S. B.; Das, N. Separation of Carrier Free ^{151,152}Tb Produced in ^{16}O Irradiated Lanthanum Oxide Matrix. *Appl. Radiat. Isot.* **1999**, *51*, 631−636.
(466) Vermeulen, C.; Steyn, G. F.; Szelecsényi, F.; Kovács, Z.; Suzuki, K.; Nagatsu, K.; Fukumura, T.; Hohn, A.; Van der Walt, T. N. Cross Sections of Proton-Induced Reactions on ^{Nat}Gd with Special Emphasis on the Production Possibilities of ^{152}Tb and ^{155}Tb. *Nucl. Instrum. Methods Phys. Res., Sect. B* **2012**, *275*, 24−32.
(467) Szelecsényi, F.; Kovács, Z.; Nagatsu, K.; Zhang, M. R.; Suzuki, K. Investigation of Deuteron-Induced Reactions on ^{Nat}Gd up to 30 MeV: Possibility of Production of Medically Relevant ^{155}Tb and ^{161}Tb Radioisotopes. *J. Radioanal. Nucl. Chem.* **2016**, *307*, 1877−1881.
(468) Duchemin, C.; Guertin, A.; Haddad, F.; Michel, N.; Métivier, V. Deuteron Induced Tb-155 Production, a Theranostic Isotope for SPECT Imaging and Auger Therapy. *Appl. Radiat. Isot.* **2016**, *118*, 281−289.
(469) Lehenberger, S.; Barkhausen, C.; Cohrs, S.; Fischer, E.; Grünberg, J.; Hohn, A.; Köster, U.; Schibli, R.; Türler, A.; Zhernosekov, K. The Low-Energy β^- and Electron Emitter ^{161}Tb as an Alternative to ^{177}Lu for Targeted Radionuclide Therapy. *Nucl. Med. Biol.* **2011**, *38*, 917−924.
(470) Aziz, A.; Artha, W. T. Radiochemical Separation of ^{161}Tb from Gd/Tb Matrix Using Ln Resin Column. *Indones. J. Chem.* **2016**, *16*, 283−288.
(471) Cotton, S. A. *Lanthanide and Actinide Chemistry*; John Wiley & Sons: West Sussex, 2006.
(472) Bünzli, J.-C. G. Review: Lanthanide Coordination Chemistry: From Old Concepts to Coordination Polymers. *J. Coord. Chem.* **2014**, *67*, 3706−3733.
(473) Moore, E. G.; Samuel, A. P. S.; Raymond, K. N. From Antenna to Assay: Lessons Learned in Lanthanide Luminescence. *Acc. Chem. Res.* **2009**, *42*, 542−552.
(474) Deng, G. Terbium Glows Green. *Nat. Chem.* **2017**, *10*, 110.
(475) Selvin, P. R.; Hearst, J. E. Luminescence Energy Transfer Using a Terbium Chelate: Improvements on Fluorescence Energy Transfer. *Proc. Natl. Acad. Sci. U. S. A.* **1994**, *91*, 10024−10028.
(476) Trout, T. K.; Bellama, J. M.; Faltynek, R. A.; Parks, E. J.; Brinckman, F. E. Effect of pH on the Emission Properties of Aqueous Tris(2,6-Dipicolinato)Terbium(III) Complexes. *Inorg. Chim. Acta* **1989**, *155*, 13−15.
(477) Bailey, M. P.; Rocks, B. F.; Riley, C. Terbium Chelate for Use as a Label in Fluorescent Immunoassays. *Analyst* **1984**, *109*, 1449−1450.
(478) Wang, Y.; Jiang, Z.; Lv, Y.; Zhang, Y.; Ma, D.; Zhang, F.; Tan, B. Study of Synthesis and Luminescent Properties of a Novel Terbium Rare Earth Complex Tb(PCAD)$_3$Phen. *Synth. Met.* **2011**, *161*, 655−658.
(479) Poonam; Kumar, R.; Boora, P.; Khatkar, A.; Khatkar, S. P.; Taxak, V. B. Synthesis, Photoluminescence and Biological Properties of Terbium(III) Complexes with Hydroxyketone and Nitrogen Containing Heterocyclic Ligands. *Spectrochim. Acta, Part A* **2016**, *152*, 304−310.
(480) Mayer, F.; Tiruvadi Krishnan, S.; Schühle, D. T.; Eliseeva, S. V.; Petoud, S.; Tóth, É.; Djanashvili, K. Luminescence Properties of Self-Aggregating Tb^{III}-DOTA-Functionalized Calix[4]Arenes. *Front. Chem.* **2018**, *6*, 1−9.

DOI: 10.1021/acs.chemrev.8b00294
Chem. Rev. 2019, 119, 902−956

(481) Aarons, R. J.; Notta, J. K.; Meloni, M. M.; Feng, J.; Vidyasagar, R.; Narvainen, J.; Allan, S.; Spencer, N.; Kauppinen, R. A.; Snaith, J. S.; et al. A Luminescent Probe Containing a Tuftsin Targeting Vector Coupled to a Terbium Complex. *Chem. Commun.* **2006**, *8*, 909−911.
(482) Faulkner, S.; Pope, S. J. A. Lanthanide-Sensitized Lanthanide Luminescence: Terbium-Sensitized Ytterbium Luminescence in a Trinuclear Complex. *J. Am. Chem. Soc.* **2003**, *125*, 10526−10527.
(483) Hanna, J. R.; Allan, C.; Lawrence, C.; Meyer, O.; Wilson, N. D.; Hulme, A. N. Optimizing the Readout of Lanthanide-DOTA Complexes for the Detection of Ligand-Bound Copper(I). *Molecules* **2017**, *22*, 802−812.
(484) Li, M.; Selvin, P. R. Luminescent Polyaminocarboxylate Chelates of Terbium and Europium: The Effect of Chelate Structure. *J. Am. Chem. Soc.* **1995**, *117*, 8132−8138.
(485) Beeby, A.; Clarkson, I. M.; Dickins, R. S.; Faulkner, S.; Parker, D.; Royle, L.; de Sousa, A. S.; Williams, J. A. G.; Woods, M. Non-Radiative Deactivation of the Excited States of Europium, Terbium and Ytterbium Complexes by Proximate Energy-Matched OH, NH and CH Oscillators: An Improved Luminescence Method for Establishing Solution Hydration States. *J. Chem. Soc., Perkin Trans. 2* **1999**, *3*, 493−504.
(486) Harris, M.; Carron, S.; Vander Elst, L.; Laurent, S.; Muller, R. N.; Parac-Vogt, T. N. Magnetofluorescent Micellar Complexes of Terbium(Iii) as Potential Bimodal Contrast Agents for Magnetic Resonance and Optical Imaging. *Chem. Commun.* **2015**, *51*, 2984−2986.
(487) Spaulding, L.; Brittain, H. G. Intermolecular Energy Transfer between Lanthanide Complexes. 9. Terbium(III) Donor and Europium(III) Acceptor Complexes of Amino Polycarboxylic Acids. *Inorg. Chem.* **1983**, *22*, 3486−3488.
(488) Canfi, A.; Bailey, M. P.; Rocks, B. F. Fluorescent Terbium Chelates Derived from Diethylenetriaminepentaacetic Acid and Heterocyclic Compounds. *Analyst* **1989**, *114*, 1405−1406.
(489) Zhang, Y. J.; Chen, Y.; Liu, Q. De; Wang, X. G.; Li, J. R.; Liu, H. Synthesis, Characterization and Luminescent Properties of Terbium and Europium Complexes with Ligands from DTPA and PAS. *J. Alloys Compd.* **2000**, *307*, 137−140.
(490) Delgado, R.; Félix, V.; Lima, L. M. P.; Price, D. W. Metal Complexes of Cyclen and Cyclam Derivatives Useful for Medical Applications: A Discussion Based on Thermodynamic Stability Constants and Structural Data. *Dalton Trans* **2007**, *26*, 2734−2745.
(491) Woods, M.; Aime, S.; Botta, M.; Howard, J. A. K.; Moloney, J. M.; Navet, M.; Parker, D.; Port, M.; Rousseaux, O. Correlation of Water Exchange Rate with Isomeric Composition in Diastereoisomeric Gadolinium Complexes of Tetra(Carboxyethyl)Dota and Related Macrocyclic Ligands. *J. Am. Chem. Soc.* **2000**, *122*, 9781−9792.
(492) Vojtíšek, P.; Cígler, P.; Kotek, J.; Rudovský, J.; Hermann, P.; Lukeš, I. Crystal Structures of Lanthanide(III) Complexes with Cyclen Derivative Bearing Three Acetate and One Methylphosphonate Pendants. *Inorg. Chem.* **2005**, *44*, 5591−5599.
(493) Baum, R. P.; Singh, A.; Benešová, M.; Vermeulen, C.; Gnesin, S.; Köster, U.; Johnston, K.; Müller, D.; Senftleben, S.; Kulkarni, H. R.; et al. Clinical Evaluation of the Radiolanthanide Terbium-152: First-in-Human PET/CT with ^{152}Tb-DOTATOC. *Dalton Trans* **2017**, *46*, 14638−14646.
(494) Müller, C.; Reber, J.; Haller, S.; Dorrer, H.; Bernhardt, P.; Zhernosekov, K.; Türler, A.; Schibli, R. Direct in Vitro and in Vivo Comparison of ^{161}Tb and ^{177}Lu Using a Tumour-Targeting Folate Conjugate. *Eur. J. Nucl. Med. Mol. Imaging* **2014**, *41*, 476−485.
(495) Byegård, J.; Skarnemark, G.; Skålberg, M. The Stability of Some Metal EDTA, DTPA and DOTA Complexes: Application as Tracers in Groundwater Studies. *J. Radioanal. Nucl. Chem.* **1999**, *241*, 281−290.
(496) Cacheris, W. P.; Nickle, S. K.; Sherry, A. D. Thermodynamic Study of Lanthanide Complexes of 1,4,7-Triazacyclononane-N,N′,N″-Triacetic Acid and 1,4,7,10-Tetraazacyclododecane-N,N′,N″,N‴-Tetraacetic Acid. *Inorg. Chem.* **1987**, *26*, 958−960.
(497) Beyer, G.-J.; Miederer, M.; Vranješ-Đurić, S.; Čomor, J. J.; Künzi, G.; Hartley, O.; Senekowitsch-Schmidtke, R.; Soloviev, D.; Buchegger, F. Targeted Alpha Therapy in Vivo: Direct Evidence for Single Cancer Cell Kill Using ^{149}Tb-Rituximab. *Eur. J. Nucl. Med. Mol. Imaging* **2004**, *31*, 547−554.
(498) Hindie, E.; Zanotti-Fregonara, P.; Quinto, M. A.; Morgat, C.; Champion, C. Dose Deposits from ^{90}Y, ^{177}Lu, ^{111}In, and ^{161}Tb in Micrometastases of Various Sizes: Implications for Radiopharmaceutical Therapy. *J. Nucl. Med.* **2016**, *57*, 759−764.
(499) Milenic, D. E.; Garmestani, K.; Chappell, L. L.; Dadachova, E.; Yordanov, A.; Ma, D.; Schlom, J.; Brechbiel, M. W. In Vivo Comparison of Macrocyclic and Acyclic Ligands for Radiolabeling of Monoclonal Antibodies with ^{177}Lu for Radioimmunotherapeutic Applications. *Nucl. Med. Biol.* **2002**, *29*, 431−442.
(500) Bodei, L.; Cremonesi, M.; Ferrari, M.; Pacifici, M.; Grana, C. M.; Bartolomei, M.; Baio, S. M.; Sansovini, M.; Paganelli, G. Long-Term Evaluation of Renal Toxicity after Peptide Receptor Radionuclide Therapy with ^{90}Y-DOTATOC and ^{177}Lu-DOTATATE: The Role of Associated Risk Factors. *Eur. J. Nucl. Med. Mol. Imaging* **2008**, *35*, 1847−1856.
(501) Kwekkeboom, D. J.; Bakker, W. H.; Kooij, P. P.; Konijnenberg, M. W.; Srinivasan, A.; Erion, J. L.; Schmidt, M. A.; Bugaj, J. L.; de Jong, M.; Krenning, E. P. [^{177}Lu-DOTA^{0},Tyr^{3}]-Octreotate: Comparison with [^{111}In-DTPA^{0}]Octreotide in Patients. *Eur. J. Nucl. Med.* **2001**, *28*, 1319−1325.
(502) FDA approves lutetium Lu 177 dotatate for treatment of GEP-NETS; https://www.fda.gov/Drugs/InformationOnDrugs/ApprovedDrugs/ucm594105.htm (accessed Apr 1, 2018).
(503) Dash, A.; Pillai, M. R. A.; Knapp, F. F. Production of ^{177}Lu for Targeted Radionuclide Therapy: Available Options. *Nucl. Med. Mol. Imaging* **2015**, *49*, 85−107.
(504) Thermal Cross Sections & Resonance Integrals; https://www.nndc.bnl.gov/atlas/atlasvalues.html (accessed Aug 27, 2018).
(505) Toporov, Y. G.; Tarasov, V. A.; Andreyev, O. I.; Zotov, E. A.; Gavrilov, V. D.; Kupriyanov, A. L.; Kuznetsov, R. A. *Development of Therapeutic Radiopharmaceuticals Based on ^{177}Lu for Radionuclide Therapy*; An International Atomic Energy Agency Publication: Vienna, 2009.
(506) Pillai, M. R. A.; Chakraborty, S.; Das, T.; Venkatesh, M.; Ramamoorthy, N. Production Logistics of ^{177}Lu for Radionuclide Therapy. *Appl. Radiat. Isot.* **2003**, *59*, 109−118.
(507) Lahiri, S.; Nayak, D.; Nandy, M.; Das, N. Separation of Carrier Free Lutetium Produced in Proton Activated Ytterbium with HDEHP. *Appl. Radiat. Isot.* **1998**, *49*, 911−913.
(508) Balasubramanian, P. S. Separation of Carrier-Free Lutetium-177 from Neutron Irradiated Natural Ytterbium Target. *J. Radioanal. Nucl. Chem.* **1994**, *185*, 305−310.
(509) Horwitz, E. P.; McAlister, D. R.; Bond, A. H.; Barrans, R. E.; Williamson, J. M. A Process for the Separation of ^{177}Lu from Neutron Irradiated ^{176}Yb Targets. *Appl. Radiat. Isot.* **2005**, *63*, 23−36.
(510) Hashimoto, K.; Matsuoka, H.; Uchida, S. Production of No-Carrier-Added ^{177}Lu via the ^{176}Yb(n,γ)$\rightarrow$^{177}Lu Process. *J. Radioanal. Nucl. Chem.* **2003**, *255*, 575−579.
(511) Van So, L.; Morcos, N.; Zaw, M.; Pellegrini, P.; Greguric, I. Alternative Chromatographic Processes for No-Carrier Added ^{177}Lu Radioisotope Separation. *J. Radioanal. Nucl. Chem.* **2008**, *277*, 663−673.
(512) Bilewicz, A.; Żuchowska, K.; Bartoś, B. Separation of Yb as $YbSO_4$ from the ^{176}Yb Target for Production of ^{177}Lu via the ^{176}Yb(n,γ)^{177}Yb$\rightarrow$^{177}Lu Process. *J. Radioanal. Nucl. Chem.* **2009**, *280*, 167−169.
(513) Chakravarty, R.; Das, T.; Dash, A.; Venkatesh, M. An Electro-Amalgamation Approach to Isolate No-Carrier-Added ^{177}Lu from Neutron Irradiated Yb for Biomedical Applications. *Nucl. Med. Biol.* **2010**, *37*, 811−820.
(514) Lebedev, N. A.; Novgorodov, A. F.; Misiak, R.; Brockmann, J.; Rösch, F. Radiochemical Separation of No-Carrier-Added ^{177}Lu as Produced via the ^{176}Yb(n, γ)^{177}Yb$\rightarrow$^{177}Lu Process. *Appl. Radiat. Isot.* **2000**, *53*, 421−425.

DOI: 10.1021/acs.chemrev.8b00294
Chem. Rev. 2019, 119, 902−956

(515) Hermanne, A.; Takacs, S.; Goldberg, M. B.; Lavie, E.; Shubin, Y. N.; Kovalev, S. Deuteron-Induced Reactions on Yb: Measured Cross Sections and Rationale for Production Pathways of Carrier-Free, Medically Relevant Radionuclides. *Nucl. Instrum. Methods Phys. Res., Sect. B* **2006**, *247*, 223−231.
(516) Medvedev, D. G.; Mausner, L. F.; Greene, G. A.; Hanson, A. L. Activation of Natural Hf and Ta in Relation to the Production of ^{177}Lu. *Appl. Radiat. Isot.* **2008**, *66*, 1300−1306.
(517) Manenti, S.; Bonardi, M. L.; Gini, L.; Groppi, F. Physical Optimization of Production by Deuteron Irradiation of High Specific Activity ^{177g}Lu Suitable for Radioimmunotherapy. *Nucl. Med. Biol.* **2014**, *41*, 407−409.
(518) Aime, S.; Barge, A.; Botta, M.; Fasano, M.; Danilo Ayala, J.; Bombieri, G. Crystal Structure and Solution Dynamics of the Lutetium(III) Chelate of DOTA. *Inorg. Chim. Acta* **1996**, *246*, 423−429.
(519) Perk, L. R.; Visser, G. W.; Vosjan, M. J.; Stigter-van Walsum, M.; Tijink, B. M.; Leemans, C. R.; van Dongen, G. A. ^{89}Zr as a PET Surrogate Radioisotope for Scouting Biodistribution of the Therapeutic Radiometals ^{90}Y and ^{177}Lu in Tumor-Bearing Nude Mice after Coupling to the Internalizing Antibody Cetuximab. *J. Nucl. Med.* **2005**, *46*, 1898−1906.
(520) Stimmel, J. B.; Kull, F. C. Samarium-153 and Lutetium-177 Chelation Properties of Selected Macrocyclic and Acyclic Ligands. *Nucl. Med. Biol.* **1998**, *25*, 117−125.
(521) Watanabe, S.; Hashimoto, K.; Ishioka, N. S. Lutetium-177 Complexation of DOTA and DTPA in the Presence of Competing Metals. *J. Radioanal. Nucl. Chem.* **2015**, *303*, 1519−1521.
(522) Asti, M.; Tegoni, M.; Farioli, D.; Iori, M.; Guidotti, C.; Cutler, C. S.; Mayer, P.; Versari, A.; Salvo, D. Influence of Cations on the Complexation Yield of DOTATATE with Yttrium and Lutetium: A Perspective Study for Enhancing the ^{90}Y and ^{177}Lu Labeling Conditions. *Nucl. Med. Biol.* **2012**, *39*, 509−517.
(523) Pandey, U.; Gamre, N.; Lohar, S. P.; Dash, A. A Systematic Study on the Utility of CHX-A''-DTPA-NCS and NOTA-NCS as Bifunctional Chelators for ^{177}Lu Radiopharmaceuticals. *Appl. Radiat. Isot.* **2017**, *127*, 1−6.
(524) Novy, Z.; Laznickova, A.; Mandikova, J.; Barta, P.; Laznicek, M.; Trejtnar, F. The Effect of Chelator Type on in Vitro Receptor Binding and Stability in ^{177}Lu-Labeled Cetuximab and Panitumumab. *J. Labelled Compd. Radiopharm.* **2014**, *57*, 448−452.
(525) Swärd, C.; Bernhardt, P.; Johanson, V.; Schmitt, A.; Ahlman, H.; Stridsberg, M.; Forssell-Aronsson, E.; Nilsson, O.; Kölby, L. Comparison of [^{177}Lu-DOTA^0,Tyr^3]-Octreotate and [^{177}Lu-DOTA^0,Tyr^3]-Octreotide for Receptor-Mediated Radiation Therapy of the Xenografted Human Midgut Carcinoid Tumor GOT1. *Cancer Biother.Radiopharm.* **2008**, *23*, 114−120.
(526) Makis, W.; McCann, K.; Buteau, F. A.; McEwan, A. J. B. Resolution of Malignant Ascites and Stabilization of Metastases in a Patient With Small Bowel Neuroendocrine Tumor With ^{177}Lu-DOTATATE Following Progression After 17 ^{131}I-MIBG Treatments and Chemotherapy. *Clin. Nucl. Med.* **2015**, *40*, 564−566.
(527) Sandström, M.; Ilan, E.; Karlberg, A.; Johansson, S.; Freedman, N.; Garske-Román, U. Method Dependence, Observer Variability and Kidney Volumes in Radiation Dosimetry of ^{177}Lu-DOTATATE Therapy in Patients with Neuroendocrine Tumours. *EJNMMI Phys.* **2015**, *2*, 24.
(528) Ilan, E.; Sandstrom, M.; Wassberg, C.; Sundin, A.; Garske-Roman, U.; Eriksson, B.; Granberg, D.; Lubberink, M. Dose Response of Pancreatic Neuroendocrine Tumors Treated with Peptide Receptor Radionuclide Therapy Using ^{177}Lu-DOTATATE. *J. Nucl. Med.* **2015**, *56*, 177−182.
(529) Bodei, L.; Kidd, M.; Paganelli, G.; Grana, C. M.; Drozdov, I.; Cremonesi, M.; Lepensky, C.; Kwekkeboom, D. J.; Baum, R. P.; Krenning, E. P.; et al. Long-Term Tolerability of PRRT in 807 Patients with Neuroendocrine Tumours: The Value and Limitations of Clinical Factors. *Eur. J. Nucl. Med. Mol. Imaging* **2015**, *42*, 5−19.
(530) Ianniello, A.; Sansovini, M.; Severi, S.; Nicolini, S.; Grana, C. M.; Massri, K.; Bongiovanni, A.; Antonuzzo, L.; Di Iorio, V.; Sarnelli, A.; et al. Peptide Receptor Radionuclide Therapy with ^{177}Lu-DOTATATE in Advanced Bronchial Carcinoids: Prognostic Role of Thyroid Transcription Factor 1 and ^{18}F-FDG PET. *Eur. J. Nucl. Med. Mol. Imaging* **2016**, *43*, 1040−1046.
(531) Sundlöv, A.; Sjögreen-Gleisner, K.; Svensson, J.; Ljungberg, M.; Olsson, T.; Bernhardt, P.; Tennvall, J. Individualised ^{177}Lu-DOTATATE Treatment of Neuroendocrine Tumours Based on Kidney Dosimetry. *Eur. J. Nucl. Med. Mol. Imaging* **2017**, *44*, 1480−1489.
(532) Strosberg, J.; El-Haddad, G.; Wolin, E.; Hendifar, A.; Yao, J.; Chasen, B.; Mittra, E.; Kunz, P. L.; Kulke, M. H.; Jacene, H.; et al. Phase 3 Trial of ^{177}Lu-Dotatate for Midgut Neuroendocrine Tumors. *N. Engl. J. Med.* **2017**, *376*, 125−135.
(533) Elf, A.-K.; Bernhardt, P.; Hofving, T.; Arvidsson, Y.; Forssell-Aronsson, E.; Wängberg, B.; Nilsson, O.; Johanson, V. NAMPT Inhibitor GMX1778 Enhances the Efficacy of ^{177}Lu-DOTATATE Treatment of Neuroendocrine Tumors. *J. Nucl. Med.* **2017**, *58*, 288−292.
(534) Garske-Román, U.; Sandström, M.; Fröss Baron, K.; Lundin, L.; Hellman, P.; Welin, S.; Johansson, S.; Khan, T.; Lundqvist, H.; Eriksson, B.; et al. Prospective Observational Study of ^{177}Lu-DOTA-Octreotate Therapy in 200 Patients with Advanced Metastasized Neuroendocrine Tumours (NETs): Feasibility and Impact of a Dosimetry-Guided Study Protocol on Outcome and Toxicity. *Eur. J. Nucl. Med. Mol. Imaging* **2018**, *45*, 970−988.
(535) Baum, R. P.; Kluge, A. W.; Kulkarni, H.; Schorr-Neufing, U.; Niepsch, K.; Bitterlich, N.; van Echteld, C. J. A. [^{177}Lu-DOTA]^0-D-Phe^1-Tyr^3-Octreotide (^{177}Lu-DOTATOC) For Peptide Receptor Radiotherapy in Patients with Advanced Neuroendocrine Tumours: A Phase-II Study. *Theranostics* **2016**, *6*, 501−510.
(536) Weineisen, M.; Schottelius, M.; Simecek, J.; Baum, R. P.; Yildiz, A.; Beykan, S.; Kulkarni, H. R.; Lassmann, M.; Klette, I.; Eiber, M.; et al. ^{68}Ga- and ^{177}Lu-Labeled PSMA I&T: Optimization of a PSMA-Targeted Theranostic Concept and First Proof-of-Concept Human Studies. *J. Nucl. Med.* **2015**, *56*, 1169−1176.
(537) Ahmadzadehfar, H.; Rahbar, K.; Kürpig, S.; Bögemann, M.; Claesener, M.; Eppard, E.; Gärtner, F.; Rogenhofer, S.; Schäfers, M.; Essler, M. Early Side Effects and First Results of Radioligand Therapy with ^{177}Lu-DKFZ-617 PSMA of Castrate-Resistant Metastatic Prostate Cancer: A Two-Centre Study. *EJNMMI Res.* **2015**, *5*, 36.
(538) Kabasakal, L.; AbuQbeitah, M.; Aygün, A.; Yeyin, N.; Ocak, M.; Demirci, E.; Toklu, T. Pre-Therapeutic Dosimetry of Normal Organs and Tissues of ^{177}Lu-PSMA-617 Prostate-Specific Membrane Antigen (PSMA) Inhibitor in Patients with Castration-Resistant Prostate Cancer. *Eur. J. Nucl. Med. Mol. Imaging* **2015**, *42*, 1976−1983.
(539) Delker, A.; Fendler, W. P.; Kratochwil, C.; Brunegraf, A.; Gosewisch, A.; Gildehaus, F. J.; Tritschler, S.; Stief, C. G.; Kopka, K.; Haberkorn, U.; et al. Dosimetry for ^{177}Lu-DKFZ-PSMA-617: A New Radiopharmaceutical for the Treatment of Metastatic Prostate Cancer. *Eur. J. Nucl. Med. Mol. Imaging* **2016**, *43*, 42−51.
(540) Heck, M. M.; Retz, M.; D'Alessandria, C.; Rauscher, I.; Scheidhauer, K.; Maurer, T.; Storz, E.; Janssen, F.; Schottelius, M.; Wester, H. J.; et al. Systemic Radioligand Therapy with ^{177}Lu Labeled Prostate Specific Membrane Antigen Ligand for Imaging and Therapy in Patients with Metastatic Castration Resistant Prostate Cancer. *J. Urol.* **2016**, *196*, 382−391.
(541) Rahbar, K.; Ahmadzadehfar, H.; Kratochwil, C.; Haberkorn, U.; Schäfers, M.; Essler, M.; Baum, R. P.; Kulkarni, H. R.; Schmidt, M.; Drzezga, A.; et al. German Multicenter Study Investigating ^{177}Lu-PSMA-617 Radioligand Therapy in Advanced Prostate Cancer Patients. *J. Nucl. Med.* **2017**, *58*, 85−90.
(542) Ahmadzadehfar, H.; Eppard, E.; Kürpig, S.; Fimmers, R.; Yordanova, A.; Schlenkhoff, C. D.; Gärtner, F.; Rogenhofer, S.; Essler, M. Therapeutic Response and Side Effects of Repeated Radioligand Therapy with ^{177}Lu-PSMA-DKFZ-617 of Castrate-Resistant Metastatic Prostate Cancer. *Oncotarget* **2016**, *7*, 12477−12488.
(543) Baum, R. P.; Kulkarni, H. R.; Schuchardt, C.; Singh, A.; Wirtz, M.; Wiessalla, S.; Schottelius, M.; Mueller, D.; Klette, I.; Wester, H. J.

DOI: 10.1021/acs.chemrev.8b00294
Chem. Rev. 2019, 119, 902−956

^{177}Lu-Labeled Prostate-Specific Membrane Antigen Radioligand Therapy of Metastatic Castration-Resistant Prostate Cancer: Safety and Efficacy. *J. Nucl. Med.* **2016**, *57*, 1006−1013.
(544) Kratochwil, C.; Giesel, F. L.; Stefanova, M.; Benesova, M.; Bronzel, M.; Afshar-Oromieh, A.; Mier, W.; Eder, M.; Kopka, K.; Haberkorn, U. PSMA-Targeted Radionuclide Therapy of Metastatic Castration-Resistant Prostate Cancer with ^{177}Lu-Labeled PSMA-617. *J. Nucl. Med.* **2016**, *57*, 1170−1176.
(545) von Eyben, F. E.; Roviello, G.; Kiljunen, T.; Uprimny, C.; Virgolini, I.; Kairemo, K.; Joensuu, T. Third-Line Treatment and ^{177}Lu-PSMA Radioligand Therapy of Metastatic Castration-Resistant Prostate Cancer: A Systematic Review. *Eur. J. Nucl. Med. Mol. Imaging* **2018**, *45*, 496−508.
(546) Ferdinandus, J.; Violet, J.; Sandhu, S.; Hofman, M. S. Prostate-Specific Membrane Antigen Theranostics: Therapy with Lutetium-177. *Curr. Opin. Urol.* **2018**, *28*, 197−204.
(547) Emmett, L.; Willowson, K.; Violet, J.; Shin, J.; Blanksby, A.; Lee, J. Lutetium ^{177} PSMA Radionuclide Therapy for Men with Prostate Cancer: A Review of the Current Literature and Discussion of Practical Aspects of Therapy. *J. Med. Radiat. Sci.* **2017**, *64*, 52−60.
(548) Fendler, W. P.; Rahbar, K.; Herrmann, K.; Kratochwil, C.; Eiber, M. ^{177}Lu-PSMA Radioligand Therapy for Prostate Cancer. *J. Nucl. Med.* **2017**, *58*, 1196−1200.
(549) Vallabhajosula, S. Radioimmunotherapy of Prostate Cancer Using ^{90}Y- and ^{177}Lu-Labeled J591 Monoclonal Antibodies: Effect of Multiple Treatments on Myelotoxicity. *Clin. Cancer Res.* **2005**, *11*, 7195s−7200s.
(550) Vallabhajosula, S.; Kuji, I.; Hamacher, K. A.; Konishi, S.; Kostakoglu, L.; Kothari, P. A.; Milowski, M. I.; Nanus, D. M.; Bander, N. H.; Goldsmith, S. J. Pharmacokinetics and Biodistribution of ^{111}In- and ^{177}Lu-Labeled J591 Antibody Specific for Prostate-Specific Membrane Antigen: Prediction of ^{90}Y-J591 Radiation Dosimetry Based on ^{111}In or ^{177}Lu? *J. Nucl. Med.* **2005**, *46*, 634−641.
(551) Vallabhajosula, S.; Goldsmith, S. J.; Hamacher, K. A.; Kostakoglu, L.; Konishi, S.; Milowski, M. I.; Nanus, D. M.; Bander, N. H. Prediction of Myelotoxicity Based on Bone Marrow Radiation-Absorbed Dose: Radioimmunotherapy Studies Using ^{90}Y- and ^{177}Lu-Labeled J591 Antibodies Specific for Prostate-Specific Membrane Antigen. *J. Nucl. Med.* **2005**, *46*, 850−858.
(552) Bander, N. H.; Milowsky, M. I.; Nanus, D. M.; Kostakoglu, L.; Vallabhajosula, S.; Goldsmith, S. J. Phase I Trial of ^{177}Lutetium-Labeled J591, a Monoclonal Antibody to Prostate-Specific Membrane Antigen, in Patients With Androgen-Independent Prostate Cancer. *J. Clin. Oncol.* **2005**, *23*, 4591−4601.
(553) Tagawa, S. T.; Milowsky, M. I.; Morris, M.; Vallabhajosula, S.; Christos, P.; Akhtar, N. H.; Osborne, J.; Goldsmith, S. J.; Larson, S.; Taskar, N. P.; et al. Phase II Study of Lutetium-177-Labeled Anti-Prostate-Specific Membrane Antigen Monoclonal Antibody J591 for Metastatic Castration-Resistant Prostate Cancer. *Clin. Cancer Res.* **2013**, *19*, 5182−5191.
(554) Nicolas, G. P.; Mansi, R.; McDougall, L.; Kaufmann, J.; Bouterfa, H.; Wild, D.; Fani, M. Biodistribution, Pharmacokinetics, and Dosimetry of ^{177}Lu-, ^{90}Y-, and ^{111}In-Labeled Somatostatin Receptor Antagonist OPS201 in Comparison to the Agonist ^{177}Lu-DOTATATE: The Mass Effect. *J. Nucl. Med.* **2017**, *58*, 1435−1441.
(555) Nicolas, G.; Baum, R.; Herrmann, K.; Lassmann, M.; Hicks, R.; Haug, A.; Navalkissoor, S.; Oberwittler, H.; Wang, T.; Wild, D. Phase 1/2 Open-Label Trial to Assess the Safety and Preliminary Efficacy of ^{177}Lu-OPS201 as Peptide Receptor Radionuclide Therapy in Patients with Somatostatin Receptor-Positive, Progressive Neuroendocrine Tumours. In *10th NANETS Annual Meeting*, Philadelphia, 2017.
(556) Membreno, R.; Cook, B. E.; Fung, K.; Lewis, J. S.; Zeglis, B. M. Click-Mediated Pretargeted Radioimmunotherapy of Colorectal Carcinoma. *Mol. Pharmaceutics* **2018**, *15*, 1729−1734.
(557) Yong, K.; Brechbiel, M. W. Towards Translation of ^{212}Pb as a Clinical Therapeutic; Getting the Lead In! *Dalton Trans* **2011**, *40*, 6068−6076.
(558) Pfost, B.; Seidl, C.; Autenrieth, M.; Saur, D.; Bruchertseifer, F.; Morgenstern, A.; Schwaiger, M.; Senekowitsch-Schmidtke, R. Intravesical α-Radioimmunotherapy with ^{213}Bi-Anti-EGFR-MAb Defeats Human Bladder Carcinoma in Xenografted Nude Mice. *J. Nucl. Med.* **2009**, *50*, 1700−1708.
(559) Fazel, J.; Rötzer, S.; Seidl, C.; Feuerecker, B.; Autenrieth, M.; Weirich, G.; Bruchertseifer, F.; Morgenstern, A.; Senekowitsch-Schmidtke, R. Fractionated Intravesical Radioimmunotherapy with ^{213}Bi-Anti-EGFR-MAb Is Effective without Toxic Side-Effects in a Nude Mouse Model of Advanced Human Bladder Carcinoma. *Cancer Biol. Ther.* **2015**, *16*, 1526−1534.
(560) Teiluf, K.; Seidl, C.; Blechert, B.; Gaertner, F. C.; Gilbertz, K. P.; Fernandez, V.; Bassermann, F.; Endell, J.; Boxhammer, R.; Leclair, S.; et al. α-Radioimmunotherapy with ^{213}Bi-Anti-CD38 Immunoconjugates Is Effective in a Mouse Model of Human Multiple Myeloma. *Oncotarget* **2015**, *6*, 4692−4703.
(561) Fichou, N.; Gouard, S.; Maurel, C.; Barbet, J.; Ferrer, L.; Morgenstern, A.; Bruchertseifer, F.; Faivre-Chauvet, A.; Bigot-Corbel, E.; Davodeau, F.; et al. Single-Dose Anti-CD138 Radioimmunotherapy: Bismuth-213 Is More Efficient than Lutetium-177 for Treatment of Multiple Myeloma in a Preclinical Model. *Front. Med.* **2015**, *2*, 76.
(562) Senekowitsch-Schmidtke, R.; Schuhmacher, C.; Becker, K.-F.; Nikula, T. K.; Seidl, C.; Becker, I.; Miederer, M.; Apostolidis, C.; Adam, C.; Huber, R.; et al. Highly Specific Tumor Binding of a ^{213}Bi-Labeled Monoclonal Antibody against Mutant E-Cadherin Suggest Its Usefulness for Locoregional α-Radioimmunotherapy of Diffuse-Type Gastric Cancer. *Cancer Res.* **2001**, *61*, 2804−2808.
(563) Friesen, C.; Glatting, G.; Koop, B.; Schwarz, K.; Morgenstern, A.; Apostolidis, C.; Debatin, K. M.; Reske, S. N. Breaking Chemoresistance and Radioresistance with [^{213}Bi]Anti-CD45 Antibodies in Leukemia Cells. *Cancer Res.* **2007**, *67*, 1950−1958.
(564) Rizvi, S. M. A.; Song, E. Y.; Raja, C.; Beretov, J.; Morgenstern, A.; Apostolidis, C.; Russell, P. J.; Kearsley, J. H.; Abbas, K.; Allen, B. J. Preparation and Testing of Bevacizumab Radioimmunoconjugates with Bismuth-213 and Bismuth-205/Bismuth-206. *Cancer Biol. Ther.* **2008**, *7*, 1547−1554.
(565) Heskamp, S.; Hernandez, R.; Molkenboer-Kuenen, J. D. M.; Essler, M.; Bruchertseifer, F.; Morgenstern, A.; Steenbergen, E. J.; Cai, W.; Seidl, C.; McBride, W. J.; et al. α-Versus β-Emitting Radionuclides for Pretargeted Radioimmunotherapy of Carcinoembryonic Antigen−Expressing Human Colon Cancer Xenografts. *J. Nucl. Med.* **2017**, *58*, 926−933.
(566) Sgouros, G.; Ballangrud, A. M.; Jurcic, J. G.; McDevitt, M. R.; Humm, J. L.; Erdi, Y. E.; Mehta, B. M.; Finn, R. D.; Larson, S. M.; Scheinberg, D. A. Pharmacokinetics and Dosimetry of an α-Particle Emitter Labeled Antibody: ^{213}Bi-HuM195 (Anti-CD33) in Patients with Leukemia. *J. Nucl. Med.* **1999**, *40*, 1935−1946.
(567) Jurcic, J. G.; Larson, S. M.; Sgouros, G.; McDevitt, M. R.; Finn, R. D.; Divgi, C. R.; Ballangrud, A. M.; Hamacher, K. A.; Ma, D.; Humm, J. L.; et al. Targeted α Particle Immunotherapy for Myeloid Leukemia. *Blood* **2002**, *100*, 1233−1239.
(568) Rosenblat, T. L.; McDevitt, M. R.; Mulford, D. A.; Pandit-Taskar, N.; Divgi, C. R.; Panageas, K. S.; Heaney, M. L.; Chanel, S.; Morgenstern, A.; Sgouros, G.; et al. Sequential Cytarabine and α-Particle Immunotherapy with Bismuth-213-Lintuzumab (HuM195) for Acute Myeloid Leukemia. *Clin. Cancer Res.* **2010**, *16*, 5303−5311.
(569) Jurcic, J. G. What Happened to Anti-CD33 Therapy for Acute Myeloid Leukemia? *Curr. Hematol. Malig. Rep.* **2012**, *7*, 65−73.
(570) Jurcic, J. G.; Rosenblat, T. L. Targeted Alpha-Particle Immunotherapy for Acute Myeloid Leukemia. *Am. Soc. Clin. Oncol. Educ. B* **2014**, *34*, e126−e131.
(571) McDevitt, M. R.; Barendswaard, E.; Ma, D.; Lai, L.; Curcio, M. J.; Sgouros, G.; Ballangrud, A. M.; Yang, W.; Finn, R. D.; Pellegrini, V.; et al. An α-Particle Emitting Antibody ([213 Bi] J591) for Radioimmunotherapy of Prostate Cancer. *Cancer Res.* **2000**, *60*, 6095−6100.
(572) Ballangrud, A. M.; Yang, W. H.; Charlton, D. E.; McDevitt, M. R.; Hamacher, K. A.; Panageas, K. S.; Ma, D.; Bander, N. H.; Scheinberg, D. A.; Sgouros, G. Response of LNCaP Spheroids after

DOI: 10.1021/acs.chemrev.8b00294
Chem. Rev. 2019, 119, 902−956

Treatment with an α-Particle Emitter (^{213}Bi)-Labeled Anti-Prostate-Specific Membrane Antigen Antibody (J591). *Cancer Res.* **2001**, *61*, 2008−2014.
(573) Friesen, C.; Roscher, M.; Hormann, I.; Leib, O.; Marx, S.; Moreno, J.; Miltner, E. Anti-CD33-Antibodies Labelled with the Alpha-Emitter Bismuth-213 Kill CD33-Positive Acute Myeloid Leukaemia Cells Specifically by Activation of Caspases and Break Radio- and Chemoresistance by Inhibition of the Anti-Apoptotic Proteins X-Linked Inhibitor of Apoptosis Protein and B-cell Lymphoma-Extra Large. *Eur. J. Cancer* **2013**, *49*, 2542−2554.
(574) Kim, Y. S.; Brechbiel, M. W. An Overview of Targeted Alpha Therapy. *Tumor Biol.* **2012**, *33*, 573−590.
(575) Gansow, O. A.; Atcher, R. W.; Link, D. C.; Friedman, A. M.; Seevers, R. H.; Anderson, W.; Scheinberg, D. A.; Strand, M. Generator-Produced Bi-212. In *Radionuclide Generators*; Knapp, F. F., Butler, T. A., Eds.; American Chemical Society: 1984; pp 215−227.
(576) Atcher, R. W.; Friedman, A. M.; Hines, J. J. An Improved Generator for the Production of ^{212}Pb and ^{212}Bi from ^{224}Ra. *Appl. Radiat. Isot.* **1988**, *39*, 283−286.
(577) Su, F. M.; Beaumier, P.; Axworthy, D.; Atcher, R.; Fritzberg, A. Pretargeted Radioimmunotherapy in Tumored Mice Using an in Vivo ^{212}Pb/^{212}Bi Generator. *Nucl. Med. Biol.* **2005**, *32*, 741−747.
(578) Rotmensch, J.; Atcher, R. W.; Hines, J.; Toohill, M.; Herbst, A. L. Comparison of Short-Lived High-LET α-Emitting Radionuclides Lead-212 and Bismuth-212 to Low-LET X-Rays on Ovarian Carcinoma. *Gynecol. Oncol.* **1989**, *35*, 297−300.
(579) Boldyrev, P. P.; Bortash, A. I.; Zagryadskii, V. A.; Zakharov, A. S.; Nikolaev, V. I.; Proshin, M. A.; Chuvilin, D. Y.; Shatrov, A. V.; Vesnovskii, S. P. ^{212}Pb/^{212}Bi Generator for Nuclear Medicine. *At. Energy* **2012**, *111*, 422−427.
(580) Hassfjell, S. A ^{212}Pb Generator Based on a ^{228}Th Source. *Appl. Radiat. Isot.* **2001**, *55*, 433−439.
(581) Zucchini, G. L.; Friedman, A. M. Isotopic Generator for ^{212}Pb and ^{212}Bi. *Int. J. Nucl. Med. Biol.* **1982**, *9*, 83−84.
(582) Brechbiel, M. W.; Dadachova, E. Radiobismuth for Therapy. In *Biological Chemistry of Arsenic, Antimony and Bismuth*; John Wiley & Sons: Chichester, 2010; pp 311−329.
(583) Ma, D.; McDevitt, M. R.; Finn, R. D.; Scheinberg, D. A. Breakthrough of ^{225}Ac and Its Radionuclide Daughters from an ^{225}Ac/^{213}Bi Generator: Development of New Methods, Quantitative Characterization, and Implications for Clinical Use. *Appl. Radiat. Isot.* **2001**, *55*, 667−678.
(584) Norman, N. C. *Chemistry of Arsenic, Antimony and Bismuth*; Springer: Netherlands, 1997.
(585) Sadler, P. J.; Li, H.; Sun, H. Coordination Chemistry of Metals in Medicine: Target Sites for Bismuth. *Coord. Chem. Rev.* **1999**, *185*−*186*, 689−709.
(586) Cukrowski, I.; Hancock, R. D.; Luckay, R. C. Formation Constant Calculation for Non-Labile Complexes Based on a Labile Part of the Metal-Ligand System. A Differential Pulse Polarographic Study at Fixed Ligand to Metal Ratio and Varied pH: Application to Polarographically Inactive Complexes. *Anal. Chim. Acta* **1996**, *319*, 39−48.
(587) Lima, L. M. P.; Beyler, M.; Delgado, R.; Platas-Iglesias, C.; Tripier, R. Investigating the Complexation of the Pb^{2+}/Bi^{3+} Pair with Dipicolinate Cyclen Ligands. *Inorg. Chem.* **2015**, *54*, 7045−7057.
(588) Cordier, D.; Forrer, F.; Bruchertseifer, F.; Morgenstern, A.; Apostolidis, C.; Good, S.; Müller-Brand, J.; Mäcke, H.; Reubi, J. C.; Merlo, A. Targeted Alpha-Radionuclide Therapy of Functionally Critically Located Gliomas with ^{213}Bi-DOTA-[Thi^{8},Met(O2)^{11}]-Substance P: A Pilot Trial. *Eur. J. Nucl. Med. Mol. Imaging* **2010**, *37*, 1335−1344.
(589) Wild, D.; Frischknecht, M.; Zhang, H.; Morgenstern, A.; Bruchertseifer, F.; Boisclair, J.; Provencher-Bolliger, A.; Reubi, J. C.; Maecke, H. R. Alpha- versus Beta-Particle Radiopeptide Therapy in a Human Prostate Cancer Model (^{213}Bi-DOTA-PESIN and ^{213}Bi-AMBA versus ^{177}Lu-DOTA-PESIN). *Cancer Res.* **2011**, *71*, 1009−1018.
(590) Garmestani, K.; Yao, Z.; Zhang, M.; Wong, K.; Park, C. W.; Pastan, I.; Carrasquillo, J. A.; Brechbiel, M. W. Synthesis and Evaluation of a Macrocyclic Bifunctional Chelating Agent for Use with Bismuth Radionuclides. *Nucl. Med. Biol.* **2001**, *28*, 409−418.
(591) Lima, L. M. P.; Beyler, M.; Oukhatar, F.; Le Saec, P.; Faivre-Chauvet, A.; Platas-Iglesias, C.; Delgado, R.; Tripier, R. H_2Me-Do2pa: An Attractive Chelator with Fast, Stable and Inert $^{Nat}Bi^{3+}$ and $^{213}Bi^{3+}$ Complexation for Potential α-Radioimmunotherapy Applications. *Chem. Commun.* **2014**, *50*, 12371−12374.
(592) Brechbiel, M. W.; Gansow, O. A.; Pippin, C. G.; Rogers, R. D.; Planalp, R. P. Preparation of the Novel Chelating Agent N-(2-Aminoethyl)-trans-1,2-Diaminocyclohexane- N,N',N''-Pentaacetic Acid (H_5CyDTPA), a Preorganized Analogue of Diethylenetriaminepentaacetic Acid (H_5DTPA), and the Structures of $Bi^{III}(CyDTPA)^{2-}$ and $Bi^{III}(H_2DTPA)$ Complexes. *Inorg. Chem.* **1996**, *35*, 6343−6348.
(593) Kozak, R. W.; Waldmann, T. A.; Atcher, R. W.; Gansow, O. A. Radionuclide-Conjugated Monoclonal Antibodies: A Synthesis of Immunology, Inorganic Chemistry and Nuclear Science. *Trends Biotechnol.* **1986**, *4*, 259−264.
(594) Ruegg, C. L.; Anderson-Berg, W. T.; Brechbiel, M. W.; Mirzadeh, S.; Gansow, O. A.; Strand, M. Improved in Vivo Stability and Tumor Targeting of Bismuth-Labeled Antibody. *Cancer Res.* **1990**, *50*, 4221−4226.
(595) Milenic, D. E.; Roselli, M.; Mirzadeh, S.; Pippin, C. G.; Gansow, O. A.; Colcher, D.; Brechbiel, M. W.; Schlom, J. In Vivo Evaluation of Bismuth-Labeled Monoclonal Antibody Comparing DTPA-Derived Bifunctional Chelates. *Cancer Biother.Radiopharm.* **2001**, *16*, 133−146.
(596) Brechbiel, M. W.; Gansow, O. A. Synthesis of C-Functionalized Trans-Cyclohexyldiethylenetriaminepenta-Acetic Acids for Labelling of Monoclonal Antibodies with the Bismuth-212 α-Particle Emitter. *J. Chem. Soc., Perkin Trans. 1* **1992**, *9*, 1173−1178.
(597) Montavon, G.; Le Du, A.; Champion, J.; Rabung, T.; Morgenstern, A. DTPA Complexation of Bismuth in Human Blood Serum. *Dalton Trans* **2012**, *41*, 8615−8623.
(598) Chong, H. S.; Milenic, D. E.; Garmestani, K.; Brady, E. D.; Arora, H.; Pfiester, C.; Brechbiel, M. W. In Vitro and in Vivo Evaluation of Novel Ligands for Radioimmunotherapy. *Nucl. Med. Biol.* **2006**, *33*, 459−467.
(599) Chong, H. S.; Song, H. A.; Birch, N.; Le, T.; Lim, S.; Ma, X. Efficient Synthesis and Evaluation of Bimodal Ligand NETA. *Bioorg. Med. Chem. Lett.* **2008**, *18*, 3436−3439.
(600) Chong, H. S.; Song, H. A.; Ma, X.; Milenic, D. E.; Brady, E. D.; Lim, S.; Lee, H.; Baidoo, K.; Cheng, D.; Brechbiel, M. W. Novel Bimodal Bifunctional Ligands for Radioimmunotherapy and Targeted MRI. *Bioconjugate Chem.* **2008**, *19*, 1439−1447.
(601) Kang, C. S.; Song, H. A.; Milenic, D. E.; Baidoo, K. E.; Brechbiel, M. W.; Chong, H. S. Preclinical Evaluation of NETA-Based Bifunctional Ligand for Radioimmunotherapy Applications Using ^{212}Bi and ^{213}Bi: Radiolabeling, Serum Stability, and Biodistribution and Tumor Uptake Studies. *Nucl. Med. Biol.* **2013**, *40*, 600−605.
(602) Song, H. A.; Kang, C. S.; Baidoo, K. E.; Milenic, D. E.; Chen, Y.; Dai, A.; Brechbiel, M. W.; Chong, H. S. Efficient Bifunctional Decadentate Ligand 3p-C-DEPA for Targeted α-Radioimmunotherapy Applications. *Bioconjugate Chem.* **2011**, *22*, 1128−1135.
(603) McDevitt, M. R.; Finn, R. D.; Ma, D.; Larson, S. M.; Scheinberg, D. A. Preparation of α-Emitting ^{213}Bi-Labeled Antibody Constructs for Clinical Use. *J. Nucl. Med.* **1999**, *40*, 1722−1727.
(604) Rizvi, S.; Allen, B.; Lee, C.; Bruchertseifer, F.; Apostolidis, C.; Morgenstern, A.; Clarke, R. Orthotopic Administration of ^{213}Bi−bevacizumab Inhibits Progression of PC3 Xenografts in the Prostate. *Immunotherapy* **2012**, *4*, 549−554.
(605) Norenberg, J. P.; Krenning, B. J.; Konings, I. R. H. M.; Kusewitt, D. F.; Nayak, T. K.; Anderson, T. L.; de Jong, M.; Garmestani, K.; Brechbiel, M. W.; Kvols, L. K. ^{213}Bi-[DOTA^{0},Tyr^{3}]-Octreotide Peptide Receptor Radionuclide Therapy of Pancreatic Tumors in a Preclinical Animal Model. *Clin. Cancer Res.* **2006**, *12*, 897−903.

DOI: 10.1021/acs.chemrev.8b00294
Chem. Rev. 2019, 119, 902−956

(606) Nayak, T. K.; Norenberg, J. P.; Anderson, T. L.; Prossnitz, E. R.; Stabin, M. G.; Atcher, R. W. Somatostatin-Receptor-Targeted α-Emitting ^{213}Bi Is Therapeutically More Effective than β-Emitting ^{177}Lu in Human Pancreatic Adenocarcinoma Cells. *Nucl. Med. Biol.* **2007**, *34*, 185−193.
(607) Giesel, F. L.; Wulfert, S.; Zechmann, C. M.; Haberkorn, U.; Kratochwil, C.; Flechsig, P.; Kuder, T.; Schwartz, L. H.; Brucherstseifer, F. Contrast-Enhanced Ultrasound Monitoring of Perfusion Changes in Hepatic Neuroendocrine Metastases after Systemic versus Selective Arterial ^{177}Lu/^{90}Y-DOTATOC and ^{213}Bi-DOTATOC Radiopeptide Therapy. *Exp. Oncol.* **2013**, *35*, 122−126.
(608) Kratochwil, C.; Giesel, F. L.; Bruchertseifer, F.; Mier, W.; Apostolidis, C.; Boll, R.; Murphy, K.; Haberkorn, U.; Morgenstern, A. ^{213}Bi-DOTATOC Receptor-Targeted Alpha-Radionuclide Therapy Induces Remission in Neuroendocrine Tumours Refractory to Beta Radiation: A First-in-Human Experience. *Eur. J. Nucl. Med. Mol. Imaging* **2014**, *41*, 2106−2119.
(609) Chan, H. S.; Konijnenberg, M. W.; Daniels, T.; Nysus, M.; Makvandi, M.; de Blois, E.; Breeman, W. A.; Atcher, R. W.; de Jong, M.; Norenberg, J. P. Improved Safety and Efficacy of ^{213}Bi-DOTATATE-Targeted Alpha Therapy of Somatostatin Receptor-Expressing Neuroendocrine Tumors in Mice Pre-Treated with L-Lysine. *EJNMMI Res.* **2016**, *6*, 83.
(610) Chan, H. S.; Konijnenberg, M. W.; de Blois, E.; Koelewijn, S.; Baum, R. P.; Morgenstern, A.; Bruchertseifer, F.; Breeman, W. A.; de Jong, M. Influence of Tumour Size on the Efficacy of Targeted Alpha Therapy with ^{213}Bi-[DOTA^0,Tyr^3]-Octreotate. *EJNMMI Res.* **2016**, *6*, 6.
(611) Chan, H. S.; de Blois, E.; Konijnenberg, M. W.; Morgenstern, A.; Bruchertseifer, F.; Norenberg, J. P.; Verzijlbergen, F. J.; de Jong, M.; Breeman, W. A. P. Optimizing Labelling Conditions of ^{213}Bi-DOTATATE for Preclinical Applications of Peptide Receptor Targeted Alpha Therapy. *EJNMMI Radiopharm. Chem.* **2017**, *1*, 9.
(612) Sathekge, M.; Knoesen, O.; Meckel, M.; Modiselle, M.; Vorster, M.; Marx, S. ^{213}Bi-PSMA-617 Targeted Alpha-Radionuclide Therapy in Metastatic Castration-Resistant Prostate Cancer. *Eur. J. Nucl. Med. Mol. Imaging* **2017**, *44*, 1099−1100.
(613) Kratochwil, C.; Schmidt, K.; Afshar-Oromieh, A.; Bruchertseifer, F.; Rathke, H.; Morgenstern, A.; Haberkorn, U.; Giesel, F. L. Targeted Alpha Therapy of mCRPC: Dosimetry Estimate of ^{213}Bismuth-PSMA-617. *Eur. J. Nucl. Med. Mol. Imaging* **2018**, *45*, 31−37.
(614) Zhang, H.; Schuhmacher, J.; Waser, B.; Wild, D.; Eisenhut, M.; Reubi, J. C.; Maecke, H. R. DOTA-PESIN, a DOTA-Conjugated Bombesin Derivative Designed for the Imaging and Targeted Radionuclide Treatment of Bombesin Receptor-Positive Tumours. *Eur. J. Nucl. Med. Mol. Imaging* **2007**, *34*, 1198−1208.
(615) Krolicki, L.; Królicki, B.; Morgenstern, A.; Kunikowska, J.; Koziara, H.; Jakuciński, M.; Apostolidis, C.; Bruchertseifer, F. Recurrent Glioblastoma Multiforme − Targeted Alpha Therapy with ^{213}Bi-DOTA-Substance P. *Radiother. Oncol.* **2016**, *118*, S16.
(616) Ranson, M.; Tian, Z.; Andronicos, N. M.; Rizvi, S.; Allen, B. J. In Vitro Cytotoxicity of Bismuth-213 (^{213}Bi)-Labeled-Plasminogen Activator Inhibitor Type 2 (Alpha-PAI-2) on Human Breast Cancer Cells. *Breast Cancer Res. Treat.* **2002**, *71*, 149−159.
(617) Li, Y.; Rizvi, S. M. A.; Ranson, M.; Allen, B. J. ^{213}Bi-PAI2 Conjugate Selectively Induces Apoptosis in PC3Metastatic Prostate Cancer Cell Line and Shows Anti-Cancer Activity in a Xenograft Animal Model. *Br. J. Cancer* **2002**, *86*, 1197−1203.
(618) Song, Y. J.; Qu, C. F.; Rizvi, S. M. A.; Li, Y.; Robertson, G.; Raja, C.; Morgenstern, A.; Apostolidis, C.; Perkins, A. C.; Allen, B. J. Cytotoxicity of PAI2, C595 and Herceptin Vectors Labeled with the Alpha-Emitting Radioisotope Bismuth-213 for Ovarian Cancer Cell Monolayers and Clusters. *Cancer Lett.* **2006**, *234*, 176−183.
(619) Allen, B. J.; Tian, Z.; Rizvi, S. M. A.; Li, Y.; Ranson, M. Preclinical Studies of Targeted α-Therapy for Breast Cancer Using ^{213}Bi-Labelled-Plasminogen Activator Inhibitor Type 2. *Br. J. Cancer* **2003**, *88*, 944−950.
(620) Qu, C. F.; Song, E. Y.; Li, Y.; Rizvi, S. M. A.; Raja, C.; Smith, R.; Morgenstern, A.; Apostolidis, C.; Allen, B. J. Pre-Clinical Study of ^{213}Bi Labeled PAI2 for the Control of Micrometastatic Pancreatic Cancer. *Clin. Exp. Metastasis* **2005**, *22*, 575−586.
(621) Song, E. Y.; Rizvi, S. M. A.; Qu, C. F.; Raja, C.; Brechbiel, M. W.; Morgenstern, A.; Apostolidis, C.; Allen, B. J. Pharmacokinetics and Toxicity of ^{213}Bi-Labeled PAI2 in Preclinical Targeted Alpha Therapy for Cancer. *Cancer Biol. Ther.* **2007**, *6*, 898−904.
(622) Drecoll, E.; Gaertner, F. C.; Miederer, M.; Blechert, B.; Vallon, M.; Müller, J. M.; Alke, A.; Seidl, C.; Bruchertseifer, F.; Morgenstern, A.; et al. Treatment of Peritoneal Carcinomatosis by Targeted Delivery of the Radio-Labeled Tumor Homing Peptide ^{213}Bi-DTPA-[F3]$_2$ into the Nucleus of Tumor Cells. *PLoS One* **2009**, *4*, e5715.
(623) Jurcic, J. G. Targeted Alpha-Particle Immunotherapy with Bismuth-213 and Actinium-225 for Acute Myeloid Leukemia. *J. Postgrad. Med. Educ. Res.* **2013**, *47*, 14−17.
(624) Robertson, A. K. H.; Ramogida, C. F.; Rodríguez-Rodríguez, C.; Blinder, S.; Kunz, P.; Sossi, V.; Schaffer, P. Multi-Isotope SPECT Imaging of the ^{225}Ac Decay Chain: Feasibility Studies. *Phys. Med. Biol.* **2017**, *62*, 4406−4420.
(625) Miederer, M.; Henriksen, G.; Alke, A.; Mossbrugger, I.; Quintanilla-Martinez, L.; Senekowitsch-Schmidtke, R.; Essler, M. Preclinical Evaluation of the α-Particle Generator Nuclide ^{225}Ac for Somatostatin Receptor Radiotherapy of Neuroendocrine Tumors. *Clin. Cancer Res.* **2008**, *14*, 3555−3561.
(626) Pandya, D. N.; Hantgan, R.; Budzevich, M. M.; Kock, N. D.; Morse, D. L.; Batista, I.; Mintz, A.; Li, K. C.; Wadas, T. J. Preliminary Therapy Evaluation of ^{225}Ac-DOTA-c(RGDyK) Demonstrates That Cerenkov Radiation Derived from ^{225}Ac Daughter Decay Can Be Detected by Optical Imaging for In Vivo Tumor Visualization. *Theranostics* **2016**, *6*, 698−709.
(627) Kratochwil, C.; Bruchertseifer, F.; Rathke, H.; Bronzel, M.; Apostolidis, C.; Weichert, W.; Haberkorn, U.; Giesel, F. L.; Morgenstern, A. Targeted α-Therapy of Metastatic Castration-Resistant Prostate Cancer with ^{225}Ac-PSMA-617: Dosimetry Estimate and Empiric Dose Finding. *J. Nucl. Med.* **2017**, *58*, 1624−1631.
(628) Kratochwil, C.; Bruchertseifer, F.; Giesel, F. L.; Weis, M.; Verburg, F. A.; Mottaghy, F.; Kopka, K.; Apostolidis, C.; Haberkorn, U.; Morgenstern, A. ^{225}Ac-PSMA-617 for PSMA-Targeted -Radiation Therapy of Metastatic Castration-Resistant Prostate Cancer. *J. Nucl. Med.* **2016**, *57*, 1941−1944.
(629) Wadas, T. J.; Pandya, D. N.; Solingapuram Sai, K. K.; Mintz, A. Molecular Targeted α-Particle Therapy for Oncologic Applications. *AJR, Am. J. Roentgenol.* **2014**, *203*, 253−260.
(630) Koch, L.; Apostolidis, C.; Janssens, W.; Molinet, R.; Van Geel, J. Production of Ac-225 and Application of the Bi-213 Daughter in Cancer Therapy. *Czech. J. Phys.* **1999**, *49*, 817−822.
(631) *Technical Meeting on Alpha Emitting Radionuclides and Radiopharmaceuticals for Therapy*; IAEA: 2013.
(632) Boll, R. A.; Malkemus, D.; Mirzadeh, S. Production of Actinium-225 for Alpha Particle Mediated Radioimmunotherapy. *Appl. Radiat. Isot.* **2005**, *62*, 667−679.
(633) Apostolidis, C.; Molinet, R.; Rasmussen, G.; Morgenstern, A. Production of Ac-225 from Th-229 for Targeted α Therapy. *Anal. Chem.* **2005**, *77*, 6288−6291.
(634) Dockx, K.; Bruchertseifer, F.; Cocolios, T. E.; Dierckx, M.; Fedosseev, V. N.; Fenwick, A.; Giles, T.; Houngbo, D.; Judge, S.; Keightley, J.; et al. *Towards Reliable Production of ^{225}Ac for Medical Applications: Systematic Analysis of the Production of Fr, Ra and Ac Beams*; 2017.
(635) Makvandi, M.; Dupis, E.; Engle, J. W.; Nortier, F. M.; Fassbender, M. E.; Simon, S.; Birnbaum, E. R.; Atcher, R. W.; John, K. D.; Rixe, O.; et al. Alpha-Emitters and Targeted Alpha Therapy in Oncology: From Basic Science to Clinical Investigations. *Target. Oncol.* **2018**, *13*, 189−203.
(636) Griswold, J. R.; Medvedev, D. G.; Engle, J. W.; Copping, R.; Fitzsimmons, J. M.; Radchenko, V.; Cooley, J. C.; Fassbender, M. E.; Denton, D. L.; Murphy, K. E.; et al. Large Scale Accelerator Production of ^{225}Ac: Effective Cross Sections for 78−192 MeV

DOI: 10.1021/acs.chemrev.8b00294
Chem. Rev. 2019, 119, 902−956

Protons Incident on ^{232}Th Targets. *Appl. Radiat. Isot.* **2016**, *118*, 366−374.
(637) Apostolidis, C.; Molinet, R.; McGinley, J.; Abbas, K.; Möllenbeck, J.; Morgenstern, A. Cyclotron Production of Ac-225 for Targeted Alpha Therapy. *Appl. Radiat. Isot.* **2005**, *62*, 383−387.
(638) Boll, R. A.; Garland, M. A.; Mirzadeh, S. Production of Thorium-229 at the ORNL High Flux Isotope Reactor. In *ANS Annual Meeting: Isotopes for Medicine and Industry*, Anaheim, 2008.
(639) Griswold, J. R. *Thick Target Yield of Th-229 via Low Energy Proton Bombardment of Th-232*; University of Tennessee: 2014.
(640) Melville, G.; J Allen, B. Cyclotron and Linac Production of Ac-225. *Appl. Radiat. Isot.* **2009**, *67*, 549−555.
(641) Melville, G.; Meriarty, H.; Metcalfe, P.; Knittel, T.; Allen, B. J. Production of Ac-225 for Cancer Therapy by Photon-Induced Transmutation of Ra-226. *Appl. Radiat. Isot.* **2007**, *65*, 1014−1022.
(642) Melville, G.; Melville, P. A. Theoretical Model for the Production of Ac-225 for Cancer Therapy by Neutron Capture Transmutation of Ra-226. *Appl. Radiat. Isot.* **2013**, *72*, 152−157.
(643) Lefort, M.; Simonoff, G. N.; Tarrago, X. Réactions Nucléaires de Spallation Induites Sur Le Thorium Par Des Protons de 150 et 82 MeV. *Nucl. Phys.* **1961**, *25*, 216−247.
(644) Gauvin, H. Réactions (p,2pxn) Sur Le Thorium 232 de 30 à 120 MeV. *J. Phys. Radium* **1963**, *24*, 836−838.
(645) Moskvin, L. N.; Tsaritsyna, L. G. Isolation of Actinium and Radium from a Thorium Target Irradiated by 600 MeV Protons. *At. Energy* **1968**, *24*, 475−476.
(646) Bonetti, R.; Chiesa, C.; Guglielmetti, A.; Matheoud, R.; Migliorino, C.; Pasinetti, A. L.; Ravn, H. L. Nuclear Structure Effects in the Exotic Decay of ^{225}Ac via ^{14}C Emission. *Nucl. Phys. A* **1993**, *562*, 32−40.
(647) Zhuikov, B. L.; Kalmykov, S. N.; Ermolaev, S. V.; Aliev, R. A.; Kokhanyuk, V. M.; Matushko, V. L.; Tananaev, I. G.; Myasoedov, B. F. Production of ^{225}Ac and ^{223}Ra by Irradiation of Th with Accelerated Protons. *Radiochemistry* **2011**, *53*, 73−80.
(648) Weidner, J. W.; Mashnik, S. G.; John, K. D.; Hemez, F.; Ballard, B.; Bach, H.; Birnbaum, E. R.; Bitteker, L. J.; Couture, A.; Dry, D.; et al. Proton-Induced Cross Sections Relevant to Production of ^{225}Ac and ^{223}Ra in Natural Thorium Targets below 200MeV. *Appl. Radiat. Isot.* **2012**, *70*, 2602−2607.
(649) Engle, J. W.; Weidner, J. W.; Ballard, B. D.; Fassbender, M. E.; Hudston, L. A.; Jackman, K. R.; Dry, D. E.; Wolfsberg, L. E.; Bitteker, L. J.; Ullmann, J. L.; et al. Ac, La, and Ce Radioimpurities in ^{225}Ac Produced in 40−200 MeV Proton Irradiations of Thorium. *Radiochim. Acta* **2014**, *102*, 569−581.
(650) Weidner, J. W.; Mashnik, S. G.; John, K. D.; Ballard, B.; Birnbaum, E. R.; Bitteker, L. J.; Couture, A.; Fassbender, M. E.; Goff, G. S.; Gritzo, R.; et al. ^{225}Ac and ^{223}Ra Production via 800MeV Proton Irradiation of Natural Thorium Targets. *Appl. Radiat. Isot.* **2012**, *70*, 2590−2595.
(651) Aliev, R. A.; Ermolaev, S. V.; Vasiliev, A. N.; Ostapenko, V. S.; Lapshina, E. V.; Zhuikov, B. L.; Zakharov, N. V.; Pozdeev, V. V.; Kokhanyuk, V. M.; Myasoedov, B. F.; et al. Isolation of Medicine-Applicable Actinium-225 from Thorium Targets Irradiated by Medium-Energy Protons. *Solvent Extr. Ion Exch.* **2014**, *32*, 468−477.
(652) Marinov, G.; Marinova, A.; Milanova, M.; Happel, S.; Lebedev, N. A.; Drokhlyansky, A.; Mirzayev, N.; Karaivanov, D. V.; Filosofov, D. V. Sorption of Rare-Earth Elements and Ac on UTEVA Resin in Different Acid Solutions. *Solvent Extr. Ion Exch.* **2017**, *35*, 280−291.
(653) Radchenko, V.; Engle, J. W.; Wilson, J. J.; Maassen, J. R.; Nortier, F. M.; Taylor, W. A.; Birnbaum, E. R.; Hudston, L. A.; John, K. D.; Fassbender, M. E. Application of Ion Exchange and Extraction Chromatography to the Separation of Actinium from Proton-Irradiated Thorium Metal for Analytical Purposes. *J. Chromatogr. A* **2015**, *1380*, 55−63.
(654) Radchenko, V.; Mastren, T.; Meyer, C. A. L.; Ivanov, A. S.; Bryantsev, V. S.; Copping, R.; Denton, D.; Engle, J. W.; Griswold, J. R.; Murphy, K.; et al. Radiometric Evaluation of Diglycolamide Resins for the Chromatographic Separation of Actinium from Fission Product Lanthanides. *Talanta* **2017**, *175*, 318−324.
(655) Ostapenko, V.; Vasiliev, A.; Lapshina, E.; Ermolaev, S.; Aliev, R.; Totskiy, Y.; Zhuikov, B.; Kalmykov, S. Extraction Chromatographic Behavior of Actinium and REE on DGA, Ln and TRU Resins in Nitric Acid Solutions. *J. Radioanal. Nucl. Chem.* **2015**, *306*, 707−711.
(656) Kirby, H. W.; Morss, L. R. Actinium. In *The Chemistry of the Actinide and Transactinide Elements*; Morss, L. R., Edelstein, N. M., Fuger, J., Eds.; Springer: Dordrecht, 2006; pp 18−51.
(657) Ferrier, M. G.; Stein, B. W.; Batista, E. R.; Berg, J. M.; Birnbaum, E. R.; Engle, J. W.; John, K. D.; Kozimor, S. A.; Lezama Pacheco, J. S.; Redman, L. N. Synthesis and Characterization of the Actinium Aquo Ion. *ACS Cent. Sci.* **2017**, *3*, 176−185.
(658) Deblonde, G. J.-P.; Abergel, R. J. Active Actinium. *Nat. Chem.* **2016**, *8*, 1084.
(659) Kennel, S. J.; Chappell, L. L.; Dadachova, K.; Brechbiel, M. W.; Lankford, T. K.; Davis, I. A.; Stabin, M.; Mirzadeh, S. Evaluation of ^{225}Ac for Vascular Targeted Radioimmunotherapy of Lung Tumors. *Cancer Biother.Radiopharm.* **2000**, *15*, 235−244.
(660) McDevitt, M. R.; Ma, D.; Simon, J.; Frank, R. K.; Scheinberg, D. A. Design and Synthesis of ^{225}Ac Radioimmunopharmaceuticals. *Appl. Radiat. Isot.* **2002**, *57*, 841−847.
(661) Deal, K. A.; Davis, I. A.; Mirzadeh, S.; Kennel, S. J.; Brechbiel, M. W. Improved in Vivo Stability of Actinium-225 Macrocyclic Complexes. *J. Med. Chem.* **1999**, *42*, 2988−2992.
(662) Maguire, W. F.; McDevitt, M. R.; Smith-Jones, P. M.; Scheinberg, D. A. Efficient 1-Step Radiolabeling of Monoclonal Antibodies to High Specific Activity with ^{225}Ac for α-Particle Radioimmunotherapy of Cancer. *J. Nucl. Med.* **2014**, *55*, 1492−1498.
(663) Chappell, L. L.; Deal, K. A.; Dadachova, E.; Brechbiel, M. W. Synthesis, Conjugation, and Radiolabeling of a Novel Bifunctional Chelating Agent for ^{225}Ac Radioimmunotherapy Applications. *Bioconjugate Chem.* **2000**, *11*, 510−519.
(664) Thiele, N. A.; Brown, V.; Kelly, J. M.; Amor-Coarasa, A.; Jermilova, U.; MacMillan, S. N.; Nikolopoulou, A.; Ponnala, S.; Ramogida, C. F.; Robertson, A. K. H.; et al. An Eighteen-Membered Macrocyclic Ligand for Actinium-225 Targeted Alpha Therapy. *Angew. Chem., Int. Ed.* **2017**, *56*, 14712−14717.
(665) Roca-Sabio, A.; Mato-Iglesias, M.; Esteban-Gómez, D.; Tóth, E.; Blas, A. de; Platas-Iglesias, C.; Rodríguez-Blas, T. Macrocyclic Receptor Exhibiting Unprecedented Selectivity for Light Lanthanides. *J. Am. Chem. Soc.* **2009**, *131*, 3331−3341.
(666) McLaughlin, M. F.; Woodward, J.; Boll, R. A.; Wall, J. S.; Rondinone, A. J.; Kennel, S. J.; Mirzadeh, S.; Robertson, J. D. Gold Coated Lanthanide Phosphate Nanoparticles for Targeted Alpha Generator Radiotherapy. *PLoS One* **2013**, *8*, e54531.
(667) Miederer, M.; Scheinberg, D. A.; McDevitt, M. R. Realizing the Potential of the Actinium-225 Radionuclide Generator in Targeted Alpha Particle Therapy Applications. *Adv. Drug Delivery Rev.* **2008**, *60*, 1371−1382.
(668) Wang, G.; de Kruijff, R. M.; Rol, A.; Thijssen, L.; Mendes, E.; Morgenstern, A.; Bruchertseifer, F.; Stuart, M. C. A.; Wolterbeek, H. T.; Denkova, A. G. Retention Studies of Recoiling Daughter Nuclides of ^{225}Ac in Polymer Vesicles. *Appl. Radiat. Isot.* **2014**, *85*, 45−53.
(669) Sofou, S.; Kappel, B. J.; Jaggi, J. S.; McDevitt, M. R.; Scheinberg, D. A.; Sgouros, G. Enhanced Retention of the α-Particle-Emitting Daughters of Actinium-225 by Liposome Carriers. *Bioconjugate Chem.* **2007**, *18*, 2061−2067.
(670) Woodward, J.; Kennel, S. J.; Stuckey, A.; Osborne, D.; Wall, J.; Rondinone, A. J.; Standaert, R. F.; Mirzadeh, S. $LaPO_4$ Nanoparticles Doped with Actinium-225 That Partially Sequester Daughter Radionuclides. *Bioconjugate Chem.* **2011**, *22*, 766−776.
(671) de Kruijff, R.; Wolterbeek, H.; Denkova, A. A Critical Review of Alpha Radionuclide Therapy—How to Deal with Recoiling Daughters? *Pharmaceuticals* **2015**, *8*, 321−336.
(672) Song, H.; Hobbs, R. F.; Vajravelu, R.; Huso, D. L.; Esaias, C.; Apostolidis, C.; Morgenstern, A.; Sgouros, G. Radioimmunotherapy

DOI: 10.1021/acs.chemrev.8b00294
Chem. Rev. 2019, 119, 902−956

of Breast Cancer Metastases with -Particle Emitter ^{225}Ac: Comparing Efficacy with ^{213}Bi and ^{90}Y. *Cancer Res.* **2009**, *69*, 8941−8948.
(673) Kennel, S. J.; Brechbiel, M. W.; Milenic, D. E.; Schlom, J.; Mirzadeh, S. Actinium-225 Conjugates of MAb CC49 and Humanized ΔCH_2CC49. *Cancer Biother.Radiopharm.* **2002**, *17*, 219−231.
(674) Schwartz, J.; Jaggi, J. S.; O'Donoghue, J. A.; Ruan, S.; McDevitt, M.; Larson, S. M.; Scheinberg, D. A.; Humm, J. L. Renal Uptake of Bismuth-213 and Its Contribution to Kidney Radiation Dose Following Administration of Actinium-225-Labeled Antibody. *Phys. Med. Biol.* **2011**, *56*, 721−733.
(675) Jaggi, J. S.; Seshan, S. V.; McDevitt, M. R.; LaPerle, K.; Sgouros, G.; Scheinberg, D. A. Renal Tubulointerstitial Changes after Internal Irradiation with α-Particle-Emitting Actinium Daughters. *J. Am. Soc. Nephrol.* **2005**, *16*, 2677−2689.
(676) Jaggi, J. S.; Seshan, S. V.; McDevitt, M. R.; Sgouros, G.; Hyjek, E.; Scheinberg, D. A. Mitigation of Radiation Nephropathy after Internal α-Particle Irradiation of Kidneys. *Int. J. Radiat. Oncol., Biol., Phys.* **2006**, *64*, 1503−1512.
(677) Borchardt, P. E.; Yuan, R. R.; Miederer, M.; McDevitt, M. R.; Scheinberg, D. A. Targeted Actinium-225 in Vivo Generators for Therapy of Ovarian Cancer. *Cancer Res.* **2003**, *63*, 5084−5090.
(678) Ballangrud, A. M.; Yang, W.-H.; Palm, S.; Enmon, R.; Borchardt, P. E.; Pellegrini, V. A.; McDevitt, M. R.; Scheinberg, D. A.; Sgouros, G. Alpha-Particle Emitting Atomic Generator (Actinium-225)-Labeled Trastuzumab (Herceptin) Targeting of Breast Cancer Spheroids: Efficacy versus HER2/Neu Expression. *Clin. Cancer Res.* **2004**, *10*, 4489−4497.
(679) McDevitt, M. R.; Ma, D.; Lai, L. T.; Simon, J.; Borchardt, P.; Frank, R. K.; Wu, K.; Pellegrini, V.; Curcio, M. J.; Miederer, M.; et al. Tumor Therapy with Targeted Atomic Nanogenerators. *Science* **2001**, *294*, 1537−1540.
(680) Miederer, M.; McDevitt, M. R.; Sgouros, G.; Kramer, K.; Cheung, N. V.; Scheinberg, D. A. Pharmacokinetics, Dosimetry, and Toxicity of the Targetable Atomic Generator, ^{225}Ac-HuM195, in Nonhuman Primates. *J. Nucl. Med.* **2004**, *45*, 129−137.
(681) Jurcic, J. G.; Rosenblat, T. L.; McDevitt, M. R.; Pandit-Taskar, N.; Carrasquillo, J. A.; Chanel, S. M.; Ryan, C.; Frattini, M. G.; Cicic, D.; Larson, S. M.; et al. Phase I Trial of the Targeted Alpha-Particle Nano-Generator Actinium-225 (^{225}Ac-Lintuzumab) (Anti-CD33; HuM195) in Acute Myeloid Leukemia (AML). *J. Clin. Oncol.* **2011**, *29*, 6516.
(682) Miederer, M.; McDevitt, M. R.; Borchardt, P.; Bergman, P.; Kramer, K.; Cheung, N. V.; Scheinberg, D. A. Treatment of Neuroblastoma Meningeal Carcinomatosis with Intrathecal Application of α-Emitting Atomic Nanogenerators Targeting Disialo-Ganglioside GD2. *Clin. Cancer Res.* **2004**, *10*, 6985−6992.
(683) Batra, J. S.; Liu, H.; Kim, S.; Navarro, V. N.; Vallabhajosula, S.; Tagawa, S. T.; Bander, N. H. PSMA-Targeted Alpha Radioimmunotherapy for Prostate Cancer with ^{225}Ac-J591. *Cancer Res.* **2017**, *77*, 5201.
(684) Tagawa, S. T.; Vallabhajosula, S.; Jhanwar, Y.; Ballman, K. V.; Hackett, A.; Emmerich, L.; Babich, J.; Sartor, A. O.; Harshman, L. C.; Beltran, H.; et al. Phase I Dose-Escalation Study of ^{225}Ac-J591 for Progressive Metastatic Castration Resistant Prostate Cancer (mCRPC). *J. Clin. Oncol.* **2018**, *36*, TPS399.
(685) Kratochwil, C.; Bruchertseifer, F.; Rathke, H.; Hohenfellner, M.; Giesel, F. L.; Haberkorn, U.; Morgenstern, A. Targeted Alpha Therapy of mCRPC with ^{225}Actinium-PSMA-617: Swimmer-Plot Analysis Suggests Efficacy Regarding Duration of Tumor-Control. *J. Nucl. Med.* **2018**, *59*, 795−802.
(686) Heppeler, A.; André, J. P.; Buschmann, I.; Wang, X.; Reubi, J.; Hennig, M.; Kaden, T. A.; Maecke, H. R. Metal-Ion-Dependent Biological Properties of a Chelator-Derived Somatostatin Analogue for Tumour Targeting. *Chem. - Eur. J.* **2008**, *14*, 3026−3034.
(687) Parker, D. Tumour Targeting with Radiolabelled Macrocycle−Antibody Conjugates. *Chem. Soc. Rev.* **1990**, *19*, 271−291.
(688) Kazmierczak, P. M.; Todica, A.; Gildehaus, F.-J.; Hirner-Eppeneder, H.; Brendel, M.; Eschbach, R. S.; Hellmann, M.; Nikolaou, K.; Reiser, M. F.; Wester, H.-J.; et al. ^{68}Ga-TRAP-$(RGD)_3$ Hybrid Imaging for the In Vivo Monitoring of $\alpha_v\beta_3$-Integrin Expression as Biomarker of Anti-Angiogenic Therapy Effects in Experimental Breast Cancer. *PLoS One* **2016**, *11*, e0168248.
(689) Finnen, D. C.; Pinkerton, A. A.; Dunham, W. R.; Sands, R. H.; Funk, M. O. Structures and Spectroscopic Characteristics of Iron(III) Diethylenetriaminepentaacetic Acid Complexes. A Non-Heme Iron-(III) Complex with Relevance to the Iron Environment in Lipoxygenases. *Inorg. Chem.* **1991**, *30*, 3960−3964.
(690) Nelson, W. O.; Karpishin, T. B.; Rettig, S. J.; Orvig, C. Aluminum and Gallium Compounds of 3-Hydroxy-4-Pyridinones: Synthesis, Characterization, and Crystallography of Biologically Active Complexes with Unusual Hydrogen Bonding. *Inorg. Chem.* **1988**, *27*, 1045−1051.
(691) Engle, J. W.; Hong, H.; Zhang, Y.; Valdovinos, H. F.; Myklejord, D. V.; Barnhart, T. E.; Theuer, C. P.; Nickles, R. J.; Cai, W. Positron Emission Tomography Imaging of Tumor Angiogenesis with a ^{66}Ga-Labeled Monoclonal Antibody. *Mol. Pharmaceutics* **2012**, *9*, 1441−1448.
(692) Mathias, C. J.; Lewis, M. R.; Reichert, D. E.; Laforest, R.; Sharp, T. L.; Lewis, J. S.; Yang, Z.-F.; Waters, D. J.; Snyder, P. W.; Low, P. S.; et al. Preparation of ^{66}Ga- and ^{68}Ga-Labeled Ga(III)-Deferoxamine-Folate as Potential Folate-Receptor-Targeted PET Radiopharmaceuticals. *Nucl. Med. Biol.* **2003**, *30*, 725−731.
(693) Walker, R. C.; Smith, G. T.; Liu, E.; Moore, B.; Clanton, J.; Stabin, M. Measured Human Dosimetry of ^{68}Ga-DOTATATE. *J. Nucl. Med.* **2013**, *54*, 855−860.
(694) Koudelková, M.; Vinšová, H.; Jedináková-Křížová, V. Isotachophoretic Determination of Stability Constants of Ho and Y Complexes with Diethylenetriaminepentaacetic Acid and 1,4,7,10-Tetraazadodecane-N,N′,N″,N‴-Tetraacetic Acid. *J. Chromatogr. A* **2003**, *990*, 311−316.
(695) Chang, C. A.; Francesconi, L. C.; Malley, M. F.; Kumar, K.; Gougoutas, J. Z.; Tweedle, M. F.; Lee, D. W.; Wilson, L. J. Synthesis, Characterization, and Crystal Structures of M(DO3A) (M = Fe, Gd) and Na[M(DOTA)] (M = Fe, Y, Gd). *Inorg. Chem.* **1993**, *32*, 3501−3508.
(696) Kumar, K.; Chang, C. A.; Francesconi, L. C.; Dischino, D. D.; Malley, M. F.; Gougoutas, J. Z.; Tweedle, M. F. Synthesis, Stability, and Structure of Gadolinium(III) and Yttrium(III) Macrocyclic Poly(Amino Carboxylates). *Inorg. Chem.* **1994**, *33*, 3567−3575.
(697) Broan, C. J.; Cox, J. P. L.; Craig, A. S.; Kataky, R.; Parker, D.; Harrison, A.; Randall, A. M.; Ferguson, G. Structure and Solution Stability of Indium and Gallium Complexes of 1,4,7-Triazacyclononanetriacetate and of Yttrium Complexes of 1,4,7,10-Tetraazacyclododecanetetraacetate and Related Ligands: Kinetically Stable Complexes for Use in Imaging and Radioimmunotherapy. X-Ray Molecular Structure of the Indium and Gallium Complexes of 1,4,7-Triazacyclononane-1,4,7-triacetic Acid. *J. Chem. Soc., Perkin Trans. 2* **1991**, *1*, 87−99.
(698) Wadas, T. J.; Wong, E. H.; Weisman, G. R.; Anderson, C. J. Coordinating Radiometals of Copper, Gallium, Indium, Yttrium, and Zirconium for PET and SPECT Imaging of Disease. *Chem. Rev.* **2010**, *110*, 2858−2902.
(699) Kodama, M.; Koike, T.; Mahatma, A. B.; Kimura, E. Thermodynamic and Kinetic Studies of Lanthanide Complexes of 1,4,7,10,13-Pentaazacyclopentadecane-N,N′,N″,N‴,N⁗-Pentaacetic Acid and 1,4,7,10,13,16-Hexaazacyclooctadecane-N,N′,N″,N‴,N⁗,N⁗′-Hexaacetic Acid. *Inorg. Chem.* **1991**, *30*, 1270−1273.
(700) Chinol, M.; Bodei, L.; Cremonesi, M.; Paganelli, G. Receptor-Mediated Radiotherapy With ^{90}Y-DOTA-DPhe^1-Tyr^3-Octreotide: The Experience of the European Institute of Oncology Group. *Semin. Nucl. Med.* **2002**, *32*, 141−147.
(701) Perk, L. R.; Visser, O. J.; Stigter-Van Walsum, M.; Vosjan, M. J. W. D.; Visser, G. W. M.; Zijlstra, J. M.; Huijgens, P. C.; Van Dongen, G. A. M. S. Preparation and Evaluation of ^{89}Zr-Zevalin for Monitoring of ^{90}Y-Zevalin Biodistribution with Positron Emission Tomography. *Eur. J. Nucl. Med. Mol. Imaging* **2006**, *33*, 1337−1345.

DOI: 10.1021/acs.chemrev.8b00294
Chem. Rev. 2019, 119, 902−956

(702) Lee, F. T.; Mountain, A. J.; Kelly, M. P.; Hall, C.; Rigopoulos, A.; Johns, T. G.; Smyth, F. E.; Brechbiel, M. W.; Nice, E. C.; Burgess, A. W.; et al. Enhanced Efficacy of Radioimmunotherapy with ^{90}Y-CHX-A″- DTPA-Hu3S193 by Inhibition of Epidermal Growth Factor Receptor (EGFR) Signaling with EGFR Tyrosine Kinase Inhibitor AG1478. *Clin. Cancer Res.* **2005**, *11*, 7080s−7086s.
(703) Martell, A. E.; Smith, R. M. *Critical Stability Constants*; Plenum Press: New York, 1989; Vol. *1*−*6*.
(704) Geraldes, C. F. G. C.; Delgado, R.; Urbano, A. M.; Costa, J.; Jasanada, F.; Nepveu, F. Complexes of Ga^{3+} and In^{3+} with the N,N″-Bis(Butylamide) Derivative of Diethylenetriaminepentaacetic Acid: Stability Constants and Nuclear Magnetic Resonance Studies in Aqueous Solution. *J. Chem. Soc., Dalton Trans.* **1995**, *3*, 327−335.
(705) Jasanada, F.; Urizzi, P.; Souchard, J.-P.; Le Gaillard, F.; Favre, G.; Nepveu, F. Indium-111 Labeling of Low Density Lipoproteins with the DTPA−Bis(Stearylamide): Evaluation as a Potential Radiopharmaceutical for Tumor Localization. *Bioconjugate Chem.* **1996**, *7*, 72−81.
(706) Bakker, W. H.; Albert, R.; Bruns, C.; Breeman, W. A. P.; Hofland, L. J.; Marbach, P.; Pless, J.; Pralet, D.; Stolz, B.; Koper, J. W.; et al. [^{111}In-DTPA-D-Phe^{1}]-Octreotide, a Potential Radiopharmaceutical for Imaging of Somatostatin Receptor-Positive Tumors: Synthesis, Radiolabeling and in Vitro Validation. *Life Sci.* **1991**, *49*, 1583−1591.
(707) Tóth, É.; Brücher, E. Stability Constants of the Lanthanide(III)-1,4,7,10-Tetraazacyclododecane-N,N′,N″,N‴-Tetraacetate Complexes. *Inorg. Chim. Acta* **1994**, *221*, 165−167.
(708) Moreau, J.; Guillon, E.; Pierrard, J.-C.; Rimbault, J.; Port, M.; Aplincourt, M. Complexing Mechanism of the Lanthanide Cations Eu^{3+}, Gd^{3+}, and Tb^{3+} with 1,4,7,10-Tetrakis(Carboxymethyl)-1,4,7,10-Tetraazacyclododecane (dota)— Characterization of Three Successive Complexing Phases: Study of the Thermodynamic and Structural Properties of the Complexes by Potentiometry, Luminescence Spectroscopy, and EXAFS. *Chem. - Eur. J.* **2004**, *10*, 5218−5232.
(709) Moreau, J.; Guillon, E.; Aplincourt, P.; Pierrard, J. C.; Rimbault, J.; Port, M.; Aplincourt, M. Thermodynamic and Structural Properties of Eu^{3+}, Gd^{3+} and Tb^{3+} Complexes with 1,4,7,10-Tetra(2-Glutaryl)-1,4,7,10-Tetraazacyclododecane in Solution: EXAFS, Luminescence, Potentiometric Studies, and Quantum Calculations. *Eur. J. Inorg. Chem.* **2003**, *2003*, 3007−3020.
(710) Caravan, P.; Ellison, J. J.; McMurry, T. J.; Lauffer, R. B. Gadolinium(III) Chelates as MRI Contrast Agents: Structure, Dynamics, and Applications. *Chem. Rev.* **1999**, *99*, 2293−2352.
(711) Loncin, M. F.; Desreux, J. F.; Merciny, E. Coordination of Lanthanides by Two Polyamino Polycarboxylic Macrocycles: Formation of Highly Stable Lanthanide Complexes. *Inorg. Chem.* **1986**, *25*, 2646−2648.
(712) Inomata, Y.; Sunakawa, T.; Howell, F. S. The Syntheses of Lanthanide Metal Complexes with Diethylenetriamine-N,N,N′,N″,N″-Pentaacetic Acid and the Comparison of Their Crystal Structures. *J. Mol. Struct.* **2003**, *648*, 81−88.
(713) Aime, S.; Barge, A.; Benetollo, F.; Bombieri, G.; Botta, M.; Uggeri, F. A Novel Compound in the Lanthanide(III) DOTA Series. X-Ray Crystal and Molecular Structure of the Complex Na[La(DOTA)La(HDOTA)]·10H_2O. *Inorg. Chem.* **1997**, *36*, 4287−4289.
(714) Thakur, P.; Conca, J. L.; Dodge, C. J.; Francis, A. J.; Choppin, G. R. Complexation Thermodynamics and Structural Studies of Trivalent Actinide and Lanthanide Complexes with DTPA, MS-325 and HMDTPA. *Radiochim. Acta* **2013**, *101*, 221−232.
(715) Shannon, R. D. Revised Effective Ionic Radii and Systematic Studies of Interatomic Distances in Halides and Chalcogenides. *Acta Crystallogr., Sect. A: Cryst. Phys., Diffr., Theor. Gen. Crystallogr.* **1976**, *32*, 751−767.
(716) Baes, C. F. J.; Mesmer, R. E. *The Hydrolysis of Cations*; Wiley-Interscience: New York, 1976.
(717) See Figures 4 and 5 for structures of all discussed ligands.

DOI: 10.1021/acs.chemrev.8b00294
Chem. Rev. 2019, 119, 902−956